Polymer-Based Drug Delivery Systems for the Targeted and Controlled Release of Cancer Drugs in Triple-Negative Breast Cancer (TNBC) Treatment

A Dissertation Presented to the Department of

Materials Science and Engineering

African University of Science and Technology

In Partial Fulfillment of the Requirements for the Degree of

Doctor of Philosophy

By

Sandra Musu Jusu (ID No. 70177)

Advisor: Professor Winston O. Soboyejo
Co-advisor: Dr. Olushola S. Odusanya

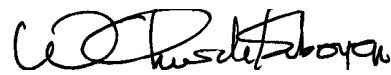### September, 2021.

CERTIFICATION

This is to certify that the dissertation titled "Polymer-Based Drug Delivery Systems for the Targeted and Controlled Release of Cancer Drugs in Triple-Negative Breast Cancer (TNBC) Treatment" submitted to the school of postgraduate studies, African University of Science and Technology (AUST), Abuja, Nigeria for the award of the Doctor of Philosophy is a record of original research carried out by Sandra Musu Jusu in the Department of Materials Science and Engineering.

POLYMER-BASED DRUG DELIVERY SYSTEMS FOR THE TARGETED AND CONTROLLED RELEASE OF CANCER DRUGS IN TRIPLE-NEGATIVE BREAST CANCER (TNBC) TREATMENT

By

Sandra Musu Jusu

A DISSERTATION APPROVED BY THE MATERIALS SCIENCE AND ENGINEERING DEPARTMENT

RECOMMENDED: Advisor: Professor Winston O. Soboyejo

Co-advisor Dr. Olushola S. Odusanya

Head, Department of Materials Science and Engineering: Prof. Peter Onwualu

APPROVED:

Chief Academic Officer

Abstract

Cancer is a disease that exists globally. Among women, breast cancer is most prevalent. Breast cancer exhibits different degrees of aggressiveness. Triple-Negative Breast Cancer (TNBC), which accounts for approximately twenty percent of breast cancer cases, is one of the most aggressive types of breast cancer, and it disproportionately affects women of African and Hispanic origins. Because TNBC is characterized by lack of expression of estrogen receptors (ER), progesterone receptors (PR), and human epidermal growth factor 2 receptors (HER2), all of which are essential targets for established hormonal therapies and anti-HER2 agents, it is difficult to treat. Currently, conventional methods such as chemotherapy and radiation are used to treat TNBC. Those treatment methods, however, are not very effective because they lack specificity, and they are undesirable due to their high dose requirement, low therapeutic indices, poor bioavailability, and other adverse side effects. To improve TNBC treatment outcomes, therefore, it is essential to explore and develop targeted cancer drug delivery systems that pass muster where current, conventional TNBC treatment methods fail. This thesis, part of which has been published, encapsulates the use of materials science and engineering approaches to develop targeted drug delivery systems for controlled and localized treatment of TNBC. The thesis contains six chapters. Chapter one covers the introduction, and chapter two covers the literature review. Chapter three discusses the results of an *in vitro* and *in vivo* study of a unique blend of polymers [poly (lactic-co-glycolic acid) - polyethylene glycol] microspheres that encapsulated LHRH-conjugated and unconjugated drugs, respectively. Chapter four highlights the use of poly (lactic-co-glycolic acid) – chitosan – polyethylene glycol microspheres encapsulating model anti-cancer drugs [prodigiosin and paclitaxel] for controlled drug delivery in TNBC treatment. Chapter five presents the results of a combined experimental and analytical *in vitro* and *in vivo* study of blended FDA-approved polymers [poly (lactic-co-glycolic acid), polyethylene glycol, and polycaprolactone] with the potential for sustained localized cancer drug release. Chapter six contains conclusions and suggestions for future work.

Keywords: triple-negative breast cancer, drug delivery, thermodynamics, kinetics, biodegradable polymers, prodigiosin, paclitaxel, microspheres, scaffolds, chitosan, poly (lactic-co-glycolic acid), polyethylene glycol, polycaprolactone, luteinizing hormone releasing hormone.

Dedication

I dedicate this dissertation to:

- God Almighty, my creator, for giving me wisdom, knowledge and understanding, protecting me and always making a way for me where there seems to be no way;

- My parents (Mr. Sylvester M. Jusu & Mrs. Millicent J. Kamara) for being beacons of hope, inspiration, love and provision in my life;

- My grandmother (Late Mrs. Marie Junisa-Demby) for instilling the importance of education in me and other females in my family even though she, herself, did not go to school;

- My brothers and sisters (Mr. Victor Kamara, Mrs. Victoria Makavore and Mrs. Sylvia Cole) for always being there for me and encouraging me to run towards the finished line; and

- The love of my life (Mr. Samuel Borbor-Sawyer, Esq.) for being loving, caring and all-round amazing. You are God's special gift to me; you bring out the best in me; and I love you with all my heart.

Preface

This dissertation is submitted in partial fulfillment of the requirements for award of the degree of Doctor of Philosophy at African University at Science and Technology, Abuja, Nigeria. This research was conducted under the supervision of Prof. Winston O. Soboyejo, Senior Vice President and Provost, Worcester Polytechnic Institute in Worcester, MA, USA. This research encapsulates the use of materials science and engineering principles to design and fabricate robust drug delivery systems (DDS) to target Triple-Negative Breast Cancer (TNBC), which is an aggressive subtype of breast cancer with poor prognosis. This research contributes to the body of cancer research by providing new insights for the development of drug delivery systems that have a viable potential to effectively treat breast cancer. This research was supported by the African Union Commission (Mwalimu Nyerere Scholarship), and World Bank African Center of Excellence (ACE) Program through the Pan-African Materials Institute (PAMI) (Grant No. P126974).

Part of this work has been published in Nature's Scientific Reports, Materials Science & Engineering C and Applied Sciences journal, as shown below:

Jusu, S.M, Obayemi, J.D., Salifu, A.A. *et al., Drug-encapsulated blend of PLGA-PEG microspheres: in vitro and in vivo study of the effects of localized/targeted drug delivery on the treatment of triple-negative breast cancer*. Scientific Reports 10, 14188(2020). https://doi.org/10.1038/s41598-020-71129-0

Jusu, S.M.; Obayemi, J.D.; Salifu, A.A.; Nwazojie, C.C.; Uzonwanne, V.O.; Odusanya, O.S.; Soboyejo, W.O. PLGA-CS-PEG Microparticles for Controlled Drug Delivery in the Treatment of TripleNegative Breast Cancer Cells.*Appl.Sci.* 2021,*11*,7112. https://doi.org/10.3390/app11157112

J.D. Obayemi, Jusu S.M., Salifu A.A., *et al., Degradable Porous Drug-loaded Polymer Scaffolds for Localized Cancer Drug Delivery and Breast Cell/Tissue Growth*, Materials Science & Engineering C (2020), https://doi.org/10.1016/ j.msec.2020.110794

Obayemi, J.D., Salifu, A.A., Eluu, S.C., Uzonwanne V. O., Jusu S. M., Nwazojie C. C., Onyekanne C. E., Ojelabi O., Payne L., Moore C. M., King J. A. and Soboyejo W. O. *LHRH-Conjugated Drugs as Targeted Therapeutic Agents for the Specific Targeting and Localized Treatment of Triple Negative Breast Cancer*,Scientific Reports 10, 8212(2020). https://doi.org/10.1038/s41598-020-64979-1

Acknowledgments

My deep appreciation goes to my friends for their moral support and understanding, and for sticking close, even though I was invariably unavailable as I worked long and hard on this project. Special thanks to my course mates and lab mates for all the intellectually stimulating discussions and for being excellent teammates through the projects we worked together on.

A special mention to the love of my life, Samuel Borbor-Sawyer Esq., for his love, his belief in my potential, and his strides to help me fulfill purpose. You are a great motivator to me, and your ability to quickly grasp complex science concepts and engage me in deep conversations about such concepts really helped broaden my horizon as a scientist.

I express my gratitude to the Seray Jah family for helping me adjust to Nigeria.

I am sincerely grateful to everyone who directly or indirectly rendered assistance to me during my PhD journey, but who, because of limited time and space, could not be mentioned in this section. God bless you.

Finally, I wish to express my profound and resounding thanks to the African Union Commission (Mwalimu Nyerere Scholarship) and World Bank African Center of Excellence (ACE) Program for granting me a scholarship/fellowship award that made it possible for me to pursue and attain my PhD.

Table of Contents

List of Figures

List of Tables

List of Abbreviations

ATCC	American Type Culture Collection
BC	Breast Cancer
BSA	Bovine Serum Albumin
CDR	Cumulative Drug Release
CS	Chitosan
DCM	Dichloromethane
DDS	Drug Delivery System
DEE	Drug Encapsulation Efficiency
DLE	Drug Loading Efficiency
DLS	Dynamic Light Scattering
DPBS	Dulbecco's phosphate-buffered saline
DSC	Differential Scanning Calorimetry
ECM	Extracellular Matrix
EDTA	Ethylenediamine-tetra-acetic acid
ER	Estrogen Receptors
FBS	Fetal Bovine Serum
FTIR	Fourier Transform Infrared Spectroscopy
H&E	Hematoxylin and eosin
HEPES	2-[4-(2-hydroxyethyl) piperazin-1-yl] ethanesulfonic acid
HER2	Human Epidermal growth factor Receptor 2
L-15	Leibovitz's 15 medium
LHRH	Luteinizing Hormone Releasing Hormone
LHRH-R	Luteinizing Hormone Releasing Hormone Receptor
MDA-MB-231	M.D. Anderson Metastatic Breast Cancer
NMR	Nuclear Magnetic Resonance Spectroscopy
PBS	Phosphate Buffered Saline
PCL	Polycaprolactone
PEG	Polyethylene glycol
PGS	Prodigiosin
PGS-LHRH	Luteinizing Hormone Releasing Hormone-Conjugated Prodigiosin
PLA	Poly Lactic Acid
PLGA	Polylactic-co-glycolic acid
PNIPA	Poly-n-isopropyl-acrylamide
PR	Progesterone receptors
PTX	Paclitaxel
PTX-LHRH	Luteinizing Hormone Releasing Hormone-Conjugated Paclitaxel
PVA	Poly (vinyl alcohol)
SEM	Scanning Electron Microscopy

TBD	Trypan Blue Dye
TE	Tissue Engineering
TGA	Thermogravimetric Analysis
TNBC	Triple-Negative Breast Cancer

Chapter 1

1.0 Introduction

1.1 Background and Motivation

Cancer is the second leading cause of death globally. In 2020, approximately 19.3 million new cancer cases and almost 10.0 million cancer death occurred [1]. The Global Cancer Statistics projects that 28.4 million cancer cases will occur by 2040 [1]. At its core, cancer is a complex serial progression of disease conditions that create an arena of cells with uncontrolled growth and the potential to escape the body's natural cell death mechanism [2]. In more simple terms, cancer is the uncontrolled growth of abnormal cells that supersedes the growth of normal cells, thereby causing abnormal growth. There are about 200 types of cancer [3]. Current scientific evidence suggests that cancer can be triggered by environmental and genetic factors [4]. Genetic and epigenetic mutations caused by some viral infections and continuous exposure to carcinogens like ultraviolet light, tobacco smoke, and insistent tissue injury ultimately lead to this disease's initiation, progression, and metastasis [2,5,6] . Despite all the recent technological improvements, some cancer-death results from recurrence and metastasis [7]. Metastasis is a sequential and complex process during which cancer cells migrate to distant organs, making it more difficult to treat cancer [8].

 Breast cancer contributes greatly to cancer-related deaths, and is the most common form diagnosed cancer in women globally [9–11]. It is also one of the leading causes of death amongst women, particularly in low-resource countries [12,13]. The rate of survival is high when breast cancer is detected and treated early. However, women's access to timely, affordable, and effective health care services is limited by several factors, which can be social, economic, or geographic,

with a high proportion of low-resource and middle resources countries being diagnosed with later-stage breast cancer [14]. Triple-negative breast cancer (TNBC) is defined by what it lacks. TNBC, lacks the expression of estrogen receptors (ER), progesterone receptors (PR), and human epidermal growth factor receptor 2 (HER2) [15]. The therapeutic implication of this is that TNBC cannot be treated using established hormonal therapies, given that they are ER and PR negative [16,17]. Also, because TNBC is HER2 negative, it cannot be treated using anti-HER2 agents. TNBC is a heterogeneous disease with several proposed molecular sub-classifications, and it accounts for 15-20 % of breast cancer cases [16–19]. The disease exhibits higher incidences in women of African and Hispanic origins [20]. Furthermore, TNBC has aggressive malignancy [21,22] with early relapse and metastatic spread to the lungs, liver, and central nervous system, thus decreasing the possibility of survival [19]. The mean survival time for patients diagnosed with metastatic TNBC is about 13 months [23]. Current treatment modalities for TNBC include radiotherapy, chemotherapy, surgical removal, or a combination of any. These conventional treatment methods often induce multiple side effects that can have a long-lasting impact on a patient's quality of life [24–26].

Over the years, drug delivery systems (DDS) have offered a unique platform to circumvent the challenges associated with conventional methods of breast cancer treatment. Modern-day medicine seeks to address those challenges, and concepts regarding efficient drug delivery are pivotal in those efforts [27]. Drug delivery systems (DDS) are used to deliver drugs to desired cells, tissues, organs, and sub-cellular organs for drug release and adsorption through various drug carriers [28]. Their desirable features include improving the pharmaceutical activities of therapeutic drugs and alleviating the side effects of therapeutic drugs, thus addressing the problem

of low bioavailability, lack of selectivity, limited solubility, poor biodistribution, and drug aggregation [28]. Modern medicine has investigated the use of controlled drug delivery technology to optimize the therapeutic effect of anti-cancer drugs. Controlled drug delivery evaluates how one can maintain the drug release profile within the therapeutic window for an extended period. This area of drug delivery not only aims to control the duration of drug release or its levels but also target it to the desired location.

Polymeric materials with various architectures are often considered the primary choice material for drug delivery applications [29]. Progress in creating polymeric materials with desirable properties has increased the possibility of their use for biomedical applications. For a targeted drug delivery system to be deemed effective, it must be able to retain, target, and release drugs, as well as evade the reticuloendothelial system (RES) [30]. Drug targeting can either be passive or active. Passive tumor targeting is based on an accumulation of drugs in the regions around the tumors with leaky vasculature and does not have a ligand for specific tissue/organ binding [31–33]. Active targeting is achieved through specific ligand–receptor interactions between drug/drug carriers and the target tumor cells [34–39]. Such specific targeting may reduce the potential side effects of breast cancer treatment. Prior studies have also revealed that triple-negative breast cancer cells overexpress LHRH receptors [40–44]. The binding of LHRH to its receptors (LHRH-R) appears to be controlled by receptor micro-aggregation and internalization of the peptide [45]. In order to improve breast cancer therapy and impede tumor metastasis, there is a need to develop targeted drug delivery systems for the controlled release of cancer drugs to combat the side effects associated with conventional breast cancer treatment methods. Moreover, it is very crucial to establish a clear understanding of the kinetics and thermodynamics parameters of drug release

from these drug delivery systems, as this would explain and describe the drug release mechanisms, thereby aiding safe and effective therapy. This dissertation uses a materials science and engineering approach by combining experimental and theoretical studies to provide new insights for the development of drug delivery systems that have viable potential in breast cancer treatment.

1.2 Unresolved Issues and Research Objectives

TNBC lacks estrogen receptors (ER), progesterone receptors (PR), and human epidermal growth factor receptor 2 (HER2), all of which are essential for targeted treatment of the disease. The challenges associated with TNBCs emerge from aggressive tumor growth, poor prognosis, accentuated side effects, and limited targeted therapies. The current methods of breast cancer treatment are associated with side effects due to their non-specific targeting, poor bioavailability, high dose requirement, low therapeutic indices, and propensity to cause multiple drug resistance. These side effects warrant numerous revisiting therapies. Therefore, there is a profound need to develop drug delivery systems for targeted, controlled, and localized drug delivery that will, among other things, alleviate the harsh side effects associated with conventional TNBC treatments. There is also a need for more relevant literature focusing on correlating the thermodynamics and kinetics of drug release from those drug delivery systems. The objectives of the current work are as follows:

1. To assess, *in vitro* and *in vivo*, the effects of localized/targeted drug delivery on the treatment of triple-negative breast cancer using a drug-encapsulated blend of polylactic-*co*-glycolic acid (PLGA)- polyethylene glycol (PEG)] microspheres;

2. To assess, *in vitro*, the use of PLGA, chitosan (CS), and polyethylene (PEG) to form PLGA-CS-PEG microparticles for controlled drug delivery in the treatment of triple-negative breast cancer cells;

3. To assess, *in vitro* and *in vivo*, the use of porous drug-loaded degradable [polylactic-*co*-glycolic acid (PLGA)- polyethylene glycol (PEG)] and [polylactic-*co*-glycolic acid (PLGA)- polycaprolactone (PCL)] scaffolds for localized cancer drug delivery and breast cell/ tissue growth;

1.3 Scope and Organization of the Work

This dissertation begins with Chapter 1, which covers the background, the introduction, the unresolved issues, and the scope of the work. Chapter 2 covers a literature review. This is followed by chapter 3, which highlights the results of an *in vitro* and *in vivo* study of a unique blend of polymers polylactic-*co*-glycolic acid (PLGA)- polyethylene glycol (PEG)] microspheres that encapsulated LHRH conjugated and unconjugated drugs, respectively. Chapter 4 highlights the *in vitro* effects of hydrophilic polymers on drug release using drug-encapsulated PLGA microspheres coated with chitosan (CS) and polyethylene (PEG)] for controlled and localized TNBC treatment, while chapter 5 presents an *in vitro* and *in vivo* assessment of the use of porous drug-loaded degradable [polylactic-*co*-glycolic acid (PLGA)- polyethylene glycol (PEG)] and [polylactic-*co*-glycolic acid (PLGA)- polycaprolactone (PCL)] scaffolds for localized cancer drug deliver and breast cell/ tissue growth. Salient conclusions from the study are then presented in chapter 6, along with some suggestions for future work.

Chapter 2

2.0 Literature Review

2.1 Introduction

The American cancer society has defined cancer as the uncontrolled growth and spread of abnormal cells that could cause death [46]. Cancer originates from the Greek word *"Karkinoma,"* which means appendage-like projections [47]. To date, cancer remains a health problem globally, and the associated death rates are very high. Histological and biological criteria are often used to classify this malignant disease. The causes of cancer are not fully understood, but certain risk factors can autonomously or in sequence initiate and or promote cancer growth [46]. These factors include repeated exposure to carcinogens, insistent tissue injury, viral infections such as (HPV), and environmental factors or influences such as tobacco smoking and ultraviolet light, all of which can cause genetic and epigenetic mutation [5,6,48]. Although cancers can be prevented through lifestyle changes (e.g., lung cancer) or vaccination (e.g., cervical cancer caused by HPV), or treated through conventional means such as chemotherapy [49], early detection of cancer, or analysis of its potential to occur, is an indispensable element in effectively preventing, managing, or treating the disease. Cancer survival is lower in sub-Saharan Africa than in other world regions, with breast cancer, for example, accounting for 24% of cancer deaths in sub-Saharan African women [50]. Cancer treatment can include localized therapies, and or systemic therapies used alone or in combination [51]. The critical step in cancer treatment, however, is developing and effectively utilizing drug delivery systems that would cause anti-cancer drugs to target and kill cancer cells without killing normal cells specifically.

2.2 Breast Cancer

The breast is a glandular organ on the chest; both males and females possess it. It is made up of two main tissues: glandular tissues and stromal (supporting) tissues, with female breasts, ordinarily having more glandular tissues than those of males [52,53]. Stromal tissues are composed of adipose tissues, which are fatty in nature, as well as fibrous connective tissues and ligaments [53,54]. Cellular fluid and waste are removed from the breast via the lymphatic tissue-immune system tissue [53]. There are 12–20 lobes in the female breast, which are subdivided into several lobules connected via milk ducts [54,55]. The heterogenous nature of the breast tissue makes it sensitive to hormonal changes in the body during the menstrual cycle [56].

Globally, breast cancer is the most common form of cancer diagnosed in women [9–11]. Projections show that 1 in 8 women worldwide have a risk of being diagnosed with invasive breast cancer and that 1 in 39 women will die from breast cancer [57]. Although breast cancer presents no symptoms when the tumor is small, the signs and symptoms of breast cancer include a painless lump, breast heaviness, unusual breast pain or discomfort, changes in the physical appearance of the breast [57,58].

A breast cancer diagnosis is critical in breast cancer therapy. Medical imaging techniques used for diagnosis include: mammography, Magnetic resonance imaging (MRI), Infrared therapy, and ultrasound (US) [11,59,60]. There are also new studies focusing on machine learning techniques to assist radiologists and physicians in identifying abnormalities and interpreting images [59,61]. The use of new biomarkers such as DNAs, microRNAs, mRNAs, and various molecules also improve breast cancer diagnosis and management [11,60].

After breast cancer is diagnosed, it is assigned a stage. The stage breast cancer is assigned is determined by the extent to which the cancer has spread at the time of assignment. The assignment helps in choosing treatment options and results in a better disease prognosis [57]. The two main staging systems for cancer are the American Joint Committee on Cancer (AJCC) staging system and the Surveillance, Epidemiology and End Results (SEER) summary staging system [57].

Breast cancer is a heterogenous and complex disease. According to the site of the cancer, there are two main types of breast cancer (Invasive and Non-invasive/*in situ*) [54]. For *in situ* breast cancer, the term "*in situ*" describes "in place," meaning cells that are confined and do not invade surrounding fatty and connective tissues of the breast [54]. The two main types of *in situ* breast cancer are ductal carcinoma *in situ* (DCIS) and lobular carcinoma *in situ* (LCIS) [57]. DCIS is confined to the breast ducts, and LCIS is confined to the breast lobules.

The four main molecular categories of breast cancer are Luminal A (HR+/HER2-), Luminal B (HR+/HER2+), Basal-like (HR-/HER2-), and HER2-enriched (HR-/HER2+) [57]. HR means hormone receptor, HER2 means human epidermal growth factor receptor 2. Luminal A represents 73% of all breast cancers, while Luminal B subtype is characterized clinically as HER2 positive and or protein Ki67 positive [57]. Luminal B breast cancers are higher grade; hence they tend to have a poorer prognosis than luminal A breast cancers [62,63].

Despite the alarming statistic of cancer death, early detection and treatment can considerably improve the disease outcomes. Breast cancer management is aimed at preserving the quality of life and prolonging the life expectancy of breast cancer patients [54]. Presently, the following

approaches are used for breast cancer treatment: targeted therapies, hormonal treatment, surgery, radiation therapy, and chemotherapy [54]. Surgery is the principal strategy used in breast cancer management for scenarios where the breast cancer has not metastasized and is also an option for further complex stages of breast cancer [64–66]. There are various forms of breast cancer surgery which include: breast-conserving surgery, mastectomy, and reconstructive surgery [54]. Women that undergo mastectomy are normally presented with the option of reconstructive surgery, which involves breast renovation [67]. Radiation therapy uses high-energy X-rays/gamma rays to kill cancer cells [53]. Chemotherapy involves the use of drugs to kill cancer cells [68,69]. It can be given in both situations, before surgery, to shrink the tumor and after surgery in cycles/dose fashion [53,54,57].

2.3 Metastasis

When cancer cells leave their primary site, they migrate to another site by either invasion or metastasis [70]. Invasion involves the movement of cancerous cells into surrounding tissues, while metastasis involves the spread of cancerous cells via the bloodstream, lymphatic system, or body spaces to distant sites [70,71]. Metastasis proceeds through sequential steps that must be complete and could, therefore, be halted if there is a failure to complete any of the sequential steps [72,73]. The five major steps of the metastatic cascade are: dissociation, invasion, intravasation, extravasation, and dormancy [74]. During dissociation, the single tumor cell detaches from the primary tumor due to the lack of cell-cell adhesion and migrates into adjacent tissues [74,75]. This is followed by invasion, where the dissociated tumor cells penetrate nearby stroma and invade and migrate through the basement membrane aiding the local blood endothelium and or lymphatics [74]. This critical event allows cancer cells to change their shape and transform a growing tumor

9

into a metastatic disease [74]. The third step is intravasation, where a locally invasive tumor cell enters the body's circulatory system [74]. Fourthly, extravasation occurs when the detached tumor cells migrate to distant body organs via lymphatic flow, leaving the vasculature [74]. The final stage is dormancy, where invaded tumor cells may remain "silent" for a long time [74].

2.4 Triple-Negative Breast Cancer

TNBC lacks the expression of progesterone receptor (PR), estrogen receptor (ER), and HER 2 [15]. TNBC makes up for 15-20% of breast cancer cases and is notorious for having a higher recurrence rate and a poorer patient survival rate compared to other types of breast cancer [76,77]. TNBC has aggressive malignancy [21,22] and disproportionately affects women of African and Hispanic origins and younger women [20,78–80]. There are incidences of TNBC in premenopausal women and those with BRCA1 gene mutation [81]. Unfortunately, women struck with TNBC have only three years of freedom from recurrence in contrast to women with other breast cancers (63 vs. 76%, $p < .0001$) [82,83]. Gene expression profiling analysis features a high overlap ratio between TNBC and basal-like breast cancer (56%-90%), in contrast to the ratio between non-TNBC and non-basal-like breast cancer (11.5%) [84,85]. Metastatic TNBC has a high proliferation rate and metastases to visceral organs and the central nervous system [86]. A better comprehension of the clinical and pathological features of TNBC would facilitate the design of novel individualized treatments.

2.4.1 Challenges with Current Triple-Negative Breast Cancer (TNBC) Treatment

TNBC lacks ER, PR, and HER2 is invariably unresponsive to hormonal therapies and HER2 agents, making it difficult to detect and treat [87,88]. Tumor metastasis is often associated with

10

TNBC and incidentally accounts for 90% of cancer-related deaths [89,90]. Furthermore, usual forms of breast cancer treatment, namely chemotherapy, radiation therapy, and surgery (or their combination) are linked with harsh side effects and warrant numerous revisiting therapies [24,91]. In early-stage cases of TNBC, chemotherapy has been successful to some extent and shown some effectiveness, but at advanced stages, the response remains poor [88]. TNBC is very heterogeneous and is associated with challenges, which include a high risk of metastasis and recurrence, lack of effective chemotherapeutic agents; poor prognosis; and absence of therapeutic targets [88]. Several approaches have been used to resolve the problems associated with TNBC treatment, which include targeted drug delivery systems, the development of nanotechnology-based formulations, and the discovery or of potential and drug-responsive targets for TNBC [88]. Recent medical investigations have indicated that using controlled and targeted drug delivery systems to optimize the therapeutic effect of anti-cancer drugs and specifically target breast cancer cells can potentially reduce the side effects of present breast cancer treatment.

2.4.2 Role of Luteinizing Hormone-Releasing Hormone (LHRH) in TNBC Treatment

In an effort to identify potential and drug-responsive targets specifically pertinent to TNBC, LHRH has shown to be an ideal target in TNBC therapy. LHRH expression is scarce in healthy tissues while LHRH receptors have been shown to be overexpressed in many tumors, including breast (about 50%), ovarian and endometrial (about 80%), 32–50% of pancreatic tumors, 80% of renal tumor and prostate (about 86%) tumors [44,92–95]. This makes LHRH an ideal tumor target for breast cancer treatment [96,97]. The binding of LHRH to its receptors (LHRH-R) appears to be controlled by receptor micro-aggregation and internalization of the peptide [45].

Over the past few decades, several researchers have initiated studies on using LHRH receptors as targets in TNBC therapy. Here, we briefly discussed some of the *in vivo* studies. Kahan *et al.,* (1999) studied the effects of a targeted cytotoxic somatostatin analog (AN-238) formed by linking the highly active doxorubicin (DOX) derivative 2-pyrrolino-DOX (AN-201) to octapeptide RC-121 (D-Phe-Cys-Tyr-D-Trp-Lys-Val-Cys-Thr-NH2) in three human breast cancer models [98]. In 2000, this group showed *in vivo* that a single dose of AN-207 significantly inhibited the tumor for three weeks after injection [99]. Föst *et al.,* (2011) analyzed whether cytotoxic LHRH agonist AEZS-108 (AN-152) is a suitable drug for an efficacious and less toxic therapy for TNBC that expresses LHRH receptors [96]. Buchholz *et al.,* (2009) evaluated the expression of LHRH receptors in TNBC human specimens and investigated if these receptors are suitable targets for the treatment with the LHRH antagonist Cetrorelix *in vitro* and *in vivo* [42]. Seitz *et al.,* (2014) confirmed that a significant proportion of TNBC express LHRH-receptors and can be successfully used as homing sites for cytotoxic analogs of LHRH, such as AEZS-108 and AEZS-125 [97]. Significant efforts have also been made by the Soboyejo group to demonstrate the specific targeting of TNBC *in vivo*. Hu *et al.,* (2020) demonstrated the application of coated LHRH-MNPs for the enhancement of magnetic resonance imaging contrast using subcutaneous xenograft tumor models [100]. Also, LHRH-conjugated PGS and LHRH-conjugated PTX were studied for the specific targeting and localized drug delivery in TNBC treatment [43,101]. Ultimately, all previous *in vivo* investigations cited concluded that LHRH receptors represent potential therapeutic targets.

2.5 Cancer Drugs

2.5.1 Paclitaxel (PTX) and Conjugated Paclitaxel Drugs

Paclitaxel is a natural taxane compound isolated from the bark of the Pacific yew tree (*Taxus brevifolia*) discovered by Dr. Monre Wall and Dr. Mansukh Wani [102,103]. Its chemical structure was elucidated by X-ray diffraction and has a molecular formula structure $C_{47}H_{51}NO_{14}$, which corresponds to the molecular weight of 853 Da [103,104]. PTX is a crystalline powder that is white or off-white in color [105]. PTX shows promising results in preclinical studies for its antitumor action, and this could be attributed to its unique features of a complex C-13 side chain attached to the taxane ring [105]. The U.S. Food and Drug Administration (FDA) approved PTX in 1992 for ovarian and breast cancer treatment [106,107]. Gene expression is not affected by PTX [108]. It is complicated to obtain PTX on an industrial scale due to the slow growth of yew trees with low content [102,109,110]. A clinical limitation of PTX is its hydrophobicity, with a fusion point of approximately 216°C and its high attraction to lipid molecules [105]. Also, PTX is not tumor cell-specific, thus causing side effects, small therapeutic window, can be trapped or lost in systemic circulation, and there are also cases of getting multidrug resistance of tumor after long-term exposure to PTX [102,105,111,112]. PTX works by suppressing the microtubule spindle dynamics, thus resulting in metaphase-anaphase transitions being blocked and eventually hindering mitosis and inducing apoptosis [113]. PTX specifically stabilizes microtubules by binding selectively to the subunit β of tubulin, thereby preventing tubulin disassembly and promoting their polymerization [114,115]. PTX model conjugates are being developed. Hyukjin *et al.,* (2008) conjugated hyaluronic acid to PTX, which were self-assembled to form micelles that could be potentially used for tumor-specific targeting [116]. Ahmad *et al.,* (2003) conjugated PTX to Erbitux (C225) to serve as a model monoclonal antibody-mediated drug delivery compound

[117]. Sahoo S. K. & Labhasetwar (2005) studied the molecular mechanism of conjugated Transferrin ligand to PTX on breast cancer cell line [118]. Regina *et al.,* (2008) conjugated PTX molecules to Angiopep-2 to produce a PTX–Angiopep-2 conjugate named ANG1005 and studied the antitumor effects [119]. Dosio *et al.,* (1997) covalently attached PTX to human serum albumin, and the antitumor activity of free drug and PTX-conjugates was tested on three different tumor cell lines [120]. Yang J. *et al.,* (2018) synthesized bioresponsive albumin-conjugated PTX prodrugs for cancer therapy using a maleimide group [121].

2.5.2 Prodigiosin and Conjugated Prodigiosin Drugs

Prodigiosins (PGS) represent the family of natural red pigments produced by various bacteria and Gram-positive actinomycetes [122–124]. PGS possesses a common pyrrolyl pyrromethene skeleton [123,125]. Previous studies have been done to develop synthetic PGS derivatives, and these PGS-conjugates are more active and less toxic compared to native PGS compounds [126,127]. Several PGS have antifungal, antimicrobial, antitumor, immunosuppressive properties, and apoptotic effects *in vitro* [128–131]. PGS could also be used in the food industry as colorants [132]. PGS has shown apoptotic effects in human cancer cell lines, in tissue culture, in primary culture, and in hepatocellular carcinoma xenograft. The mode of action of PGS in inducing apoptosis remains unclear due to the multiple cellular targets and confer resistance to other anticancer agents via its several multidrug resistance pumps [125,133–135]. PGS has been found in the nucleus, granules near the nucleus, cytoplasm, and in the membrane of the mitochondrion as these positions would assist in better understanding of the mechanism of action of PGS [135–138]. The presence of PGS in the nucleus could support the assumption of DNA cleavage as proapoptotic activity [125]. PGS-conjugates have also been studied. Obayemi *et al.,* (2020)

synthesized PGS conjugated to LHRH peptides [43]. These PGS-conjugates significantly targeted drug delivery to TNBC tumor sites. Ayatollahi *et al.,* (2018) synthesized prodigiosin-conjugated aptamer to attach to the surface of brain cancer cells [139].

2.6 Drug Delivery System (DDS)

The process by which a pharmaceutical compound is administered to humans or animals to bring about a therapeutic effect is referred to as drug delivery [140]. Drug delivery systems (DDS) serve as a vehicle to transport these pharmaceutical drugs in the body to the desired site for drug release and absorption, thereby achieving the desired therapeutic effect [28]. In that regard, the main aim of DDS is to improve the pharmacological activities of therapeutic drugs, including enhancing the drug's aqueous solubility and chemical stability, bioavailability, biodistribution, and reducing drug aggregation as well as side effects [28]. Furthermore, DDS increases drug efficacy and, consequently, lowers drug dosage frequency as well as overall treatment cost and improves patient compliance [141–144]. Ultimately, providing and maintaining therapeutic drug concentration is the goal of any DDS [141–144]. Diverse materials have been used to fabricate DDS for various drug delivery routes, and they could be functionalized with peptides, metalloids, polymers, lipids, etc. [43,141,142].

2.7 Tumor-Targeted Drug Delivery

It is a method used to predominantly accumulate drugs with a zone of interest that is independent of the drug administration method and route [145]. Targeted drug delivery aims to concentrate the drug at the target zone in comparison to other parts, thus reducing the relative drug concentration and any toxicity that may arise otherwise [146,147]. The targeted drug delivery system is

comprised of three components: a drug, a targeting moiety, and a pharmaceutical carrier system [145]. The delivery system used for drug targeting depends on the drug delivery route selected [33]. An effective targeted drug delivery system must be able to retain, evade, target, and release [30]. This implies that the pharmaceutical carrier should be able to load the drug efficiently and capable of escaping barriers that may degrade it. Meeting these criteria is crucial in extending circulation time, thereby causing the carrier to reach the target site and release the drug there in time. Targeted drug delivery systems improve therapeutic efficacy and bestow several other advantages. These advantages include simplifying drug administration protocols, reducing overall drug concentration needed, thus reducing the cost of therapy, increasing drug concentration at the target zone without toxic effects on non-target zones, and inhibiting drug-resistant tumor cells [34,145]. Researchers and clinicians in the field of drug targeting have employed several schemes to advance drug targeting, including the direct application of drugs into the target organ/tissue, passive targeting through leaky vasculature, magnetic targeting of drugs attached to paramagnetic carriers, and employing physical targeted systems based on temperature-sensitive and pH-sensitive drug carriers. These schemes utilize vector molecules that possess a high specific affinity toward the target region [145]. Targeting may either be passive or active. Passive tumor targeting is based on the accumulation of drugs in the regions around the tumors with leaky vasculature and does not have a ligand for specific tissue/organ binding [31–33]. Active targeting is achieved through specific ligand–receptor interactions between drug/drug carriers and the target tumor cells [34–39].

2.8 Polymer Blending

Polymers are either natural or synthetic. The unique edge synthetic polymers have over natural polymers is that they can be altered to obtain a wide array of products [148]. The functional group found in some natural polymers is useful in biomedical applications because they are less prone to toxic results, but their presence together with contaminants present in the material of natural origin might create unwanted immunological effects [149]. Nevertheless, synthetic polymers possess chemical linkages that significantly alter the degradation and other properties [148]. Polymer blends are convenient physical modifications to merge the properties of different polymers to generate novel properties through a thermodynamically driven blending of the polymers [150]. Polymer blends and or chemically linked polymers can be utilized to obtain intermediate properties of two or more polymers [148]. Several formulations of polymeric blends include a combination of: (I) synthetic and natural polymers, (II) natural–natural polymers, and (III) synthetic-synthetic polymers [151].

Additionally, the first category of blends provides a controlled degradation rate as the degradation kinetics of the polymer blend is directly proportional to the amount of natural polymer [152]. Examples of natural and synthetic polymer blends are PLA/CS, PLA/HA; PLG/gelatin/elastin; and PLA/starch, PCL/starch, etc. Synthetic/synthetic polymer blends are developed to enhance processability, mechanical and biocompatible properties, and reduce the cost compared to the parent material [153]. Some drawbacks associated with polymer blends include having difficult miscibility in blend formation and processability for scaffold applications [152].

2.9 Microparticles for drug delivery

By definition, microspheres are "monolithic spheres or therapeutic agents distributed all over the matrix either as a molecular dispersion of particles or a structure made up of continuous phases of one or more miscible polymers in which the drug particles are dispersed at the molecular or macroscopic level" [154]. This is to say that microspheres are monolithic systems in which the pharmaceutical ingredient is homogeneously dispersed within the polymer matrix or wax, where it is impossible to point out a distinct nucleus [155–157]. Microspheres have aspherical morphology with a size range of one to three hundred microns (1- 300 μm) [154]. Microspheres provide continuous and extended therapeutic effects, thereby decreasing the dosing frequency and causing improved patient compliance [154]. Based on the round shape and smaller size, microspheres can be introduced into the body via several routes and personalized based on requirement profiles and targeted drug delivery [154,158]. Microspheres do not cross into the interstitium over the size of 100 nm transported by the lymph and thus act locally, which is an advantage over nanoparticles [159]. Microspheres are characterized as powders made up of a natural or synthetic polymer, which are biodegradable, and the choice of polymer used is crucial [158]. Considering that polymers are widely used for synthesizing microspheres, they also protect the drugs and enhance bioavailability [160]. Marison *et al.,* (2004) categorized microspheres production methods into chemical, physiochemical, mechanical [161]. The chemical method can be subdivided into *in situ* polymerization and interfacial polymerization [162,163]. The physiochemical method involves complex coacervation [164], while the mechanical method includes spray-drying and extrusion-based methods [165,166].

2.10 Tissue Engineering (TE)

TE is a multidisciplinary and interdisciplinary field that focuses on creating a functional biological replacement that restores, maintains, or improves tissue function by integrating a scaffold, cells, and biological molecule [167–169]. This makes tissue engineering a vital tool that could be applied to improve several clinal situations [170]. A porous scaffold is a requirement to produce an engineered tissue as it provides a three-dimensional environment [171,172]. Additionally, an ideal scaffold should be biocompatible, tunable biodegradation rate, nontoxic degradation products, three-dimensional and high porous and interconnected pore network to facilitate nutrients and waste transport, mechanical strength, and appropriate surface chemistry for cells interaction [173,174]. Almost all tissue-engineered scaffolds introduced into a patient's body are meant to degrade and be replaced by fresh tissue gradually [175]. Three-dimensional scaffolds mimic the natural ECM of connective tissues that assist cell proliferation, cell differentiation, and cell biosynthesis and provide architectural support [176,177]. The use of tissue engineering has been dramatically increasing in breast cancer research. These scaffolds have also been used as drug delivery systems in cancer research, and there are studies that have focused on the kinetics of drug release from these systems [178]. Subia *et al.,* (2015) evaluated the *in vitro* three-dimensional model of the breast cancer cells and the bone microenvironment to understand the cellular interactions in the presence of a targeted anticancer drug delivery system [179]. Tissue engineering can be used for breast reconstruction that gives a realistic appearance of the breast, unlike silicone-based implants and current research shows promising results. Wang *et al.,* (2013) fabricated an adipose tissue engineering platform for soft tissue defect repair [180]. Wu *et al.*, (2017) prepared a Tamoxifen-loaded RADA16-I peptide hydrogel scaffold with hADSCs for breast reconstruction [181]. Baldwin *et al.,* (2020) investigated the biocompatibility of tannic acid-collagen type I injectable bead scaffold for breast reconstruction [182]. Rehnke *et al.,* (2019)

reported breast reconstruction using a three-dimensional absorbable mesh scaffold and subsequent autologous fat grafting (AFG) [183].

2.11 Polymer Degradation Mechanisms

The controlled alteration in polymer strength and color is referred to as degradation and is affected by factors such as temperature and chemicals [184]. Polymer degradation and erosion play a role for all polymers [185]. All polymers degrade and the time duration of degradation and application depends on whether the polymer is degradable or non-degradable [185]. Typically, degradable polymers degrade during their application or immediately afterward; non-degradable polymers require an extended time [185]. Degradation is a process in which monomers are formed from monomers due to cleavage of polymer chains, while erosion refers to the material because of monomers and oligomers leaving the polymer [186]. Polymer degradation could be mechanical degradation, thermal degradation, photodegradation, and chemical degradation [185].

In polymer blends, the macroradicals of both components may react between them or with the macromolecules of the other phases [187]. There are six possible degradation routes that this can take place by, and they are characterized by competitive reactions that form chemical species that can significantly change the degradation scheme and its degradation effect on the blend's final properties [187]. These routes are as follows: reactions between macroradicals and macromolecules, reactions between two different macroradicals, reactions between macromolecules and small molecules, reactions between macromolecules and small radicals, reactions between macroradicals and small molecules, and reactions between two small molecules [187].

Polymer degradation can be monitored by changes in their morphology using Scanning Electron Microscopy (SEM) to examine the changes in the shape of the polymer due to enzymatic degradation [188]. Previous studies have revealed the use of atomic force microscopy (AFM) to observe real-time polymer degradation as it enables one to estimate the material's roughness at very low magnification [189–192]. Gel permeation chromatography (GPC) can also be used to monitor the degradation rate reduction of the polymer molecular weight (Mw) [193]. FTIR and ^{1}H NMR can also be used to measure the change in the chemical composition of the polymer as a result of degradation [194].

Differential Scanning Calorimetry (DSC) and wide-angle X-ray diffraction (WAXD) can be used to access the changes in crystallinity in the polymer due to degradation [195,196]. Some of the analytical techniques used to understand the mechanism of enzymatic degradation, assess the potential toxicity, and investigate the intermediates and end products of degradation are High-Performance Liquid Chromatography (HPLC), anion exchange HPLC, Liquid Chromatography with Mass Spectrometry LC-MS, and UV-visible absorption spectrophotometer [194,197–200].

Chapter 3

3.0 Drug-Encapsulated Blend of PLGA-PEG Microspheres: *In vitro* **and** *In vivo* **Study of the Effects of Localized/Targeted Drug Delivery on the Treatment of Triple-Negative Breast Cancer**

3.1 Introduction

Cancer has been estimated to account for 9.6 million deaths in 2018 [201]. It is the second leading cause of death and is second only to cardiovascular disease which is the leading cause of death in the world [202]. The World Health Organization (WHO) has projected that over 13.1 million cancer-related deaths will occur by 2030, a time when cancer would likely overtake cardiovascular disease as the leading cause of death in humans [203]. Cancer can affect different parts of the body in both men and women. In the case of women, breast cancer, persists as the most commonly diagnosed cancer in women globally [201,204]. Notably, triple-negative breast cancer is the leading cause of death of women, especially in low-resource countries [12,205]. TNBC is an aggressive and immunopathology subtype of breast cancer that usually does not respond to drugs that target ER, PR and HER2 [16,17,206,207] with relatively high mortality rate [16,17,206]. This is due to the poor prognosis that could result to late diagnosis, ineffective treatment options [16,17,206].

TNBC has been shown accounts for 15-20 % of breast cancer cases in which there is a lack of estrogen receptors (ER), progesterone receptors (PR) and human epidermal growth factor receptor 2 (HER2) [16,17,207]. In such cases, bulk chemotherapy, radiation therapy and surgery (or their combination) are often used as cancer treatment strategies [207–209]. However, the side effects of

treatments are often severe and cancer may also recur, triggering the need for revisiting therapies [24,91].

Significant efforts have been made to develop drugs for the treatment of TNBC using platinum compounds [210], EGFR inhibitors [211,212], antiangiogenics therapy [213], PARP inhibitors [214], mammalian targets with rapamycin (mTOR) [215,216], kinase inhibitors of SRC, Kit, and other kinases [213,217]. Recent efforts have also explored the use of implantable encapsulated drug systems [218], drug-loaded/encapsulated microspheres [219,220], nanospheres/nanoparticles [221,222], liposomes [223], dendrimers [224], micelles [225] and scaffolds [178] for breast cancer treatment. Novel gold and magnetite nanocomposite heating systems have also been proposed for localized breast cancer treatment (via hyperthermia) and/or thermal ablation [222,226]. However, some of these approaches lack specificity and selectivity in their targeting of tumor cells.

Hence, in recent years, significant efforts have been made to develop targeted anti-cancer drugs for the improved treatment of cancer [227,228]. In most cases, targeted anti-cancer drugs can be engineered using specific Molecular Recognition Units (MRUs) or antibodies that interact specifically with receptors that are overexpressed on the surfaces of cancer cells [229–231]. Such specific targeting of cancer cells may, therefore, have the potential to reduce the potential side effects of cancer treatment. Since over 50% of human breast cancer cells express binding sites (receptors) for luteinizing hormone releasing hormone (LHRH), LHRH is one of the specific targeting receptors that can be used for the treatment of breast cancer [41,96,97].

Polymeric materials are primary choices for controlled localized and targeted cancer drug delivery [232,233]. Polylactide-co-glycolide (PLGA) and polyethylene glycol (PEG) are FDA-approved polymers and have been widely explored for applications in drug delivery. This is due largely to their biocompatibility [234–236]. Furthermore, Poly (ethylene glycol) (PEG), a hydrophilic polymer, which decreases its interactions with blood components [235]. The proportion of poly lactic acid (PLA) and poly glycolic acid (PGA) in poly lactic acid co glycolic acid (PLGA) can also be used to control the degradation rates or drug release rates during controlled release from PLGA [234].

Prior work has shown that the release of cancer drugs from biodegradable polymers can occur by diffusion [232,237–239], solvent activation via osmosis or swelling of the system [237,240,241], chemical or enzymatic reactions, or cleavage of the drug from the system [185,236,237,239]. Extended release over durations comparable to cancer treatment regimens is often a challenge. However, to the best of our knowledge, none of the prior studies have explored encapsulated new targeted cancer drug (PGS-LHRH) with FDA approved blend of polymer (PLGA and PEG) [242,243]. Furthermore, there has been no study that has explored the thermodynamics and kinetics of drug delivery from drug-loaded blends of polymer microspheres. Such studies are needed to provide insights into the thermodynamic driving forces and the release mechanisms that are associated with the release of targeted cancer drugs from microparticles for the localized treatment and prevention of recurred triple-negative breast tumors after surgical resection.

This study presents the results of an experimental study of a unique proportion of blend of polymers (PLGA and PEG) that were used to encapsulate targeted drugs (PGS-LHRH or PTX-

LHRH) for the enhancement of sustained and localized delivery of targeted drugs for breast cancer treatment. This studies offer outstanding advantages that include targeted drug for controlled and prolong release period [244]. The *in vitro* drug release kinetics and thermodynamics with their degradation mechanisms were elucidated for micro-spherical drug-loaded polymer blends. Results from the drug release *in vitro* and *in vivo* experiment showed that the effect of targeted-loaded drug leads to decrease the viability of TNBC cells (MDA-MB-231). The induced cytotoxicity and changes in the underlying cytoskeletal structures of the MDA-MB-231 cells (that are associated with controlled cancer drug release) are also explored via Confocal Microscopy. The implications of the results are then discussed for the development of polymeric microspheres that are encapsulated with targeted cancer drugs. Such drugs are shown to have the potential for the controlled delivery of cancer drugs that prevent the regrowth or loco-regional recurrence of TNBC after surgical resection.

3.2 Materials & Experimental Methods

3.2.1 Materials

Poly (D,L-lactide-co-glycolide) (PLGA 65:35, viscosity 0.6 dL/g), poly vinyl alcohol (PVA) (98% hydrolyzed, MW= 13,000 – 23,000), Bovine Serum Albumin (BSA) and 4% paraformaldehyde were obtained from Sigma Aldrich (St. Louis, MO, USA). Polyethylene glycol (PEG) (8 kD), Dichloromethane (DCM) and Phosphate Buffered Saline (PBS) solution that were used for *in vitro* drug release at pH of 7.4 were purchased from Fisher Scientific (Hampton, NH, USA). Prodigiosin (PGS) were biosynthesized and chemically conjugated with Luteinizing hormone-releasing hormone (LHRH) at the Soboyejo Lab at the Worcester Polytechnic Institute (WPI), Worcester,

MA, USA. Paclitaxel was obtained from ThermoFisher Scientific (Waltham, MA, USA) and was conjugated to LHRH.

Cell culture medium Leibovitz's-15 (L-15), trypsin-ethylenediamine-tetra-acetic acid (Trypsin-EDTA), Fetal Bovine Serum (FBS), penicillin-streptomycin, Alamar Blue^{TM} Cell Viability Assay, Dulbecco's phosphate-buffered saline (DPBS), vinculin Mouse Monoclonal Antibody, Goat anti-Mouse IgG (H+L) Superclonal™ Secondary Antibody, Alexa Fluor® 488 conjugate Alexa Fluor® 555 Rhodamine Phalloidin, Triton™ X-100, Trypan Blue Solution (0.4%) were also procured from ThermoFisher Scientific (Waltham, MA, USA). MDA-MB-231 cell line used in this study was obtained from American Type Culture Collection (ATCC) (Manassas, VA, USA). All of the reagents that were used were of analytical grade, as provided by the suppliers.

3.2.2 Preparation of Drug-loaded PLGA-PEG Microspheres

Targeted drug-loaded microspheres (PGS-LHRH-loaded PLGA-PEG and PTX-LHRH-loaded PLGA-PEG blend microspheres) and non-targeted drug-loaded microspheres (PGS-loaded PLGA-PEG and PTX-loaded PLGA-PEG blend microparticles) were prepared, respectively, using the emulsion solvent evaporation technique, described in prior work by Obayemi *et al.,* (2020) [219]. Although, in this study physical blends consisting of PLGA and PEG polymer in the ratio of 1:1 were dissolved in an organic solvent (DCM) to form a primary system. In separate vials, 5mg/ml drug concentration (PGS or PGS-LHRH or PTX or PTX-LHRH) were prepared and emulsified in a 3% PVA stabilizer. These were then transferred under homogenization to the primary solution.

The resulting drug-polymer mixtures were sonicated to form a homogenous initial oil-water system. The homogeneous emulsion was then transferred dropwise into an aqueous 3 % PVA solution (prepared with deionized water). The mixture formed was homogenized with an Ultra Turrax T10 basic homogenizer (Wilmington, NC, USA) that was operated at 30,000 rpm for 5 minutes. The resulting oil-water emulsion was then stirred with a magnetic stirrer for 3 hours to enable the evaporation of the DCM.

The excess amount of PVA in the stirred mixture was removed by washing four times with tap water and centrifuging for 10 minutes at 4,500 rpm with an Eppendorf Model 5804 Centrifuge (Hauppauge, NY, USA). The emulsifier/stabilizer and non-incorporated drugs were then washed off, while the drug-encapsulated microparticles were recovered after centrifugation. Finally, the resulting microparticles were lyophilized for 48 hours with a VirTis BenchTop Pro freeze dryer (VirTis SP Scientific, NY, USA). The lyophilized microparticles powder were stored at -20°C, prior to the material characterization and drug release experiments. PLGA-PEG microparticles (without drugs) were also prepared as controls.

3.2.3 PLGA-PEG Microparticles Characterization

The hydrodynamic diameters and polydispersity index of the lyophilized drug-loaded and control PLGA-PEG microparticles were analyzed using a Malvern Zetasizer Nano ZS (Zetasizer Nano ZS, Malvern Instrument, Malvern, UK). The morphologies of the microparticles were also characterized using Scanning Electron Microscopy, (SEM) (JEOL 7000F, JEOL Inc. MA, USA). Prior to SEM, the freeze-dried microparticles were mounted initially on double-sided copper tape on an aluminum stub. The resulting particles were then sputter-coated with a 5 nm thick layer of

gold. The mean diameter of the microparticles were then analyzed using the ImageJ software package (National Institutes of Health, Bethesda, MD, USA).

Fourier Transform Infrared Spectroscopy (FTIR) (IRSpirit, Shimadzu Corporation, Tokyo, Japan) was used to characterize the physicochemical properties of the drug-loaded PLGA–PEG microparticles. This was used to evaluate the chemical bonds/functional groups that were associated with the drug-loaded and unloaded PLGA-PEG microparticles. The lyophilized samples were scanned at 4 mm/s at a resolution of 2 cm^{-1} over a wavenumber range of 600–3600 cm^{-1}. This was done using the IR solution software package (ver.1.10) (IRSpirit, Shimadzu Corporation, Tokyo, Japan).

Nuclear Magnetic Resonance Spectroscopy (NMR) was also used to study the structure of unloaded and drug-loaded PLGA-PEG microparticles. This was done using a Bruker Advance 400 MHz (Bruker BioSpin Corporation, Billerica, MA, USA). First, 10 mg of PLGA-PEG microparticles were dissolved in 1 ml of chloroform ($CDCl_3$). HNMR spectra of drug-loaded and control PLGA-PEG microparticles were obtained and analyzed using Bruker's TopSpin™ Software package (ver 3.1) (Bruker Biospin GmbH, Rheinstetten, Germany).

Finally, the thermal properties of the drug-loaded PLGA-PEG microparticles and their control were measured using Thermogravimetric Analysis (TGA) (TG 209 F1 Libra, NETZSCH, Selb, Germany) and Differential Scanning Calorimetry (DSC) (DSC 214 Polyma, NETZSCH, Selb, Germany). This was done to evaluate the possible interactions of the drugs with the polymer blends

(PLGA-PEG). TGA thermograms were obtained between 25°C and 900°C with a constant heating rate of 20 K/min under nitrogen gas. This was done using alumina crucibles containing 10 mg of sample.

For the DSC analysis, 10 mg of the freeze-dried drug-loaded and control PLGA-PEG microparticles was weighed, respectively. In each case, samples were sealed in aluminum pans. They were then heated in an inert nitrogen atmosphere with a nitrogen flow rate of 20 ml/min that was subjected to a heating cycle between 20°C and 250°C with an empty reference aluminum pan. The data obtained was then analyzed by NETZSCH Proteus-7.0 software (NETZSCH, Selb, Germany). Similar procedure was followed for DSC analysis of PTX and PGS. This was used to identify the decomposition temperatures, the glass transition temperatures (T_g) and the melting temperatures (T_m), respectively.

3.2.4 *In vitro* Drug Release

Sixty-two-day *in vitro* drug release experiments were performed on PLGA-PEG microparticles that were encapsulated with PGS or PGS-LHRH or PTX or PTX-LHRH. These were carried out at 37°C, 41°C and 44°C in an effort to study the kinetics and thermodynamics of drug release under *in vitro* conditions. The temperatures were chosen to correspond to the normal human body temperature (37°C) and hyperthermic temperatures (41°C and 44°C).

First, triplicate 10 mg measures of drug-loaded microparticles were suspended separately in 10 ml of PBS of pH 7.4 containing 0.2% Tween 80, using 15 ml screw-capped tubes. The sample tubes were then placed in orbital shakers (Innova 44 Incubator, Console Incubator Shaker, New Brunswick, NJ, USA) rotating at 80 rpm and maintained at temperatures of 37°C, 41°C, and 44°C, respectively. At 24-hour intervals, over a period of 62 days, the tubes were centrifuged at 3000 rpm for 5 minutes to obtain 1.0 ml of the centrifuged supernatant (known release study samples). 1 ml of freshly prepared-drug free PBS was then used to replace the removed supernatant to conserve the sink conditions. The test samples were then swirled and placed back into the shaker incubator for the continuous release study.

The amount of released drug in each of the supernatant samples (released at 37°C, 41°C and 44°C) was characterized using a UV-Visible spectrophotometer (UV-1900 Shimadzu Corporation, Tokyo, Japan). The wavelength of the UV-Visible spectrophotometer was fixed at a wavelength of 535 nm (PGS and PGS-LHRH) and 229 nm (PTX and PTX-LHRH), respectively, in order to measure the absorbance. A standard curve was used to determine the concentrations of drug (PGS, PGS-LHRH, PTX and PTX-LHRH) released from their respective drug-loaded microparticles [245].

The drug encapsulation efficiencies of the microspheres were also determined. First, 10 mg of microparticles was dissolved in DCM. The amount of drug encapsulated was then determined with a UV-Visible spectrophotometer (UV-1900 Shimadzu Corporation, Tokyo, Japan) at a fixed maximum wavelength of 535 nm for PGS and PGS-LHRH and 229 nm for PTX and PTX-LHRH,

respectively. The amount of drug that was encapsulated into the PLGA-PEG microparticles was then determined from the weight of the initial drug-loaded microparticles and the amount of drug incorporated, using a method developed by Park *et al.,* (2005) [246].

The Drug Loading Efficiency and Drug Encapsulation Efficiency (DEE) of drug-loaded PLGA-PEG microparticles was determined from equation (1) and (2), respectively:

$$Drug\ Loading\ Efficiency\ (DLE) = \frac{MD}{MD+MP} \times 100 \tag{1}$$

$$Drug\ Encapsulation\ Efficiency\ (DEE) = \frac{M_X}{M_Z} \times 100 \tag{2}$$

where MD is the mass of drug uptake into the microspheres, MP of polymer in the microsphere, M_x is the amount of encapsulated drug and M_z is the amount of drug used for the preparation of the microparticle.

Since drug release is often enabled by capsule degradation [239], the degradation of the drug-loaded microparticles was studied after each week of degradation under *in vitro* conditions. This was done using Scanning Electron Microscopy, (SEM) (JEOL 7000F, JEOL Inc. MA, USA), which was used to characterize the microstructural morphologies of the drug-loaded polymer blend.

3.2.5 *In vitro* Cell Viability and Cytotoxicity

The MDA-MB-231 breast cancer cells were cultured in Leibovitz's 15 (L-15) medium, supplemented with 10 % FBS and penicillin/streptomycin (50 U/ml penicillin; 50 μg/ml

streptomycin). This complete cell culture medium containing L-15 and other supplements (10 % FBS and 2% penicillin/streptomycin) is referred to as L-15$^+$.

In vitro cell viability and cytotoxicity studies were performed using the Alamar Blue^{TM} Cell Assay as described in our recent studies[178]. This was used to explore the possible effects of drug-induced toxicity on triple-negative breast cancer (MDA-MB-231) cells. 10^4 cells/well were seeded in 24-well plates (n = 4) in L-15$^+$ culture medium [178]. Furthermore, three hours after cell attachment, the culture medium was replaced with 1 ml of culture medium containing 0.5 mg/ml drug-loaded PLGA-PEG microparticles.

Cell viability was monitored at durations of 0, 6, 24, 48 72 and 96 hours after drug-loaded microparticle addition. At each of these time points, the culture medium (L-15$^+$) was replaced with 1 ml of culture medium (L-15$^+$) containing 10 % alamar blue solution. The resulting cells in the 24 well-plates were then incubated in a humidified incubator at 37°C for 3 hours. 100 µl aliquots were transferred into duplicate wells of a black opaque 96-well plate (Thermo Fisher Scientific, Waltham, MA) for fluorescence intensities measurement at 544 nm excitation and 590 nm emission using a 1420 Victor3 multilabel plate reader (Perkin Elmer, Waltham, MA) [178]. All of the experiments were repeated thrice.

The percentage of alamar blue reduction and the percentage of cell growth inhibition were determined from equation (3) and (4) [178]:

$$\% \ Alamar \ Blue \ Reduction = \frac{FI_{sample} - FI_{10\%AB}}{FI_{100\%R} - FI_{10\%AB}} \times 100 \qquad (3)$$

$$\% \ Growth \ Inhibition = \left(1 - \frac{FI_{sample}}{FI_{cells}}\right) \times 100 \qquad (4)$$

where FI_{sample} is the fluorescence intensity of the samples, $FI_{10\%AB}$ is the fluorescence intensity of 10 % Alamar Blue[TM] reagent (negative control), $FI_{100\%R}$ is the fluorescence intensity of 100 % reduced Alamar Blue[TM] (positive control) and FI_{cells} is the fluorescence intensity of untreated cells [178].

The loss of cell viability was characterized using a dye exclusion assay. This works based on the concept that viable cells do not take up impermeable dyes (like Trypan Blue), while dead cells are permeable and take up the dye because their membranes lose their integrity. Hence, we adopted previous method reported in our prior work [219]. In this work Trypan Blue Dye (TBD) staining was used to quantify the loss of cell viability. This utilized a 0.4 % solution of TBD in buffered isotonic salt solution with a pH of 7.3. 0.1 mL of TBD stock solution was added to 1 mL of cells, mixed gently and incubated at 25°C for 1 min. A hemocytometer was then used to count the number of blue staining cells, and the total number of cells under an optical microscope (Nikon TS100, Nikon Instruments Inc., Melville, New York, USA) that was operated at low magnification [219]. Equation (5) was used to calculate the number of viable cells.

$$\% \ Viable \ Cells \ (VC) = 1 - (Number \ of \ blue \ cells \div Number \ of \ total \ cells) \times 100 \qquad (5)$$

3.2.6 Cellular Drug Uptake

MDA-MB-231 cells were seeded on coverslips (CELLTREAT Scientific Products, Pepperell, MA, USA) in 12-well plates using 1 ml growth medium (L-15$^+$). The cells were then incubated in a humidified incubator at 37°C until cells were about 70% confluent. Post attachment, the cells were incubated with 1 ml of 0.1mg/ml drug-loaded microspheres dissolved in growth medium (L-15$^+$). After 5 hours, the cells were washed twice with 5% (v/v) Dulbecco's phosphate-buffered saline (DPBS) (Washing solvent). After washing, the cells were then fixed with 4% paraformaldehyde for 12 minutes, before rinsing thrice with 5% (v/v) DPBS. 0.1% Triton™ X-100 was added for 10 minutes to permeabilize the cells [247]. This was then blocked with 1% BSA for 1 hour at room temperature (25°C). The BSA-treated ECM were then rinsed thrice with the 5% (v/v) DPBS, before labeling with vinculin Mouse Monoclonal Antibody at 2 µg/ml and incubating for 3 hours at room temperature (25°C).

The washing solvent was used to rinse the resulting samples, which were then labeled with Goat anti-Mouse IgG (H+L) Superclonal™ Secondary Antibody, Alexa Fluor® 488 conjugate for 45 minutes at room temperature. F-actin was stained with Alexa Fluor® 555 Rhodamine Phalloidin for 30 minutes. The coverslips were then mounted on glass slides and sealed. The cells were visualized with HEPES buffer (pH 8) using HCX PL APO CS 40X 1.25 oil objective in Leica SP5 Point Scanning Confocal Microscope (Buffalo Grove, IL, USA) and representative images were obtained.

3.2.7 *In vivo* Studies

In vivo animal studies similar to our recent studies [178]were carried in this work using thirty 3-week old healthy immunocompromised female athymic nude-Foxn1nu mice. These mice were purchased from Envigo (South Easton, MA, USA) and have a weight of ~16 g. These mice were kept in the vivarium (to acclimatize) until they are 4-weeks old. They were then used in *in vivo* studies to explore the extent to which encapsulated localized and targeted drug delivery systems can be used to prevent the breast tumor regrowth or loco-regional recurrence, following surgical resection [178].

All the animal procedures described in this work were performed in accordance with the approved animal guidelines by the Worcester Polytechnic Institute (WPI), Institutional Animal Care and Use Committee (WPI IACUC) with approval number #A3277-01. The mice were also maintained in accordance with the approved IACUC protocol and were provided with autoclaved standard diet [178]. All the experimental protocols in these studies were performed under an approved ethical procedure and guidelines provided by the Worcester Polytechnic Institute IACUC. The sample group are based on the agent that are implanted into the mice for the treatment. The number of mice per this sample group (n) was determined to be n=5 based on power law and from our prior work. The thirty mice were randomly divided into six groups of five mice each. Each of this group was exposed to one of the following: (PLGA-PEG_PGS, PLGA-PEG_PGS-LHRH, PLGA-PEG_PTX, PLGA-PEG_PTX-LHRH), positive control (PLGA-PEG) and control group (without microspheres).

When the mice in each study group were 4-weeks-old, we induced interscapular subcutaneous TNBC tumors via the subcutaneous injection of 5.0×10^6 MDA-MB-231 cells that were harvested

35

from monolayer *in vitro* cell cultures [178]. Subcutaneous tumors were allowed to grow for over 4 weeks until they were large enough to enable tumor surgery and microsphere implantation (28 days after tumor induction). The expected size of the induced subcutaneous xenograft tumor after 28 days of induction is 300 ± 21 mm^3 [178]. The tumor formation was investigated by palpation, which was measured on a daily basis with digital calipers. During this period, the mice were monitored for changes in weight, abnormalities, and infections. For baseline evaluation, control mice (without microspheres) were also monitored for comparisons with the mice injected with drug-loaded microspheres.

Tumor volume was calculated from the following formula shown in equation (6) [248,249]:

$$Tumor = a \times {b^2}/{2} \qquad (6)$$

where a and b are the respective longest and shortest diameters of the tumors that were measured using a digital Vernier caliper.

Surgical removal of ~ 90 percent of the tumor was performed randomly on each group member using the recommended anesthesia and pain suppressant. In each case, 200 mg/ml of PLGA-PEG_PGS, PLGA-PEG_PGS-LHRH, PLGA-PEG_PTX, PLGA-PEG_PTX-LHRH, positive controls (PLGA-PEG) and control were implanted locally at the location where the source resected tumor was removed [178]. The statistical rationale for each treatment group was based on power law and from our prior work [178]. Within each group, localized cancer drug release was monitored for the period of 18 weeks. The body weight of each mice was monitored and measured every 3 days up to 126 days to check for any possible weight loss/gain, physiological changes, toxicity to the drugs, and well-being of the mice for the different treatment groups. This was done

to check for possible tumor regrowth [178]. In a similar fashion, after the 18 weeks of study, the mice were euthanized and their tumors and lungs were then excised [178]. This was followed by cryo-preservation to check for any toxicity and metastasis.

Following weight analysis, we compared the survival rate of the various treatment groups as a function of recurrence of the TNBC tumor. Survival study of mice was done post-surgical removal of tumor and during treatment period. The mice were observed for 18 weeks post-treatment for signs of cancer recurrence, if any. This was to allow enough time for recurrence. Thirty female nude mice were randomly divided into the following six groups (n=6): Control, PLGA-PEG, PLGA-PEG_PGS, PLGA-PEG_PGSLHRH, PLGA-PEG_PTX, PLGA-PEG_PTXLHRH, PLGA-PEG. Survival curves were made using Kaplan-Meier plots, and the statistical difference was evaluated using the log-rank test in SPSS. The mice in this study were euthanized when reoccurrence was observed. At the end of week 18, the surviving mice were also euthanized.

3.2.8 Histopathological Study and Immunofluorescence Staining

The histopathology of the lungs, and in some cases regrowth/reoccurred tumor were evaluated. The samples that were used for the histological examination of the lungs were sectioned into 5 μm thicknesses along the longitudinal axis using similar technique from our recent studies [247]. They were then placed on a glass slide. First, the slides were hydrated by passing them through 100, 90 and 70 % of alcohol baths. The hydrated samples (on the slides) were then stained with hematoxylin and eosin (H&E). The stained slides were finally examined using light microscopy (with a 20x objective lens) in a model TS100F Nikon microscope (Nikon Instruments Inc., Melville, NY, USA) that was coupled to a DS-Fi3 C mount that was attached to a Nikon camera.

Receptor staining via immunofluorescence (IF) staining was used to characterize the overexpressed LHRH receptors on the TNBC tumor and organs. This was crucial to show evidence of regrowth or the presence of metastasis in the organs using the IF staining method as described in prior work [178]. Optimum cutting temperature (OCT) compound-Embedded frozen tumor/tissue were processed in a cryostat (Leica CM3050 S Research Cryostat, Leica Biosystems Inc., Buffalo Grove, IL, USA)[178]. The stained samples were then imaged at a magnification of 40x in a Leica TCS SP5 Spectral Confocal microscope that was coupled to an Inverted Leica DMI 6000 CS fluorescence microscope (Leica, Buffalo Grove, IL, USA)[178].

3.2.9 Statistical Analysis

The results are reported as mean ± standard deviation for n = 3 (unless otherwise stated). In both *in vitro* study of drug release, cell viability studies as well as the *in vivo* study of the effects of drug release, statistical differences between the treatment groups were analyzed using one-way ANOVA. Differences in *in vitro* cell viabilities between the different treatment groups at different durations were analyzed using two-way ANOVA with post hoc Tukey HSD multiple comparisons tests using IBM SPSS Statistics 25 package. The differences were considered to be significant when the p-value was < 0.05.

3.3 Kinetics and Thermodynamics Modeling

3.3.1 Kinetics Modeling of *In vitro* Drug Release**.**

The drug release kinetics of drug-loaded PLGA-EG microparticles were determined by fitting the release data to Zeroth order kinetics, First Order Kinetics, Higuchi Model and Korsmeyer– Peppas Model. We initially used Zeroth order kinetics to describes the release from the drug-loaded microspheres in which the release rate is independent of concentration [250]. Hence, the plot of % Cumulative Drug Release (CDR) versus time was obtained based equation (7) below:

$$Q_t = Q_O + K_0.t \tag{7}$$

where Q_t is the cumulative amount of drug released in time 't' (release occurs rapidly after drug dissolves), Q_0 is the initial amount of drug in the solution and K_0 is the zeroth order release constant and 't' is time in hours.

In the case of first order kinetics, our release rate was shown to depend on concentration [251]. A plot of log of % Cumulative Drug Release (CDR) versus time that gives a straight line was plotted based on equation (8):

$$\log Q_t = \log Q_0 + {Kt}/{2.303} \tag{8}$$

where Q_t is the cumulative amount of drug release in time 't', Q_0 is the initial amount of drug in the solution, K is the first order release constant, and 't' is time. First order kinetics is often observed during the dissolution of water-soluble drugs in porous matrices [252].

Furthermore, the Higuchi model was used to characterize the release of the drugs incorporated into polymer matrices [155,253]. Typically, the Higuchi model describes the drug release from insoluble matrix as a square root of time, based on Fick's first law [57,58]. A plot of % Cumulative

Drug Release (CDR) versus the square root of time $(\sqrt{t})$ as shown by equation (9) was used to describe the kinetics of drug release.

$$Q_t = K_H . t^{1/2} \qquad (9)$$

where Q_t is the cumulative amount of drug released at time (t), K_H is Higuchi constant and 't' is time.

Finally, the Korsmeyer-Peppas (K-P) model was also used to explore the drug release kinetics from the polymeric matrix systems. For K-P drug release, a plot of log $\frac{M_t}{M_\infty}$ versus log t was plotted where 'n' represents the slope of the line, which corresponds to the underlying mechanism of drug release. The diffusion exponent (*n* value) of Korsmeyer-Peppas model was then used to identify the different drug release mechanism. For example, $n < 0.45$ corresponds to a Fickian diffusion mechanism, while $0.45 < n < 0.89$ corresponds to non-Fickian transport, $n = 0.89$ corresponds to Case II (relaxational) transport, while $n > 0.89$ corresponds to super case II transport [238,251,253]. The K-P model is given by equation (10):

$$\frac{M_t}{M_\infty} = Kt^n \qquad (10)$$

where $\frac{M_t}{M_\infty}$ is a fraction of drug released after time 't', 'K' is the kinetic constant, n is the release exponent, and 't' is time. In most cases, the K-P model is only applicable to the first 60% of drug release [251,252].

3.3.2 Thermodynamics of *In vitro* Drug Release.

The drug release studies were used to obtain the Gibbs free energy (ΔG), the enthalpy (ΔH), and the entropy (ΔS) changes associated with drug release from the drug-loaded PLGA-PEG microparticles at different temperatures [254,255]. The values of ΔG, ΔH and ΔS obtained were then used to explain the thermodynamic properties and the spontaneity of the underlying drug release processes from the drug-loaded microspheres.

Initially, the experimental data obtained from our drug release experiments (at different temperatures) were used to estimate the activation energy (E_a). This is done using the Arrhenius equation (11). The underlying thermodynamical mechanisms were then elucidated from equations (11) and (12). These give:

$$K_t = D_f e^{\frac{E_a}{RT}} \tag{11}$$

and

$$lnK_t = lnD_f - \frac{E_a}{R} \times \frac{1}{T} \tag{12}$$

where R is the universal gas constant (8.314 J mol^{-1} K^{-1}), K_t is the thermodynamic equilibrium constant, T is given as the absolute temperature (K), E_a is the activation energy, D_f is the pre-exponential factor and K_t is the thermodynamic equilibrium constant. The activation energy, E_a (kJ mol^{-1}), was estimated from a Van Hoff plot of lnK_t versus $1/T$. Hence, the slope of the plot gives $-\frac{E_a}{R}$. The Eyring expression for K_t gives equation (13):

$$\ln \frac{K_t}{T} = -\frac{\Delta H}{R}\frac{1}{T} + \ln\frac{K_B}{h} + \frac{\Delta S}{R} \tag{13}$$

In cases in which the plot of $\ln K_t$ versus $1/T$ is linear, then the underlying enthalpy ΔH (slope) and entropy ΔS (intercept) can be determined, respectively, from the slopes and intercepts of the plots [254]. Hence, the slope 'm' is given as $-\frac{\Delta H}{R}$ and the intercept 'c' is given by $\ln\frac{K_B}{h} + \frac{\Delta S}{R}$.

where ΔH is the enthalpy change, ΔS is the entropy change, K_B is the Boltzmann constant (1.38065 m^2 kg s^{-2} k^{-1}), and h is the Planck's constant (6.626× 10^{-34}J sec). Finally, the changes in the free energy ΔG can be obtained by substituting the calculated values of ΔH and ΔS into equation (14) ` at a given temperature, T.

Finally, the Gibbs free energy change is given by equation (14):

$$\Delta G = \Delta H - T\Delta S \tag{14}$$

where ΔS is the entropy change, ΔH is the enthalpy change and ΔG is Gibbs free energy change.

3.4 Results and Discussion

3.4.1 PLGA-PEG Microparticle Characterization

SEM images of the polymer blend drug-loaded microspheres with their and control microspheres are presented in Figures 3.1(A-E). Our results show that there are no significant morphological differences between the drug-loaded PLGA-PEG microspheres and the control PLGA-PEG microspheres. This suggests that the presence of drug did not significantly affect the morphologies of the drug-loaded microspheres. Furthermore, the mean particle sizes of the microparticles were between 0.84 μm and 1.23 μm (Figure 3.1F). The hydrodynamic diameter obtained from the DLS (Table 3.1) were greater than the mean diameter obtained from the SEM (Figure 3.1F). This could

be attributed to the PEG being soluble in the DLS medium leading to a swollen structure with high water content [256].
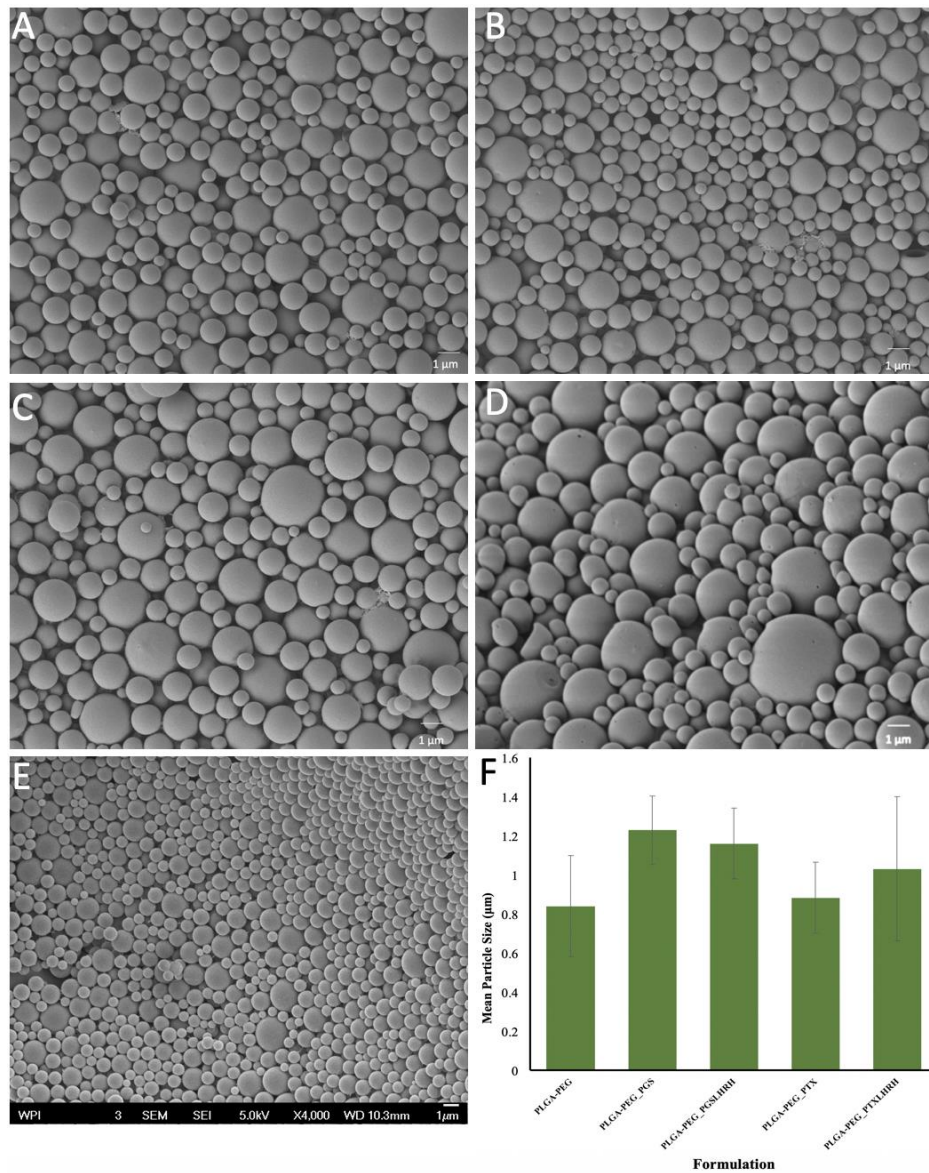
Figure 3.1: SEM images of (A) PLGA-PEG_PGS (B) PLGA-PEG_PGS-LHRH (C) PLGA-PEG_PTX (D) PLGA-PEG_PTX-LHRH (E) PLGA-PEG microspheres (F) Mean particle size distributions of drug-loaded and control PLGA-PEG microspheres.

Table 3.1: The mean diameter (SEM), the hydrodynamic hydrometer (DLS) and the polydispersity index (PDI) values for the various PLGA-PEG microspheres formulations.

Formulation	SEM (μm)	DLS (μm)	PDI
PLGA-PEG	0.80±0.26	3.14±0.09	0.82
PLGA-PEG_PGS	1.23±0.18	5.44±0.23	0.67
PLGA-PEG_ PGS-LHRH	1.16±0.18	6.92±0.44	0.47
PLGA-PEG_PTX	0.88±0.18	5.26±0.53	0.58
PLGA-PEG_PTX-LHRH	1.03±0.37	6.02±0.80	0.39

The FTIR spectra obtained for the drug-loaded PLGA-PEG microspheres were similar to those of the control PLGA-PEG microspheres (Figure 3.2). This indicates that there was no significant modification on the chemical groups of PLGA and PEG due to drug loading. Hence, in each case, the characteristic peaks that were obtained for PLGA and the PEG polymer. These were present before and after drug loading. Thus, the FTIR spectra obtained for the drug-loaded and control PLGA-PEG microspheres showed a strong band at 1749 cm^{-1}. This corresponds to the C=O stretch in the lactide and glycoside structure [243,257–259]. A characteristic peak of PEG was revealed at 1084 cm^{-1}. This is equivalent to the C-O stretch [257,260,261]. Clearly, the identical FTIR spectra of the drug-loaded microspheres (PLGA-PEG_PGS, PLGA-PEG_PGSLHRH, PLGA-PEG_PTX and PLGA-PEG-PTXLHRH) correspond to those of the spectrum of the blend of polymer (PLGA-PEG). Results from the drug-loaded spectra show the absence of characteristic intense bands of the drugs used (PTX, PG, PTXLHRH or PGSLHRH). In each case, the absence of the peaks may have been masked by the bands produced by the blend of polymer [262]. This

result suggests the presence of drugs as a molecular dispersion in the blend polymer matrix due to

the absence of chemical interaction between the blend of polymer (PLGA-PEG).
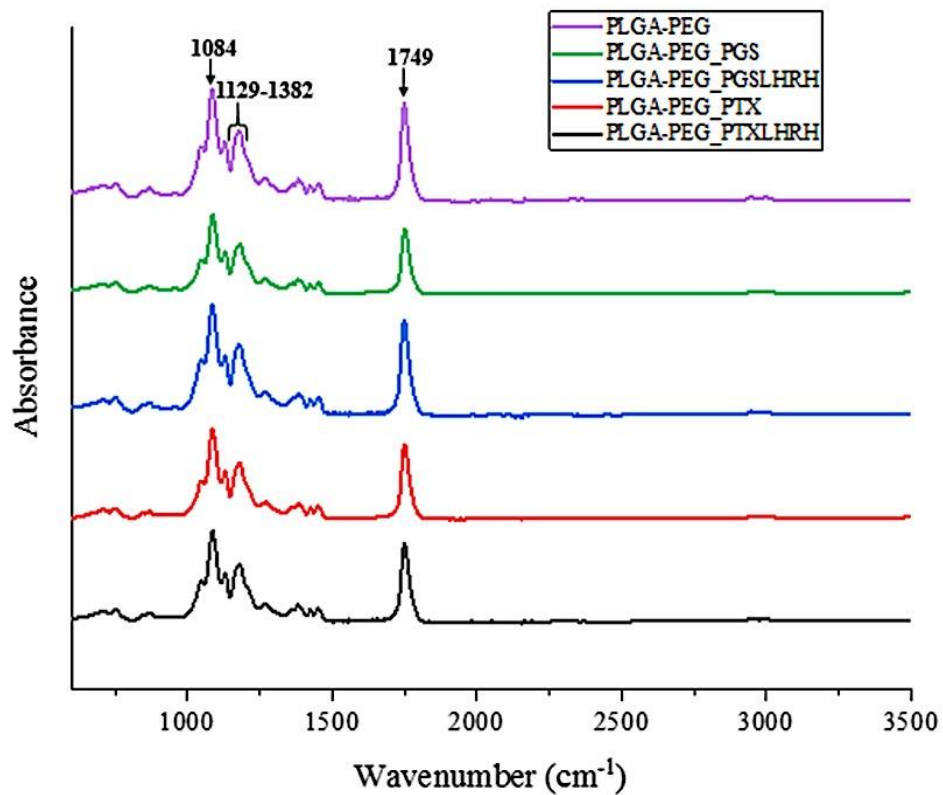
Figure 3.2: FTIR spectra of the synthesized drug-loaded (PLGA-PEG_PGS, PLGA-PEG_PGS-LHRH, PLGA-PEG_PTX, PLGA-PEG_PTX-LHRH) microspheres and control (PLGA-PEG) microspheres
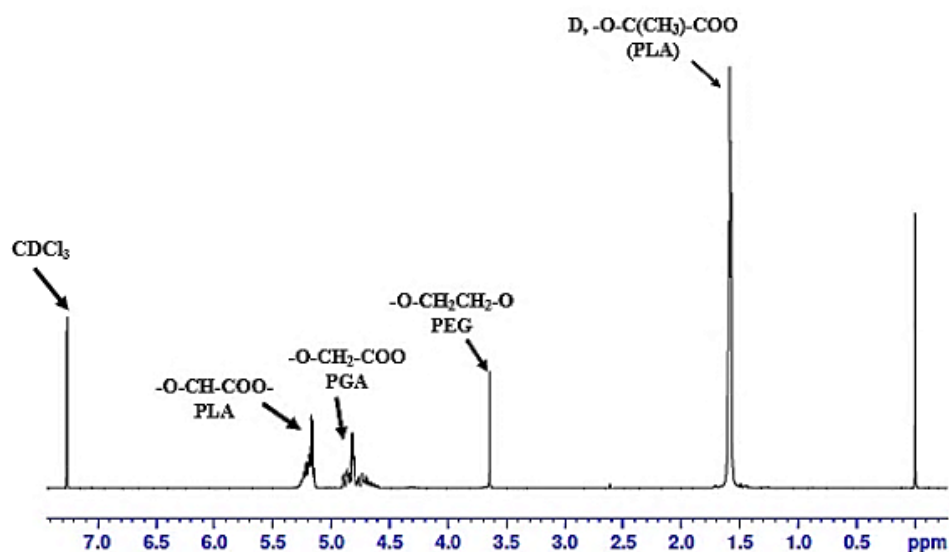
Figure 3.3: A representative 1HNMR spectrum for drug-loaded PLGA-PEG microspheres

Similar HNMR spectra were obtained for all the PLGA-PEG microsphere formulations, with four sets of principal peaks (ppm). Figure 3.3 shows representative HNMR spectra for the different formulations of PLGA-PEG microspheres. The peak at 3.64 ppm corresponds to the hydrogen atoms in the methylene groups of the PEG moiety[242,263]. Hydrogen atoms in the methyl groups of the D- and L-lactic acid repeat units resonated at 1.57 ppm with an overlapping pair[263,264]. A highly complex peak, due to several different glycolic acid, D-lactic, L-lactic sequences in the polymer backbone, was observed at 4.81 ppm and 5.20 ppm. This corresponds to the glycolic acid CH_2 and the lactic acid CH, respectively[263]. Deuterated chloroform was used as a solvent and a chemical shift was seen at 7.26 ppm. These results suggest that the blend of polymers did not undergo chemical modification during drug loading and encapsulation.

Figure 3.4 below, shows the thermal decomposition process of control PLGA-PEG microspheres and drug-loaded PLGA-PEG microspheres obtained via Thermogravimetric Analysis (TGA). The

TGA thermograms reveal one stage of weight loss. This suggests that the polymers and respective drugs mix but do not interact. The one step decomposition in the TGA analysis (Figure 3.4) may be due to the decomposition of the PLGA moiety in the blend [265]. The decomposition temperatures of the control PLGA-PEG microspheres and the drug-loaded PLGA-PEG microspheres are presented in Figure 3.4. The results show that the decomposition temperature decreases with drug loading.
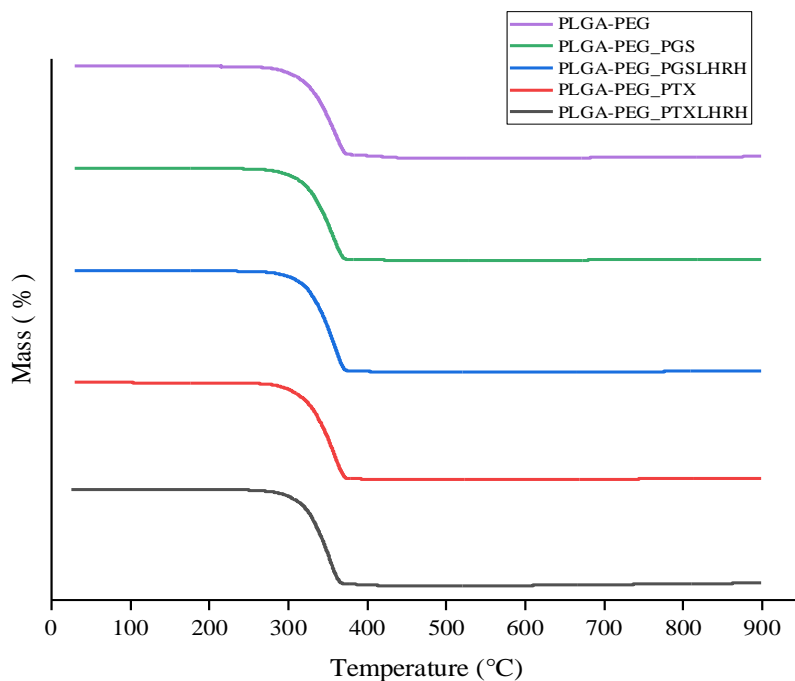
Figure 3.4: TGA curves of control PLGA-PEG microspheres and drug-loaded PLGA-PEG microspheres.
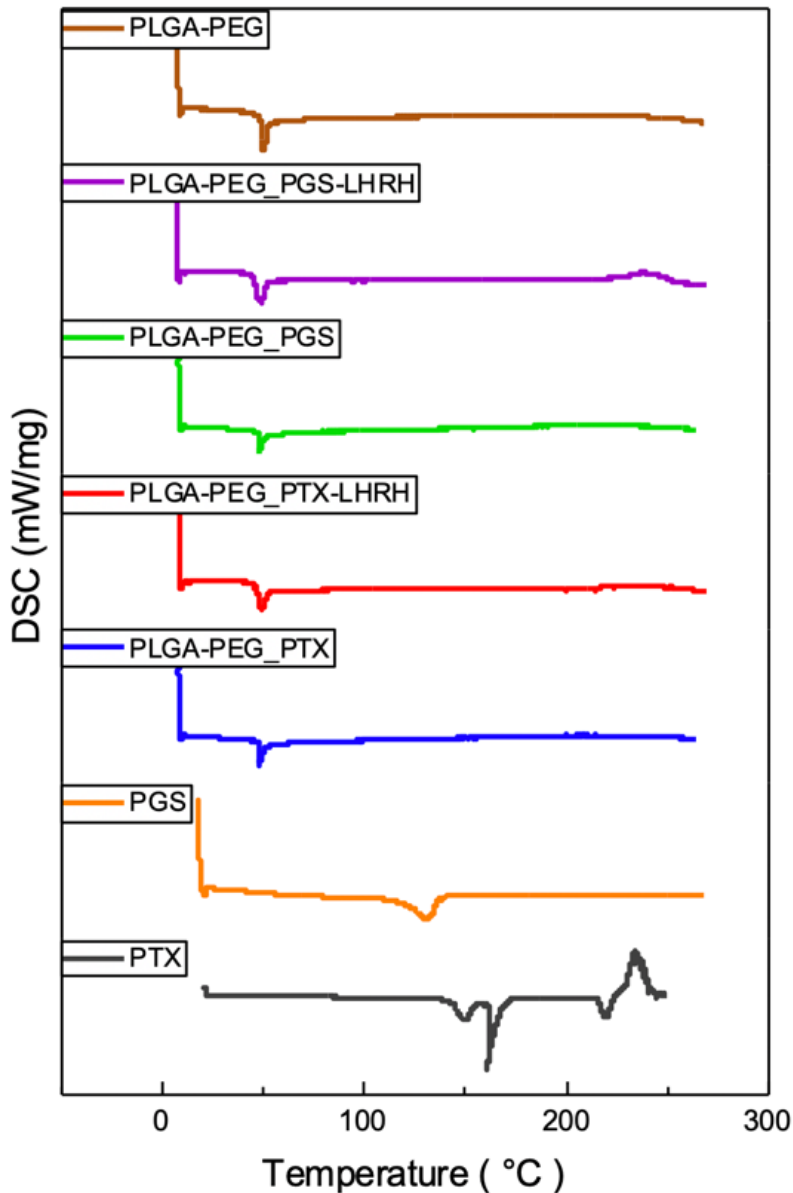
Figure 3.5: DSC thermographs of freeze-dried drug-loaded and control PLGA-PEG microspheres, respectively.

The DSC thermograms are presented in Figure 3.5. This reveals that the control PLGA-PEG microspheres and drug-loaded PLGA-PEG microspheres exhibited similar endothermic events with a single defined peak. This suggests that the drug-loading did not affect the polymer structure. In the case of the control PLGA-PEG microspheres, the glass transition temperature (Tg) and the melting temperature (T_m) were measured to be 48.3°C and 51.3°C, respectively (Table 3.2). The

48

ΔCp corresponds to 0.411 J/(g*K). However, in the case of drug-loaded PLGA-PEG microspheres, the T_g and T_m were lower than those of the control PLGA-PEG microspheres, leading to higher ΔCp values. These changes in the measured values are attributed to the effects of the respective drugs, which act as a plasticizers for the polymer (PLGA) [266].

Furthermore, it was also observed that crystalline PTX had an endothermic peak corresponding to a melting point of 220 °C. Similarly, in the case of case of PGS, an endothermic peak was observed at 132 °C. It should be noted that due to the concentration and the very low drug loading of the drug in the respective microspheres, there was no any noticeable signature peaks of corresponding drug formed in each drug-loaded system. This result indicate that each drug encapsulated did not crystallize in the blend of polymer microspheres [267]. Generally, it was observed that the encapsulation of drug into the polymer microspheres did not significantly change the thermal properties of the drug-loaded polymer systems.

Table 3.2: The Glass transition temperature (Tg), Endothermic peak and Delta Heat Capacity (ΔCp) values for the various PLGA-PEG microspheres formulations.

Drug-Loaded Composition	Glass transition temperature (Tg) (°C)	Endothermic peak (°C)	Delta Heat Capacity (ΔCp) J/(g*K)	Decomposition Temperature (°C)
PLGA-PEG	48.3	51.3	0.411	334.4
PLGA-PEG_PGS	47.0	49.3	0.635	327.2
PLGA-PEG_PGS-LHRH	47.8	50.2	0.497	322.3
PLGA-PEG_PTX	47.3	49.6	0.495	330.5
PLGA-PEG_PTX-LHRH	47.6	50.1	0.479	325.7

3.4.2 *In vitro* Drug Release

Figures 3.6(a-d) show the time dependence of the percentage of cumulative drug release from the drug-loaded PLGA-PEG microspheres. All of the drug-loaded formulations revealed similar release profiles. However, the initial burst release after 48 hours was strongly affected by the type of drug that was encapsulated. In the case of PLGA-PEG microspheres that were loaded with PGS or PGS-LHRH, lower levels of burst release were observed, compared to those obtained from PLGA-PEG microspheres that were loaded with PTX or PTX-LHRH. This was attributed to the hydrophilic and hydrophobic moieties in the PGS-based drugs [178].

(a)

(b)

51

(c)

Legend:
- PLGA-PEG_PTX @37°C
- PLGA-PEG_PTX @41°C
- PLGA-PEG_PTX @44°C

Y-axis: % Cummulative Drug Release

X-axis: Day (s)

(d)
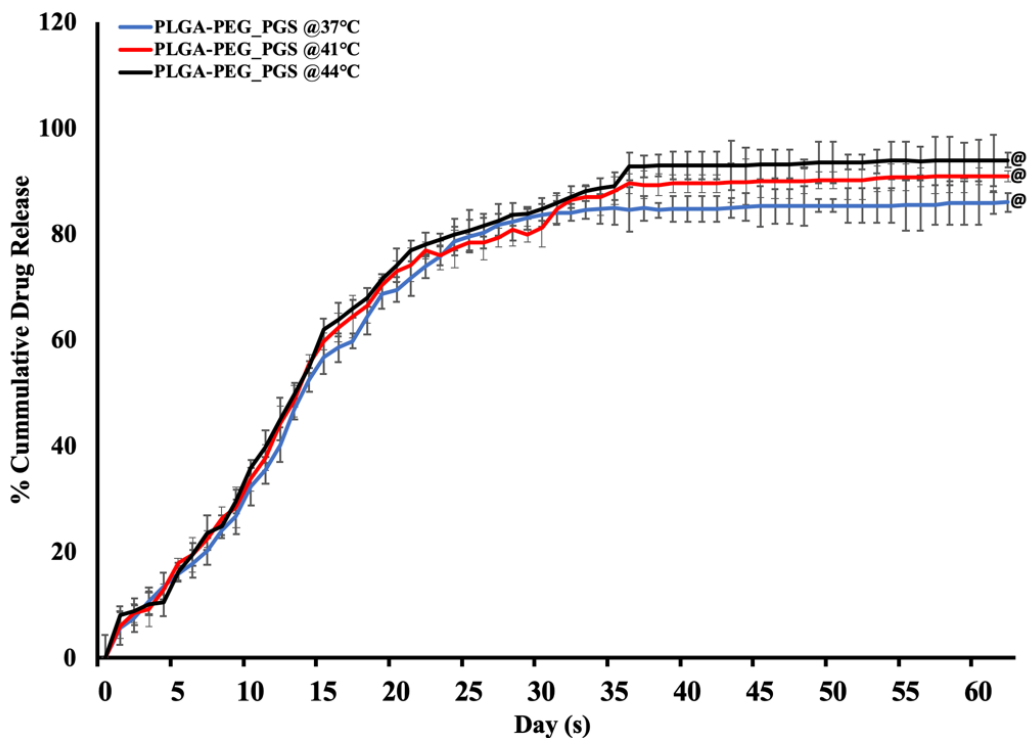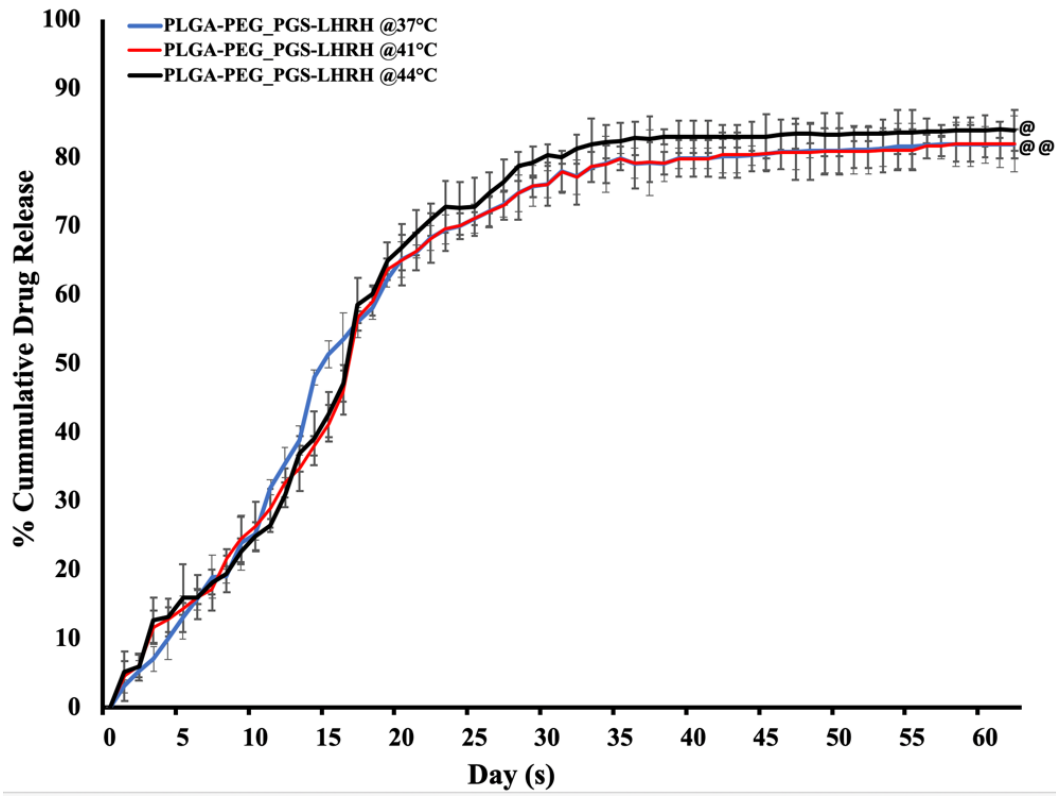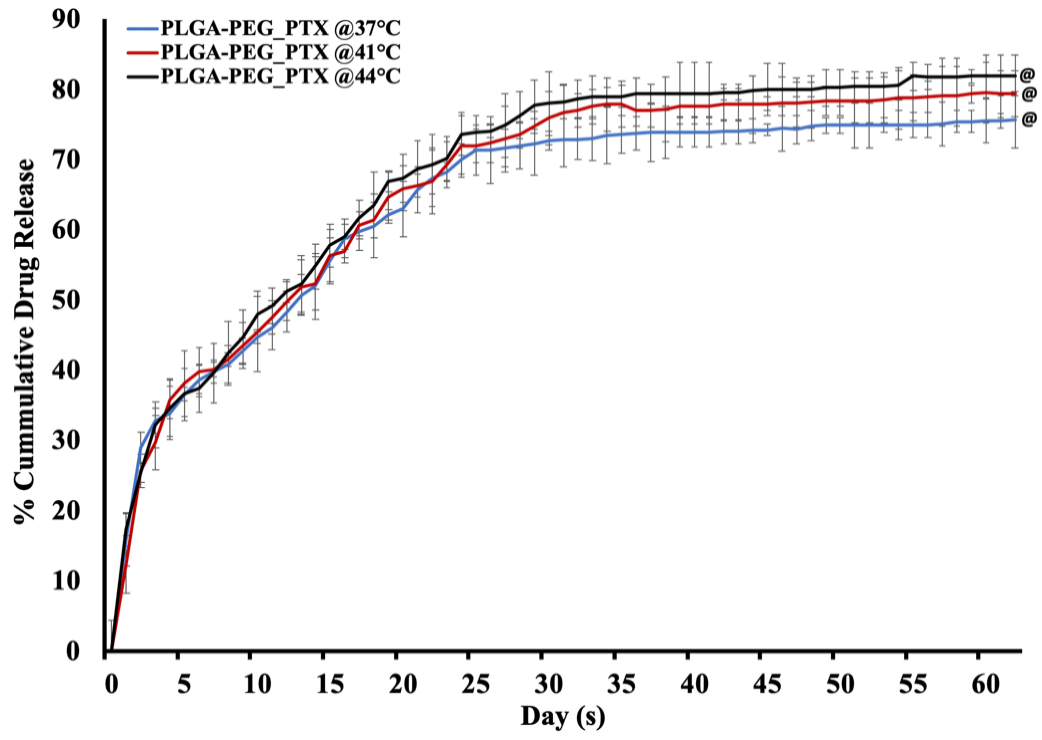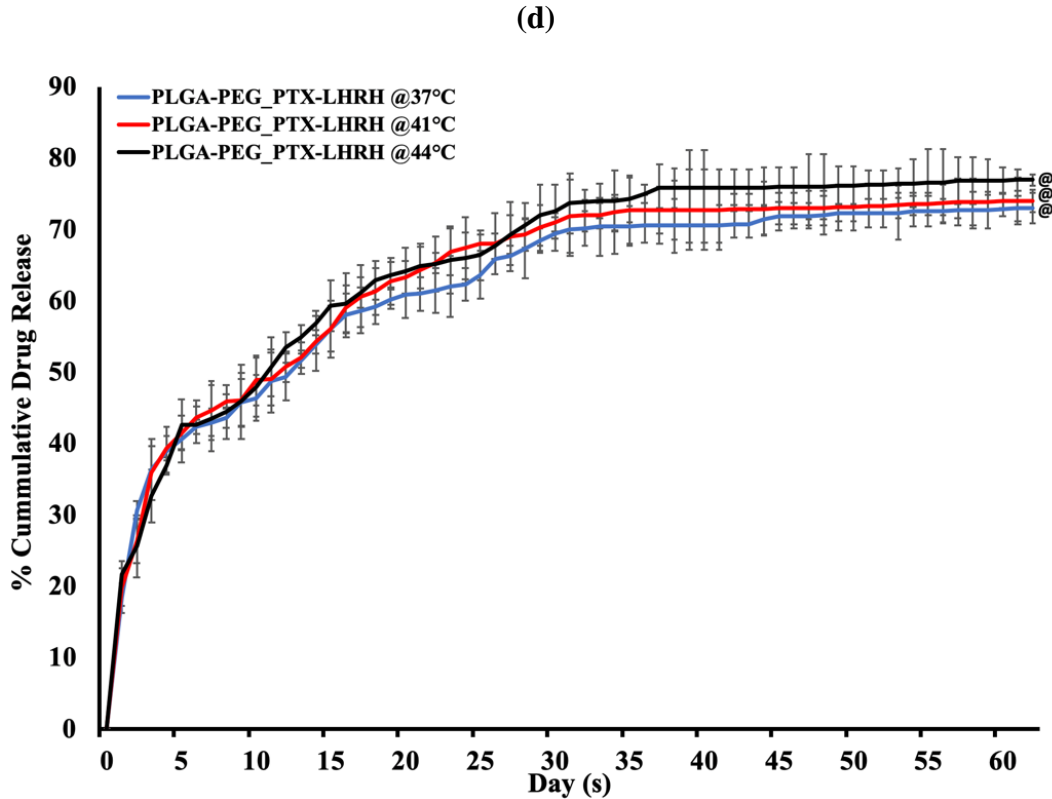
Figure 3.6: *In vitro* release profile of (a) PLGA-PEG-PGS microspheres (b) PLGA-PEG-PTX (c) PLGA-PEG-PGS-LHRH (d) PLGA-PEG-PTX-LHRH drug-loaded microspheres at 37°C, 41°C and 44°C, respectively. In all cases (n = 3, [@]p > 0.05 vs. control)

After 62 days, ~ 80% of PTX and PTX-LHRH drugs was released, while ~ 85% of PGS and PGS-LHRH was released over the same period. The slight decrease in the percentage of cumulative drug release from the PTX and PTX-LHRH drug is attributed to the stronger hydrophobic domain of PTX-based drugs. Finally, in this section, it is important to note that controlled release occurred from the microspheres (with ~ 60% release) within ~ 40 days. The respective drug encapsulation efficiencies and their drug loading efficiency obtained for the drug-loaded PLGA-PEG_PGS, PLGA-PEG_PGS-LHRH, PLGA-PEG_PTX, PLGA-PEG_PTX-LHRH, were determined to be ~ 46%, 40%, 72%, 38% and 12.3%, 14.2%, 16.1%, 9.8%, respectively. In each case of the drug release studies, the results were not significant since the p value for each drug at different temperatures considered are greater than 0.05. This implies that there was no significant difference

when we use different temperatures. However, comparing the respective cumulative drug release, the results were considered to be significant with a p value < 0.05.

3.4.3 *In vitro* Drug Release Kinetics

The drug release kinetics (Table 3.3) obtained from the drug release data that were fitted in the kinetic models [zero order ($Q_t = Q_O + K_0.t$), first order ($\log Q_t = \log Q_0 + {Kt}/{2.303}$), Higuchi model ($Q_t = K_H.t^{1/2}$) and Korsmeyer–Peppas model ($\frac{M_t}{M_\infty} = Kt^n$)] showed clearly that the Korsmeyer–Peppas model provided the best fit to the experimental data obtained for the different drug-loaded PLGA-PEG microsphere formulations. In some cases, the release exponent 'n' was between 0.446 and 0.889, which is consistent with drug release by anomalous transport or non-Fickian diffusion that involves two phenomena: drug diffusion and relaxation of the polymer matrix [268].

Table 3.3: The kinetic constant (K), correlation coefficient (R^2) and Release exponent (n) of kinetic data analysis of drug released from the various PLGA-PEG microspheres formulations.

Formulations	Temperature °C	Zero Order		First order		Higuchi model		Koresmeyer-Peppas		
		K	R^2	K	R^2	K	R^2	K	R^2	n
PLGA-PEG_PGS		1.232	0.711	0.014	0.505	12.786	0.857	1.920	0.973	**0.870**
PLGA-PEG_PGS-LHRH	37	1.226	0.749	0.015	0.529	12.578	0.882	1.837	0.977	**0.889**
PLGA-PEG_PTX		0.769	0.692	0.008	0.330	8.137	0.867	3.271	0.962	**0.459**
PLGA-PEG_PTX-LHRH		0.680	0.704	0.007	0.294	7.802	0.845	3.340	0.848	**0.490**
PLGA-PEG_PGS		1.315	0.752	0.014	0.513	13.533	0.875	1.982	0.969	**0.855**
PLGA-PEG_PGS-LHRH	41	1.236	0.760	0.015	0.548	12.607	0.884	1.785	0.976	**0.885**
PLGA-PEG_PTX		0.853	0.718	0.009	0.354	8.964	0.886	3.398	0.969	**0.447**
PLGA-PEG_PTX-LHRH		0.685	0.672	0.007	0.288	7.316	0.856	3.431	0.912	**0.446**
PLGA-PEG_PGS		1.371	0.757	0.014	0.519	13.987	0.867	2.034	0.953	**0.842**
PLGA-PEG_PGS-LHRH	44	1.281	0.749	0.015	0.551	13.085	0.873	1.809	0.966	**0.881**
PLGA-PEG_PTX		0.881	0.728	0.009	0.357	9.224	0.951	3.210	0.985	**0.490**
PLGA-PEG_PTX-LHRH		0.753	0.712	0.008	0.311	7.939	0.885	3.302	0.968	**0.450**

3.4.4 Thermodynamics of *In vitro* Drug Release

The thermodynamic parameters (ΔG, ΔH, ΔS and E_a) that were obtained from this study are presented in Table 3.4. The change in the Gibb's free energy (ΔG) was negative for all of the PLGA-PEG microsphere formulations. This indicates the feasibility and non-spontaneous nature of the drug release from the PLGA-PEG microspheres at all temperatures. Figure 3.7 shows a plot of Gibb's free energy versus Temperature for various PLGA-PEG formulations. The negative values obtained for the change in entropy (ΔS) also confirm that there is a decrease in the disorder associated with drug release from the various PLGA-PEG microspheres. Furthermore, the positive values obtained for the change in enthalpy (ΔH) confirm that the drug release process (from all of the PLGA-PEG microspheres formulations containing PGS, PGS-LHRH or PTX-LHRH respectively) was endothermic. However, a positive E_a was obtained for the drug release from all the PLGA-PEG formulations, indicating that in all cases, the rate of drug release increased with increasing temperature.

Table 3.4: Thermodynamic parameters for the various PLGA-PEG microspheres.

Formulations	Temperature °C/K	E_a (kJ mol^{-1})	ΔS (kJ mol^{-1} K^{-1})	ΔH (kJ mol^{-1})	ΔG (kJ mol^{-1})
PLGA-PEG_PGS	37 / 310.15	6.720	-0.170	6.720	52.871
	41 / 314.15				53.553
	44 / 317.15				54.064
PLGA-PEG_PGS-LHRH	37 / 310.15	4.379	-0.178	4.379	59.586
	41 / 314.15				60.298
	44 / 317.15				60.832
PLGA-PEG_PTX	37 / 310.15	7.714	-0.163	7.714	58.268
	41 / 314.15				58.920
	44 / 317.15				59.409
PLGA-PEG_PTX-LHRH	37 / 310.15	5.444	-0.170	5.444	58.170
	41 / 314.15				58.850
	44 / 317.15				59.360
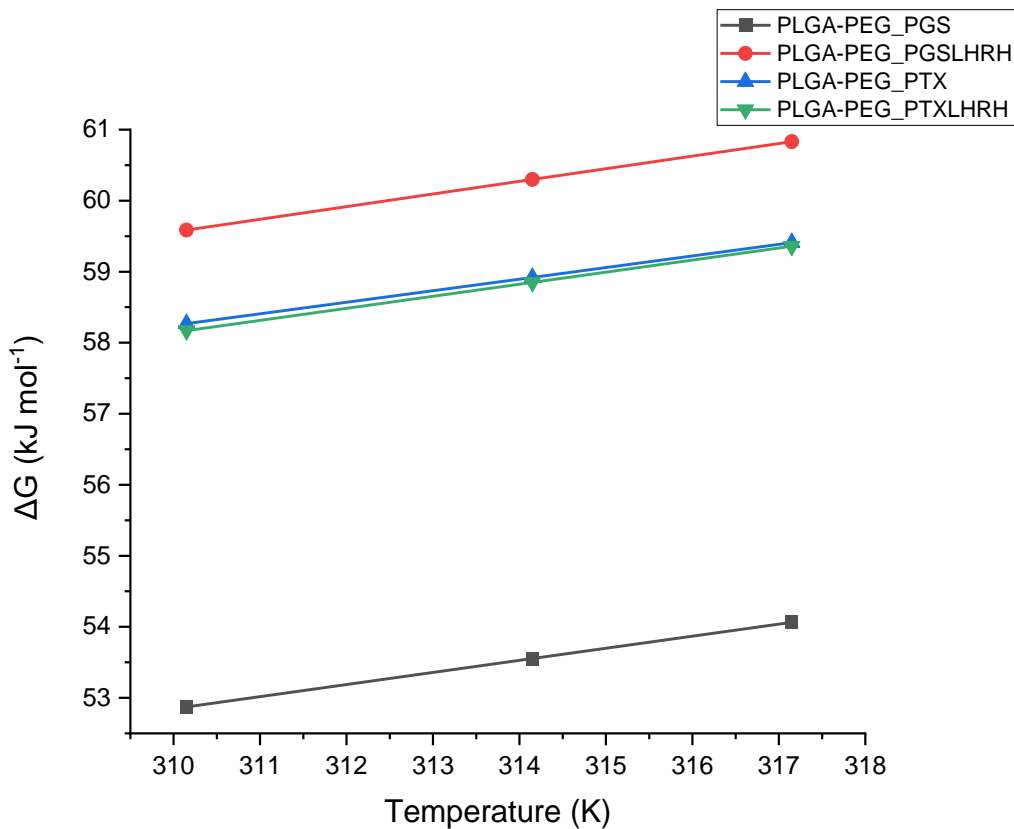
Figure 3.7: A plot of Gibb's free energy versus Temperature for various drug-loaded PLGA-PEG formulations.

3.4.5 *In vitro* Degradation of Drug-loaded Microspheres

SEM images of the degradation of the drug-loaded microspheres are presented in Figure 3.8. Gradual morphological changes were observed within the 56-day period of the drug release experiments. After 24 hours of exposure to the release medium (PBS, pH=7.4), the surfaces of the drug-loaded PLGA-PEG microspheres were still smooth with micropores. However, by day 14, morphological changes were observed. These included microsphere agglomeration, distinct

micropores and less spherical shapes. Evidence of microsphere agglomeration and void formation was observed by Day 28. After 42 days of drug elution, the surfaces of the PLGA-PEG microspheres were completely eroded visibly larger pores. Further evidence of material removal was also observed after 56 days of drug elution, which was found to result in more porous structures than those that were observed before drug elution. The increased erosion is attributed to the hydrolytic degradation of the ester and drug leaching [269].
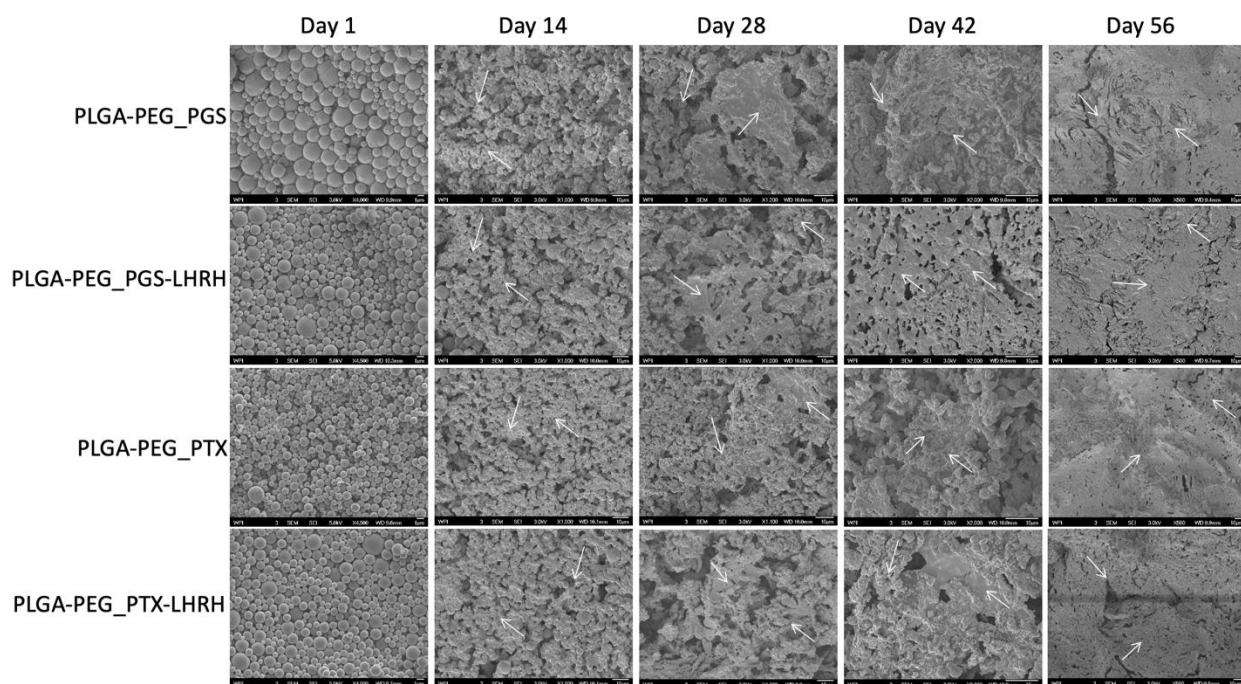
Figure 3.8: SEM images of surfaces of drug-loaded PLGA-PEG microspheres after 57 days exposure to phosphate buffer saline at pH 7.4: and cross-sections (note the different magnifications/scaling bars). The white arrows show evidence of the progression of material removal and degradation site.

3.4.6 *In vitro* Cell Viability and Drug Cytotoxicity

Figures 3.9 and 3.10 compares the percentage alamar blue reduction and percentage cell growth inhibition, respectively, for cells only (MDA-MB-231 cells), drug-loaded and control PLGA-PEG

microspheres 6, 24, 48, 72 and 96 hours post-treatment. The percentage alamar blue reduction measures the cell metabolic activity, which is a function of the cell viability and cell population. This implies that a higher percentage of alamar blue reduction value corresponds to a higher cell growth and, by extension, a higher cell viability. A two-way ANOVA with post hoc Tukey HSD multiple comparisons tests showed that, generally, the cell viability was significantly lower ($p <$ 0.05) for the cells treated with drug-loaded PLGA-PEG microspheres than cells that were not exposed to drug elution from microspheres. Furthermore, the cells treated with PLGA-PEG microspheres loaded with conjugated drugs (PGS-LHRH, PTX-LHRH) were less viable than their counterparts that were loaded with unconjugated drugs (PGS, PTX). This means that the conjugated drugs were more effective at reducing the metabolic activities of the MDA-MB-231 cells than their unconjugated counterparts. The statistically significant group pairs of interest ($p <$ 0.05) are highlighted in Figure 3.9 and 3.10.

There was a slight reduction in cell viability when the cells were exposed to the control PLGA-PEG microspheres (no drugs), attributed to the cytotoxic effects of leached residual DCM solvent that was used to process the microspheres. However, the reduction in cell viabilities (Figure 3.9 and increase in cell growth inhibition (Figure 3.10) by the drug-loaded microspheres were higher than those by the control microspheres (no drugs) ($p < 0.05$), providing evidence of the cytotoxicity and anti-proliferative effects the encapsulated drugs

The stronger effects of the conjugated drugs (PGS-LHRH, PTX-LHRH) are attributed to the conjugation of the LHRH ligand to the anticancer drugs. This is likely to increase the specificity of the binding of the released drugs to the overexpressed LHRH receptors on the MDA-MB-231

cells. Thus, the LHRH-conjugated anticancer drugs are much more effective in targeting the MDA-

MB-231 cells than the unconjugated drugs (PGS or PTX).
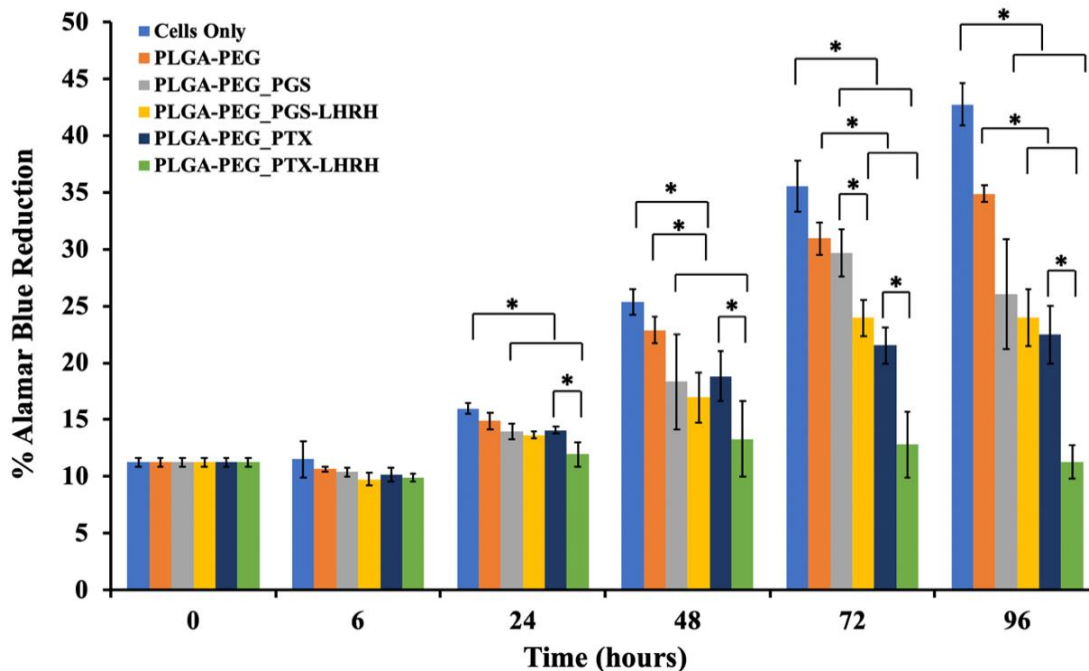
Figure 3.9: Percentage Alamar Blue reduction for cells only (MDA-MB-231 cells), drug-loaded and control PLGA-PEG microspheres 6, 24, 48, 72 and 96 hours post-treatment.
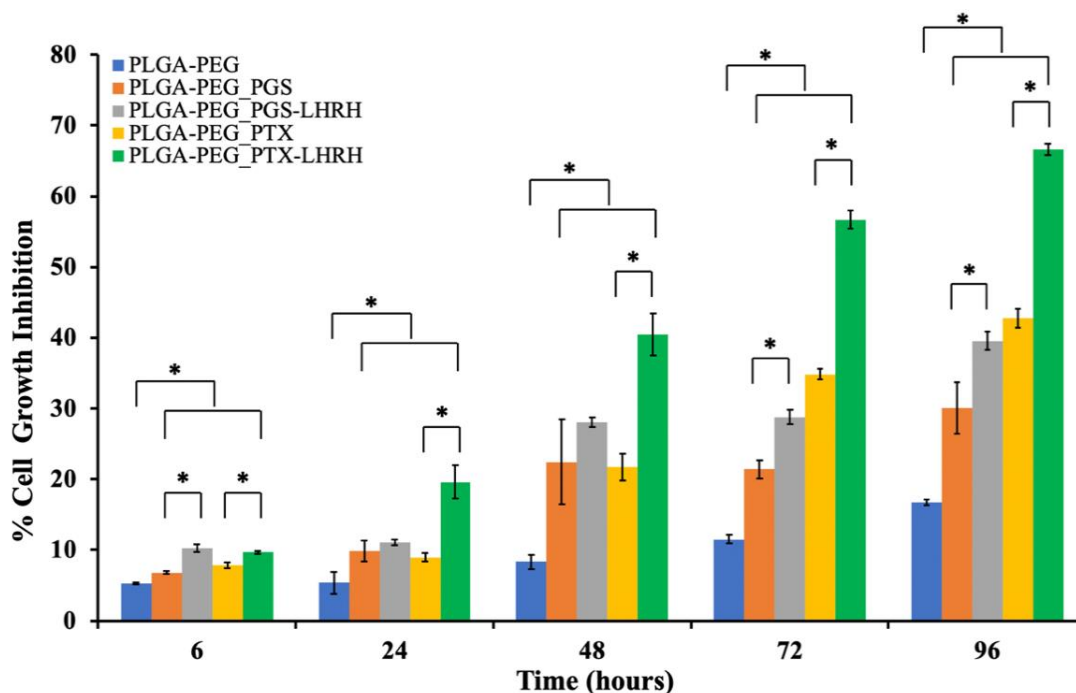
Figure 3.10: Percentage cell growth inhibition for drug-loaded and control PLGA-PEG microspheres after 6, 24, 48, 72 and 96 hours' post-treatment [*p < 0.05 (n = 4)].

3.4.7 *In vitro* Cytotoxicity and Drug Uptake

In this study, we consider the cytotoxicity to be a measure of the percentage of cell growth inhibition. Figure 3.11 shows the extent to which the addition of the drug-loaded PLGA-PEG microspheres inhibited MDA-MB-231 cell growth after 6, 24, 48, 72 and 96 hours of exposure, when compared to the inhibition of untreated cells. Higher cytotoxicity levels (due to drug-treatment) correspond to higher percentages of cell growth inhibition. The results show that cell growth was clearly inhibited by the release of drugs from the drug-loaded PLGA-PEG microspheres (compared to control unloaded PLGA-PEG microspheres).

Furthermore, the cells treated with PLGA-PEG microspheres loaded with conjugated drugs (PGS-LHRH, PTX-LHRH) exhibited higher percentages of cell growth inhibition than their counterparts loaded with unconjugated drugs (PGS, PTX). Hence, the LHRH-conjugated drug-loaded microspheres were more effective at inhibiting cell growth than the unconjugated drug-loaded microspheres. The increased effectiveness of the LHRH-conjugated drugs is attributed to the specific targeting of the LHRH receptors on the MDA-MB-231 cells.

Finally, the Trypan blue dye (TBD) cell count was used to confirm the effects of the drug-loaded PLGA-PEG microsphere treatment on MDA-MB-231 cell viability. An exponential increase in the cell viability/proliferation of the MDA-MB-231 cells (control) was observed throughout the incubation period. In agreement with the alamar blue^{TM} assay results, the viability of the MDA MB 231 cells treated with PLGA-PEG microspheres (loaded with conjugated drug) were significantly reduced, in comparison to MDA-MB-231 cells treated with PLGA-PEG microspheres loaded with unconjugated drugs. This again shows that the conjugated drugs were effective at reducing cell viability than the unconjugated drugs. In summary, the TBD revealed that ~ 95% of the cells were dead (with ~ 5% of viable cells remaining) after 96 hours of exposure to targeted encapsulated drug-loaded PLGA-PEG microspheres. The results show a significant difference between the cell viability of encapsulated targeted-drug system (PLGA-PEG_PGSLHRH, PLGA-PEG_PTXLHRH) and PLGA-PEG_PGS, PLGA-PEG_PTX since the p-value calculated is < 0.05.

(a)
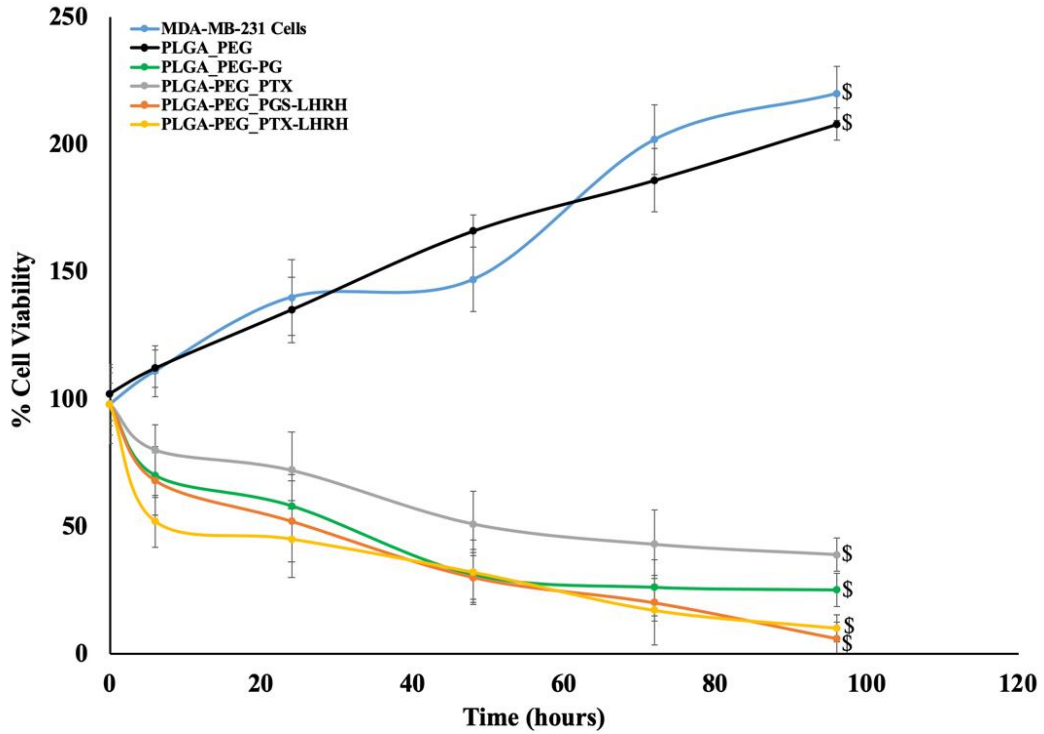
Figure 3.11: Cell viability study of MDA-MB-231 cells showing the effect of the treatment time when incubated with drug-loaded and unloaded PLGA-PEG microspheres after for a period of 240 h with MDA-MB-231 cells acting as a control.

	MDA-MB-231	PGS MS	PGSLHRH MS	PTX MS	PTXLHRH MS
ACTIN					
VINCULIN					
MERGE					
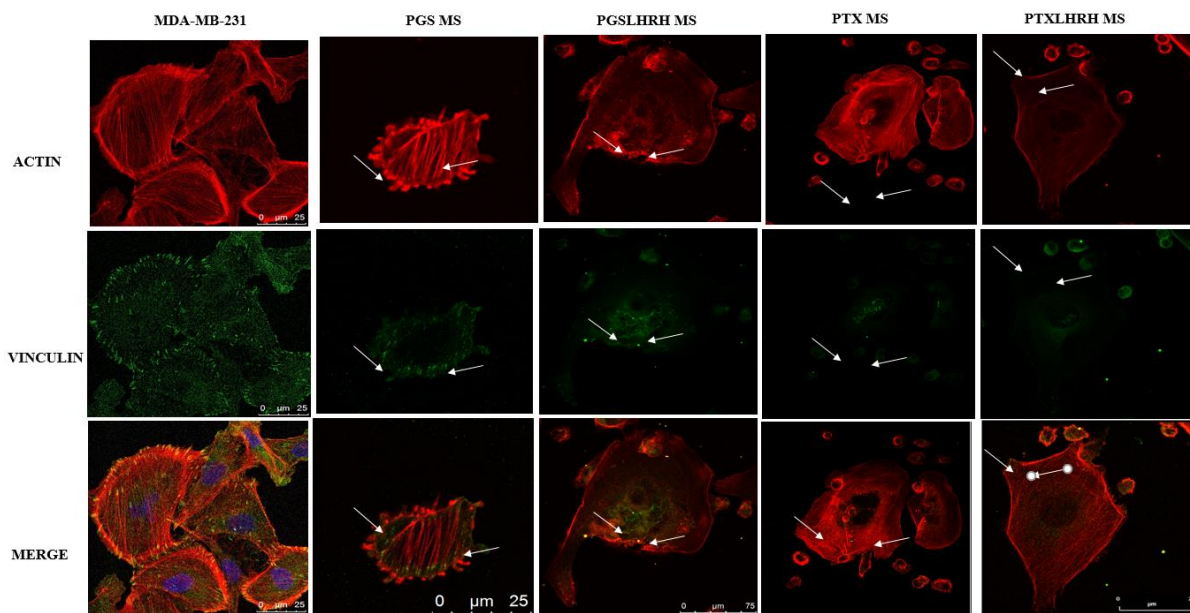
Figure 3.12: Representative confocal images of MDA-MB-231 cells after 5 hours incubation with respective drug-loaded PLGA-PEG microspheres at 37°C. Red staining reveals actin-filaments and green staining indicates vinculin. All cells were stained and imaged under the same conditions. White arrows indicate the initiation of cytoskeleton disruption/disintegration (n = 3, $^\$p < 0.05$ vs. control).

The network of the cytoskeleton of actin microfilaments, intermediate filaments, and microtubules make up the cytoplasm which controls the mechanical structure and shape of the cell [270]. Hence, the disruption of the spatial organization of the cytoskeleton networks (by pharmacological treatments) can affect the structure and properties of the cell [271,272]. Hence, in this section, changes in the cytoskeleton structure are elucidated following exposure to the release of cancer drugs (PGS, PTX, PGS-LHRH, PTX-LHRH). The resulting effects of the uptake of cancer drugs was elucidated via confocal laser scanning microscopy and are presented in Figure 3.12. Distinctive changes in the cytoskeletal structures were observed after 5 hours of exposure to drug release. The changes in the cytoskeletal structure also continue with increasing exposure to the

released drugs. This results suggests that the exposure to cancer drugs significantly affects the underlying cytoskeletal structure giving rise to apoptosis and cell death [273–276]

3.4.8 *In vivo* Animal Studies

Figure 3.13 presents the body weights of the mice over the therapeutic period of 18 weeks. Results showed that there was no statistical difference in the growth rate (as a function of weight) of mice treated with drug-loaded microspheres and the control group. It can be concluded that there were no significant changes in the body weight associated with any of the treatment groups as compared to the control group. This implies that the drug-loaded particles used did not create any cytotoxic effects on the general well-being of the treatment group mice during the therapeutic window/time. Although there was an increase in body weight of the treatment groups, this increase is synonymous to those of the control group indicating that there was no noticeable side effects, physiological changes, or drastic decrease in the body weight after the administration of the drugs, compared to the control mice. Consequently, during the therapeutic time, all of the mice studied appeared to be healthy with normal eyes and skin conditions. These results are similar to our previous study in which we found that the concentration of the conjugated drugs used are effective for the treatment of TNBC [43].
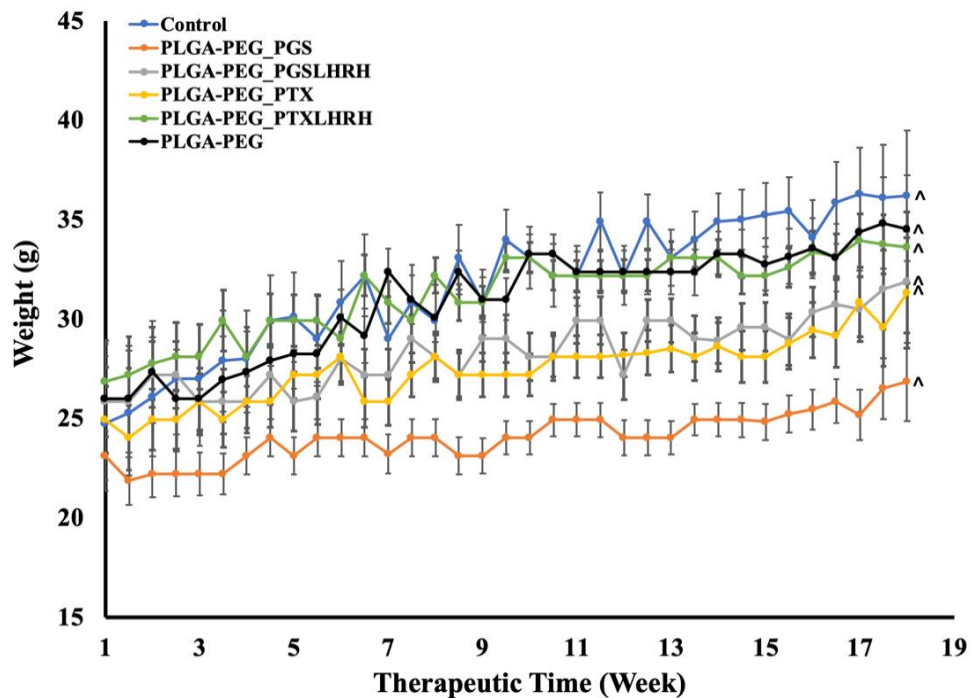
Figure 3.13: Body weight variation of subcutaneous xenograft tumor-bearing mice treated with drug-loaded microparticles in the presence of control (n = 5, ^p < 0.05)
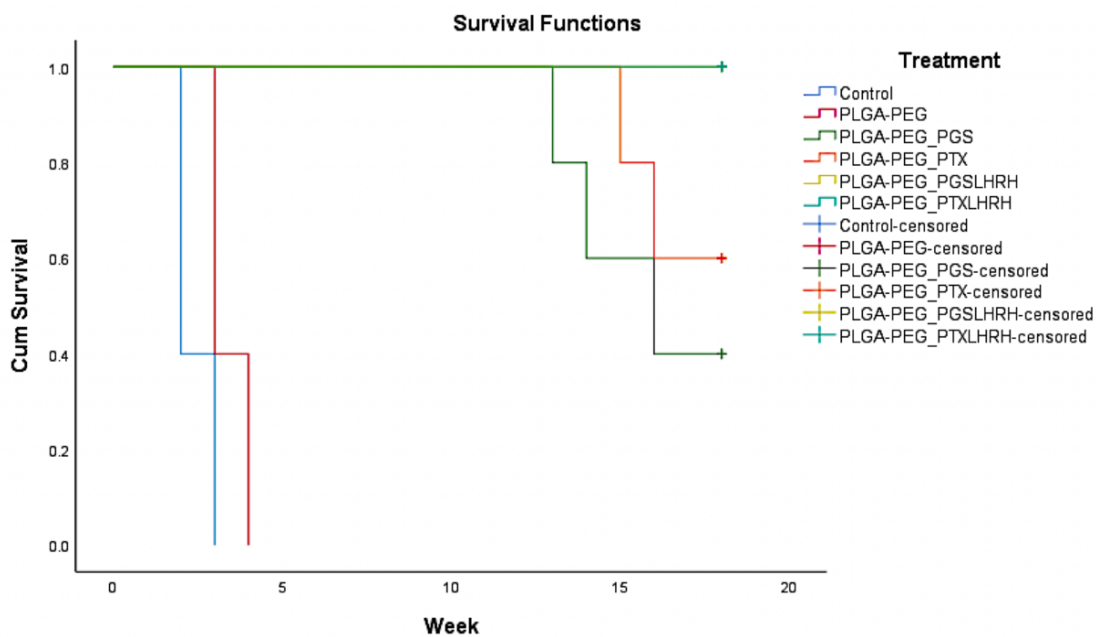
Figure 3.14: Kaplan Meier survival curves (N=30) showing the effect of all treatment groups on the survival rate of mice.

Survival rate for all the treatment groups during the therapeutic duration are shown is presented in the Kaplan-Meier curves as shown in Figure 3.14. A survival rate that describe the recurrence of the treated tumor was observed at week 13, 14, 16 for mice treated with PLGA-PEG_PGS while at week 15 and 16 week we observed a recurrence for mice treated with PLGA-PEG_PTX.. *ln vivo* animal studies results showed that the drug loaded microsphere prolonged the survival of mice and prevented the recurrence time for tumor. However, mice treated with targeted drug-loaded microspheres (PLGA-PEG_PGSLHRH and PLGA-PEG_PTXLHRH) with an overlapping curve show a prolonged survival and limits recurrence compared to the PLGA-PEG_PGS and PLGA-PEG_PTX. Overall, our results reveal that each group treated with drug-loaded microspheres had a higher cumulative survival compared to the cumulative survival noted in the untreated/control groups ($p<0.0001$). These results from are in good agreement with the *in vitro* cell viability studies.

The mean tumor volume was 310 ± 14 mm^3 28 days after the tumor was induced subcutaneously [Figure 3.15 (Ia)]. The process of surgery and the outcome of implanted drug-loaded microspheres are shown in Figure 3.15 [I]. The representative drug-loaded microspheres (PLGA-PEG_PGS-LHRH) implanted after tumor was removed revealed that there was no local recurrent of tumor after 18 weeks [Figure 3.15 (If)]. It was observed that for the case of mice implanted with targeted drug-loaded microspheres (PLGA-PEG_PGS-LHRH and PLGA-PEG_PTX-LHRH), there was no recurrence of tumor after drug released from the microspheres for 18 weeks (See representative result in Figure 3.15 (If). These results are also similar for PLGA-PEG_PTX-LHRH. PLGA-PEG_PGS, and PLGA-PEG_PTX.
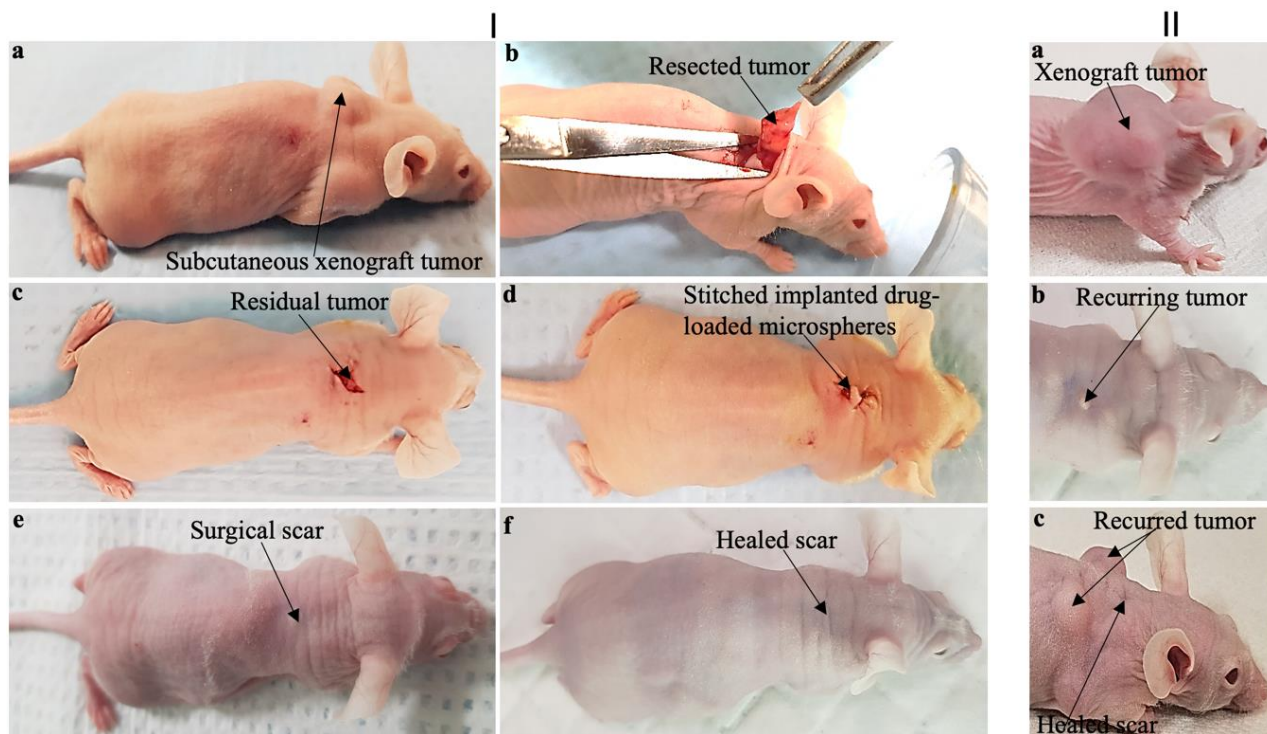
Figure 3.15: (I) Representative photographs showing the steps involved in the treatment of the TNBC tumor with drug-loaded microspheres: (a) Subcutaneous xenograft TNBC tumor; (b) Surgical tumor removal; (c) Residual tumor; (d) Stitched residual tumor with implanted drug-loaded microspheres; (e) Healing scar 8 weeks after surgery and (f) Completely healed mice 18 weeks after surgery and treatment with targeted drug-loaded microspheres (PLGA-PEG_PGSLHRH). (II) (a-c) Representative mice treated with non-drug microparticles (PLGA-PEG) with recurred tumor.

In general, for the mice treated with targeted drug-loaded microspheres, no significant weight loss or side effects were discussed. However, this groups implanted with positive control microspheres (PLGA-PEG) and the control mice (with no microspheres) exhibited noticeable multiple recurrences of the TNBC tumors [Figure 3.15 (IIa-IIc)]. These recurrences are attributed to the incomplete removal of all of the residual tumor and the absence of drug-loaded microspheres [Figure 3.15 (Ic)]. In contrast, no tumor reoccurrence was observed after the implantation of the targeted TNBC drug (PLGA-PEG_PGS-LHRH). Hence, the drug-loaded microparticles are

effective for the prevention of tumor recurrence, following surgical resection of triple-negative breast tumor.

Figures 3.16 (Ia & Ib) present immunofluorescence (IF) images of LHRH receptors showing the presence of LHRH receptors on the tumor and lungs of the control mice group that was treated with non-drug loaded microparticles. It was also noticed that after 18 weeks of surgery, the source tumor [Figure 3.16 (Ic)] showed metastases in the lungs [Figure 3.16 (Id)]. Figures 3.16 (IIa & IIb) show the lungs of mice treated with PTX-loaded PLGA-PEG and PGS-loaded PLGA-PEG microparticles, respectively, while Figures 3.16 (IIc and IId) show the lungs of mice treated with PTX-LHRH-loaded PLGA-PEG and PGS-LHRH-loaded PLGA-PEG microparticles, respectively. The results clearly show that for the control mice, there was evidence of metastasis in the lungs, due to the presence of multiple metastatic foci or nodules from H&E histological staining. Hence, both IF staining and the H&E analyses of the primary tumors and the metastases in the lungs validated the use of drug-loaded microspheres for the localized drug delivery of PGS-LHRH to tumor sites following surgical removal of the primary tumor.
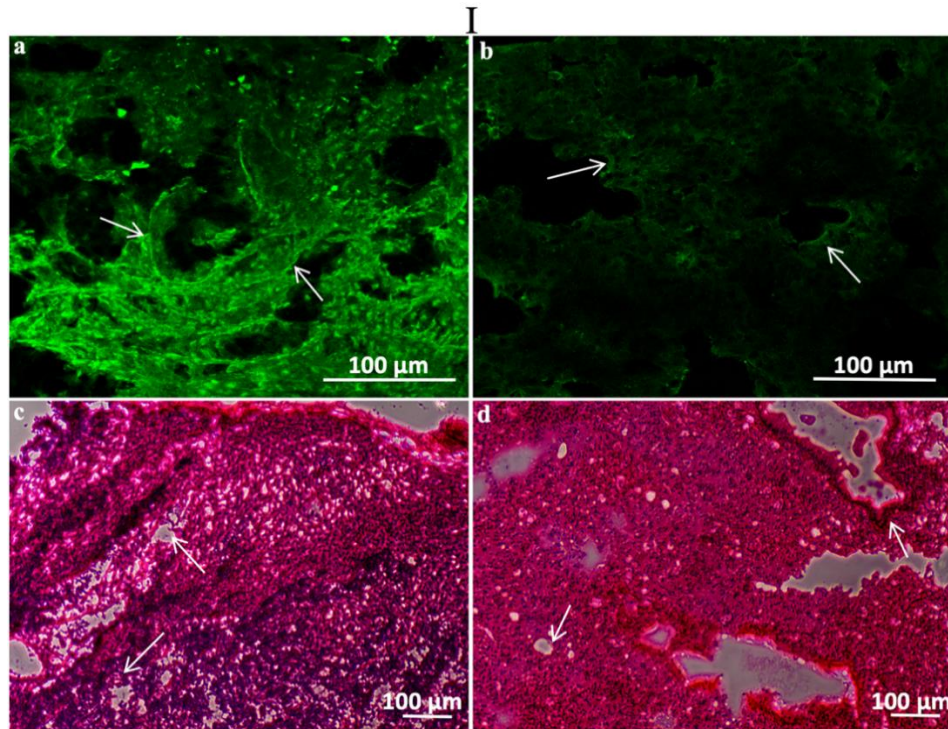
Figure 3.16 [I]: Representative immunofluorescence images of LHRH receptors (green stain) expressed on the (a) tumor, and (b) lungs of mice treated with a control microspheres (PLGA-PEG) and their corresponding H&E stain showing metastasis in the (c) tumor and (d) lungs.
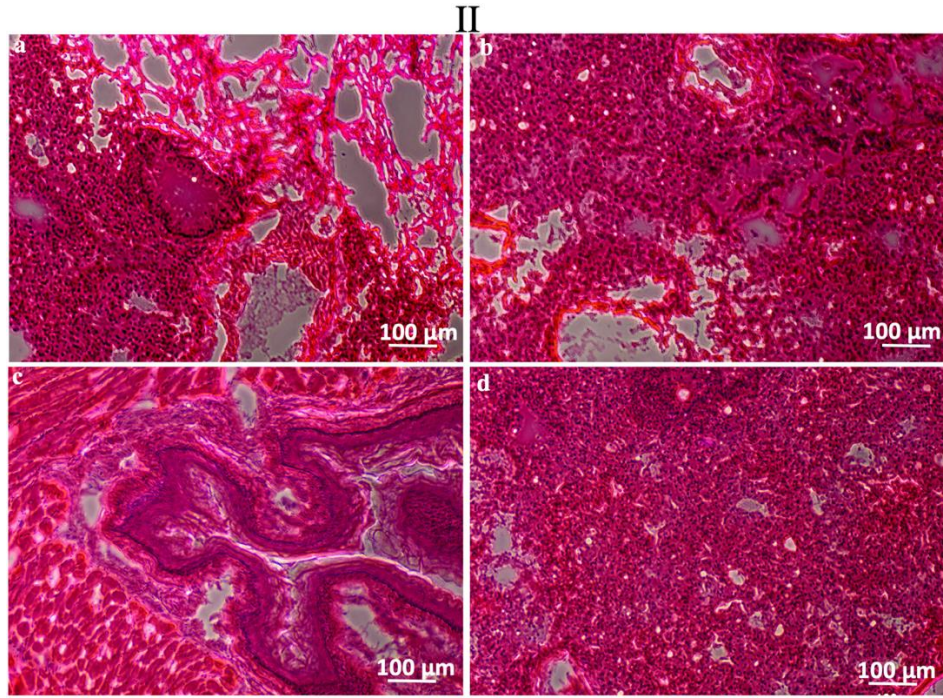
Figure 3.16 [II]: Optical images of mice lungs treated with (a) PLGA-PEG_PTX (b) PLGA-PEG_PGS (c) PLGA-PEG_PTX-LHRH (d) PLGA-PEG_PGS-LHRH microspheres.

3.5 Conclusion

The implications of the above results are very significant. First, uniquely loaded microspheres (of relevant clinical sizes) have been developed for the delivery of targeted cancer drugs (PGS-LHRH, PTX-LHRH) to TNBC cells. The microspheres, which were formulated from a distinct blend of polymers, exhibited bi-phasic release of the anti-cancer drugs. The drug release kinetics are controlled by anomalous (non-Fickian) drug diffusion following the Korseymer-Peppas model at the earlier stages of drug release. This is followed by degradation and membrane erosion, as shown in the SEM degradation images at the later stages of drug elution.

A higher level of burst release was observed for PTX-based drugs than PGS-based drugs. Similar drug release profiles were observed at different temperatures. The thermodynamic studies also confirmed the feasibility of the drug release at different temperatures, while the release kinetics were shown to be controlled by non-Fickian diffusion and polymer degradation, which was confirmed by observations of erosion on the surfaces of the PLGA-PEG microspheres after polymer degradation. These insights into the thermodynamics and kinetics of the drug release create a new dimension that describe processes that are relevant to localized drug release and their mechanisms.

Furthermore, under *in vitro* conditions, the targeted drugs (LHRH conjugated Prodigiosin /Paclitaxel) were more effective at reducing the viabilities of breast cancer cells (MDA-MB-231) than Prodigiosin/Paclitaxel alone. This suggests that the LHRH enhances the specific targeting of TNBC cells by inhibiting cancer cell growth. Distinct changes in actin cytoskeletal structure and vinculin transmembrane structures were associated with targeted drug release. The *in vivo* results

also suggest that the targeted-drug-loaded microspheres are effective at preventing the loco-regional recurrence of TNBC, following surgical resection of triple-negative breast tumors.

Chapter 4

4.0 PLGA-CS-PEG Microparticles for Controlled Drug Delivery in the Treatment of Triple-Negative Breast Cancer Cells

4.1 Introduction

Cancer is the second leading cause of death globally [201,203]. It was the cause of death for an estimated 9.6 million people in 2018 [201,203]. Based on projections, cancer deaths will continue to rise, with 13 million people projected to die of cancer in 2030. At this rate, cancer may surpass cardiovascular disease as the leading cause of death, globally [203]. Current scientific evidence suggests that cancer can be triggered by environmental and genetic factors [4]. Current treatment modalities include radiotherapy, chemotherapy, hormonal therapy, and surgical removal [277]. These conventional treatment modes, however, are known to induce multiple side effects that can have negative long-term effects on a patient's quality of life [277].

The emergence of drug delivery systems (DDS) for delivery of anticancer agents has created a profound impact on clinical therapeutics. DDS are used to deliver drugs to desired cells, tissues, organs, and sub-cellular organs for drug release and adsorption, through a variety of drug carriers [28]. In general, DDS are aimed at addressing some of the shortcomings of conventional cancer treatment methods, thereby improving treatment efficacy, while avoiding toxicity in normal cells. Their desirable features include improving the pharmaceutical activities of therapeutic drugs and alleviating the side effects of therapeutic drugs, thereby addressing the problem of low bioavailability, lack of selectivity, limited solubility, poor biodistribution, and drug aggregation [28]. Since the main aim of drug delivery is to attain and maintain the required therapeutic concentration of the drug in plasma, or at the site of action, for the period of treatment [278], controlled drug delivery presents several advantages. It reduces premature degradation, improves

drug uptake, sustains drug concentrations within the therapeutic window, and reduces side effects associated with toxicity [279]. Hence, the concept of efficient drug delivery is important in disease management [27].

Over the past three decades, polymeric materials have played an important role in the controlled release of therapeutic agents over extended periods [232]. Due to their desirable characteristics, polymers are premier choices for localized, targeted, and controlled delivery of cancer drugs [232,233]. Biodegradable polymeric drug delivery systems have also been used to achieve the controlled delivery of drugs, macromolecules, cells, and enzymes [101,178,219,280]. Biopolymers have been used extensively in drug delivery applications. Their increased use is due to their biocompatibility and favorable degradation properties. These result in the breakdown of biopolymers to produce nontoxic byproducts [281,282].

Prodigiosin (PGS) and paclitaxel (PTX) were used as our model drugs. PGS is a natural red pigment produced as a secondary metabolite by numerous bacterial species, which include *Serratia marcescens*, *Pseudomonas magneslorubra*, *Vibrio psychroerythrous, Serratia rubidaea*, *Vibrio gazogenes*, *Alteromonas rubra*, *Rugamonas rubra,* and Gram positive actinomycetes, such as *Streptoverticillium rubrireticuli* and *Streptomyces longisporus ruber* [122–125,283]. Some members of the PGS family have antifungal, antimicrobial, antitumor, and immunosuppressive properties, and apoptotic effects *in vitro* [128–131,283]. PTX, also known as Taxol, is a natural product that was isolated from the yew tree *Taxus brevifolia* [103,284]. PTX is used as a chemotherapeutic agent and has been reported to have a broad spectrum of antitumor activity [284,285].

To design controlled drug release systems for effective therapy, it is critical to understand drug release kinetics and thermodynamics. The kinetics of drug release conveys relevant knowledge

about the function of material systems [286]. Mathematical models can be used to evaluate drug release mechanisms and kinetics [250]. Furthermore, thermodynamic parameters such as enthalpy (ΔH), entropy (ΔS), and Gibbs free energy (ΔG) can be used to explain the drug kinetic release profiles [287]. Even though there has been extensive research on drug delivery systems, relating the drug release parameters with their thermodynamic parameters is still in its infancy [287,288].

In an effort address this unmet need, polymeric microspheres were developed using the W/O/W emulsion technique [289,290] in order to explore the kinetics and thermodynamics of anticancer drug release. The polymers of choice are poly (lactic-co-glycolic acid) (PLGA), chitosan, and polyethylene glycol (PEG). PLGA and PEG are biocompatible polymers that have been approved by the Food and Drug Administration (FDA) for use in the field of drug delivery [234–236]. The drug release characteristics of PLGA are tunable by altering the ratios of polylactic acid and polyglycolic acid [234]. PEG decreases interactions with blood components [235]. Chitosan is a naturally abundant polymer and is useful in medicine due to its biodegradability, biocompatibility, mucoadhesive, and nonimmunogenic properties, together with its ability to enhance the penetration of large molecules across mucosal surfaces [291]. These polymers have been used in several investigations related to drug delivery applications in cancer treatment [290,292–294].

The physicochemical and morphological properties of synthesized PLGA-CS-PEG microspheres were characterized using Fourier transform infrared spectroscopy (FTIR) and scanning electron microscopy (SEM). Mathematical models were used to analyze the kinetics and thermodynamics of the *in vitro* drug release from the microspheres at hyperthermic and human body temperatures [101,178]. Alamar blue assay was used to evaluate the cell viability and drug-induced cytotoxicity on triple-negative breast cancer cells [101,178]. The implications of the results are then discussed

as they relate to the development of drug-encapsulating microspheres for controlled release of cancer drugs in triple-negative breast cancer treatment.

4.2 Materials & Experimental Methods

4.2.1 Materials

Chitosan (low molecular weight, 75–85% deacetylated), Poly vinyl alcohol (PVA) (98% hydrolyzed, MW = 13,000–23,000), and Poly (D, L-lactide-co-glycolide) (PLGA 65:35, viscosity 0.6 dL/g) were obtained from Sigma-Aldrich (St. Louis, MO, USA). One percent glacial acetic acid, Polyethylene glycol (PEG) (8000), Phosphate Buffer Saline (PBS), and Dichloromethane (DCM) were acquired from Fisher Scientific (Hampton, NH, USA). Prodigiosin (PGS) was synthesized in Soboyejo's Laboratory at the Worcester Polytechnic Institute (WPI), Worcester, MA, USA. Ninety-six well plates and paclitaxel (PTX) were obtained from Thermo Fisher Scientific (Waltham, MA, USA). For cell culture and *in vitro* cell viability studies, Leibovitz's-15 (L-15), Fetal Bovine Serum (FBS), trypsin-ethylenediamine-tetra-acetic acid (Trypsin-EDTA), Penicillin–streptomycin, Dulbecco's phosphate-buffered saline (DPBS), and Alamar Blue Cell Viability reagent were also purchased from Thermo Fisher Scientific (Waltham, MA, USA). All reagents used were of analytical grade.

4.2.2 Preparation of Drug-loaded PLGA-CS-PEG Microspheres

Drug-loaded blend of PLGA-CS-PEG microspheres were prepared using the water-oil-water (W/O/W) emulsions method with slight modifications [289,290]. Briefly, 100 mg of PLGA polymer was dissolved in 3 mL of organic solvent (dichloromethane). This was followed by adding

5 mg/mL or 8 mg/mL of PGS or PTX, respectively, to form primary emulsions. Chitosan solution (4% *w/w*) was prepared in 1% glacial acetic acid, filtered, and then added to the aqueous PVA solution. PEG (5%, *w/w*) with a molecular weight of 8 kD was added to the aqueous PVA and chitosan solution before emulsification to produce PLGA-CS-PEG microparticles.

The emulsification was done in an aqueous PVA solution (12 mL, 2% *w/v*) to form an oil-in-water (o/w) emulsion using an Ultra Turrax T10 basic homogenizer (Wilmington, NC, USA), set at a speed of 30,000 rpm for 3 min over an ice bath. The emulsion was kept in a magnetic stirrer that was operated overnight at 1000 rpm for the evaporation of the organic solvent. Next, the emulsifier and nonincorporated drugs were rinsed off. A VirTis BenchTop Pro freeze dryer (VirTis SP Scientific, Stone Ridge, NY, USA) was used to lyophilize the recovered microparticles for 48 h. The nonloaded PLGA-CS-PEG microparticles were also prepared as described above without incorporating the drug.

4.2.3 Characterization of the microparticles

SEM (JEOL 7000F, JEOL Inc., Peabody, MA, USA) was used to characterize the structure of the microparticles. Prior to the SEM session, the freeze-dried drug-encapsulated PLGA-CS-PEG microparticles samples were mounted on double-sided copper tape, with the other end affixed to an aluminum stub. This was followed by sputter-coating the resulting microparticles with a 5 nm gold–palladium layer. The ImageJ software package (National Institutes of Health, Bethesda, MD, USA) was then used to analyze the mean diameter of the microparticles.

The physicochemical properties of the drug-loaded PLGA-CS-PEG microparticles were analyzed using Fourier transform infrared spectroscopy (FTIR) (IRSpirit, Shimadzu Corporation, Tokyo,

Japan). Using the IR solution software package (ver.1.10) (IRSpirit, Shimadzu Corporation, Tokyo, Japan), the lyophilized drug-encapsulated PLGA-CS-PEG microparticles were scanned at 4 mm/s at a resolution of 2 cm^{-1} from 400 to 3500 cm^{-1}.

4.2.4 *In vitro* drug release

After encapsulating PGS (5 mg/mL or 8 mg/mL) or PTX (5 mg/mL or 8 mg/mL) in their blend of PLGA-CS-PEG polymer, a thirty-day *in vitro* drug release study was carried out in a bid to analyze the kinetics and thermodynamics of *in vitro* drug release. The *in vitro* drug release experiments were carried out at three temperatures: 37, 41, and 44 °C. The first temperature (37 °C) corresponds to human body temperature while the later (41 °C and 44 °C) correspond to hyperthermic temperatures.

For each formulation, 10 mg of lyophilized PLGA-CS-PEG microparticles were suspended separately in a centrifuge tube containing 10 mL of PBS (pH = 7.4) with 0.01% (*v/v*) Tween 80 to maintain sink condition. This was done in triplicate for each formulation. Then, for *in vitro* drug release process, the centrifuge tubes containing samples were positioned back into the orbital shaker (Innova 44 Incubator, Console Incubator Shaker, New Brunswick, NJ, USA) rotating at 80 rpm and maintained at the respective set temperatures (37, 41, and 44 °C). At the predetermined time duration, 1 mL of the centrifuged supernatant was obtained for drug content analysis and then replaced with 1 mL PBS (pH 7.4). The samples in the centrifuge tubes were swirled gently and returned into the shaker incubator to continue the drug release study.

A UV–visible spectrophotometer manufactured by UV-1900 Shimadzu Corporation, Tokyo, Japan, was employed to evaluate the absorbance of each 1 mL supernatant sample released at set

temperatures after 24 h. To measure the absorbance for prodigiosin (PGS) analysis, the wavelength of the UV–visible spectrophotometer was fixed at 535 nm and 229 nm for PGS and PTX, respectively. The concentrations of drug (PGS or PTX) released from their respective PLGA-CS-PEG microparticles loaded with drugs were determined from a standard curve [245].

In addition, to determine the drug encapsulation efficiencies of drug-loaded PLGA-CS-PEG microspheres, a predetermined amount of drug-loaded PLGA-CS-PEG microparticles was dissolved in DCM. The UV–visible spectrophotometer was used to determine the concentration of drug in the suspension.

Equation (1) was used to determine the *Drug Encapsulation Efficiency (DEE)* of drug-loaded PLGA-CS-PEG microparticles:

$$Drug\ Encapsulation\ Efficency\ (DEE) = \frac{M_X}{M_Z} \times 100 \qquad (1)$$

where M_x represents the amount of drug that was encapsulated and M_z represents the amount of drug used for preparing the PLGA-CS-PEG microparticle.

4.2.5 *In vitro* cell viability

Several studies have demonstrated *in vitro* and *in vivo* studies that PGS, or PTX, has anticancer activity against breast cancer [43,101,178,241]. In this context, to investigate the potential anticancer effect of these drugs (PGS and PTX), Alamar blue assay was carried out on MDA-MB-231 breast cancer cells. The percentage of Alamar blue reduction was used to measure the cell viability with or without treatment with drug-loaded microparticles. A higher percent reduction value implies a higher cell growth and, by extension, a higher cell viability. The breast cancer cell line (MDA-MB-231) was obtained from American Type Culture Collection (ATCC) (Manassas,

VA, USA). The passage number of used cell culture was 10, and the cells were maintained under standard cell culture conditions to prevent contamination by mycoplasma, bacteria, fungi, and virus. The materials and supplements used for the cell culture were sterile and all cell culture procedures were carried out in a Labconco Delta Series Purifier Class II Biosafety Cabinet (Labconco Corporation, Kansas City, MO, USA). The dosage levels used was based on prior studies [43,101,178]. The cells were incubated with drug-loaded PLGA-CS-PEG microspheres or nonloaded PLGA-CS-PEG microsphere suspension at 10 mg/mL, respectively, at time intervals 0, 6, 24, 48, and 72 h. In addition, the cells were treated with free PTX and PGS at 15 µM concentration at the time intervals.

In this study, a complete cell culture medium referred to as Leibovitz's 15+ (L15+) was used. L15+ contains Leibovitz's 15 (L15), 10% FBS, and 2% penicillin/streptomycin. MDA-MB-231 cells were cultured in a T75 flask using L15+ medium and incubated in a humidified incubator set at 37 °C. The cells were harvested at 70–80% confluence (log phase of growth) using trypsin-EDTA. Alamar blue cell viability assay was used to perform the *in vitro* cell viability and drug-induced cytotoxicity studies on MDA-MB-231 cells, as described in our previous work [178]. Approximately 10^4 cells per well were seeded in 24-well plates ($n = 4$) [178]. Prior to the cell culture experiments, the drug-loaded microspheres were exposed to UV light under sterile conditions. Three hours post cell seeding, the L15+ medium was replaced with 1 mL of L15+ containing 10 mg/mL of PLGA-CS-PEG microparticles loaded with drugs and the plates were incubated at 37 °C and 5% CO_2 for 3 h in a humidified incubator. At predetermined time intervals (0, 6, 24, 48, and 72 h after the incorporation of the drug-loaded microspheres), the L15+ medium was replaced with L15+ containing 10% Alamar blue reagent. After incubating the plates for 3 h at 37 °C and 5% CO_2, 100 µL aliquots were transferred into duplicate wells of a black opaque 96-

well plate for fluorescence intensity measurements using a 1420 Victor3 multilabel plate reader (Perkin Elmer, Waltham, MA, USA) set at 544 nm excitation and 590 nm emission. Similar protocol was followed to assess the cell viability of nonloaded PLGA-CS-PEG microparticles and free drugs. The nonloaded PLGA-CS-PEG microparticles acted as the control. The percentage Alamar blue reduction data were normalized to the time 0 values (time 0) such that the initial values approximated 100% cell viability.

Equations (2) and (3) were used to determine the percentage (%) Alamar blue reduction and the percentage (%) cell growth inhibition [178]:

$$\% \, Alamar \, Blue \, Reduction = \frac{FI_{sample} - FI_{10\%AB}}{FI_{100\%R} - FI_{10\%AB}} \times 100, \qquad (2)$$

$$\% \, Growth \, Inhibition = \left(1 - \frac{FI_{sample}}{FI_{cells}}\right) \times 100, \qquad (3)$$

where FI_{sample} is the sample's fluorescence intensity, $FI_{10\%AB}$ is 10% Alamar blue reagent fluorescence intensity, $FI_{100\%R}$ is 100% reduced Alamar blue fluorescence intensity, and FI_{cells} is the fluorescence intensity of untreated cells [178].

4.2.6 Statistical analysis

Statistical analysis was carried out using the analysis of variance (ANOVA) test. The statistical analysis includes two-way ANOVA testing of the cell viability and cytotoxicity data. It also includes one-way ANOVA testing of drug release data. This was used to evaluate the differences between the control and the study groups. Thus, $p < 0.05$ was used to determine the significance. Post hoc Tukey tests were also used to distinguish between statistically significant groups. All the

experimental results were reported as mean ± standard deviation. All experiments were carried out in triplicate unless otherwise stated.

4.3 Kinetics and Thermodynamics Modeling

4.3.1 Kinetics Modeling

The mechanism of drug release from the various PLGA-CS-PEG microsphere formulations was investigated using zeroth order, first order, Higuchi, and Korsmeyer–Peppas mathematical models. The drug release data were fitted to the four kinetic models and R^2 value close to 1 was the criterion for selection of the best fit model.

Zeroth order model describes the drug release in which the release rate does not depend on concentration [250]. ***First order model*** is associated with the dissolution of water-soluble drugs in porous matrices [252]. This model reveals a release rate that depends on concentration [251]. ***Higuchi model*** characterizes the release from polymer matrices [155,253]. Using Fick's first law, the Higuchi model describes release of drug from insoluble matrix as a square root of time [252,253]. ***Korsmeyer–Peppas (K–P) model*** explores the drug release from polymeric matrix systems and is only applicable to the first 60% of drug release [251,252]. For K–P drug release, a plot of log $\frac{M_t}{M_\infty}$ vs. log t was used to obtain the slope, n, of the resulting line, which corresponds to the underlying mechanism of drug release. For example, $n < 0.45$ corresponds to a Fickian diffusion mechanism, while $0.45 < n < 0.89$ corresponds to non-Fickian transport, $n = 0.89$ corresponds to Case II (relaxational) transport, while $n > 0.89$ corresponds to super case II transport [238,251,253].

The equations for the respective models are summarized in Table 4.1

Table 4.1. Kinetic models and their respective equations

Serial Number	Kinetic Model	Equation
1	Zeroth order	$Q_t = Q_O + K.t$
2	First order	$\log Q_t = \log Q_0 + {Kt}/{2.303}$
3	Higuchi	$Q_t = K.t^{1/2}$
4	Korsmeyer–Peppas (K–P)	$\dfrac{M_t}{M_\infty} = Kt^n$

where Q_0 is the initial amount of drug in the solution, Q_t is the cumulative amount of drug released at time t, and K is the kinetic constant, t is the time, $\dfrac{M_t}{M_\infty}$ is a fraction of drug released after time t, and n is the release exponent.

4.3.2 Thermodynamics Modeling

The data for the *in vitro* release of drug from PLGA-CS-PEG microspheres were used to calculate the thermodynamic parameters: activation energy (E_a) and the enthalpy (ΔH), Gibbs free energy (ΔG), and the entropy (ΔS) changes [254,255]. This paper uses expressions from prior studies [101] to estimate the thermodynamic parameters. These are summarized in Table 4.2, where their mathematical expressions are presented. The magnitude and signs of these parameters provide insight to the spontaneity and feasibility of drug release processes from the microspheres.

Table 4.2. Thermodynamic parameters and their respective mathematical expressions.

Serial Number	Name of Equation	Mathematical Expression
1	Arrhenius (1st form)	$K_t = D_f e^{\frac{E_a}{RT}}$
2	Arrhenius (2nd form)	$lnK_t = lnD_f - \frac{E_a}{R} \times \frac{1}{T}$
3	Eyring	$\ln\frac{K_t}{T} = -\frac{\Delta H}{R}\frac{1}{T} + \ln\frac{K_B}{h} + \frac{\Delta S}{R}$
4	Change in Gibbs free energy	$\Delta G = \Delta H - T\Delta S$

In the expressions presented, R is 8.314 J mol^{-1} K^{-1}, which represents the universal gas constant, T is the absolute temperature in Kelvin, the thermodynamic equilibrium constant is K_t, E_a is the activation energy, and the pre-exponential factor is denoted by D_f. A Van Hoff plot of ln K_t vs. $1/T$ was used to estimate E_a (kJ mol^{-1}). Thus, the gradient gives $-\frac{E_a}{R}$. Given the Eyring expression for K_t, when a plot is for ln K_t vs. $1/T$ is linear, then the gradient of the plot equals the enthalpy change and intercept of the plot equals entropy change [254]. Hence, the gradient m is given as $-\frac{\Delta H}{R}$ and $\ln\frac{K_B}{h} + \frac{\Delta S}{R}$ equals the intercept c, respectively, where K_B is the Boltzmann constant with value 1.38065×10^{-34} m^2 kg s^{-2} K^{-1}, ΔS is change in entropy, h is Planck's constant (6.626×10^{-34} J sec), and ΔH is the enthalpy change.

4.4 Results and Discussion

4.4.1 Microparticle characterization

Figure 4.1(a-e) shows the morphological analysis (SEM) that the particles were spherical in shape with a smooth surface for all formulations. The morphology of the drug-loaded microspheres was not significantly different from that of the nonloaded PLGA-CS-PEG microspheres, which implies that the morphologies of the PLGA-CS-PEG microspheres were not significantly affected by drug encapsulation. Figure 4.2 reveals that the mean particle sizes of the microparticles ranged from 1.17 μm to 1.39 μm.
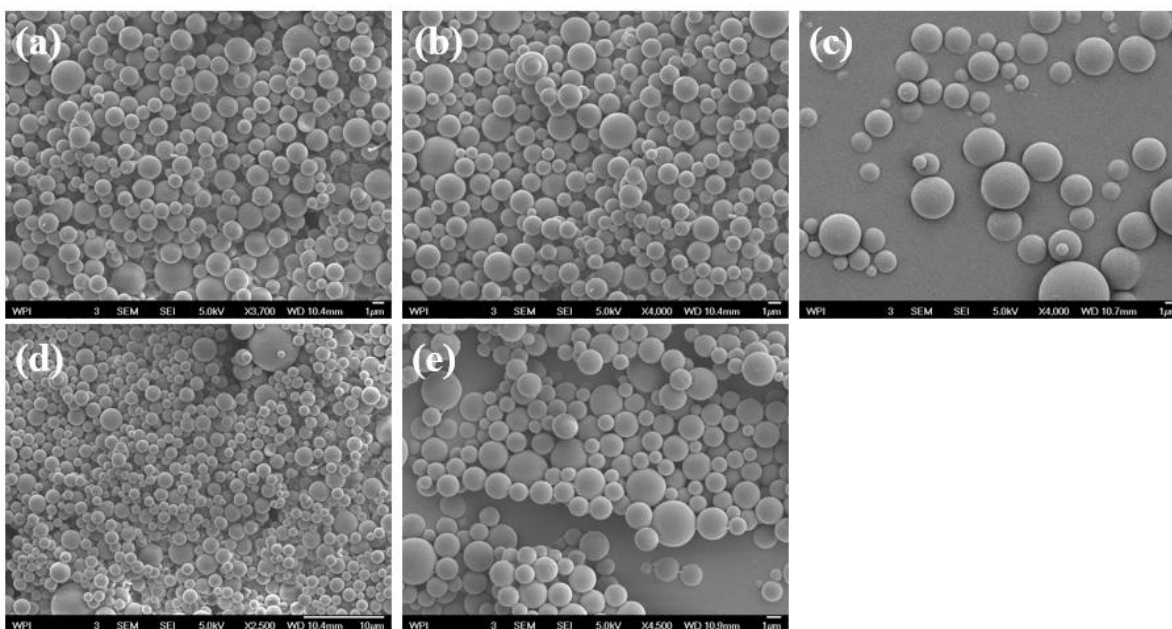
Figure 4.1. SEM pictures of PLGA-CS-PEG microsphere formulations (a) PLGA-CS-PEG_PGS5 (b) PLGA-CS-PEG_PGS8 (c) PLGA-CS-PEG (d) PLGA-CS-PEG_PTX5 (e) PLGA-PEG_PTX8 microspheres
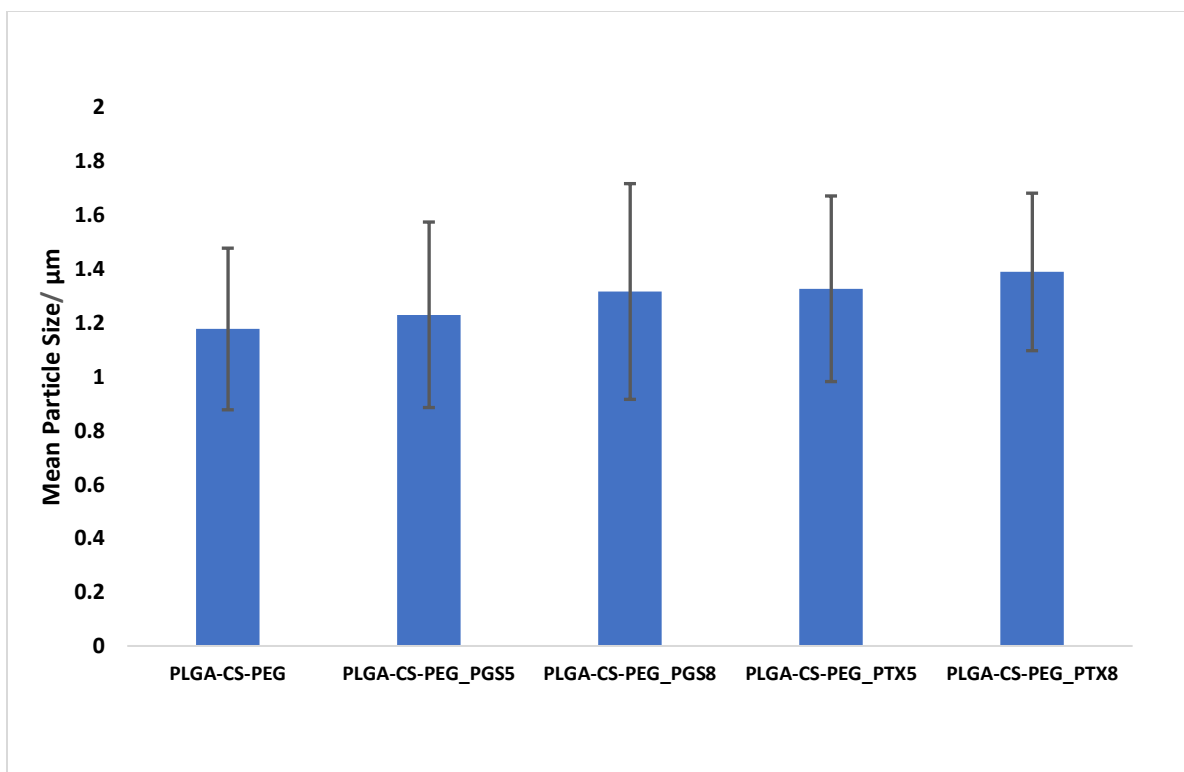
Figure 4.1(f) Mean particle size of PLGA-PEG microspheres using Image J Software**.**

FTIR analysis was used to confirm the existence of CS and PEG on PLGA-CS-PEG microspheres. It was also used to study the interactions between the drug and polymer matrix. A representative FTIR spectrum for the PLGA-CS-PEG microspheres is shown in Figure 4.2. There was no evidence of strong bonds between the respective drugs (PGS or PTX) and PLGA-CS-PEG microparticles. In the FTIR spectrum, the characteristic band at 3422 cm^{-1} is attributed to –NH$_2$ and –OH groups stretching vibration in the chitosan matrix [295] and followed by a peak at ~2995 cm^{-1} due to the amino group. The strong band at 1749 cm^{-1} corresponds to the C=O stretching vibration of the carbonyl in the lactide and glycoside structure [296]. The characteristic peak revealed at 1084 cm−1of the PEG polymer is attributed to the C–O–C stretching vibration of the repeated—OCH2CH2—units of the PEG backbone. The occurrence of these characteristic peaks

indicate that PEG and CS were successfully coated onto the microspheres. Other peaks obtained in the fingerprint region are shown in Figure 4.2.
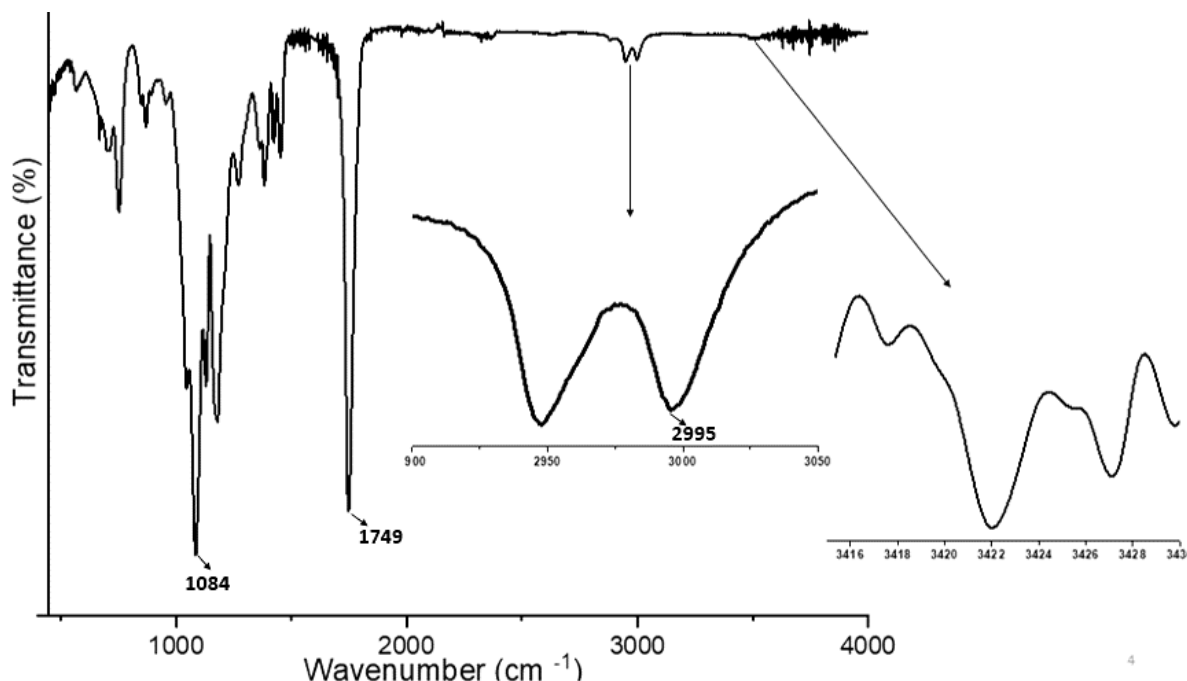
Figure 4.2: A representative FTIR spectrum for the respective PLGA-CS-PEG microspheres synthesized.

4.4.2 *In vitro* drug release

Figure 4.3(a-d) illustrates the profiles for *in vitro* drug release from PLGA-CS-PEG microspheres in PBS (pH 7.4, 0.01% Tween 80) at 37, 41, and 44 °C. The four types of PLGA-CS-PEG microsphere formulations (PLGA-CS-PEG_PGS5, PLGA-CS-PEG_PGS8, PLGA-CS-PEG_PTX5, and PLGA-CS-PEG_PTX8) all exhibited controlled drug release with over 50% release by the end of day 30. After 48 h, the initial burst release for each microsphere formulation is presented in Table 4.3. The initial burst release depended on the drug type encapsulated. In the

case of PGS loaded PLGA-CS-PEG microspheres, a lower burst release was observed. This could be as a result of the hydrophilic and hydrophobic moieties in the PGS drug [101,178]. For PLGA-CS-PEG microspheres encapsulated with PTX drug, a higher release was noticed. Similar findings have been reported in previous studies [101,178]. The results also revealed that PLGA-CS-PEG microspheres loaded with 8 mg/mL concentration of drug have an overall higher burst release than PLGA-CS-PEG microspheres loaded with a drug concentration of 5 mg/mL. On day 30, the overall cumulative drug release reveals a similar pattern for the respective drug-loaded microspheres. It is also important to note that the overall % CDR after the 30 day release was slightly lower for paclitaxel-loaded PLGA-CS-PEG microsphere than prodigiosin-loaded PLGA-CS-PEG microspheres, which could be ascribed to the hydrophobic moiety of PTX drug [101,178].

(a)

(b)

(c)

(d)
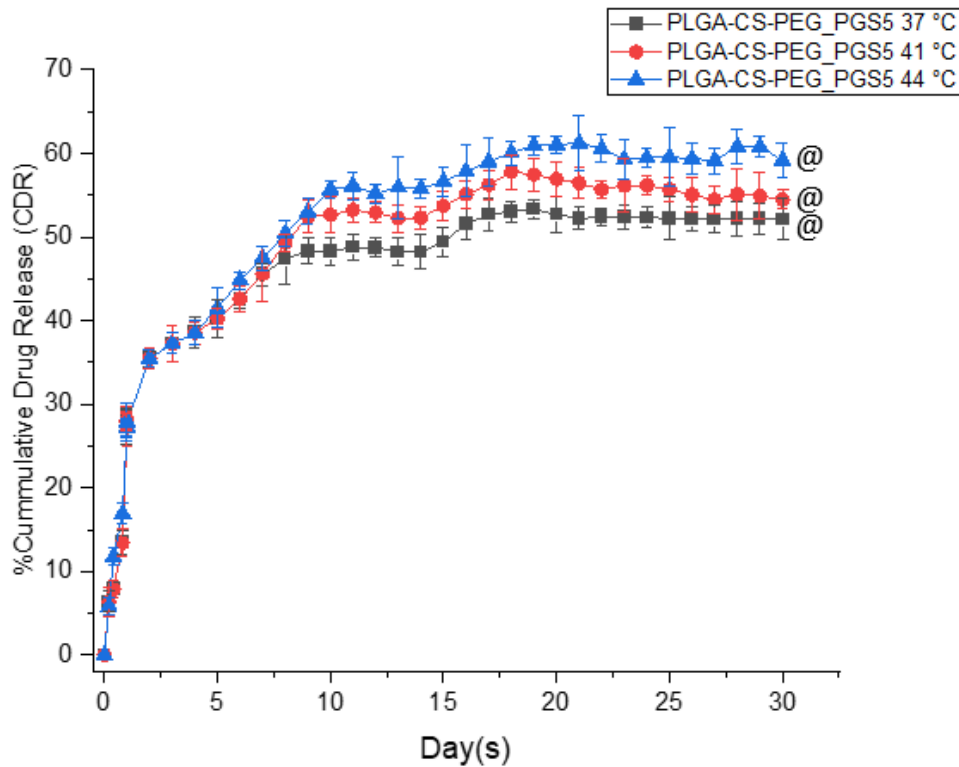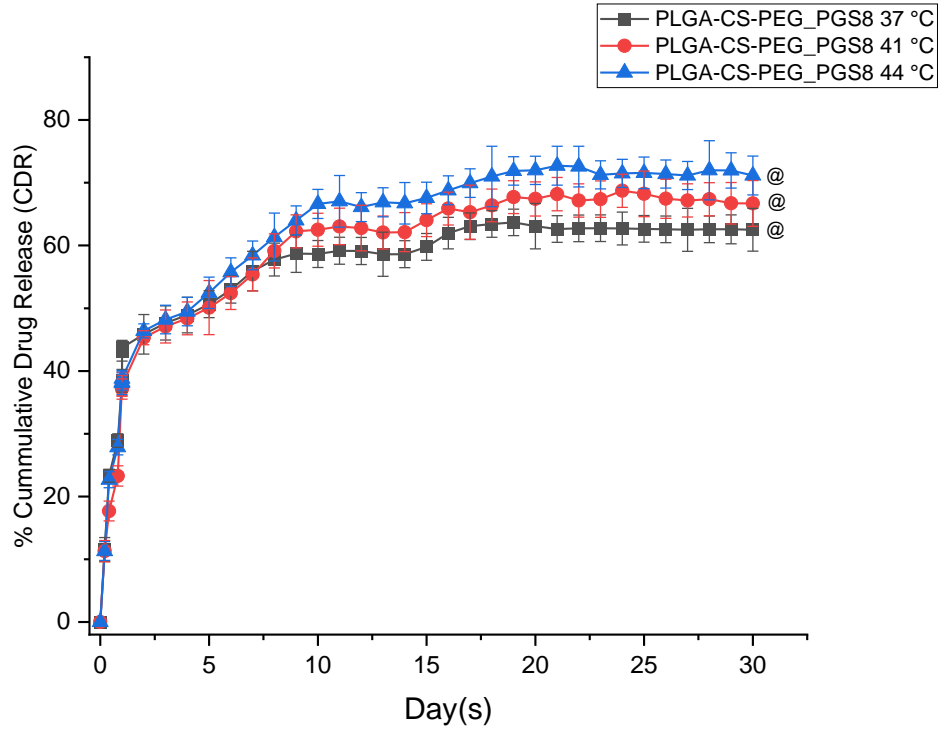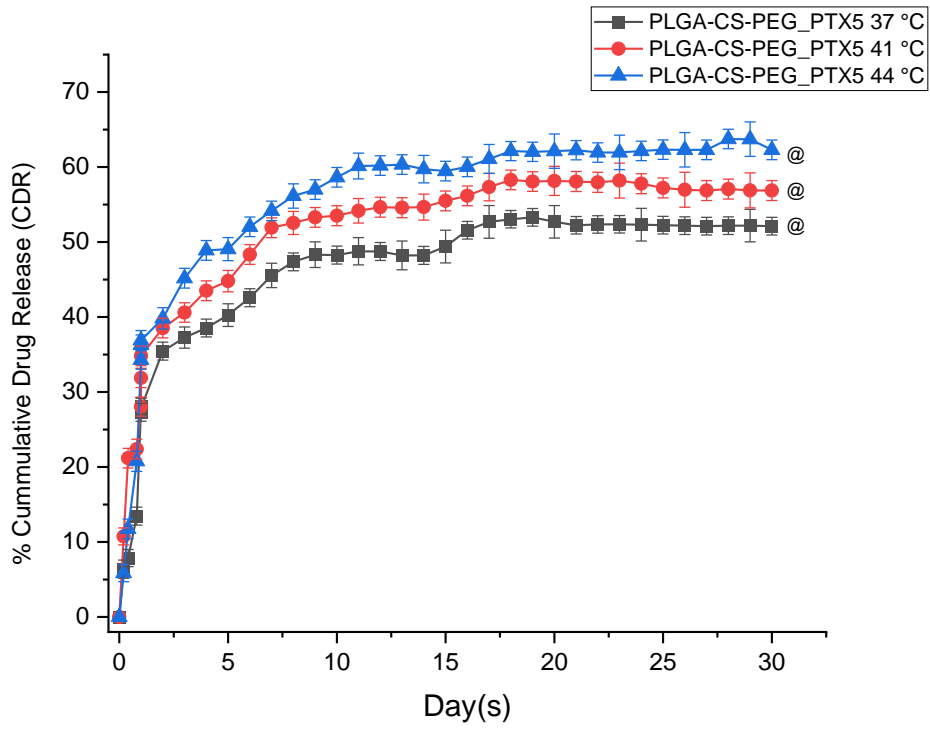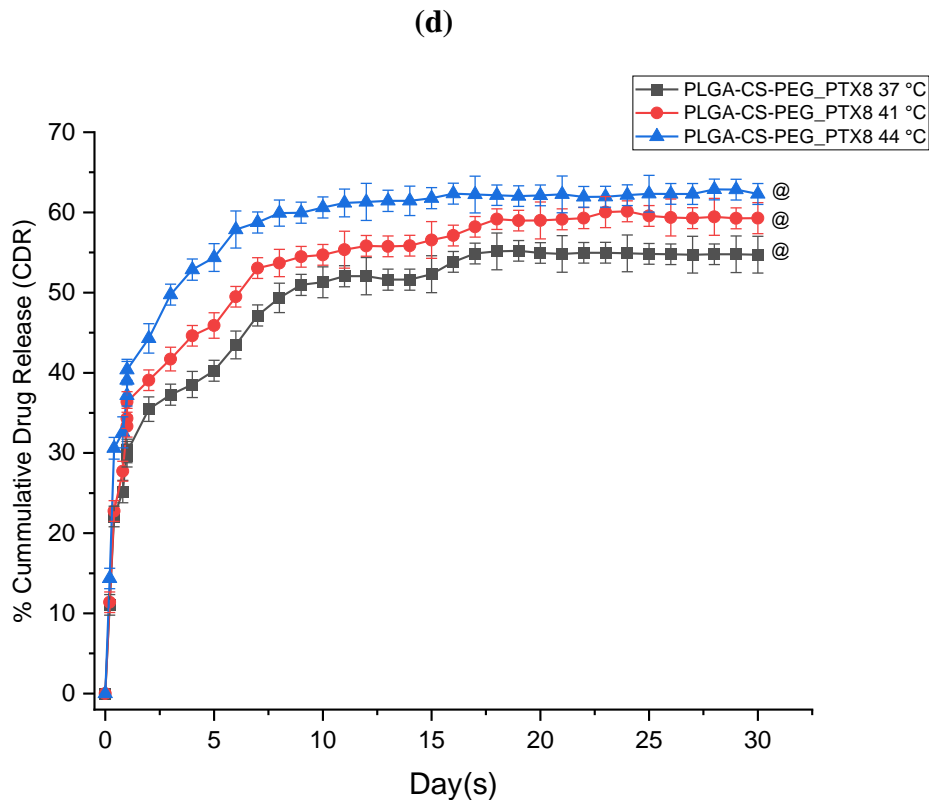
Figure 4.3. *In vitro* drug release profile of drug-loaded PLGA-CS-PEG microspheres: (**a**) PLGA-CS-PEG_PGS5, (**b**) PLGA-CS-PEG_PGS8, (**c**) PLGA-CS-PEG_PTX5, and (**d**) PLGA-CS-PEG_PTX8 performed in phosphate-buffered saline (pH = 7.4, 0.01% Tween 80) at set temperatures (37, 41, and 44 °C). In all cases ($n = 3$, @ $p > 0.05$). Error bars represent the standard deviation for $n = 3$.

The drug encapsulation efficiencies for the PLGA-CS-PEG_PGS5, PLGA-CS-PEG_PGS8, PLGA-CS-PEG_PTX5, and PLGA-CS-PEG_PTX8 microspheres were determined to be 56.5%, 58.5%, 57.5%, and 56%, respectively, and are presented in Table 4.3. Furthermore, the drug release profiles were similar at the set temperatures (37, 41, and 44 °C), which implies that the variation in temperature used during the drug release do not significantly (p-value > 0.05) influence the drug release profiles for the PLGA-CS-PEG microspheres. However, comparing the respective cumulative drug release, the results were significant with p-value < 0.05. Overall, these results

suggest the potential of drug-loaded microspheres for controlled release of therapeutic levels of anticancer drugs were within clinically relevant durations [178].

Table 4.3. Parameters for *In vitro* Drug Release from PLGA-CS-PEG Microspheres as a Function of Time and Temperature

Formulations	Drug release temperature (°C)	Percentage burst release after 48 h	Encapsulation Efficiency (%)	Percentage cumulative drug release for 30 days
PLGA-CS-PEG_PGS5	37	27.290 ±2.074	56.5	52.117±2.506
PLGA-CS-PEG_PGS5	41	27.290 ±1.031		54.471±1.095
PLGA-CS-PEG_PGS5	44	27.130 ±1.031		59.151±2.084
PLGA-CS-PEG_PGS8	37	28.910 ±1.082	58.5	62.502 ± 3.412
PLGA-CS-PEG_PGS8	41	23.277 ±1.230		66.700 ±3.641
PLGA-CS-PEG_PGS8	44	27.872 ±1.807		71.153 ± 3.103
PLGA-CS-PEG_PTX5	37	28.055 ±1.157	57.5	52.117 ±1.172
PLGA-CS-PEG_PTX5	41	28.055 ± 1.270		56.862 ±1.329
PLGA-CS-PEG_PTX5	44	34.275 ± 1.231		62.300 ±1.309
PLGA-CS-PEG_PTX8	37	30.400 ±1.310	56.0	54.728 2.290
PLGA-CS-PEG_PTX8	41	33.323 ±1.346		59.287 1.930
PLGA-CS-PEG_PTX8	44	37.176 ±1.320		62.300 1.300

4.4.3 Drug release kinetic

To understand the *in vitro* drug release kinetics from PLGA-CS-PEG microspheres, four kinetic models were explored. These include the zeroth order model, the first order model, the Higuchi model, and the Korsmeyer–Peppas (K–P) model [250]. The kinetic constant (K) and correlation coefficients (R^2) obtained for the release kinetics are presented in Table 4.4.

It is clear from Table 4.4 that the release kinetics for the various PLGA-CS-PEG microsphere formulations with the highest correlation coefficients R^2 fit the K–P model the best. The release exponents, *n*, were also found to be within the range of $0.45 < n < 0.89$, signifying that the release mechanism was by anomalous non-Fickian diffusion.

Table 4.4: The kinetic constant (K), correlation coefficient (R^2) and Release exponent (n) of kinetic data analysis of drug released from drug-loaded PLGA-CS-PEG Microspheres formulations.

Formulations	Temperature °C	Zero Order		First Order		Higuchi		Koresmeyer-peppas		
		K	R^2	K	R^2	K	R^2	K	R^2	n
PLGA-CS-PEG_PGS5	37	1.162	0.593	0.034	0.418	8.020	0.791	1.277	0.840	0.462
PLGA-CS-PEG_PGS5	41	1.295	0.611	0.037	0.438	8.902	0.809	1.279	0.860	0.482
PLGA-CS-PEG_PGS5	44	1.452	0.672	0.038	0.488	9.811	0.859	1.308	0.894	0.464
PLGA-CS-PEG_PGS8	37	1.146	0.539	0.023	0.415	8.005	0.737	1.179	0.934	0.542
PLGA-CS-PEG_PGS8	41	1.438	0.624	0.029	0.486	9.828	0.817	1.266	0.839	0.494
PLGA-CS-PEG_PGS8	44	1.546	0.648	0.029	0.509	10.507	0.838	1.205	0.948	0.536
PLGA-CS-PEG_PTX5	37	1.162	0.593	0.034	0.418	8.020	0.791	1.277	0.840	0.462
PLGA-CS-PEG_PTX5	41	1.162	0.587	0.027	0.481	8.059	0.791	1.065	0.900	0.522
PLGA-CS-PEG_PTX5	44	1.332	0.575	0.032	0.384	9.238	0.776	1.371	0.814	0.457
PLGA-CS-PEG_PTX8	37	1.122	0.626	0.026	0.530	7.681	0.822	1.081	0.908	0.488
PLGA-CS-PEG_PTX8	41	1.169	0.601	0.025	0.489	8.053	0.799	1.126	0.884	0.483
PLGA-CS-PEG_PTX8	44	1.067	0.494	0.020	0.418	7.620	0.706	1.115	0.913	0.591

4.4.4 Thermodynamics of drug release

Table 4.5 presents the values for the thermodynamic parameters that were calculated from *in vitro* drug release data in this study. The ΔG which is the most important thermodynamic parameter associated with the release process, was positive for PLGA-CS-PEG microspheres, indicating a nonspontaneous natural process. This nonspontaneous process could be attributed to the controlled release of drug from the PLGA-CS-PEG microspheres and probably aids controlled drug release over a one month period [178,281].

Table 4.5. Values for Thermodynamic Parameters for PLGA-CS-PEG Microspheres.

Formulations	Temperature °C/K	E_a (kJ mol^{-1})	ΔS (kJ mol^{-1} K^{-1})	ΔH (kJ mol^{-1})	ΔG (kJ mol^{-1})
	37 / 310.15	2.656	-0.243	0.050	75.415
PLGA-CS-PEG_PGS5	41 / 314.15				76.387
	44 / 317.15				77.116
	37 / 310.15	3.245	-0.242	0.638	75.694
PLGA-CS-PEG_PGS8	41 / 314.15				76.662
	44 / 317.15				77.388
	37 / 310.15	5.653	-0.234	3.047	75.622
PLGA-CS-PEG_PTX5	41 / 314.15				76.558
	44 / 317.15				77.260
	37 / 310.15	3.890	-0.240	1.284	75.720
PLGA-CS--PEG_PTX8	41 / 314.15				76.680
	44 / 317.15				77.400

Figure 4.4 shows a plot of ΔG (kJ mol^{-1}) vs. temperature (K) for PLGA-CS-PEG microspheres. A positive value was obtained for ΔH, which shows that the release of drug from PLGA-CS-PEG microspheres was an endothermic process. Additionally, as the drug diffused in the medium to try

to reach equilibrium, there was reduction in system disorder. This was clearly indicated by the negative values for ΔS for all PLGA-CS-PEG formulations. Such nonspontaneous release may be due to the controlled release and more likely to promote the release of the drug at a controlled rate during a period of one month. The E_a is the energy required to move the drug molecule from within the polymer matrix to the medium. A positive E_a value was obtained for the drug release from PLGA-CS-PEG formulations, with values <10 kJ/mol indicating that the *in vitro* drug release was mainly by diffusion-driven processes.
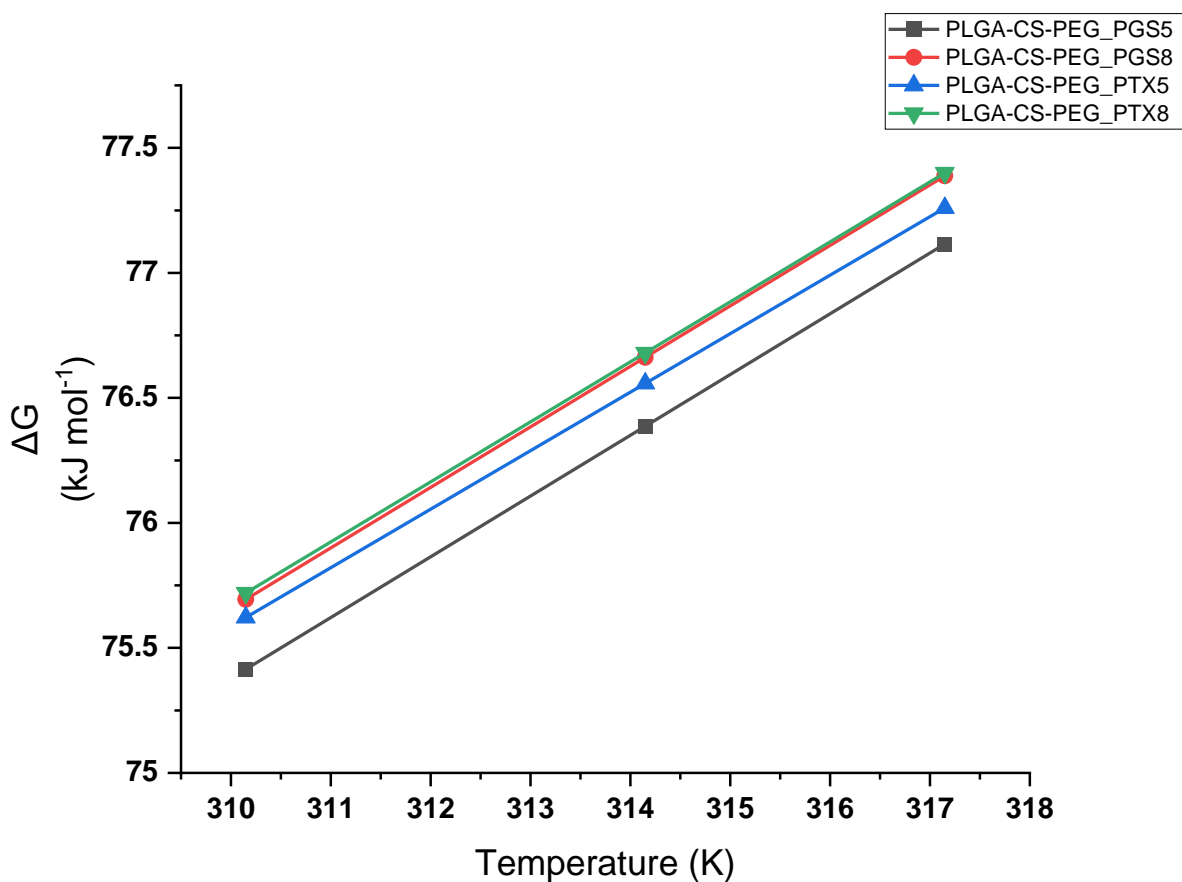
Figure 4.4. A graph of Gibb's free energy versus Temperature for PLGA-CS-PEG Microspheres at different temperatures.

4.4.5 *In vitro* Cell Viability and Cytotoxicity

The data in Figure 4.5a compare the viability of untreated cells with those treated with drug-loaded microparticles after 6, 24, 48, and 72 h post-treatment. At all durations, cell viability was lower for breast cancer MDA-MB-231 cells treated with drug-loaded PLGA-CS-PEG microparticles encapsulating drugs vs. the untreated cells. In addition, the cells treated with paclitaxel-loaded microparticles were less viable than their prodigiosin-loaded counterparts. Among the treated cells, increasing the concentration of prodigiosin and paclitaxel in PLGA-CS-PEG microparticles resulted in decreased cell viability, as manifested in the lower normalized percentage Alamar blue reduction values. There was an initial decline in the viability of the treated cells after 6 h of exposure followed by a gradual rise in cell viability until 72 h. In the case of the paclitaxel-loaded PLGA-PEG-CS microparticles at 8 mg/mL, the viability continued to decrease after 6 h. There was an initial decline in the viability of the treated cells after 6 h of exposure followed by a gradual rise in cell viability until 72 h, except for the paclitaxel-loaded PLGA-PEG-CS microparticles at 8 mg/mL concentration, which continued to decline further. The initial decline in cell viability was probably due to the initial burst release of the drugs from the microparticles that shocked the cells, which were still in their lag growth phase and in their most fragile state.
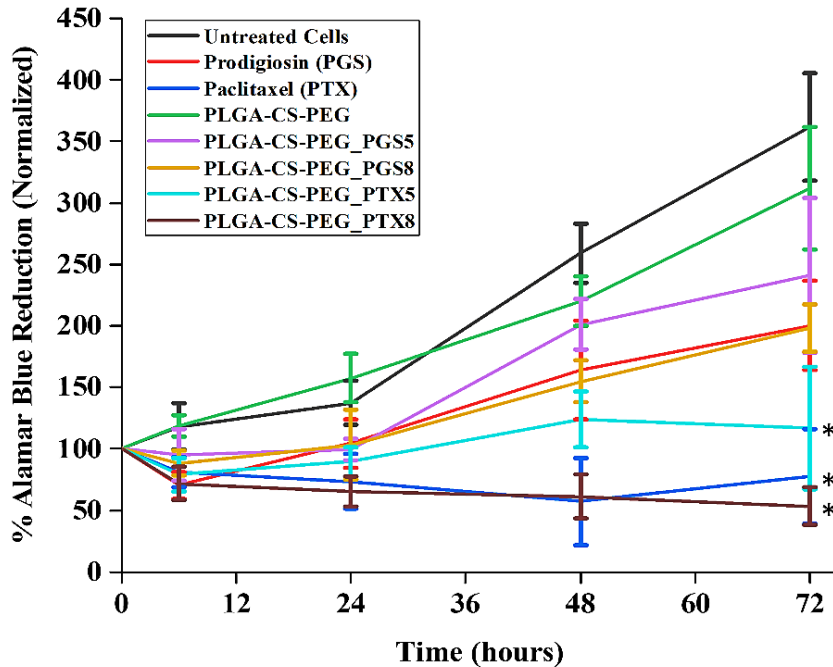
Figure 4.5(a): Percentage Alamar blue reduction for untreated MDA-MB-231 cells and MDA-MB-231 cells treated with nonloaded microspheres, PGS, PGS-loaded microspheres, PTX, and PTX-loaded microspheres at 6, 24, 48, and 72 h post-treatment. Error bars represent the standard deviation for $n = 3$; * $p < 0.05$ (significantly different from untreated cells).

The data in Figure 4.5b show the effect of adding PLGA-CS-PEG microspheres encapsulating drugs to the cells inhibit MDA-MB-231 breast cancer cell growth after 6, 24, 48 and 72 h exposure when compared to the untreated MDA-MB-231 breast cancer cells. Percentage cell growth inhibition was used as a measure of the drug-induced cytotoxicity level. A higher percent inhibition value implies an elevated cytotoxicity level due to drug treatment. Again, the data show that at all durations, paclitaxel-loaded microparticles exhibited higher percent inhibition values than prodigiosin-loaded microparticles, meaning that cells exposed to the former were more cytotoxic than the latter. In addition, increasing the concentration of drugs in the microparticles resulted in

higher cytotoxicity levels as manifested in the higher percent growth inhibition values. In effect, loading the microparticles with 8 mg/mL of paclitaxel was more effective in impeding the growth of MDA-MB-231 breast cancer cells, while prodigiosin at a concentration of 5 mg/mL was least effective.
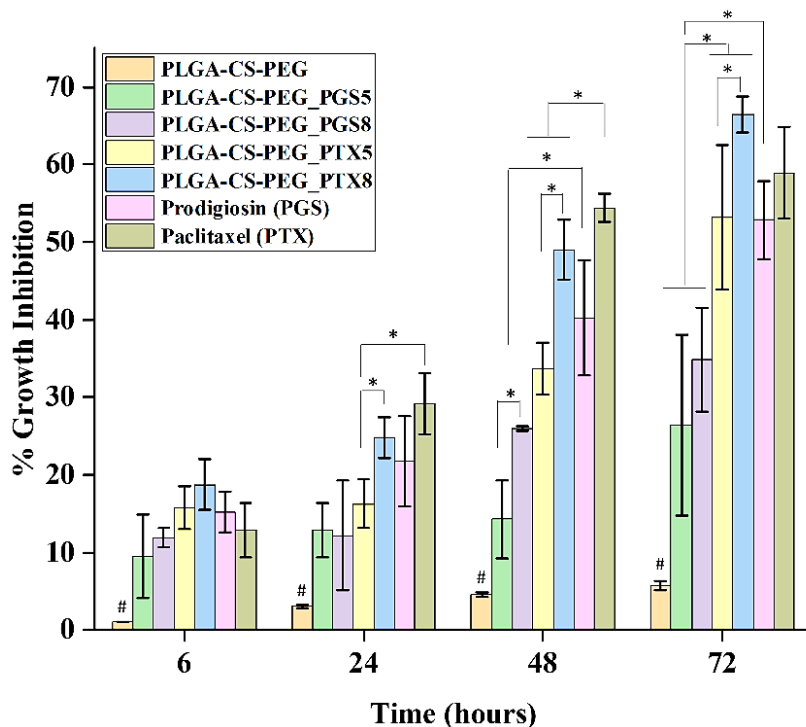
Figure 4.5(b): A graph of percentage cell growth inhibition vs. time for MDA-MB-231 cells treated with nonloaded microspheres, PGS, PGS-loaded microspheres, PTX, and PTX-loaded microspheres at 6, 24, 48 and 72 h post-treatment. Error bars represent the standard deviation for $n = 3$; * $p < 0.05$; # $p < 0.05$ (significantly lower than the others).

4.5 Conclusion

This study suggests that the combination of PLGA, CS, and PEG can be used to form microspheres for the controlled release of cancer drugs such as paclitaxel and prodigiosin into cancer cells and tissues. The purpose of this study is to explore the effects of immobilized drug-loaded

microparticles that are injected into regions from which tumor tissues have been extracted. Unlike the injectable drug-loaded nanoparticles that have sizes below certain critical sizes, the use of immobilized/implantable microparticle systems or scaffolds within a tumor site (after surgical removal of tumor to treat local regional/residual cancer tumor) has been reported to be safe [101,178].

The extended release of paclitaxel and prodigiosin also inhibits the growth (reduces the viability) of MDA-MB-231 cells under *in vitro* conditions (Figure 4.5a–b).

However, although further *in vivo* work is needed to investigate the possible outcome of extended cancer drug (prodigiosin and paclitaxel) release from the microparticles that were produced in this study, the current work does show that the combined use of PEG and CS polymer can be used to control the thermodynamics and the kinetics of the controlled release characteristics (Figure 4.4a–d and Tables 4.4 and 4.5).

Furthermore, since the extended release of prodigiosin and paclitaxel from other PLGA microparticles did not elicit any observable cytotoxic responses in our prior work [101], we are hopeful that the *in vivo* elution of the same drugs (prodigiosin and paclitaxel) from PLGA-CS-PEG PEG microparticles will not induce cytotoxic effects. This suggests that the combination of two hydrophilic polymers (PEG and CS) could be advantageous in terms of preventing the adhesion of blood proteins to the surface, thereby improving the longevity in blood circulation.

In any case, the *in vitro* drug release profiles obtained in this study (Figure 4.4a–d) exhibited a biphasic-controlled drug release from PLGA-CS-PEG microspheres with >50% drug released at day 30. This is because the result is characterized by an initial burst release of drug followed by a constant rate of drug release [297]. Thus, the burst release phase occurs because of the initial

exposure of the microspheres to the phosphate-buffered saline and the next phase basically relates the power-law relationship between cumulative amount of drug release and time [298]. A similar biphasic release was observed in the work of Suphiya Parveen and Sanjeeb K. Sahoo [290]. This controlled release can be attributed to the presence of CS and PEG as a blend, implying that they act as physical barriers that limit diffusion and erosion processes associated with drug transport through the microspheres.

Hence, it was not surprising that the best fit to the drug release data obtained in this study was the Korsmeyer–Peppas model [101,178,238,241]. This model corresponds to n values within the range $0.45 < n < 0.89$, which is consistent with anomalous drug release by a combination of non-Fickian diffusion and erosion by polymer network degradation. The initial stage of drug release is due to diffusion from the polymer microspheres. However, the remaining drugs trapped in the microspheres are only released as the polymer degrades. Therefore, it is necessary to use a degradable material to slow the release of the drugs from the PLGA-CS-PEG microspheres. The use of PLGA polymer enables controlled release of drug due to their biocompatibility and degradability properties. Typically, as the drug-loaded microspheres break down inside the body, they produce nontoxic natural byproducts such as water and carbon dioxide that are easily eliminated [281,282].

The occurrence of erosion by polymer network degradation is attributed to a two-step process in which the blend of hydrophilic polymers on the microspheres first form a swollen structure (due to water absorption) leading to the detangling of chemical, prior to the subsequent erosion of the PLGA microparticles. It is also worth mentioning that, during the burst release phase when poorly encapsulated and surface bound drugs are released, a higher level of burst release was observed

from PTX-loaded microspheres than that observed from PGS-loaded microspheres. In addition, at the set temperatures (37, 41, and 44 °C) similar drug release profiles were seen.

The values obtained for the thermodynamic parameters such as enthalpy (ΔH), entropy (ΔS), and Gibbs free energy (ΔG) showed that the drug release was feasible at 37, 41, and 44 °C. They also revealed that the drug release process was orderly, endothermic, and nonspontaneous.

Finally, it is important to note that the therapeutic potency of the various drug-loaded PLGA-CS-PEG microsphere formulations was assessed using Alamar blue assay. The results confirmed that the MDA-MB-231 breast cancer cell growth was highly repressed by PLGA-CS-PEG_PTX8 microspheres, with PLGA-CS-PEG_PGS5 microspheres being the least efficient. In any case, PLGA-CS-PEG microspheres loaded with drugs exhibited drug release and MDA-MB-231 cell growth inhibition that suggest that they are promising candidates for the controlled release of drugs (paclitaxel and prodigiosin) for triple-negative breast cancer treatment.

Before concluding, it is important to compare the results from this study to the results from a prior study by Jusu *et al.*, (2020) in which similar materials (PLGA-PEG) were used to encapsulate anticancer drugs. As in prior work by Jusu *et al.*, (2020) in which PLGA-PEG microspheres were studied, the current study in which we introduced chitosan into the polymer matrix resulted in the anomalous non-Fickian release of cancer drugs that was well characterized by the Korsmeyer–Peppas model. The drug release at the end of day 30 was also slightly lower for PLGA-CS-PEG microspheres than for PLGA-PEG microspheres at the same time duration.

The slower rate of drug release suggests that extended release of cancer drugs due to the chitosan-PEG blend in the PLGA-CS-PEG microparticles could give rise to further extensions of the drug release durations than those associated with drug release from only PEG blend with PLGA.

Finally, it is important to note here that prior *in vivo* studies of targeted drug release from implanted drug-loaded PLGAPEG microparticles did not reveal any additional cytotoxicity effects after the extended elution of targeted cancer drugs (PGS and PTX) from the microparticles [101]. This suggests that the PLGA-CS-PEG microspheres examined in this study are likely to elute targeted and untargeted drugs for longer durations at lower rates that are not likely to induce any additional cytotoxicity effects.

Chapter 5

5.0 Degradable Porous Drug-Loaded Polymer Scaffolds for Localized Cancer Drug Delivery and Breast Cell/Tissue Growth

5.1 Introduction

Current statistics in 2018 have shown that breast cancer death rates (in women) have declined by 39% over the past 16 years [299]. The progress has been attributed to awareness, improved understanding of tumor biology, as well as improvements in early detection and treatment strategies [299–301]. Despite this good news, breast cancer is still the second most commonly diagnosed, and the leading cause of death in women [301–304]. There have also been significant efforts to develop drug-based polymer scaffolds for localized cancer drug delivery [219,305–313] and other drug delivery systems [219,305–314] to mitigate specific kinds of diseases. These drug systems have been developed to reduce the overall side effects associated with bulk chemotherapy or conventional methods of treatments which often results in severe side effects associated with the transport of cancer drugs to target cancer cells/tissue [219,301,305–309,312].

Furthermore, following the detection/diagnosis of breast cancer, surgical resection of the tumor(s) is often followed by chemotherapy, radiation therapy, hormonal therapy or a combination of these treatment methods [306]. However, in most cases, these conventional cancer treatment strategies can interfere with DNA synthesis and mitosis, leading to uncertain death or rapid growth and division of normal and cancer cells [301]. Hence, an increasing number of breast cancer patients had to undergo a combination of chemotherapy and/or radiation therapy, after breast cancer surgery or mastectomy, due to the high risk of breast cancer recurrence [315].

In several cases, breast reconstruction after surgery are carried out using silicone-based implants that are used to fill the spaces left by resected tumors [316]. This reconstruction process may be associated with soft tissue irritation via capsular contracture and pain. It can also result in undesirable aesthetics [316]. There is, therefore, a need to develop 3D implantable drug-encapsulated and bioresorbable tissue engineered structures/scaffolds that can localize the controlled release of cancer drugs while supporting the subsequent regeneration of normal breast tissue in a way that avoid the need for a follow-up chemotherapy, radiation therapy or silicon-based breast implants.

Prior work [219,305–313] has explored the use of drug polymer scaffolds in localized cancer drug delivery. The studies have shown that the localized delivery of cancer drugs can result in effective treatments with much lower drug doses and limited side effects [317] , compared to those associated with bulk chemotherapy. Although there have been several efforts to develop 2D [301,312,317–320] and 3D [321–323] implantable scaffolds for breast tissue reconstruction after surgery/mastectomy [301,312,317–323], most of the studies have focused on breast tissue regeneration, and not breast reconstruction following drug release from 3D implantable microporous drug-loaded polymer scaffolds. In this study, we developed 3D drug-loaded scaffolds using a blend of FDA approved polymers [polylactic-co-glycolic acid (PLGA), polyethylene glycol (PEG) and polycaprolactone (PCL)] as a model system for breast tissue regeneration, following localized cancer therapeutics.

Since the degradation of 3D scaffolds (that are used for tissue regeneration/reconstruction) may result in the accumulation of acidic degradation products [324], miscible, drug-loaded blends of synthetic biodegradable polymers have been explored in efforts to reduce the drug domain sizes to the molecular scale [325–328]. Such structures have been shown to increase the stability of homogenous amorphous drug-polymer systems [329]with strong H-bonding, acid–base ionic interactions, dipole–dipole interactions, or/and hydrophobicity [329,330].

Furthermore, polymer scaffolds with similar Young's moduli to breast cell/tissue have been shown to result in the production of extracellular matrix (ECM) and improved cell attachment and proliferation [331]. This enhances mechanotransduction and cell signaling during tissue development [331]. 3D scaffolds of PCL with native, tissue-like mechanical properties, have compressive Young's moduli of ~ 300 MPa [332], while porous 3D scaffolds of PLGA (50:50) with tissue-like characteristics have Young's moduli of ~ 2 GPa [333,334]. In the case of PEG scaffolds, Bryant *et al.,* (2004) [335] have reported compressive Young's moduli of ~ 500 kPa for 20% PEG (MW 3000 Da) [335]. These values are much greater than the Young's moduli of human breast tumor tissue and normal breast tissue, which have been reported to have a Young's moduli in the range of ~ 4 - 100 kPa [336–338].

Although, PLGA has been widely used for drug delivery system, their hydrophobicity may be a problem for the formulation of drug delivery systems [339]. Similarly, due to the high hydrophilicity of PEG, it can create accelerated drug release [340]. Therefore, the need to use blend of these polymer was crucial to achieve a desirable drug release profile. In this work, we

leverage the unique characteristics of these individual polymer (PLGA, PEG, PCL) by the combined use of PLGA and PEG or PLGA and PCL which may help to overcome the shortcomings associated with the use of single polymers [341] for localized drug delivery.

In this chapter, we present mechanically robust 3D implantable microporous polymer scaffolds with interconnected microstructural graded pores. These scaffolds are loaded with cancer drug (prodigiosin or paclitaxel) prior to kinetics and thermodynamic studies of controlled cancer drug release. The physicochemical, thermal, mechanical and bio-structural properties of the scaffolds were elucidated. The ability of the resulting scaffolds to support breast tissue regeneration was then explored, following *in vitro* and *in vivo* studies of the effects of localized cancer drug release on cell viability and toxicity. The implications of the results are discussed for the development of 3D scaffolds for the localized chemotherapeutics and tissue regeneration.

5.2 Materials & Experimental Methods

5.2.1 Materials

Poly(lactic-co-glycolic acid) lactide: glycolide (50:50), mol. Wt. 30,000-60,000 and poly(ethylene glycol) (PEG) (Mn = 7000 to 9000) polymers that were used in this study for scaffold fabrication were purchased from Millipore Sigma (St Louis, MO, USA). Also, biodegradable polycaprolactone (PCL), with internal viscosity of 1.0-1.3 dL/g that was used for the drug delivery systems was procured from Durect Corporation (Cupertino, CA, USA), while the paclitaxel drug and dichloromethane (DCM) that was used to dissolve the polymers and the drug were obtained from Thermo Fisher Scientific (Waltham, MA, USA).

Breast cancer cell line (MDA-MB-231) and normal breast cell line (MCF-10A) were purchased from ATCC (Manassas, VA, USA), while Phosphate Buffered Saline (PBS) and 0.1% w/v Tween 80 that were used for *in vitro* drug release, and the cell culture reagents were all purchased from Thermo Fisher Scientific (Waltham, MA, USA). Also, all and the tissue cell culture plates were procured from CELLTREAT Scientific Product (Pepperell, MA, USA). Finally, the Prodigiosin (PGS) drug that was used in this study was synthesized in the Soboyejo Research Group at WPI, as reported in our previous work [219,342].

5.2.2 Fabrication of Drug-Loaded Blends of Porous Scaffolds

In the first case, a blend of PLGA-PCL was prepared by dissolving PLGA and PCL in a ratio of 3:2 in DCM. PLGA and PEG polymers were prepared in a ratio of 1:1 in DCM. The resulting mixture of polymer blend was vigorously stirred at room-temperature ($25^{o}C$) in a capped container using a magnetic stirrer. This was done for 12 h to produce a homogenous mixture. A high viscosity polymer solution was obtained after the complete dissolution of polymer.

Furthermore, in separate containers, solutions of prodigiosin (PGS) or paclitaxel (PTX) drug (each with concentration of 8 mg/ml) were prepared with DCM. These drugs were selected due to their proven anti-cancer activities [219,342]. In each case, the polymer blend and the corresponding drug solution were mixed thoroughly for 6 h to obtain the following drug-based blends of polymers: PLGA-PCL_PGS; PLGA-PCL_PTX; PLGA-PEG_PGS; PLGA-PEG_PTX, and their controls. 3D interconnected microporous scaffolds were produced by casting the resulting drug-

based mixtures in a mold consisting of salt (NaCl) particles with grain sizes < 150 um. This was done using a combination of solvent casting and particulate leaching (in deionized water) to remove NaCl particles.

The resulting scaffolds were then pre-frozen at − 80 °C for 1 h in a TSX40086A Ultra-Low Temperature Freezer (Thermo Fisher Scientific, Waltham, MA, USA), prior to lyophilization for 12 hours at − 80 °C under 110 mm Hg vacuum (BenchTop Pro with Omnitronics Freeze Dryer, SP Scientific, Warminster, PA, USA). Non-drug-loaded PLGA-PEG and PLGA-PCL scaffolds were prepared in the same manner as controls.

5.2.3 Polymer Blend Surface Wettability Analysis

Because of the hydrophobic and hydrophilic characteristics of the blend of polymers, we used contact angle with a water (PBS) droplet to evaluate the hydrophilicity of each blend. In this case, we fabricated thin films of the corresponding blend of polymers and formulations (PLGA-PEG, PLGA-PCL, PLGA-PCL_PGS, PLGA-PEG_PTX, PLGA-PCL_PGS and PLGA-PCL_PTX) using spin coating system (Ni-Lo 4 XL Spin Coater, Nilo Scientific, Ottawa, Canada) that was rotating at 3000 rpm for 1 minute. To each surface of the thin spin coated film of polymer blend, a droplet of PBS was placed before the contact angle measurement (θ) was carried out using a ramé-hart Model 100-00 Goniometer. For each sample group, the contact angle of five different spots on scaffold were measured. Final results of the average value were presented with their error bars. A thin film was used for this experiment because it is almost impossible to get a PBS droplet on the porous scaffold strut to use for the contact angle measurement.

5.2.4 Structural and Mechanical Characterization of Scaffolds.

Since the porosity and integrity of tissue engineered scaffolds are important for cell growth/migration and proliferation [343–345], we studied the porosity of the scaffolds using a liquid displacement method [346,347]. This technique was used to measure densities and porosities of the drug-loaded blend of polymer scaffolds that were prepared from PLGA, PCL, and PEG. Due to the hydrophobicity of the drug-blended polymer, ethanol was used as the penetrating solvent to quantify the porosity of the scaffolds. Ethanol was used as solvent because it does not induce any shrinkage or swelling of the scaffolds during the testing.

After measuring the dimension of the scaffolds using a Vernier caliper, the weight of each scaffold, W_s was determined using a sensitive measuring scale (Smart Weigh Premium High Precision Digital Milligram Scale, Virginia Beach, VA, USA) before submerging it into a graduated cylinder with a recorded volume of ethanol, V_i, until the entire scaffold was soaked with ethanol. Subsequently, the total volume of ethanol and ethanol-impregnated foam was then recorded as V_c. Vr describes the residual volume of ethanol after the soaked scaffold was removed. Therefore, the volume of each porous scaffold is given by, $(V_c - V_i)$, while the volume of ethanol retained in the scaffold is $(V_i - V_r)$. Also, the total volume of each scaffold is given by:

$$V_s = (V_c - V_i) + (V_i - V_r) = (V_c - V_r). \qquad (1)$$

Thus, the density of each porous scaffold was obtained from:

$$\rho_s = \frac{W_s}{(V_c - V_r)} \qquad\qquad (2)$$

while the porosity Φ_s, of each of the drug-loaded scaffold was obtained from:

$$\Phi_s = \frac{(V_i - V_r)}{(V_c - V_r)} \qquad\qquad (3)$$

In each case, the resulting scaffolds were freeze-dried and sputter-coated with 5 nm of gold prior to studies of their morphologies in a Field Emission Scanning Electron Microscope (SEM) (JSM-7000F, JEOL Ltd, Akishima, Tokyo, Japan) that was operated at an acceleration voltage of 3 kV. Consequently, the porous morphologies (mean pore sizes) in the SEM images were analyzed using the ImageJ software package (NIH Image, Scion Image for Windows, National Institute of Health, Bethesda, Maryland, USA). 3D images of the porous scaffold were obtained with high energy micro-computed X-ray tomography (micro-focus CT scanner, VJ Technology, Bohemia, NY, USA) at 12-micron spatial resolution to reveal the interior porous structure. The 2D and 3D structure were visualized and reconstructed using Volume Graphic software (VGSTUDIO MAX, Volume Graphics, Inc., Heidelberg, Germany). To visualize the scaffolds, reconstructed images were volume-rendered

The mechanical properties of the scaffolds were also characterized to provide insights into their ability to support loads and deformation during the spreading and proliferation of cells and formation of tissue [344]. In this study, the compressive mechanical properties of the porous

scaffolds were measured using an Instron model 5848 MicroTester (Instron Corporation, Canton, MA, USA). Six porous scaffold samples, each with dimensions of 10 mm x 5 mm x 5 mm, were deformed in compression at a crosshead speed of 0.5mm/min. Strains were determined from the displacement obtained during the deformation of the scaffolds using a 10 N load cell. The Young's moduli were then determined from the gradient of the initial linear (elastic) region of the stress–strain curve while the yield strength was obtained from the intersection of two tangents to the stress–strain curve at a strain of 10%.

5.2.5 Fourier Transform Infra-Red Spectroscopy and Thermal Characterization

The physicochemical characteristics of the drug-loaded porous scaffolds were characterized using Fourier Transform Infra-Red (FTIR) spectroscopy (IRTracer-100, Shimadzu, Kyoto, Japan). The spectra for each material were obtained within a wave number range between 500 cm^{-1} and 4000 cm^{-1}. The thermal properties [glass transition temperature (T_g) and melting temperature (T_m)] of the PLGA-PCL_PGS; PLGA-PCL_PTX; PLGA-PEG_PGS; PLGA-PEG_PTX scaffolds and their controls were determined using a Dynamic Scanning Calorimeter (DSC) (DSC 214 Polyma with IC40, NETZSCH, Selb, Germany). Approximately 10 mg of each sample was crimped into aluminum pans. The resulting samples were run under a heat/cool/heat cycle from −10 to 200 ºC. Heating and cooling rates were carried out, respectively, at 10 ºC/min and - 10 ºC/min, under a steady supply of nitrogen gas at 50 ml/min.

5.2.6 *In vitro* Drug Release and Degradation Studies

Prior to the release study, the drug loading in each sample was estimated to determine the actual concentration of drug (PGS or PTX) that was successfully loaded into the microporous scaffolds. In this case, dried scaffold containing PG or PTX was weighed precisely and dissolved in 1 ml of DCM. The resulting mixture was then vortexed to obtain a homogenous solution that was filtered using a 0.22 mm filter. The amount of drug in the resulting polymer solution was measured using a UV spectrophotometer (UV-1900, Shimadzu, Kyoto, Japan) that was operated at 235 nm and 535 nm. A standard calibration curve was constructed by dissolving known concentrations of PG and PTX in DCM [219].

In an effort to understand the mechanisms of drug release from a kinetics and thermodynamics perspective, a 56-day long drug release study was carried out at 37°C, 41°C and 44°C. These temperatures were selected to cover a range between the average human body temperature (~ 37°C), and possible hyperthermia temperatures between 41°C and 45°C. In each case, a triplicate of 10 mg of drug-loaded scaffold each (PLGA-PCL_PGS; PLGA-PCL_PTX; PLGA-PEG_PGS or PLGA-PEG_PTX) was immersed in a screw-capped 15 ml falcon tubes containing 10 ml of PBS that was mixed at a pH of 7.4 with 0.1% w/v Tween 80. The tubes were then placed in a Console Incubator Shaker (Innova 44 Incubator, New Brunswick, NJ, USA) and rotated at 100 rpm, maintained at 37°C, 41°C and 44°C, respectively. 1 ml each of solution (release study samples solvent) was collected from the individual tubes and replenished with fresh PBS after every 24 hours to maintain the sink conditions.

The collected samples were analyzed with a UV-Vis spectrophotometer that was operated at 235 nm (maximum absorbing wavelength of paclitaxel drug) and 535 nm (maximum absorbing wavelength of prodigiosin drug). From the Beer Lambert law [219], the concentrations of each drug released from the different drug-loaded microporous scaffolds were quantified using the PTX calibration curve (y = 2.2399x + 0.0024, R^2= 0.9949) or the PGS calibration curve (y = 0.9868x + 0.0018, R^2= 0.9972) developed in our earlier work [219].

The drug loading efficiency (DLE) and the drug encapsulation efficiency (DEE) were measured from drug-loaded microporous scaffolds using the following expressions:

$$DLE = \frac{M_d}{M_d + M_p} \times 100 \tag{4}$$

$$DEE = \frac{M_x}{M_z} \times 100 \tag{5}$$

where M_d is the mass of drug uptake into the scaffolds, and $M_d + M_p$ is sum of the masses of drug and polymer in the scaffold, M_x is the amount of encapsulated drug and M_z is the amount of drug that was used for the preparation of the scaffolds.

We hypothesize that drug release through the microporous scaffolds is sustained and controlled by three mechanisms in three phases. These mechanisms are diffusion through water-filled pores (burst release); diffusion through the polymer, and erosion/degradation of the polymer [281,348].

Since the scaffold degradation mechanisms can also affect drug release, the degradation of the scaffolds was also studied at 37°C. This was done on a weekly basis during the 56-day drug release experiments. During the degradation studies, the weights of each of the samples were measured to determine the weight loss. Visual observations of the effects of degradation (through hydrolysis of the porous scaffolds) were obtained via SEM over time at different intervals (14, 28, 42 and 56 days). The percentage weight loss in each case was obtained from:

$$\% \, Weight \, Loss = \frac{(W_o - W_t)}{W_o} \times 100 \qquad (6)$$

where W_o is the initial weight of the dry sample and W_t is the weight of dry sample at a specified duration of degradation. In each case, representative SEM images were obtained to show structural and morphological changes associated with the *in vitro* drug release processes.

5.2.7 *In vitro* Cell Viability and Drug Uptake

The effectiveness of the drug-loaded scaffolds in reducing cell viability via localized drug release was explored *in vitro* using breast cancer cells that were exposed to drugs released from the drug-loaded scaffolds. Here, triple-negative breast cancer (TNBC) cells (MDA-MB-231) in their log phase of growth, were harvested with Trypsin-EDTA after rinsing with Dulbecco phosphate-buffered saline (DPBS).

About 10^4 cells/well were sub-cultured in 12-well plates using L15+ medium (L15 medium with cell medium supplement of FBS and penicillin/streptomycin) in an incubator (Model NU-5700, Nuaire, Plymouth, MN, USA). A 60 % confluence was reached after 48 hours of incubation at 37

°C. Subsequently, a 5 mm x 5 mm x 3 mm scaffolds from each drug-loaded blend were pre-wetted via three-step immersion in ethanol. The resulting scaffolds were then washed in sterile DiH_2O and placed in cell culture medium (L15+) for 2 h (due to their hydrophobicity) prior to their immersion in the wells containing the breast cancer cells.

Cell viability and cytotoxicity were characterized using Trypan Blue after 0, 6h, 12h, 24 h, 48 h and 72 h in drug-loaded microporous scaffolds in 60 % confluence MDA-MB-231 cells. This was done by incubating the resulting well-plates with 0.4% trypan blue for 5 min, prior to counting the number of viable and non-viable cells with a hemocytometer. The cell counting was done using a model TS100F Nikon microscope (Nikon Instruments Inc., Melville, NY, USA) that was attached to a DS-Fi3 C camera at 10x.

5.2.8 *In vitro* Cell Culture and Cell Proliferation

The proliferation/regeneration of normal breast cells/tissue was characterized under *in vitro* conditions on the resulting drug-released scaffolds. This was done to explore the combined effects of localized breast cancer treatment and normal breast cell proliferation/reconstruction. After 56-days of drug release, the resulting microporous scaffolds were sterilized and used in the presence of control scaffolds (PLGA-PEG and PLGA-PCL) to study cell spreading and proliferation. Also. prior to the cell seeding, residual drugs were tested for. In each case, 5×10^4 normal breast cells were seeded onto the scaffolds (in 6-well plates) at 37°C. This was done in 5% CO_2 in 1 ml of the following medium: DMEM/F12 medium (Invitrogen # 11330-032) supplemented with 5% horse serum (Invitrogen # 16050-122), 30 ng/ml murine Epidermal Growth Factor (Peprotech #315-09),

0.5 µg/ml hydrocortisone (Sigma, #H-0888), 100 ng/ml cholera toxin (Sigma #C8052-1MG), 10 µg/ml insulin (Sigma #I-882-100MG), 1% Penicillin-Streptomycin (ATCC # or Invitrogen #15070-063), and 0.2% amphotericin (Gemini Bioproducts, #400-104) [247].

The resulting cell-seeded scaffolds were incubated at 37°C for 3 h for cell adhesion to the scaffolds. Cell viability and proliferation were then accessed by monitoring cell metabolic activities using the alamar blue cell viability and cytotoxicity reagent (Thermo Fisher Scientific, Waltham, MA, USA). This was done in triplicates at days 0, 1, 3, 7, 14, 21 and 28. At each time point, the culture media were replaced with 1 ml of 10% alamar blue solution (in the media) and incubated at 37°C for 3 hours. Thereafter, 100 µL aliquots were transferred into triplicate wells of a black opaque 96-well plate (Thermo Fisher Scientific, Waltham, MA, USA). This was followed by measurement of fluorescence intensities at 544 nm excitation and 590 nm emission using a 1420 Victor 3 multi-label plate reader (Perkin Elmer, Waltham, MA, USA). The percentage of alamar blue reduction was obtained from equation (7) below:

$$\% \, Alamar \, Blue \, Reduction = \frac{FI_{sample} - FI_{10\%AB}}{FI_{100\%R} - FI_{10\%AB}} \times 100 \tag{7}$$

where FI_{sample} is the fluorescence intensity of the (treated or untreated) cells, $FI_{10\%AB}$ is the fluorescence intensity of 10% AB reagent (negative control), and $FI_{10\%R}$ is the fluorescence intensity of 100% reduced alamar blue (positive control).

5.2.9 Fluorescence Microscopy and Scanning Electron Microscopy

At each time interval during the cell proliferation study, fluorescence staining of cell-scaffolds constructs was used to reveal the presence of growing cells. This staining was done to reveal the actin cytoskeleton and nuclei of the cells on the scaffolds. Initially, the cells on the surface structures were fixed with 4% paraformaldehyde for 15 minutes. They were then permeabilized with 0.1% Triton X-100 for 15 minutes. The resulting cell-scaffolds constructs were then blocked with 1% BSA for 1 hour at room temperature (25 $^{\circ}$C). This was followed by F-actin staining with Alexa Fluor 555 Rhodamine Phalloidin (Product # R415, 1:300, Thermo Fisher Scientific, Waltham, MA, USA). Finally, the nuclei were counterstained with SlowFade Gold Antifade Mountant with DAPI (Product # S36938, Thermo Fisher Scientific, Waltham, MA, USA). The resulting samples were kept on a glass slide and imaged with a TS100F Nikon microscope (Nikon Instruments Inc., Melville, NY, USA) that was attached to a DS-Fi3 C camera with 10X and 20X objective lenses.

Finally, SEM observations of the proliferated cells/tissue (on the scaffolds) were carried out at the same corresponding time intervals (day 0, 1, 3, 7, 14 and 21). The media was removed, and the cell-scaffold constructs were rinsed three times with PBS. These cells-scaffolds were then fixed in a 4% high grade paraformaldehyde in 0.1 M PBS solution for 15 minutes. The samples were then washed thrice in 10% of 1X PBS and 90% DiH$_2$O. Subsequently, the adhered cells on the scaffolds were dehydrated for 10 minutes in a graded series of ethanol concentrations (50%, 70%, 80%, 90% and 100 %).

Finally, the dehydrated cell-scaffold samples were chemically dried by placing them into a mixture of, hexamethyldisilizane (HMDS) and 100% ethanol (1:2) for 20 mins. This was followed by immersion in 2:1 HDMS:100% ethanol and subsequently into 100% HMDS for 20 mins. The fixed, dehydrated and dried samples were placed on double-sided copper tape on aluminium stubs, prior to sputter-coating with gold. The proliferated cells/tissue (on the blend of microporous scaffolds) were imaged in an SEM that was operated at an accelerating voltage of 3 kV (Field Emission SEM, JSM-7000F, JEOL Ltd, Akishima, Tokyo, Japan).

5.2.10 *In vivo* Animal Studies

In this section, preliminary animal studies were carried out to demonstrate a proof of concept of the use of drug-loaded scaffolds. The goal of this study is to explore localized delivery of cancer drug from the scaffolds to prevent the regrowth or loco-regional recurrence in the treatment of TNBC, following surgical resection of triple-negative breast tumor. We first carried out experimental study to induce the TNBC tumor before surgery to partially remove the tumor before implantation of drug-loaded scaffold. Twenty-one 4-week-old healthy immunocompromised Female Athymic Nude-Foxn1nu strain mice were purchased from Envigo (South Easton, MA, USA). These mice were ~ 18 g each and were kept in the WPI vivarium to acclimatized and ready for experiments until they are 5-weeks old. These animals were approved for use in the current work by the Worcester Polytechnic Institute, Institutional Animal Care and Use Committee (WPI IACUC). All animal procedures described in this work were performed in accordance with the approved animal protocol and guidelines.

All the mice were induced with subcutaneous TNBC tumor at the interscapular region via subcutaneous injection using 5.0×10^6 MDA-MB-231 cells. The induce subcutaneous tumors were monitored for the period of 28 days before surgery and placement of the implantable scaffolds. During the tumor growth, the tumor formation was checked by palpation and measured by a combination of digital caliper and MRI. For baseline evaluation, control sample groups with non-loaded scaffolds and without scaffolds were use as basis for comparison. The tumor volume was calculated using the following modified ellipsoidal formula [248,249].

$$Tumor\ Volume\ (TV) = \frac{Width^2\ x\ Length}{2} \tag{8}$$

where the *Length* was the longest axis of the tumor, and the *Width* was the longest measurement at a right angle to the length.

The mice were randomly divided into seven groups of three mice. This grouping was based on drug-loaded scaffolds formulations [PLGA-PEG_PGS, PLGA-PCL_PGS, PLGA-PEG_PTX, PLGA-PCL_PTX, PLGA-PEG, PLGA-PCL and controls (no scaffolds)]. Group five, six and seven are all control groups. In each case, partial surgical removal of the tumors was performed randomly on each member of the group with the appropriate and recommended anesthesia and pain suppressant. In each case, 6 mm x 6 mm of sterilized PLGA-PEG_PGS, PLGA-PCL_PGS, PLGA-PEG_PTX, PLGA-PCL_PTX, and control PLGA-PEG, PLGA-PCL scaffolds were implanted locally at the location where the subcutaneous tumor was removed.

In each group, localized cancer drug release was monitored for a period of 16 weeks to check for any tumor regrowth, metastasis side effect. We also monitored the mice for any changes in weight, abnormalities, and infections. After the 16 weeks study, the mice were euthanized. The lungs of the mice implanted with drug-loaded scaffolds as well as those of the controlled mice and regrowth tumor were then excised and cryo-preserved immediately to check for any toxicity and metastasis.

5.2.11 Histopathological Studies

In this section, we checked for tumor regrowth and metastasis by staining for the LHRH receptors and using hematoxylin and eosin (H&E) stain on the tumor and lungs from the sample mice. Several literatures have established the overexpression of LHRH receptors by TNBC [247]. Receptor staining via immunofluorescence (IF) staining was done to characterize and show evidence of regrowth tumor and metastases of TNBC on the lungs. LHRH receptors were done by immunofluorescence staining as described in prior work [247].

First, the samples were first incubated with 0.5 ml of 3 % bovine serum albumin (blocking agent) obtained from Sigma-Aldrich (St. Louis, MO, USA) at room-temperature (~23°C) for 60 mins. This was prepared with PBS mixed with 30 µl of triton X-100 (Life technologies Corporation, Carlsbad CA). The blocking agents were washed off three times from the sample slides and samples were further incubated over night at 4°C with three drops of anti-LHRH Antibody (Millipore Sigma, Burlington, MA, USA) a primary antibody, to detect the levels of LHRH. Finally, each of the tissue samples slides were washed and then treated with 50 µl of anti-mouse

IgG conjugated with Alexa fluoro 488 secondary antibody with concentration of 1 µg/ml for 2 hours. The stained samples were then imaged at a magnification of 40x of Leica TCS SP5 Spectral Confocal microscope couple with Inverted Leica DMI 6000 CS fluorescence microscope (Leica, Buffalo Grove, IL, USA).

Histopathology of the lungs and in some case regrown/reoccurred tumor were evaluated. The frozen tissue samples were embedded in Optimum cutting temperature (OCT) compound and processed in a cryostat (Leica CM3050 S Research Cryostat, Leica Biosystems Inc., Buffalo Grove, IL, USA). Briefly, the samples used for the histological examination were sectioned into 10 µm thickness along the longitudinal axis and placed on a glass slide. First, the tissue-slides were hydrated by passing them decreasing ethanol baths. These hydrated samples on the slides were then stained with hematoxylin and eosin (H&E). The stained slides were finally examined using light microscopy made up of a 20x objective lens of TS100F Nikon microscope (Nikon Instruments Inc., Melville, NY, USA) coupled with a DS-Fi3 C mount Nikon camera.

5.2.12 Statistics

In each case in the experiments, an independent Student t test and a one-way analysis of variance (ANOVA) test were used to study the differences between the control and the study groups. A *p*-value < 0.05 was used to determine the significance. All of the data were reported as means ± SD.

5.3 Kinetics and Thermodynamics Modeling

In this study, the release data of PGS or PTX drugs (from their respective microporous scaffolds) was used to study the mechanism and kinetics of drug release. This was done by fitting the drug release data to empirical mathematical models.

The drug release data were fitted to: Zero-order, First-order, Higuchi, Hixon-Crowell and Korsmeyer-Peppas models [349]. The results are presented in Table 5.1 along with the correlation coefficients (R^2) that were obtained from linear regression.

Table 5.1: Mathematical models applied to the drug (PGS and PTX) release data from microporous resorbable scaffolds

S/N	Kinetic Models	Expression
1	Zero Order	$D_f = K_0\,t$
2	First order	$\ln(1 - D_f) = -K_f\,t$
3	Higuchi	$D_f = K_H\,\sqrt{t}$
4	Hixon-Crowell	$W_o^{\frac{1}{2}} - W_t^{\frac{1}{2}} = K_{HC}\,t$
5	Korsmeyer-Peppas	$D_f = K_{kp}\,t^n$

In Table 5.1, D_t is the fraction of drug released up to time t, the k's represent the drug release rate constants, while n is the release exponent in the Korsmeyer-Peppas model [349]. Also, W_0 is the initial amount of drug in pharmaceutical dosage form, and W_t is the remaining amount of drug in the pharmaceutical dosage form at time t, in the Hixson-Crowell model.

The kinetics and thermodynamics of drug release can be determined using mathematical models of drug release from porous scaffolds [287]. In the cases of PGS or PTX release from microporous scaffolds, the maximum drug release coefficients or constant of reaction (D_0) and the activation energy (E_a) can be obtained (for temperatures of 37°C, 41°C, and 44°C) using the following versions of the Arrhenius:

$$D_t = D_0 Exp\left[-\frac{E_a}{R_g T}\right] \tag{9}$$

$$lnD_t = lnD_0 - \frac{E_a}{R_g} \times \frac{1}{T} \tag{10}$$

In equation (9) and (10), E_a is defined as the activation energy (J mol^{-1}); R_g is the universal gas constant, 8.314 J/mol K; T is the temperature in Kelvin, D_o is the Arrhenius constant and constant of the reaction, and D_t is the fraction of drug released at time t. The constants D_0 and E_a were obtained respectively from the plots of lnD_t versus 1/T. These resulted in linear relationships with slope of $-\frac{E_a}{R_g}$ and y-axis intercepts of lnD_0.

Furthermore, the Eyring equation (Equation shown below) was used to calculate some of the thermodynamic parameters. The thermodynamic parameters were used to identify changes in the drug release characteristics, which may be affected by the type of system, the drug release microenvironment, and polymer/polymer chains [287].

$$\ln\left(\frac{D_t}{T}\right) = \left[\ln\left(\frac{K_b}{h}\right) + \frac{\Delta S}{R_g}\right] - \frac{\Delta H}{R_g} \times \frac{1}{T} \tag{11}$$

Assuming a linear relationship:

$$y = mx + c: \text{y} = \ln\left(\frac{D_t}{T}\right); \text{x} = \frac{1}{T}; \text{c} = \left[\ln\left(\frac{K_b}{h}\right) + \frac{\Delta S}{R_g}\right] \text{ and m} = -\frac{\Delta H}{R_g} \tag{12}$$

ΔH and ΔS can be estimated from the values obtained from plots of $\ln\left(\frac{D_t}{T}\right)$ against $\frac{1}{T}$. Furthermore, the Gibbs Free Energy change is given by:

$$\Delta G = \Delta H - T\Delta S \tag{13}$$

where K_b is the Boltzmann constant (R_g/N, 1.38 x 10^{-23} J/molK), h is Planck's constant (6.62 x 10^{-34} J/s), ΔS is the entropy change, ΔH is the enthalpy change and ΔG is Gibbs free energy change. The changes in the thermodynamic activation parameters, ($\Delta S, \Delta H \text{ and } \Delta G$) were obtained using the Eyring equation [287].

5.4 Results and Discussion

5.4.1 Scaffold Polymer Blend Surface Wettability

From Figure 5.1, it can be seen that the contact angle (θ) for PLGA-PCL was higher than PLGA-PEG polymer blend ($68 \pm 3.6° > 53 \pm 2.2°$). In similar manner, the contact angle measured for the drug-loaded PLGA-PCL blend of polymer scaffolds was greater than those of drug-loaded PLGA-PEG. The presence of PEG (hydrophilic polymer) in the blend helps to decrease the contact angle which result to increase in wettability. Furthermore, our results showed that in each case of the

blend used, the drug-loaded scaffolds resulted in slightly higher contact angle measurement. This may be due to the presence of the hydrophobic drugs loaded in the polymer scaffolds.
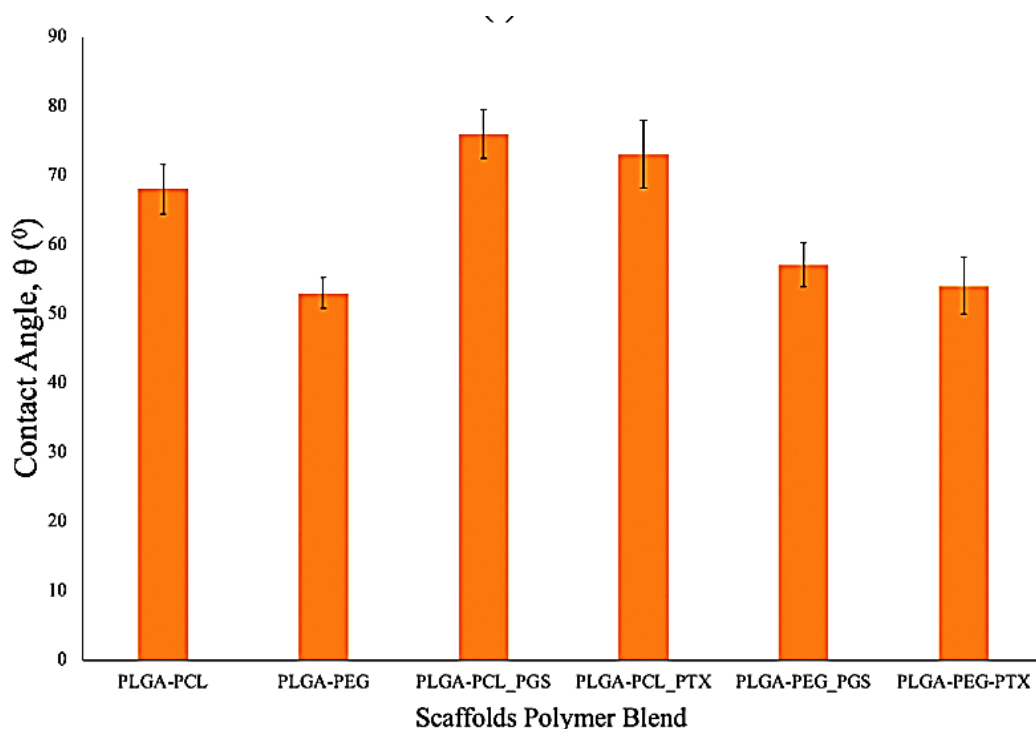
Figure 5.1: Contact angle measured for the different blends of polymers scaffolds. In all cases, the results are expressed as the mean $\pm$ SD with statistical difference $P < 0.05$.

5.4.2 Structural and Mechanical Properties of Porous Scaffold

Typical SEM images of the microporous scaffolds that were fabricated are presented in Figures 5.2. These include images of PLGA-PEG scaffolds (Figure 5.2 A), PLGA-PEG_PGS scaffolds (Figure 5.2 C), PLGA-PCL scaffolds (Figure 5.2 B) and PLGA-PCL_PGS scaffolds (Figure5.2 D). All of the scaffolds have similar structures and morphologies. The SEM images also revealed

mean pore sizes in the PLGA-PCL blend had a diameter of ~ 108.6 ± 5.2 μm, while drug-loaded

PLGA-PCL_PGS and PLGA-PCL_PTX blends had pore diameters of ~ 98.3 ± 7.5 μm and 101.8

± 9.8 μm, respectively. Thus, the loading of the drugs did not significantly alter the structures of

the microporous scaffolds (Figures 5.2A-D). Also, we have shown from our prior work that the

freeze-drying process and the 5 nm sputter-coated gold did not noticeably changed the structure of

the scaffolds [219].
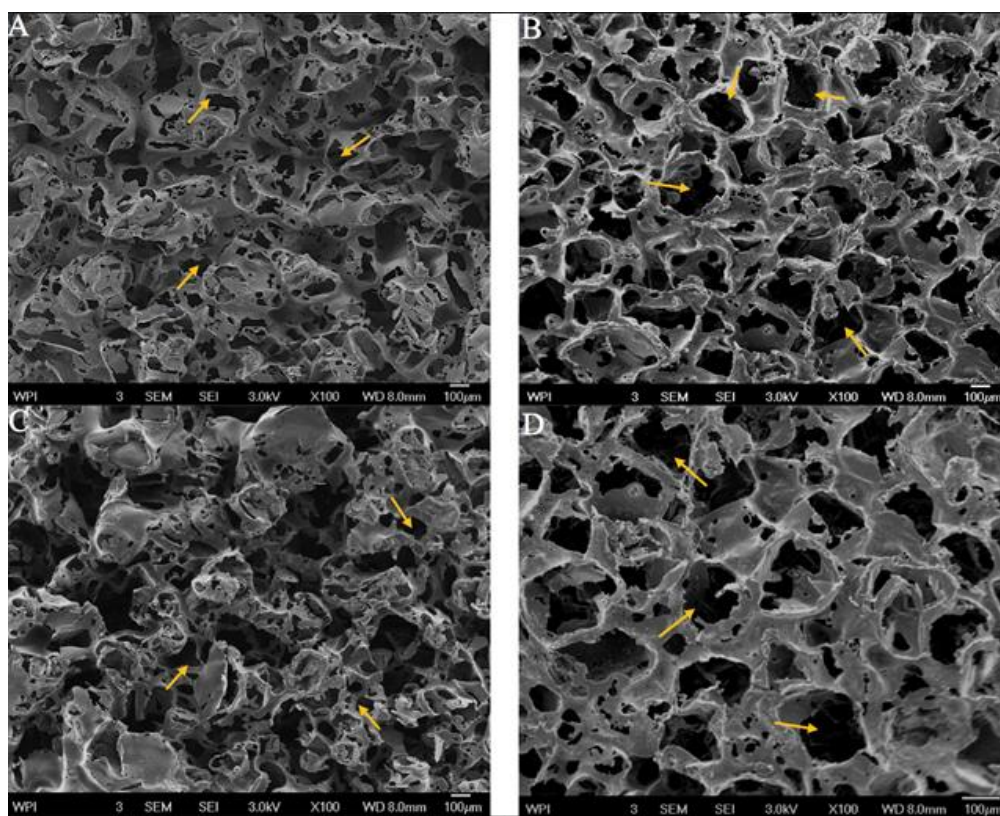
Figure 5.2: Representative SEM micrographs showing the morphological and structural features of 3D with yellow arrows pointing at the micropores (A) PLGA-PEG scaffold; (C) PLGA-PEG-PGS scaffold; (B) PLGA-PCL scaffold and (D) PLGA-PCL-PGS scaffold.

In the case of the PLGA-PEG blend, the mean pore size was measured to be 98 ± 8.6 μm, while

PLGA-PEG_PGS and PLGA-PEG_PTX blends had mean pore diameters of 88.4 ± 12.3 μm and

124

92.4 ± 8.6 µm, respectively, (Table 5.2). Hence, the drug loading did not significantly change the

pore sizes. However, the porosity (Table 5.2) of the drug-loaded scaffolds was slightly higher than

that of the non-loaded scaffolds. Furthermore, Figures 5.3 (a-d) show the cross-sections of 2D and

3D volume rendering of the porous scaffolds from a CT-scan. Clearly, the images provide a

qualitative appreciation of the 3D scaffold structures. The scaffolds are also shown to have

interconnected porosity that can support cell proliferation, nutrition and easy migration for tissue

vascularization and formation [343–345]. Hence, these interconnected porosities of the scaffolds

are evidence of their potential to support tissue growth and regeneration.

Table 5.2: Physical parameters of polymer blend microporous scaffolds

S/N	Material	Mean Pore Size (µm)	Porosity (%)
1	PLGA	131 ± 4.2	88.2
2	PEG	123.5 ± 6.4	86.5
3	PCL	146 ± 7.1	82.8
4	PLGA/PEG	98 ± 8.6	93.4
5	PLGA/PCL	108.6 ± 5.2	88.3
6	PLGA/PEG_PTX	92.4 ± 8.6	93.7
7	PLGA/PEG_PGS	88.4 ± 12.3	94.34
8	PLGA/PCL_PTX	101.8 ± 9.8	89.12
9	PLGA/PCL_PGS	98.3 ± 7.5	93.1
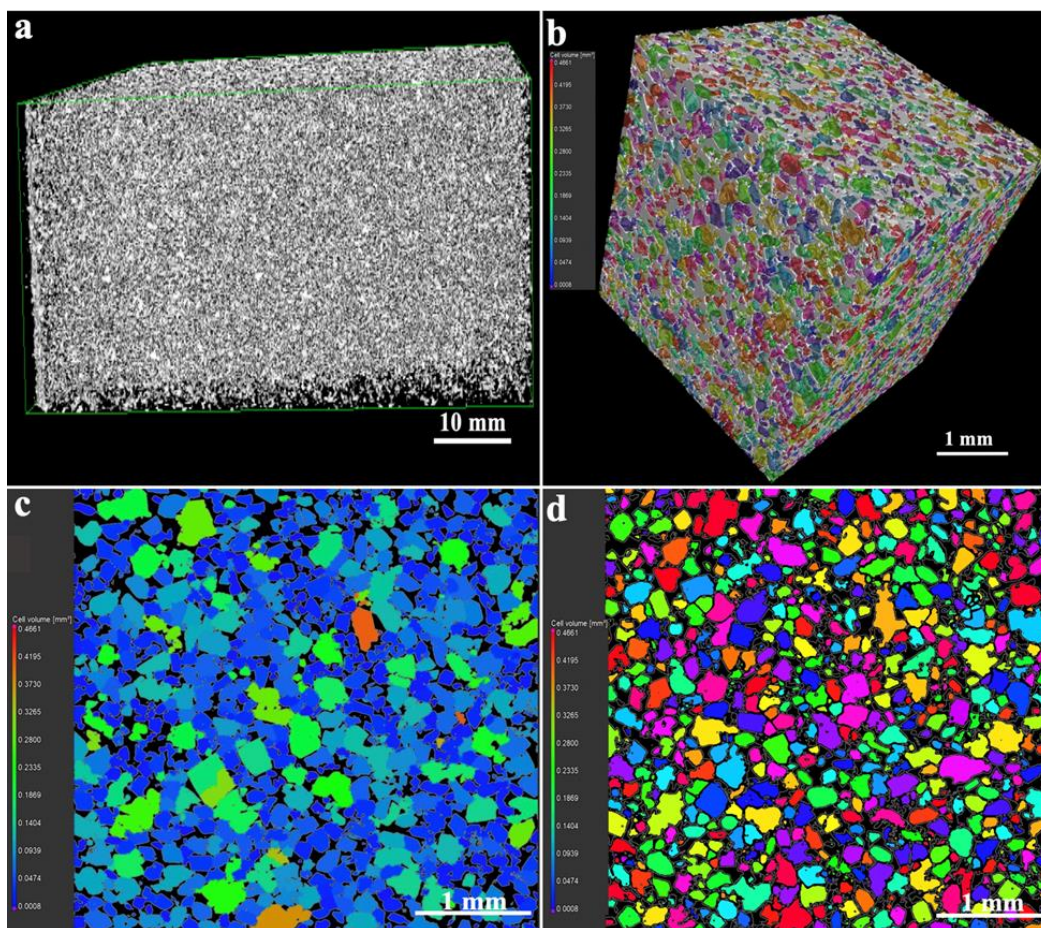
Figure 5.3: Representative X-ray micro CT Images showing distributions of the interconnected porosity of (a) 3D reconstructed images of PLGA-PEG_PGS scaffolds (b) 3D reconstructed images of PLGA-PCL_PGS scaffolds (c) 2D reconstructed images of PLGA-PEG_PGS scaffolds and (d) 2D reconstructed images of PLGA-PCL_PGS scaffolds.

The compressive stress-strain curves of the scaffolds are presented in Figure 5.4. The PLGA-PCL-based scaffolds have the highest strengths and strain to failure, while the PLGA-PEG-based scaffolds have lower strengths and strains to failure. Also, the drugs have limited influence on the stress-strain behavior of the drug-loaded scaffolds. The elastic moduli (4.5 ± 0.6 kPa – 5.6 ± 0.8 kPa) and yield strengths (5.5 ± 1.1 kPa - 6.7 ± 1.2 kPa) obtained (Table 5.3) from the stress-strain curves of the microporous scaffolds are within the range reported for actual human breast tumor

tissue and normal breast tissue [336–338,350–352]. The introduction of pores clearly helps to reduce the mechanical properties of the blends of polymer scaffolds [353], which in turn will support cell proliferation and tissue regeneration [354].
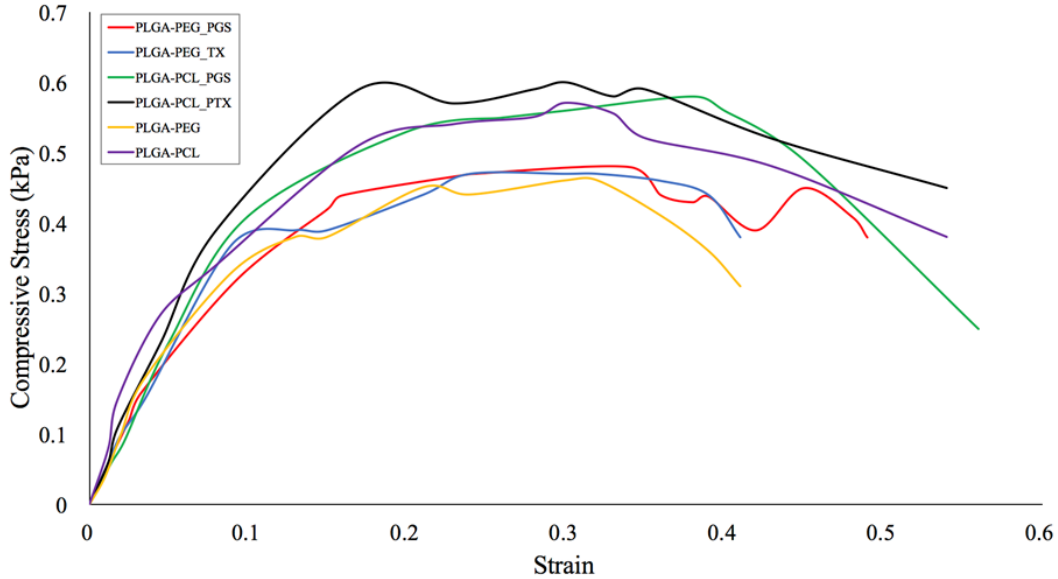
Figure 5.4: Typical compressive stress–strain curves of PLGA-PEG_PGS, PLGA-PEG_PTX, PLGA-PCL_PGS and PLGA-PCL_PTX scaffolds from compression test (0.5 mm/min).

Table 5.3: Mechanical properties of drug-loaded porous scaffolds

S/N	Porous Scaffold Blend	Yield Strength (kPa)	Compressive Young's Modulus (kPa)
1	PLGA-PEG_PTX	5.6 ± 0.8	5.5 ± 1.1
2	PLGA-PEG_PGS	4.5 ± 0.6	5.4 ± 0.7
3	PLGA-PEG	4.8 ± 1.6	5.3 ± 1.3
4	PLGA-PCL_PTX	5.1 ± 1.2	6.7 ± 1.2
5	PLGA-PCL_PGS	4.8 ± 0.4	6.3 ± 0.9
6	PLGA-PCL	4.5 ± 1.4	6.1 ± 1.7

5.4.3 Fourier Transform Infra-Red and Dynamic Scanning Calorimetry

The FTIR results from the drug/polymer formulations are presented in Figure 5.5. These results show that characteristic band formed at 2945 cm^{-1} as a result of the stretching of CH, CH$_2$ and CH$_3$ groups, while the characteristic peak at 1750 cm^{-1} was due to the stretching of the C=O bond. The peak at 1180 cm^{-1} is attributed to the stretching of C-O and C-C bonds associated with PLGA, PEG and PCL. Again, there are similarities in the spectra of PLGA-PEG or PLGA-PCL polymer and PLGA-PEG_PGS or PLGA-PCL_PTX scaffolds, as shown in Figure 5.5. The spectra obtained for each drug were masked out by those of the polymer blends such that they appear as molecular dispersions in the scaffold matrices. Furthermore, no new peaks were observed in the drug-loaded samples, suggesting that no new chemical reactions/bonds formed during the blending and drug loading/encapsulation processes.
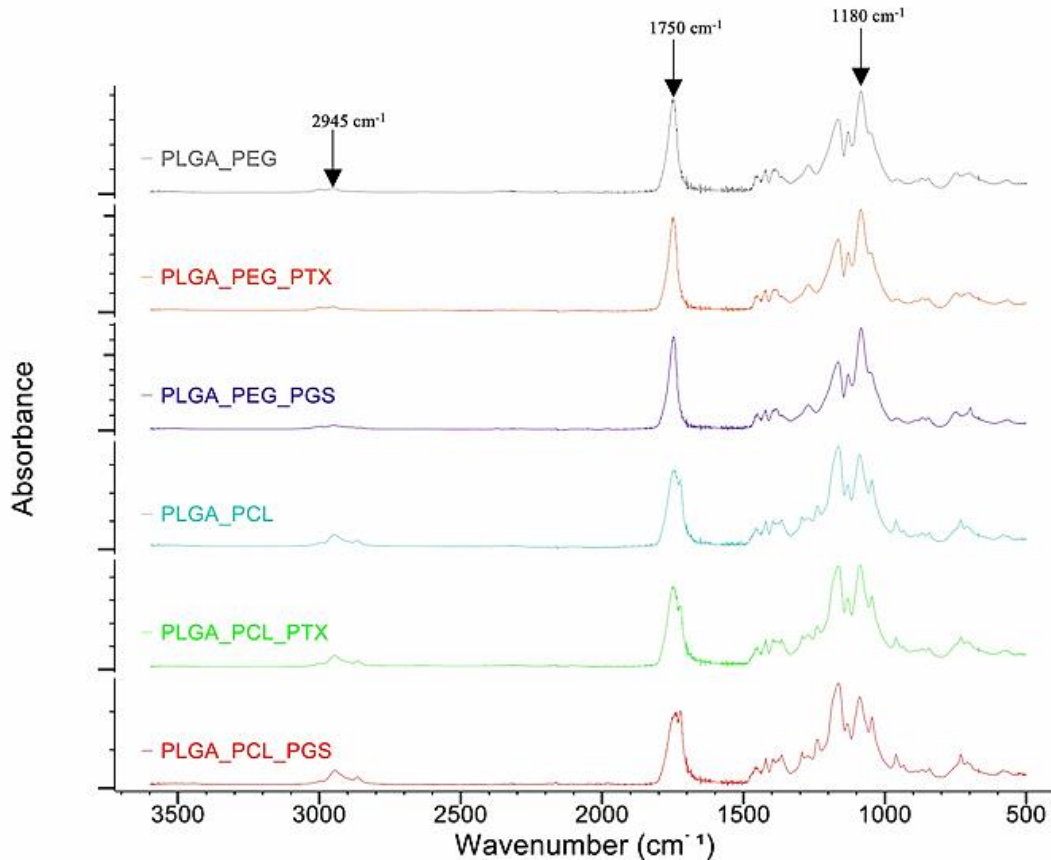
Figure 5.5: FTIR spectra of microporous blend of PLGA-PEG_PGS, PLGAPEG_PTX, PLGA-PCL_PGS, PLGA-PCL_PTX, PLGA-PEG, PLGA-PCL scaffolds as well as PGS and PTX drug used.

The results obtained from the DSC analyses (Figure 5.6) revealed that PLGA-PEG_PGS and PLGA-PEG_PTX and their control (PLGA-PEG) had similar thermal behavior from the DSC curves. Also, in the case of drug-loaded PLGA-PCL_PGS and PLGA-PCL_PTX, they appear to have similar behavior (in their thermal behavior) to the control (PLGA-PCL). However, the DSC results also revealed a single defined peak. This single peak suggests that the drug in each case was strongly miscible with their blend of polymers. The DSC curve contained a defined single peak within a relatively narrow temperature range. This revealed the melting temperature (T_m) and glass transition temperature (T_g) of the PLGA-PEG_PGS, PLGA-PEG_PTX and PLGA-PEG to

be 48°C, 49°C, 53.9°C, and 45.4°C, 45.9°C, 50.7°C, respectively. In the case of PLGA-PCL_PGS, PLGA-PCL_PTX and PLGA-PCL, their T_m and T_g were 57.9°C, 55°C, 54.9°C and 50.1°C, 49.1°C, 48.8°C, respectively (Figure 5.6). Slight changes were observed in the measured T_m and T_g values obtained for plain polymer blends (PLGA-PEG and PLGA_PCL) as well as drug-loaded scaffolds (PLGA-PEG_PGS, PLGA-PEG_PTX, PLGA-PCL_PGS, and PLGA-PCL_PTX). These changes may be attributed to the effects of the drugs, which act as strong plasticizers of the polymer blend [266].
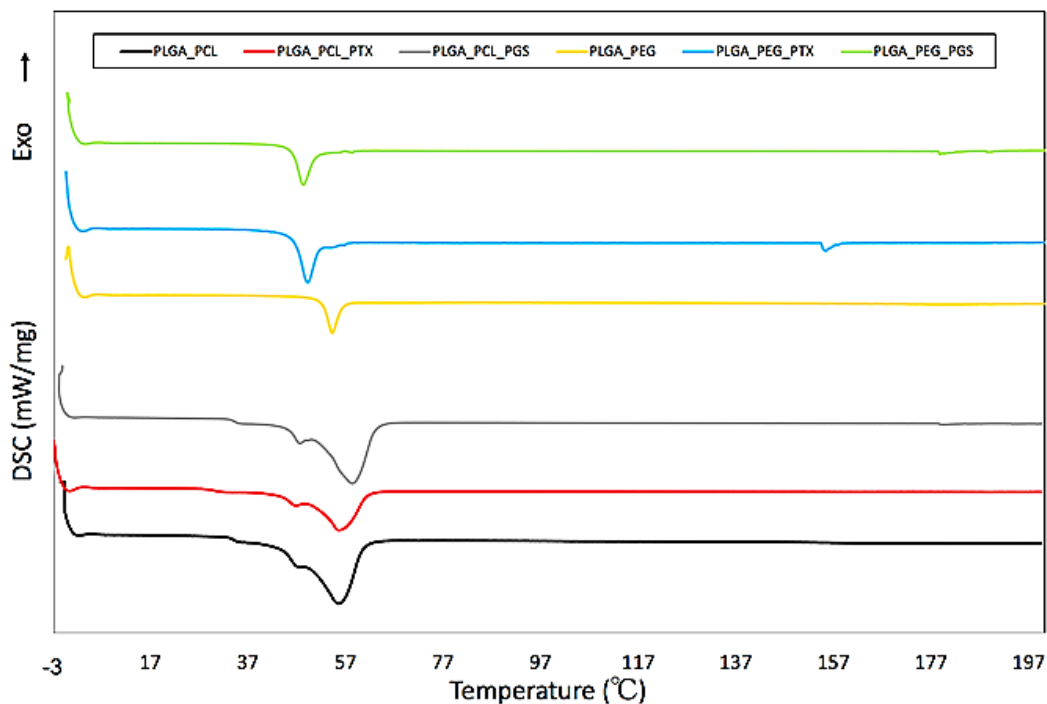
Figure 5.6: Representative DSC curves showing single peak within a relatively narrow temperature range that revealed the melting temperature (Tm) and glass transition temperature (Tg) of the polymer blend of PLGA-PEG-PGS, PLGA-PEG_PTX, PLGA-PCL_PGS, PLGA-PCL_PTX, PLGA-PEG, PLGA-PCL scaffolds.

5.4.4 *In vitro* Drug Release

Drug release at 37°C [355] revealed an initial burst release after 48 h for PLGA-PEG_PGS, PLGA-PEG_PTX, PLGA-PCL_PGS and PLGA-PCL_PTX to be 21%, 35%, 15% and 28%, respectively, as well as percentage cumulative drug release of 85.5 ± 2%, 81.5 ± 3.3%, 73.5 ± 1.3% and 66 ± 3.1%, respectively (Figure 5.7i and Table 5.4). For the drug release carried out at 41°C for PLGA-PEG_PGS, PLGA-PEG_PTX, PLGA-PCL_PGS and PLGA-PCL_PTX, we observed a burst release after 48 h to be 19%, 37%, 17% and 30%, respectively, with percentage cumulative drug release of 88 ± 2.5%, 85.5 ± 3.7%, 74.4 ± 2.5% and 68.5 2.3%, respectively (Figure 5.7ii and Table 5.4). Finally, at 44°C in the case of PLGA-PEG_PGS, PLGA-PEG_PTX, PLGA-PCL_PGS and PLGA-PCL_PTX, the burst release after 48 h corresponds to 21%, 39.5%, 19% and 21%, respectively, with percentage cumulative drug release of 89 ± 1.5%, 87 ± 3.1%, 76.5 ± 1.9% and 69 ± 2.1%, respectively (Figure 5.7iii and Table 5.4).

(i)

(ii)
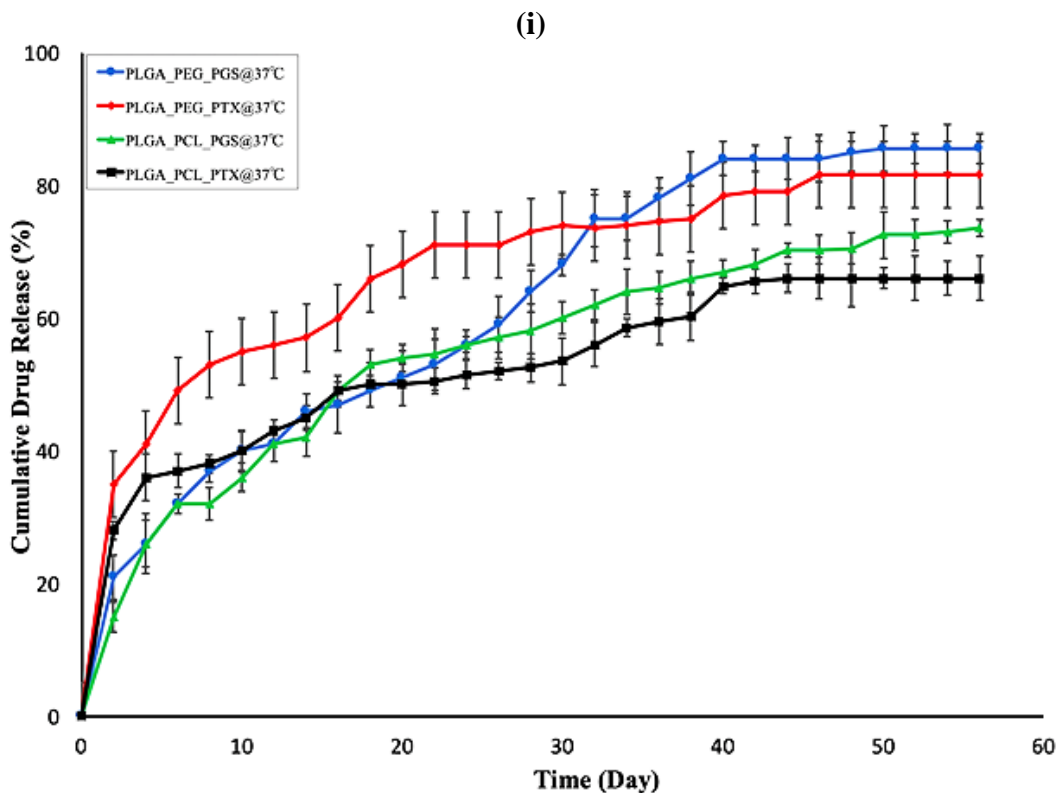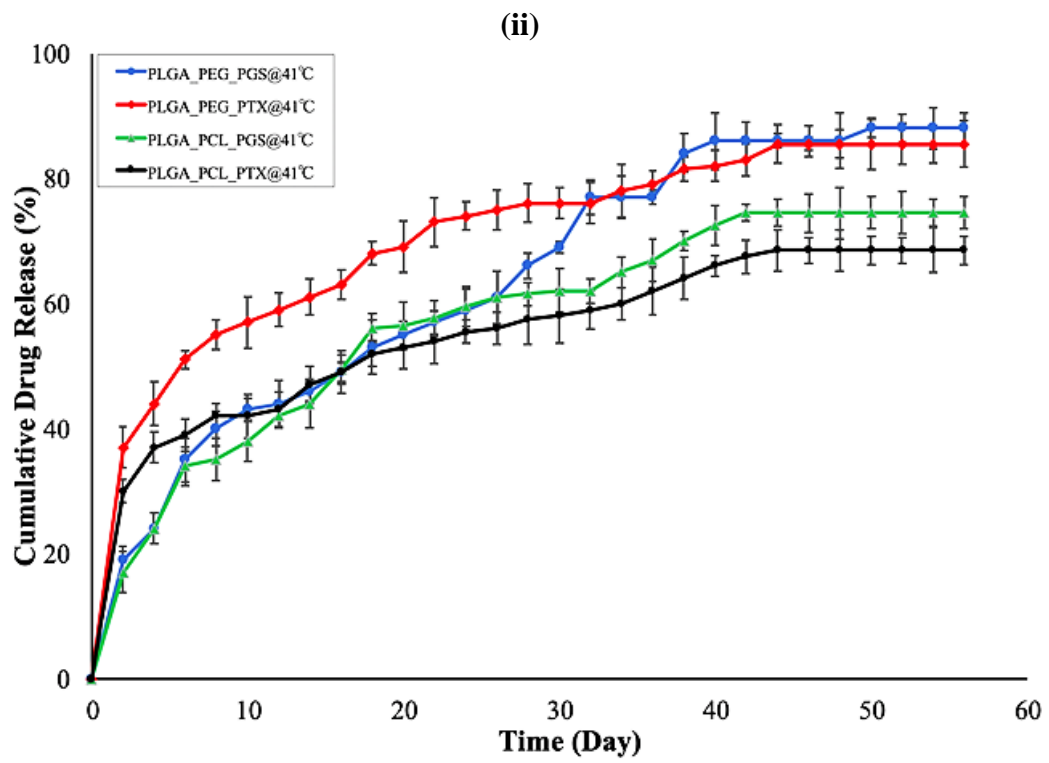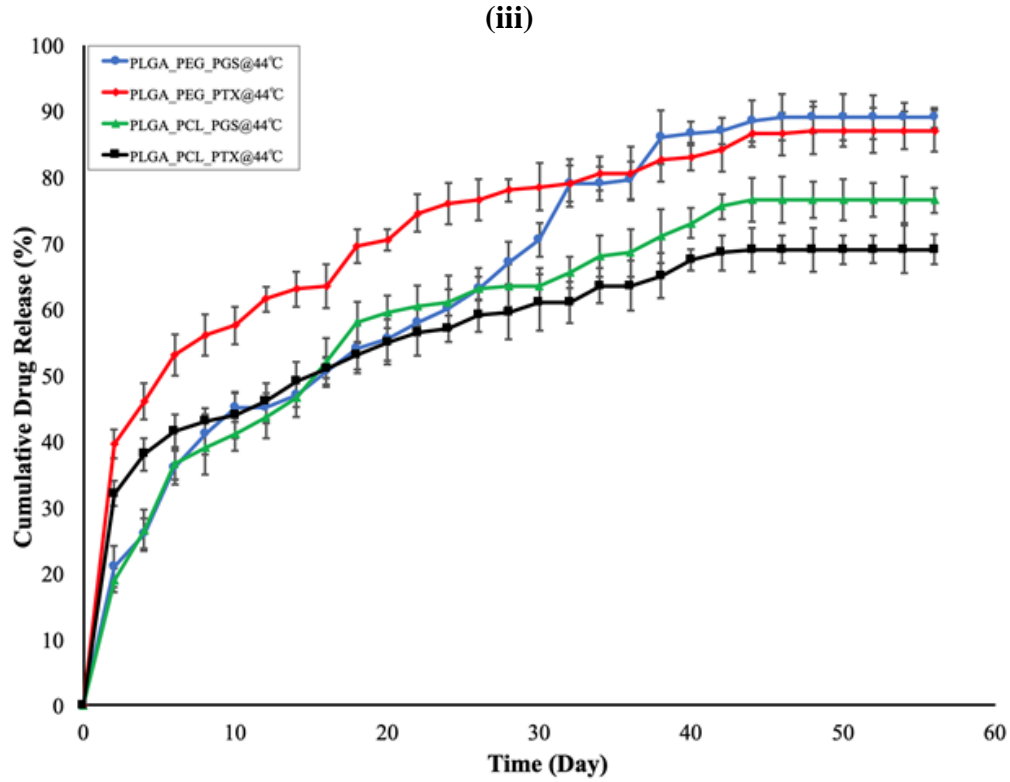
Figure 5.7: Cumulative drug release from porous blend of drug-loaded PLGA-PEG-PGS, PLGA-PEG_PTX, PLGA-PCL_PGS, PLGA-PCL_PTX scaffolds at a pH 7.4 and at release temperature of (i) 37 °C (ii) 41 °C and (iii) 44 °C, respectively. (*P*-values of<*0.05* for *Student's t-test)*.

Table 5.4: Drug release parameters from microporous scaffolds as a function of time and temperature.

S/N	Drug-loaded Scaffold System	Drug Release Temperature (°C)	Percentage Burst Release after 48 h	DLE (%)	Percentage Cumulative Drug Release for 56 Days
	PLGA-PEG_PGS	37	21	5.1	85.5 ± 2
1	PLGA-PEG_PTX	37	35	4.8	81.5 ± 3.3
	PLGA-PCL_PGS	37	15	4.3	73.5 ± 1.3
	PLGA-PCL_PTX	37	28	3.4	66 ± 3.1
	PLGA-PEG_PGS	41	19	5.1	88 ± 2.5
2	PLGA-PEG_PTX	41	37	4.8	85.5 ± 3.7
	PLGA-PCL_PGS	41	17	4.3	74.4 ± 2.5
	PLGA-PCL_PTX	41	30	3.4	$68.5\ 2.3$
	PLGA-PEG_PGS	44	21	5.1	89 ± 1.5
3	PLGA-PEG_PTX	44	39.5	4.8	87 ± 3.1
	PLGA-PCL_PGS	44	19	4.3	76.5 ± 1.9
	PLGA-PCL_PTX	44	32	3.4	69 ± 2.1

Furthermore, it can be clearly seen that the variation of temperature used during the drug release does not significantly influence the drug release profiles for the specific blend of scaffolds fabricated (Figures 5.7i-5.7iii and Table 5.4). However, it was observed that the presence of PGS slightly lowers the burst release of the drug from each of the drug-loaded scaffolds. In general, the awareness of the relationship between concentrations tested non-clinically and what is achievable in a clinical context can greatly assist in translational research [356]. For instance, the pharmacokinetic parameters of paclitaxel drug approved for human include a dose of 175 mg/m^2 within a concentration of 4.37 μmol/L. The concentrations used in this study is thought to falls within a comprehensive guide dose and clinically relevant concentration selection (when the conversion factor from humans to mice as well as to cells are considered) as approved by the FDA for cancer treatment [356].

In the case of PLGA-PEG and PLGA-PCL blend, the presence of PLGA may have been responsible in enhancing the degradation by moderating the hydrophilicity of the drug-loaded blend during control release of the drug [357]. Whereas, the PCL in the PLGA-PCL drug-loaded system played a role in the control of mass loss of PLGA and in release of the drug [358]. Thus, our results show the potential for longer-lasting and lower release amounts which could be within a safe range that may avoid potential toxicity while reducing undesirable side-effects. Hence, the current results suggest that the drug-loaded polymer blends explored in this study can be used to achieve *in vivo* therapeutic levels of release of cancer drugs at clinically-relevant time scales.

5.4.5 *In vitro* Drug Release Kinetics

From all of the five kinetic models that were used to analyze the PGS and PTX drug release from the 3D microporous scaffolds, only the Higuchi and the Korsmeyer-Peppas models (Table 5.5) were found to characterize the drug release from the scaffolds with high correlation coefficients (R^2) that closely describe the release of prodigiosin or paclitaxel from the drug-loaded scaffolds. However, the power law (Korsmeyer-Peppas) model best fitted the first 60% of drug release data that was obtained. The Korsmeyer-Peppas (KP) model provides an exponential correlation between the drug release and time [359]. The results showed that the KP model was associated with high correlation coefficients (R^2) between 0.9049 and 0.9825, within the temperature range that was considered. The release exponents, n, obtained for the PGS or PTX from each of the corresponding scaffold constituents were greater than 0.5. This suggests that the drug release mechanism was non-Fickian or anomalous. The anomalous nature of the drug release may be due to the blend of PLGA-PEG and PLGA-PCL polymer material that was used to induce reservoir effects, leading to sustained release of the PGS or PTX drugs.

Table 5.5: Results kinetic models showing kinetic constant and *in vitro* release constant of the squared correlation coefficient (R^2) and release coefficients for drug release under different temperature.

S/N	Drug-loaded Scaffold System	Tempt (°C/K)	Kinetic Model	R^2 Value	m Value	c Value	k Constant	n Constant
1	PLGA-PEG_PGS	37/310	Higuchi	0.8068	12.017	1.525	12.017 ($h^{-1/2}$)	-
	PLGA-PEG_PTX	37/310		0.8324	21.124	1.299	21.124 ($h^{-1/2}$)	-
	PLGA-PCL_PGS	37/310		0.7126	15.125	1.023	15.125 ($h^{-1/2}$)	-
	PLGA-PCL_PTX	37/310		0.7012	20.039	1.078	20.039 ($h^{-1/2}$)	-
2	PLGA-PEG_PGS	41/314	Higuchi	0.8005	14.641	1.358	14.641 ($h^{-1/2}$)	-
	PLGA-PEG_PTX	41/314		0.7119	12.800	0.954	12.800 ($h^{-1/2}$)	-
	PLGA-PCL_PGS	41/314		0.7724	16.437	1.063	16.437 ($h^{-1/2}$)	-
	PLGA-PCL_PTX	41/314		0.7974	21.910	0.798	21.910 ($h^{-1/2}$)	-
3	PLGA-PEG_PGS	44/317	Higuchi	0.6924	15.803	1.368	15.803 ($h^{-1/2}$)	-
	PLGA-PEG_PTX	44/317		0.6801	24.397	0.953	24.397 ($h^{-1/2}$)	-
	PLGA-PCL_PGS	44/317		0.7983	18.766	1.054	18.766 ($h^{-1/2}$)	-
	PLGA-PCL_PTX	44/317		0.7282	14.045	0.776	14.045 ($h^{-1/2}$)	-
4	PLGA-PEG_PGS	37/310	Korsmeyer-Peppas	0.9742	0.606	0.124	1.3305 (h^{-n})	0.606
	PLGA-PEG_PTX	37/310		0.9152	0.600	0.244	1.7539 (h^{-n})	0.600
	PLGA-PCL_PGS	37/310		0.9825	0.607	0.097	1.2503 (h^{-n})	0.607
	PLGA-PCL_PTX	37/310		0.9077	0.556	0.237	1.7258 (h^{-n})	0.556
5	PLGA-PEG_PGS	41/314	Korsmeyer-Peppas	0.9803	0.619	0.109	1.2853 (h^{-n})	0.619
	PLGA-PEG_PTX	41/314		0.9111	0.604	0.253	1.7906 (h^{-n})	0.604
	PLGA-PCL_PGS	41/314		0.9811	0.611	0.105	1.2735 (h^{-n})	0.611
	PLGA-PCL_PTX	41/314		0.9077	0.563	0.240	1.7378 (h^{-n})	0.563
6	PLGA-PEG_PGS	44/317	Korsmeyer-Peppas	0.9749	0.617	0.126	1.3366 (h^{-n})	0.617
	PLGA-PEG_PTX	44/317		0.9062	0.605	0.261	1.8239 (h^{-n})	0.605
	PLGA-PCL_PGS	44/317		0.9740	0.611	0.128	1.3428 (h^{-n})	0.611
	PLGA-PCL_PTX	44/317		0.9049	0.568	0.247	1.7660 (h^{-n})	0.568

5.4.6 *In vitro* Drug Release Thermodynamics

The evaluation of the drug release rates at the different temperatures (37°C, 41°C and 44°C) enable the extraction of important thermodynamic parameters that were associated with the release of PGS or PTX from their scaffolds. From equation 9 and 13, the activation energy (E_a), the enthalpy change (ΔH), entropy change (ΔS) and Gibbs free energy change (ΔG) were determine from the results of the drug release experiments. Typically, the magnitude of E_a provides insights into the amount of energy that is needed to move the drug molecule from the polymer matrix to the

dissolution medium (PBS). In this case, the E_a may be influenced by the type of intraparticle diffusion of the drug molecules from the drug-polymer matrix during the drug release [360]. Usually, a lower activation energy (5-40 kJ/mol) may be driven by diffusion-controlled processes, while a higher activation energy (40–800 kJ/mol) [360] may also be attributed to chemically-controlled processes [360]. The thermodynamic parameters obtained for prodigiosin and paclitaxel drug release from the respective microporous drug-loaded polymer scaffold blends are summarized in Table 5.6.

Table 5.6: Thermodynamic parameters obtained from prodigiosin and paclitaxel drug release rate from drug-loaded polymer scaffold blend.

Drug-loaded Scaffold System	Activation Energy, Ea (kJ/mol)	Enthalpy, ΔH (kJ/mol)	Entropy, ΔS (kJ/K)	Gibbs Free Energy, ΔG (kJ/mol)	
				Temp (ºC/K)	ΔG (kJ/mol)
PLGA-PEG_PGS	4.106	1.608	-0.2616	37/310	82.7040
				41/314	83.7504
				44/317	84.5352
PLGA-PEG_PTX	4.545	1.940	-0.2343	37/310	74.5730
				41/314	75.5102
				44/317	76.2131
PLGA-PCL_PGS	8.059	5.454	-0.2258	37/310	75.4520
				41/314	76.3552
				44/317	77.0326
PLGA-PCL_PTX	8.628	5.817	-0.1987	37/310	67.4140
				41/314	68.2088
				44/317	68.8049

This show that the release of PGS or PTX from the scaffolds may occurs mainly by diffusion-controlled processes, since the values of E_a were less than 10 kJ/mol (Table 5.6). Furthermore, the activation energies of PLGA-PCL_PGS and PLGA-PCL_PTX (8.059 kJ/mol and 8.628 kJ/mol, respectively) were about twice those of PLGA-PEG_PGS and PLGA-PEG_PTX (4.106 kJ/mol and 4.545 kJ/mol, respectively).

The underlying enthalpy changes are also presented in Table 5.6. The results show that drug release from all of the scaffolds occurred by endothermic processes, since $\Delta H > 0$ [361]. Also, the changes in entropy were all negative ($\Delta S < 0$), which is consistent with a decrease in disorder (in the drug-loaded scaffolds) with increasing drug release [361]. Finally, it is important to note that the measured Gibb's Energy changes (Figure 5.8 and Table 5.6) were all greater than zero ($\Delta G > 0$). These positive values show that the drug release process (from all of the scaffolds that were used in this study) were non-spontaneous in nature [362]. Such non-spontaneous release may be as a result of the controlled release and more likely to promote the release of drug at a controlled rate over a period of one month [281].
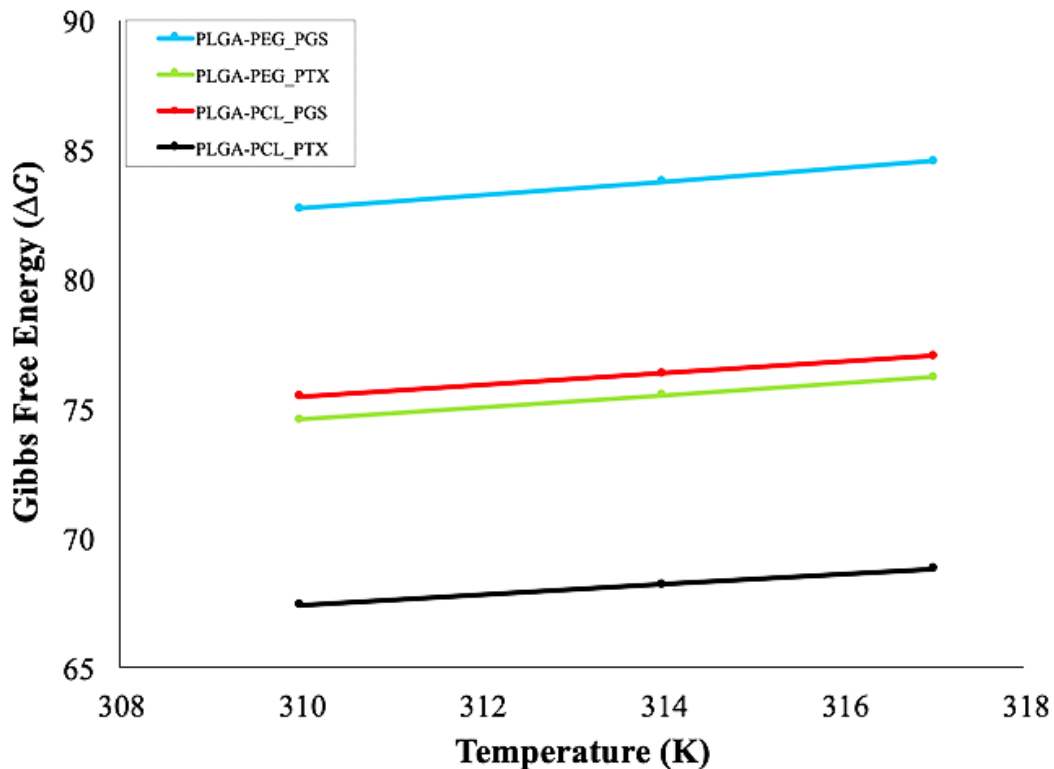
Figure 5.8: Graph of Gibbs free energy against temperature variation for the release of PGS and PTX-loaded scaffolds.

5.4.7 *In vitro* Drug-loaded Polymer Scaffold Degradation

SEM images of PLGA-PEG_PGS and PLGA-PCL_PGS drug-loaded scaffolds are presented in Figures 5.9(A-H) for scaffolds undergoing degradation for durations of 2, 4, 6 and 8 weeks at 37°C. The corresponding weight loss of the scaffolds obtained under *in vitro* conditions is presented in Figure 5.10 for the scaffolds loaded with PGS or PTX.
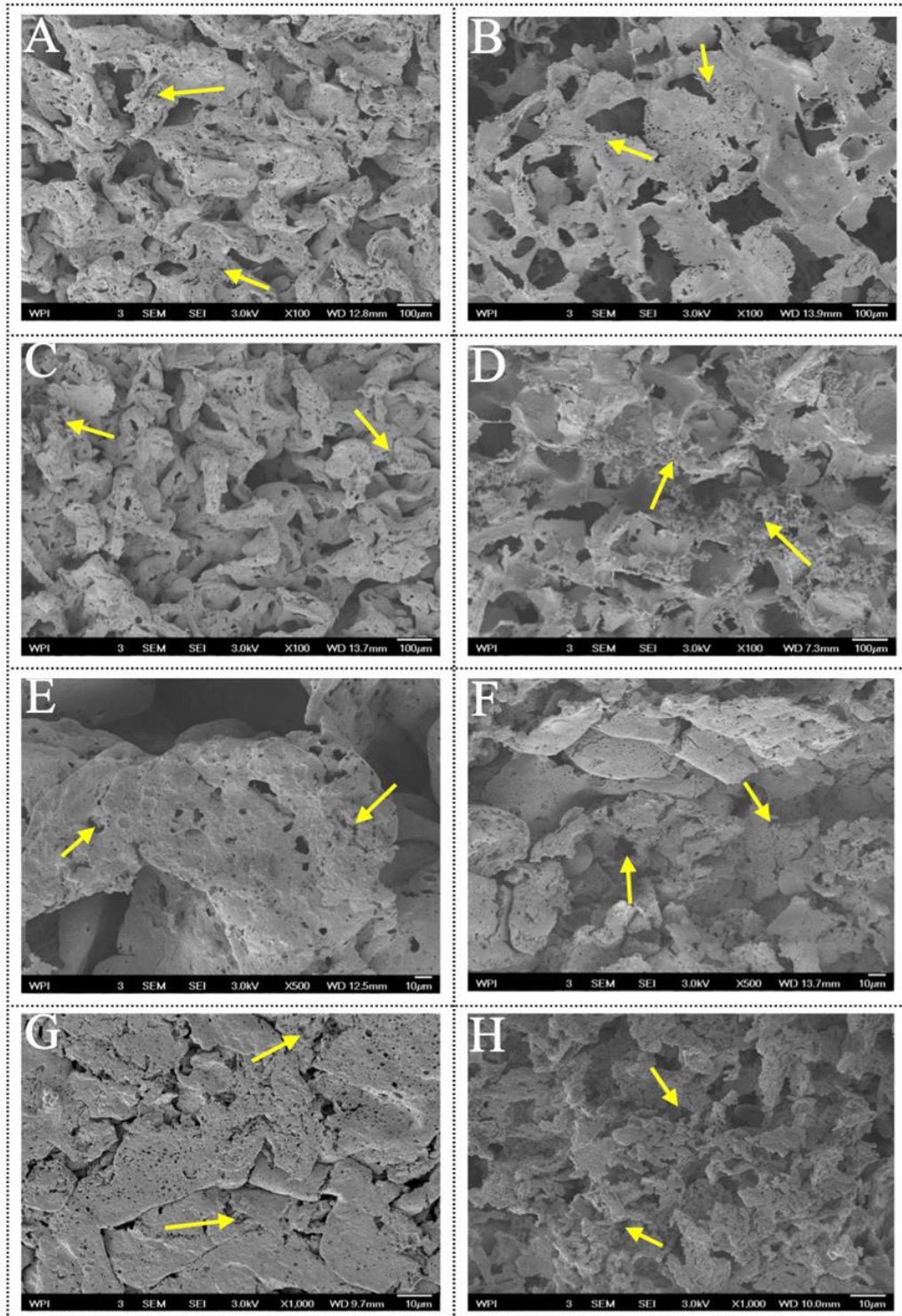
Figure 5.9: Representative SEM micrographs of PLGA-PEG_PGS (A, C, E, G) and PLGA-PCL_PGS (B, D, F, H) showing representative morphology of scaffolds degradation and degraded sites after 2- weeks (A and B), 4-weeks (C and D), 6-weeks (E and F) and 8-weeks (G and H) of *in vitro* release drug, respectively.
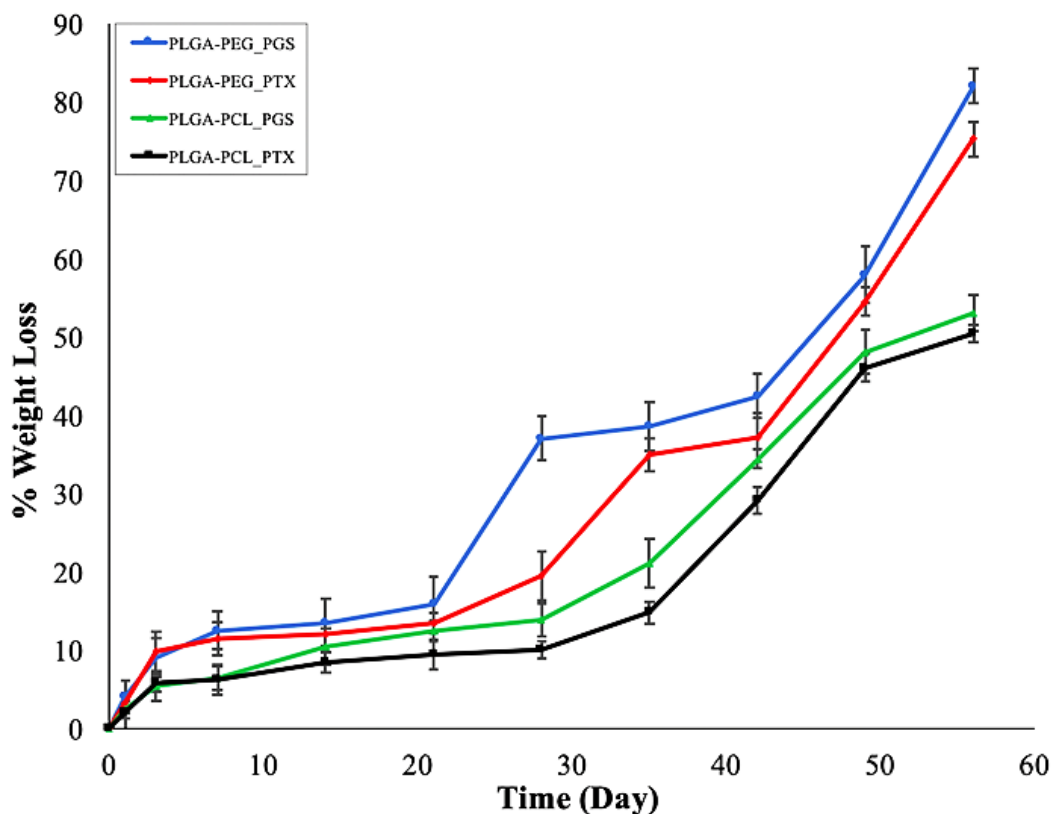
Figure 5.10: Degradation kinetics of PLGA-PEG_PGS, PLGA-PEG_PTX, PLGA-PCL_PGS and PLGA-PCL_PTX scaffolds (The curve represents the mean value of three independent degradation experiments).

In both cases, gradual morphological changes were observed in the structure of the 3D microporous scaffolds under *in vitro* conditions. After the first day (24 h), there were no noticeable structural changes.

However, clear evidence of erosion was observed on the surfaces of the PLGA-PEG_PGS scaffolds and the PLGA-PCL_PGS scaffolds after 2, 4, 6 and 8 weeks of drug release [Figure 5.9(A-H)]. The results revealed clear evidence of pit collapse, as the struts started to degrade due

to erosion. The differences between the degradation of the drug-loaded scaffolds are consistent with prior observation of degradation-induced morphological changes in drug-polymer blends in which the presence of drugs has been shown to change the degradation mechanism from bulk erosion to surface erosion [269]. Similar degradation process was observed was observed in the case of PLGA-PEG_PTX and PLGA-PCL_PTX, which shows that the drug does not noticeably contribute in the degradation process.

Furthermore, it is clear from Figure 5.10 that the PLGA-PEG drug-scaffold blend degraded faster with about 70-80% weight loss, compared to the PLGA-PCL blend in which the weight loss was about 50% after 56-days of degradation under *in vitro* conditions. In general, the degradation process in the drug-loaded PLGA-PEG and PLGA-PCL scaffolds occurred in two noticeable stages. In first stage, which occurs within the first three weeks, small weight losses (9-18%) were observed. These are attributed to the effects of diffusion through nanoporous structures and dissolution mechanisms. However, in the second phase, significant weight losses (12-85%) in the scaffolds were observed. This stage may be as a result of hydrolytic degradation of the polymer scaffolds which initially start as surface erosion that may be driven largely due to the chemical hydrolysis of the scaffolds during the later stage of *in vitro* drug release [363]. In this case, these drug-loaded polymer scaffolds exhibit a certain hydrophilicity to absorb water and thus degrade by cleavage of hydrolytically sensitive ester bonds. For example, PLGA polymer constituent degrades hydrolytically to unstable ester bonds into lactic acids and glycolic acids [364].

5.4.8 *In vitro* Cell Viability

The results obtained from the trypan blue exclusion assay (Figure 5.11) revealed the toxicity of the drug released from the drug-loaded porous scaffolds. This is consistent with prior work [219] which shows that PGS or PTX drug release tends to stop the progression of cell during the mitotic stage of the cell cycle [365] and significantly repressed the growth and proliferation of the MDA-MB-231 cells (TNBC cells) after 96 h. The 96 h study period covers to the burst release phase of the drug from the porous scaffolds. In contrast, the breast cancer cells that were not subjected to drug release were shown to proliferate in the control experiment. Hence, the reduction in cell viability (following PGS or PTX release from the scaffolds) is attributed to the induction of apoptosis [123,219,366–369].
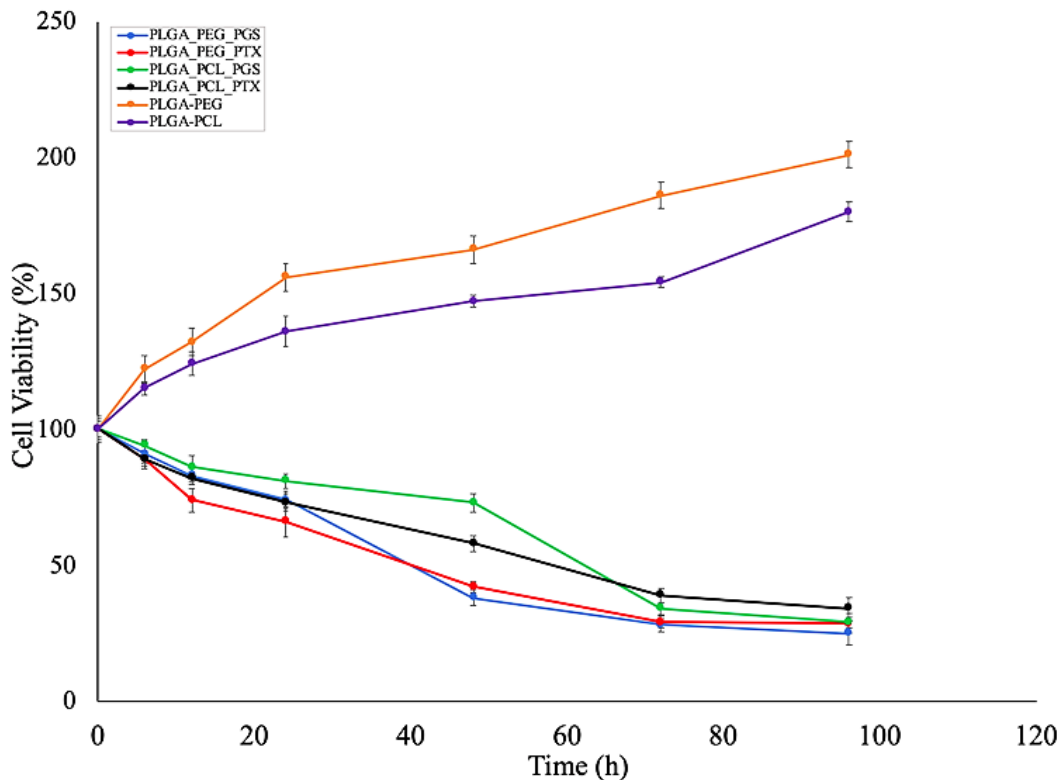
Figure 5.11: Cell viability study indicating the effect of *in vitro* released drug from PLGA-PEG and PLGA-PCL drug-loaded scaffolds incubated in MDA-MB-231 cells within a period of 72 h.

5.4.9 Breast Cell-Proliferation and Integration

Since one of the goals of this study was to enable the regeneration of normal tissue from the polymer scaffolds, following the release of the cancer drug (PGS or PTX), it is of interest to compare the cell proliferation on control (non-drug-loaded; PLGA-PCL and PLGA-PEG) scaffolds with the cell proliferation on scaffolds that were used in the drug release experiment (PLGA-PCL_PGS, PLGA-PEG_PTX, PLGA-PCL_PGS, PLGA-PCL_PTX). In all cases, from the alamar blue assay results (Figure 5.12), it was clearly seen that the percentage alamar blue reduction increased with time. This increase is as a result of higher cell metabolic activities directly associated with increase in cell viability and proliferation of the normal breast cells over the 28-day period. This increase clearly occurs as a result of absence of residual drugs in the scaffolds. Also, the presence of the complimentary properties of PLGA and PEG or PLGA and PCL in the blend are essential. For PLGA-PEG blend scaffold, the presence of PEG as stated earlier in the wettability study leads to a reduced in the contact angle as a result of the hydrophilic nature of PEG. This influence created tends to promote cell/tissue growth on the surfaces of the scaffolds [370].
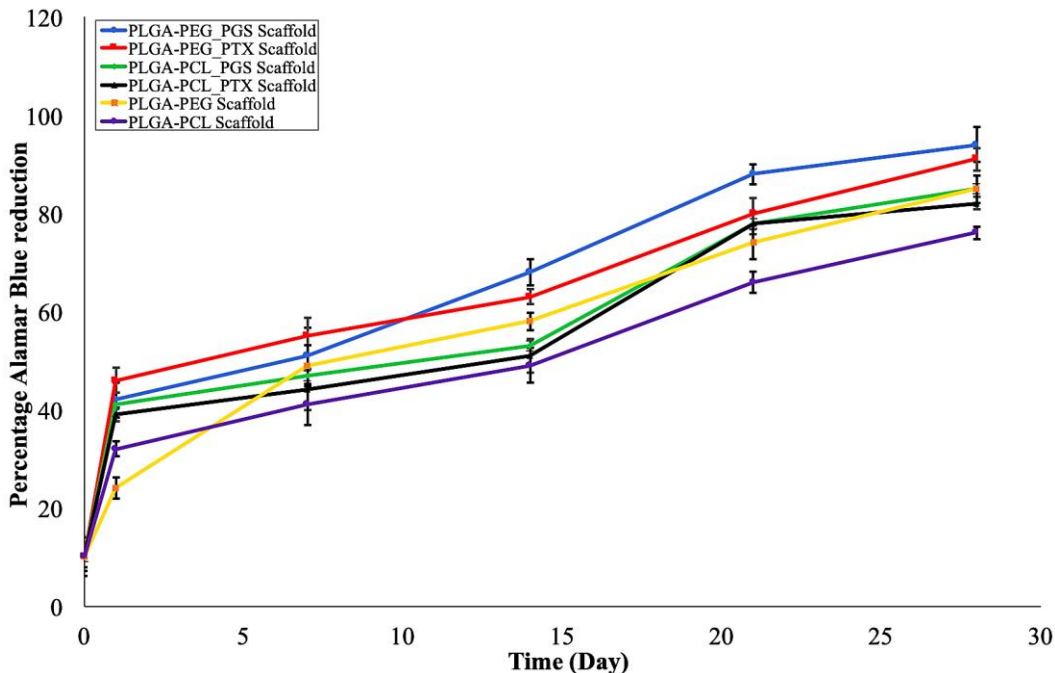
Figure 5.12: Representation of normal breast cell proliferation/viability as a percentage of alamar blue reduction for 28 days period for drug-based scaffolds whose drugs were already released from an *in vitro* experiment before cells were seeded on them.

Somewhat surprising, the viability of the normal breast cell line (MCF-10A) increased with increasing duration of exposure to scaffolds left behind after controlled release. Similar trends were also observed in the SEM images for both drug-loaded and the control (non-drug loaded) scaffolds (Figure 5.13). The Alamar Blue assay results which show denotes the viability of the cells (Figure 5.12) are consistent with SEM and fluorescence microscopy observations of the MCF-10A cells on the prior drug-loaded and non-drug-loaded scaffolds as presented in Figures 5.13 and 5.14. Again, the combined SEM and fluorescence images clearly present evidence of cell spreading and proliferation on all of the scaffold types that were examined in this study.

However, in both of the above cases, cell proliferation increased with time. Furthermore, at day 7 the cells began to spread faster by colonizing the pores and creating a homogeneous distribution of cells on the porous surfaces of the scaffolds after 14 days. The SEM results revealed clear evidence of cell attachment, and cell proliferation on the struts and pores which were completely colonized after 28 days (Figures 5.13A-O). Hence, the current results (Figures 5.12 and 5.13) confirm the biocompatibility of all of the scaffolds that were used in this study.
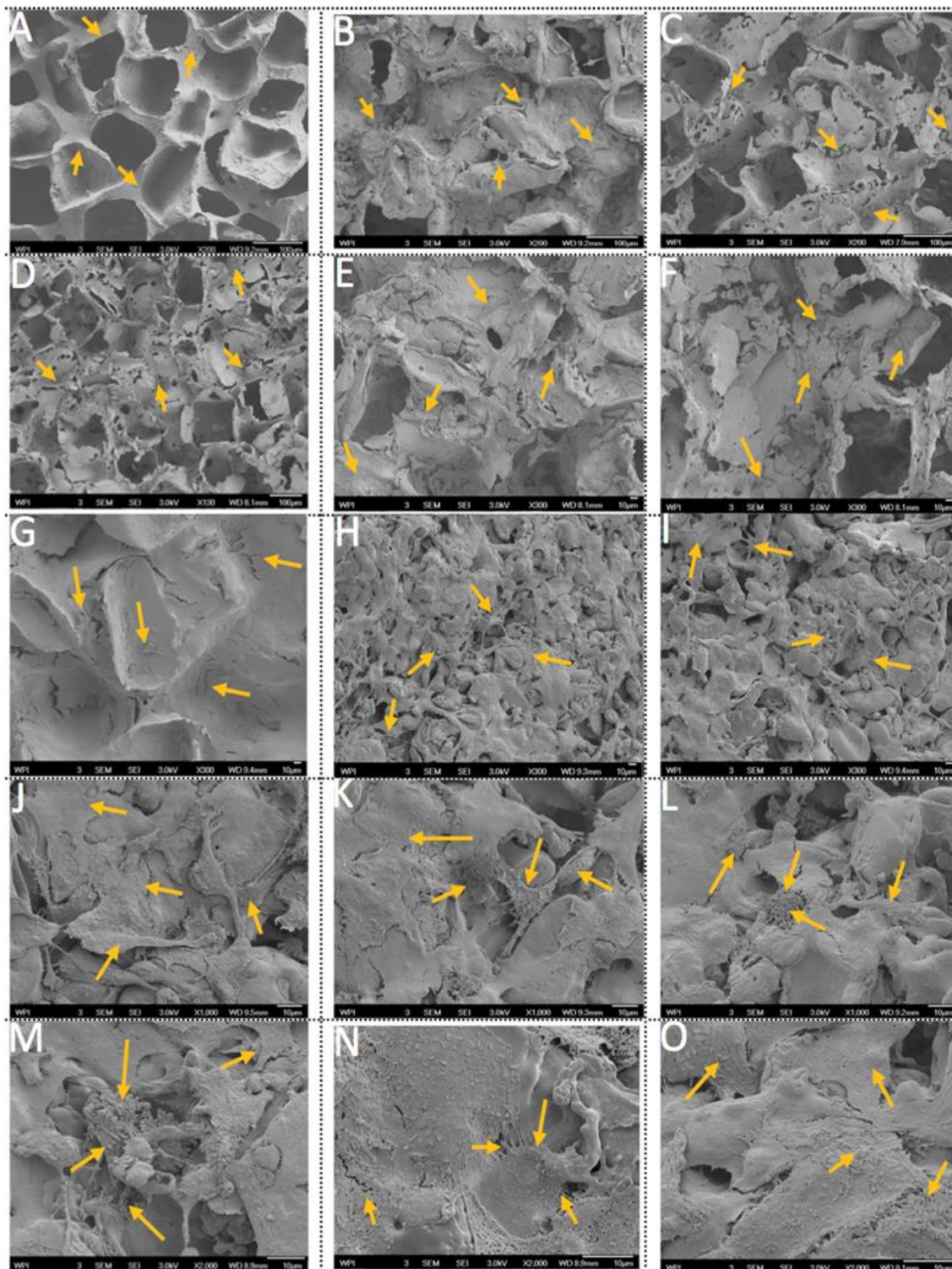
Figure 5.13: Representative SEM micrographs of proliferated normal breast cells on 3D control PLGA-PEG scaffolds (A, D, G, J, M); PLGA-PEG_PGS scaffolds (B, E, H, K, N) after *in vitro* drug release; PLGA-PCL_PGS scaffolds (C, F, I, L, O) after *in vitro* drug release.

The fluorescence images also provide some interesting insights into the distribution of the ECM and the spreading of the cells on the 3D scaffolds (Figures 5.14a-o). It is clear from these images that the extracellular matrix (ECM) covered the entire surfaces of the scaffolds. Again, the stained cell nuclei also show that most of the ECM was covered by proliferating cells on the surfaces of the 3D scaffolds (Figures 5.13 and 5.14). This was true for cell spreading and proliferation on the control (non-drug-loaded) scaffolds and the "used" scaffolds that were left behind after drug release. The current work, therefore, suggests that the "used" scaffolds (left behind scaffolds after drug release) can significantly support cell proliferation and regeneration of normal breast tissue after to controlled and localized release of cancer drug.
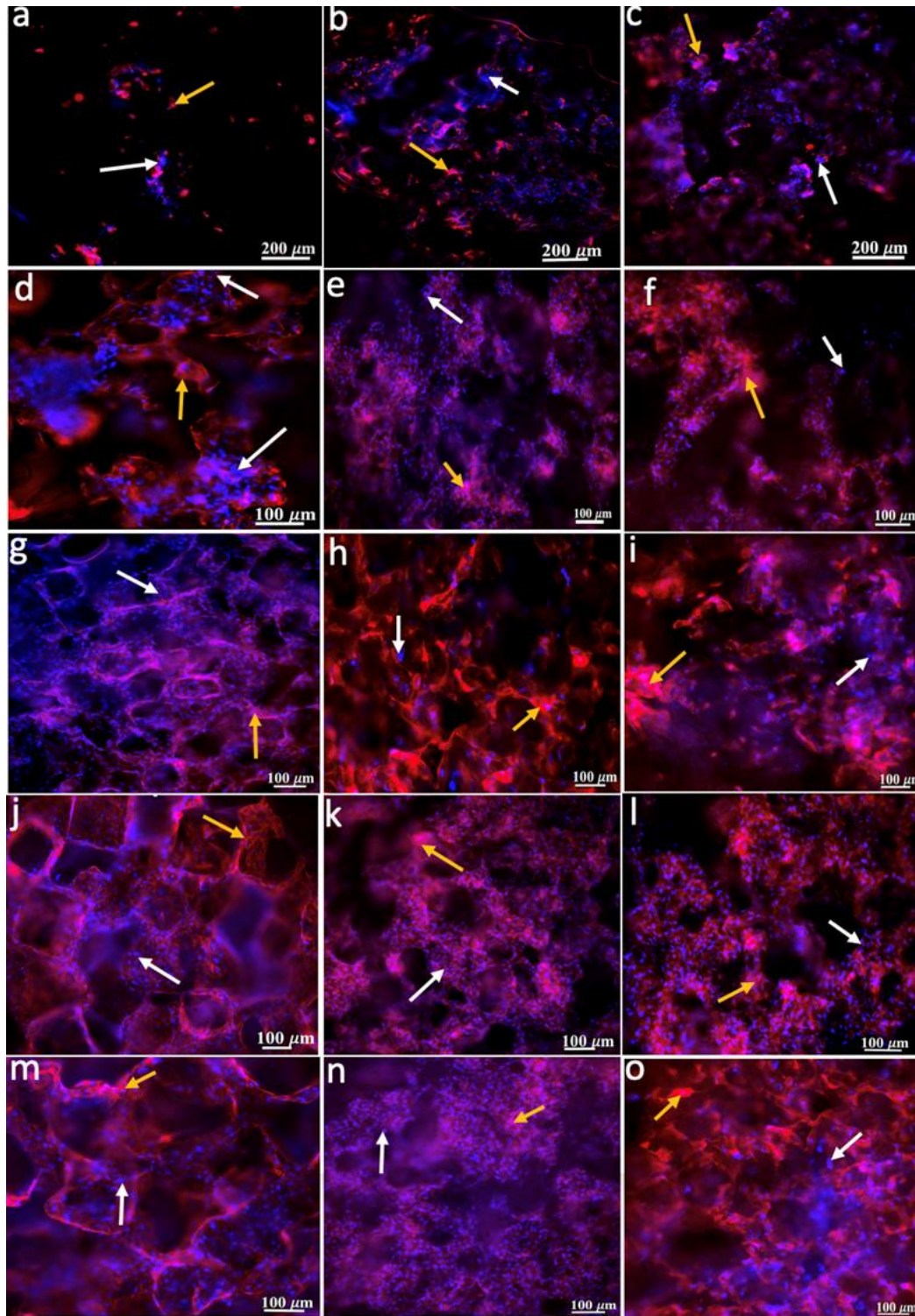
Figure 5.14: Fluorescence images of stained actin cytoskeleton and nuclei of proliferated normal breast cells on 3D control PLGA-PEG scaffolds (a, d, g, j, m); PLGAPEG_PGS scaffolds (B, E, H, K, N) after *in vitro* drug release; PLGA-PCL_PGS scaffolds (c, f, i, l, o) after *in vitro* drug release.

5.4.10 *In vivo* Animal Study

At 28 days of tumor measurement, the mean tumor volume was measured to be 300 ± 21 mm^3. Figure 5.15 show a representative process and evidences of drug-loaded scaffold (PLGA-PCL_PGS) implanted in a surgical removed tumor site. Our results revealed that there was no local regional recurrent of tumor after 16 weeks of proper monitoring of the respective mice implanted with drug-loaded scaffold (See Figure 5.15f). These results are also similar for PLGA-PEG_PTX, PLGA-PCL_PGS and PLGA-PCL_PTX. We also did not notice any side effects, significant weight loss as well as infection due to the combine effect of the surgical procedure and drug-loaded implanted scaffolds.

However, in the case of the positive control non-drug-loaded scaffold (PLGA-PCL) (Figure 5.16a), there was regrowth of tumor (Figure 5.16c). This is because of the absence of drug in the scaffold for control localized treatment of TNBC (Figure 5.16c). Similar results were obtained for the porous PLGA-PEG scaffolds. Multiple recurred TNBC tumor were observed in the case that was no scaffolds implanted 16 weeks after tumor resection (Figure 5.16d). Clearly, our results showed that the drug-loaded scaffolds can be used for the for localized drug delivery of cancer drug treatment of TNBC to prevent the regrowth or loco-regional recurrence in the treatment of TNBC, following surgical resection of triple-negative breast tumor.
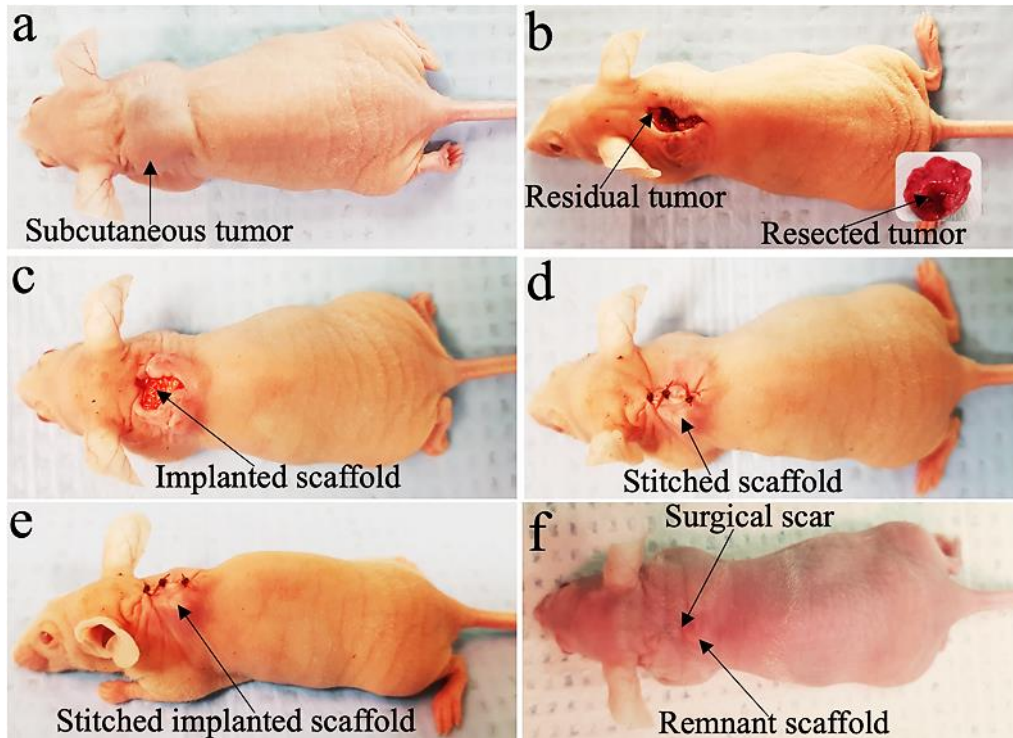
Figure 5.15: Representative anti-tumor effect of drug-loaded scaffold (PLGA-PCL_PGS) showing mice (a) with subcutaneous TNBC tumor, (b) tumor removal, (c) with implantable scaffold (d, e) with scaffolds under surgical stitches and (f) treated after 16 weeks with drug-loaded scaffold
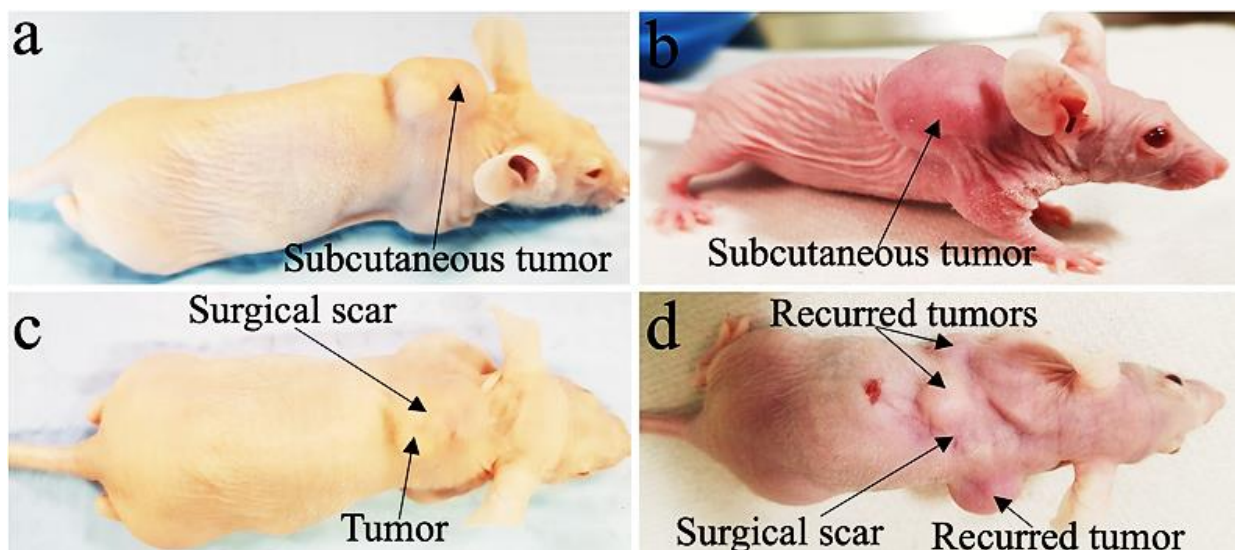
Figure 5.16: Representative of (a, b) control mice with subcutaneous tumor with (c) implantable non-drug-loaded scaffolds (PLGA-PCL) with recurred tumor 16 weeks after surgery (d) control mice with multiple recurred tumor 16 weeks after resection.

Typically, after 16 weeks of surgery as well as the introduction of implantable scaffold, it is expected that if there is any regrowth of TNBC it should have metastasize to the lungs. Thus, results from the immunofluorescence (IF) staining of LHRH to detect the presence of TNBC showed positive result for the control mice tumor which obviously exhibited metastasis in the lungs due to the presence of the LHRH (green stain) carried out [247] (Figure 5.17 a and b). The IF staining result is validated in the H&E histological analysis where multiple metastatic foci and nodules are observed in the tumor and lungs (Figure 5.17c and d).

Finally, H&E results from representative drug-loaded scaffolds (PLGA-PCL-PGS and PGA-PEG_PGS) showed that there was evidence in the regeneration of normal tissue on the residual scaffolds after localized drug delivery at 16 weeks (Figure 5.17a and c). Clearly, it can be seen that there was no multiple metastatic foci and nodules on the lungs for the mice treated with these drug-loaded scaffolds. Similar results were seen in the case of PLGA-PCL-PTX and PGA-PEG_PTX). These results validate the potential use of the drug-loaded scaffolds as implantable systems for controlled localized delivery of cancer drug for cancer treatment and for regeneration of breast tissue, following surgical resection of triple-negative breast tumor. However, a detail animal study should be further explored to fully capture the goal and to sequentially demonstrate the regeneration/reconstruction of breast tissue after controlled drug release by the drug-loaded scaffolds.
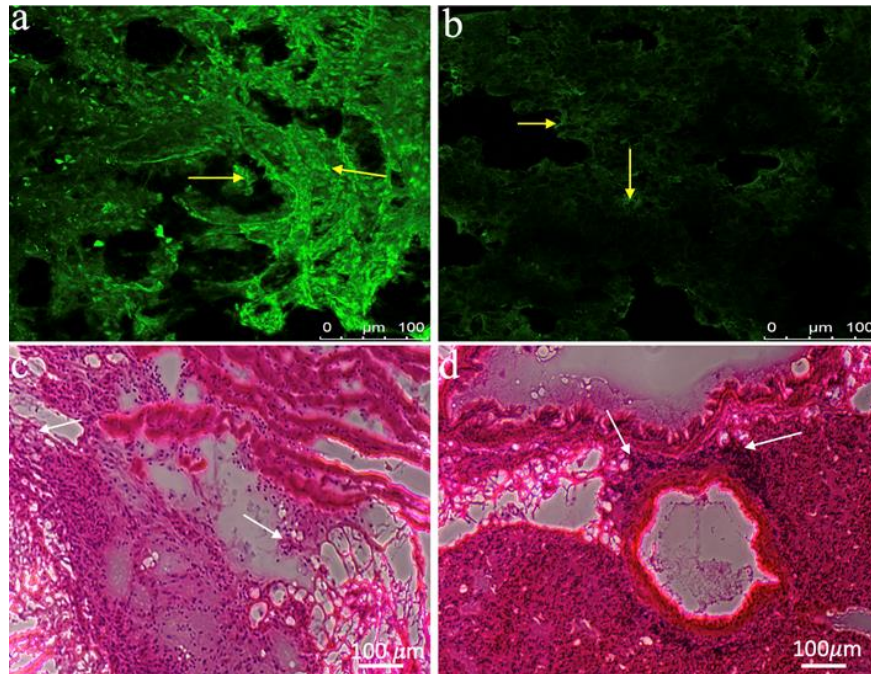
Figure 5.17: Representative images of LHRH receptors (green stain) of (a) tumor, and (b) lungs of mice treated with a control scaffold PLGA-PCL with their corresponding H&E stain showing metastasis in the (c) tumor (d) lungs
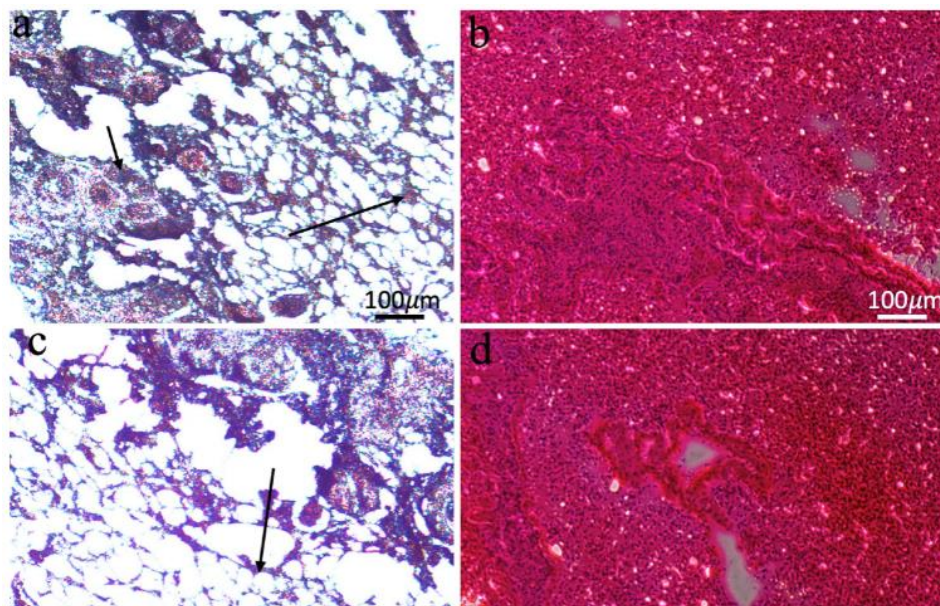
Figure 5.18: H&E staining of representative drug-loaded scaffold (a) PLGA-PCL-PGS and (c) PGA-PEG_PGS scaffolds with regenerated tissue after drug release at week 16 of implantation. While (b and d) are the optical images showing absence of metastasis in the lungs after treatment with drug-loaded PLGA-PCL-PGS and PGA-PEG_PGS scaffolds, respectively.

5.5 Conclusion

The implications of the current work are quite significant. First, they suggest that resorbable scaffolds (with mixed polymer blend) can be engineered for controlled release over extended periods that can give rise to the controlled release of cancer drugs over a period of ~ 56 days. Such controlled release, which is attributed to diffusion and dissolution phenomenon in the earlier stages, and polymer erosion in the later stages, results in the extended release of PGS or PTX, which reduces the viability of breast cancer cells/tissue around the scaffolds.

Furthermore, following the release of the cancer drugs, the current work suggests that normal breast cancer cells spread and proliferate on the surfaces as well as pores of all scaffolds that were explored in this study. Such spreading and proliferation occur on the structure of non-drug-loaded scaffolds as well those that were used initially in the drug release experiments. Also, the *in vivo* animal study clearly demonstrated the use of porous drug-loaded scaffolds for the localized cancer drug delivery to prevent tumor loco-regional recurrence and tissue regeneration, following surgical resection of triple-negative breast tumor.

Hence the current work suggests that drug eluting scaffolds can be developed for the localized release of cancer drugs to surrounding breast cells/tissue. Furthermore, upon their release, the scaffolds can be used to facilitate the regeneration of normal breast tissue via the culturing and regeneration of normal breast tissue on the residual scaffolds. They might be some need to sequentially characterize the vascularized nature of the regenerated tissue from the animal study under *ex vivo* conditions. Further work may be needed to explore in detail the application of the

porous blend of scaffolds for the localized and controlled treatment of breast cancer, and the subsequent regeneration of normal breast tissue in animal studies and clinical trials.

Chapter 6

6.1 Conclusions

This dissertation presents the results of efforts to use materials science and engineering approaches to develop drug delivery systems for the targeted treatment of triple-negative breast cancer and the regeneration of breast tissue after the excision of cancerous breast tissue. A significant aim of cancer therapy is to impede tumor metastasis; hence exploring targeted treatment options for highly metastatic tumors are in high demand. In this body of work, a series of polymer-based drug delivery systems are successfully developed for the targeted, controlled, and localized treatment of TNBC. The main scientific findings from the studies are presented below.

1. *In vitro* drug elution from the three drug delivery systems studied is best fitted to the Korsemeyer-Peppas model. This means that the mechanism of *in vitro* drug release is characterized by anomalous non-Fickian diffusion, followed by polymer degradation and surface erosion phenomena that occur during the later stages of drug elution.

2. The thermodynamic analysis of *in vitro* drug release from the three drug delivery systems revealed positive values for ΔG, ΔH, and negative values for ΔS at set temperatures of 37°C, 41 °C, and 44 °C. These are consistent with endothermic, non-spontaneous, and non-chaotic drug release processes that favor extended release from these drug delivery systems.

3. Extended drug release (over durations of 50-62 days) was observed for the drug-loaded microspheres and scaffolds. Such release durations are comparable to the duration of breast

cancer treatment regimens. They could greatly facilitate the localized clinical treatment of TNBC over clinically relevant durations of breast cancer treatment.

4. The 3D microporous scaffolds are shown to support the growth of normal breast cells/tissue on non-drug-loaded scaffolds or scaffolds that were left behind after the release of PGS or PTX cancer drugs. This is critical because it provides a dual system for drug release and a supporting matrix for breast tissue regeneration. Breast tissue regeneration is particularly important for women who undergo surgery (wide excision, quadrantectomy, and mastectomy). Hence, this approach could provide a viable alternative to silicone implants.

5. The *in vitro* release of targeted and untargeted anti-cancer drugs from all the drug delivery systems (microparticles and scaffolds) results in significant reductions in the viability of MDA-MB-231 (TNBC) cells. The extended, controlled release of targeted and untargeted anti-cancer drugs also prevents the loco-regional recurrence of TNBC from regions surrounding excised breast tumor tissue/xenografts.

6. The results also show that the elution of conjugated drugs (PGS-LHRH and PTX-LHRH) reduces cell viability more than the elution of unconjugated drugs (PGS or PTX). This is due to the interactions between the LHRH and the overexpressed receptors on the surfaces of the TNBC cells.

7. The *in vivo* animal experiments on nude mice showed that the drug release prevents the loco-regional recurrence of TNBC following tumor resection.

8. The drug-loaded PLGA-PEG microspheres extend the survival time of the treated mice post tumor resection compared with the untreated mice. Furthermore, the elution of the targeted drugs from the PLGA-PEG microspheres is more effective in extending the survival times than the elution of the untargeted drugs.

6.2 Suggestions for Future work

Based on the findings from the studies in this dissertation, the following further research is recommended.

6.2.1 Drug-Encapsulated PLGA-PEG Microspheres

The results presented in chapter 3 prove that the release of LHRH-conjugated drugs from PLGA-PEG microspheres prevents the loco-regional recurrence of triple-negative breast cancer in mice model, post tumor resection, unlike unconjugated drugs (PGS, PTX). Since findings from small rodent animals like mice may not translate into human clinical applications, it would be important to implement these studies in larger animal models [371,372]. Larger animal models better reflect the human body conformation and pathophysiology of certain naturally occurring diseases than rodent models [373]. Carrying out those studies in larger animal models will make it easier to assess and evaluate any disparity between rodent studies and large animal studies, thereby translating this research into clinical applications. Shanks *et al.,* (2009) showed the difference in bioavailability of pharmaceuticals between humans, primates, dogs, and rodents and whether they can be used to predict human outcomes [374]. As with any animal study, it is important to note

that there are ethical dimensions and limited indications, which require the specific use of animal models.

Furthermore, the cytotoxicity on other major organs like (bone, liver, spleen) are also important factors that need to be clarified for clinical applications. Additionally, under *in vitro* conditions, it would be good to examine degradation products such as lactic acid (from PLGA degradation) in the remaining buffer during the drug release experiment. One question to consider is whether the accumulation of degradation products incurs any changes in pH, for example, pH of the drug release environment, and thus affect drug release. It will also be good to assess whether multiple concentrations of drug microspheres should be selected to test the effect of different duration on cell activity to find the best concentration of drug microspheres.

6.2.2 PLGA-CS-PEG Microparticles

In this study, the *in vitro* drug release from PLGA-CS-PEG microspheres was promising. However, due to the limitation of time, no *in vivo* studies were carried out. Hence, it would be essential to demonstrate the performance of the drug-loaded PLGA-CS-PEG microspheres under *in vivo* conditions. Furthermore, the potential cytotoxicity in major organs such as lungs, and bones should also be considered because it has been observed that breast cancer metastasizes preferentially to the bones and lungs and less frequently to other organs such as the liver and brain [375]. It will also be essential to study the effects of drug release with additional cancer cell lines. Under *in vitro* conditions, it will be good to carry out more *in vitro* studies, such as non-specific toxicity to normal non-cancer cells or biodegradability assay, the degradation of these microspheres for extended periods, and examine degradation products in the remaining buffer

during the drug release experiment. It would be important to encapsulate the PLGA-CS-PEG microspheres with LHRH-conjugated drugs instead of just PGS and PTX respectively, to enhance the specific targeting of TNBC.

6.2.3 Degradable porous drug-loaded polymer scaffolds

Our findings from the *in vivo* experiments suggest that localized drug release from drug-based 3D resorbable porous scaffolds can be used to eliminate/treat local recurred triple-negative breast tumors and promote normal breast tissue regeneration after surgical resection. However, further work is also needed using larger animal models [371,372]. As stated earlier, large animals better reflect the human body conformation and pathophysiology of certain naturally occurring diseases than rodent models [373]. It would also be beneficial to encapsulate LHRH-conjugated drugs instead of unconjugated drugs, as previous studies from our group have established that LHRH-conjugated drugs are more effective in the specific targeting of TNBC [43,101].

6.2.4 3D PLA capsules embedded with poly-N-isopropyl-acrylamide (PNIPA) hydrogels.

Here, we started a study of targeted and controlled drug release from 3D printed PLA with embedded PNIPA gels for TNBC treatment. The study uses 3D printing to fabricate PLA capsules that contain drug-loaded poly-N-isopropyl-acrylamide (PNIPA)-based hydrogels. This customizable method uses computer-assisted design (CAD) files to print PLA capsules with well-controlled architectures. In this way, 3D Printable devices/capsules can be customized for patients and prepared in minutes. The *in vitro* release of the encapsulated drugs was studied at human body temperature (37°C) and hyperthermic temperatures (41 and 44°C). To continue this study, it would

be essential to analyze the *in vitro* drug release using thermodynamics and kinetics models to understand the mechanisms of drug release. Also, the *in vitro* cell viability and cytotoxicity should be examined, followed by *in vivo* studies to assess the robustness of this drug delivery device. Figure 6.1 below shows schematics of capsule configurations, while Figure 6.2 shows the *in vitro* drug release from the device for various drug formulations at 37°C, 41°C, and 44°C, respectively.
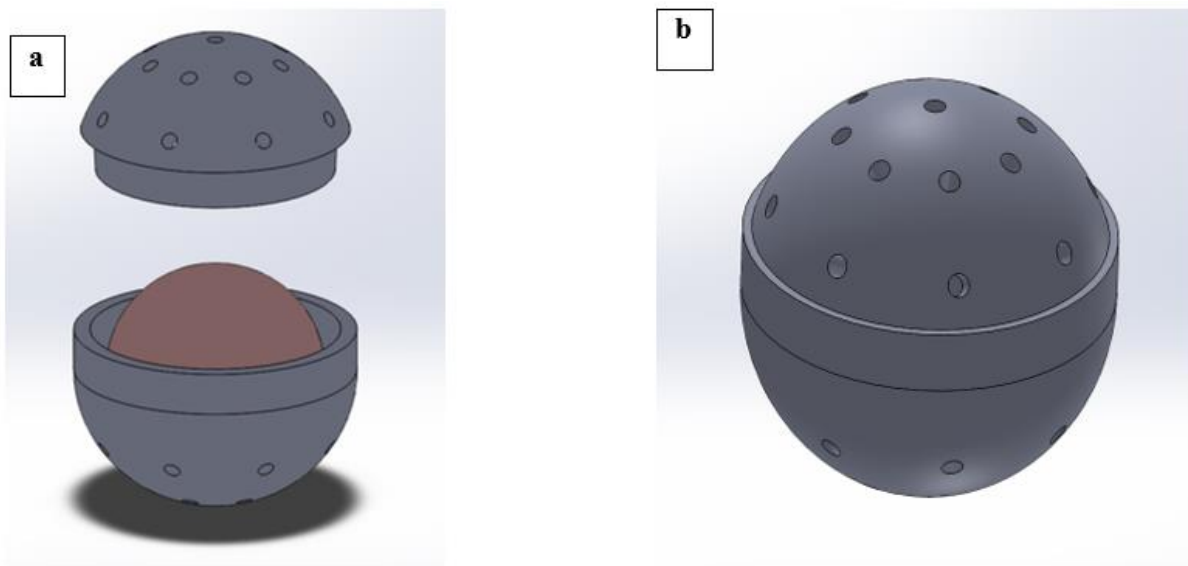
Figure 6.1: Schematics of Capsule Configurations: (a) Opened 3D-PLA capsule containing PNIPA hydrogel and (b) Sealed 3D-PLA capsule containing PNIPA hydrogel

a

b
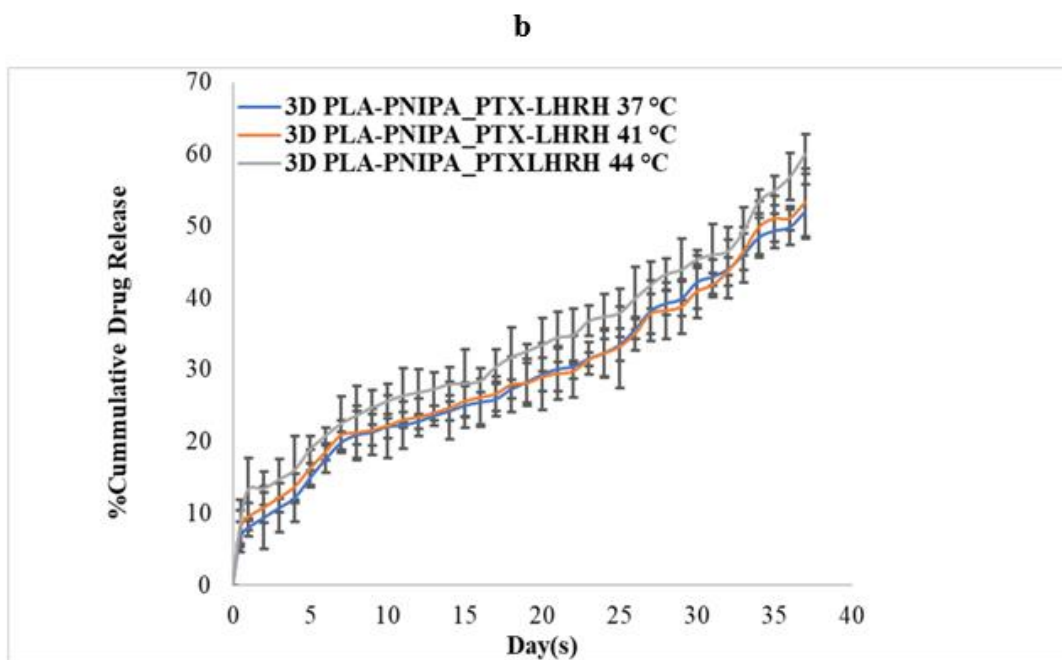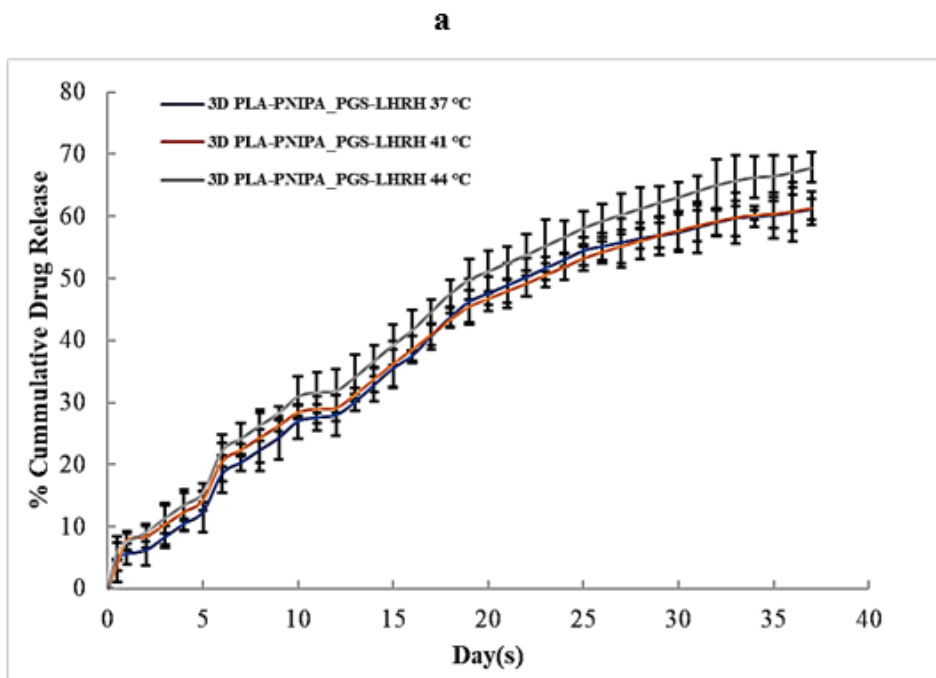
Figure 6.2. *In vitro* release profile of the various drug-loaded 3D-PLA capsule formulations (a) 3D-PLA-PNIPA_PGS-LHRH (b)3D-PLA-PNIPA_PTX-LHRH at 37°C, 41°C and 44°C, respectively.

References

[1]   H. Sung, J. Ferlay, R.L. Siegel, M. Laversanne, I. Soerjomataram, A. Jemal, F. Bray, Global Cancer Statistics 2020: GLOBOCAN Estimates of Incidence and Mortality Worldwide for 36 Cancers in 185 Countries, CA. Cancer J. Clin. 71 (2021) 209–249. https://doi.org/10.3322/caac.21660.

[2]   S. Thakkar, D. Sharma, K. Kalia, R.K. Tekade, Tumor microenvironment targeted nanotherapeutics for cancer therapy and diagnosis: A review, Acta Biomater. 101 (2020) 43–68. https://doi.org/10.1016/j.actbio.2019.09.009.

[3]   Q. Song, S.D. Merajver, J.Z. Li, Cancer classification in the genomic era: Five contemporary problems, Hum. Genomics. 9 (2015) 1–8. https://doi.org/10.1186/s40246-015-0049-8.

[4]   J. Boyle, Molecular biology of the cell, 5th edition by B. Alberts, A. Johnson, J. Lewis, M. Raff, K. Roberts, and P. Walter, Biochem. Mol. Biol. Educ. 36 (2008) 317–318. https://doi.org/10.1002/bmb.20192.

[5]   N.E. Sounni, A. Noel, Targeting the tumor microenvironment for cancer therapy, Clin. Chem. 59 (2013) 85–93. https://doi.org/10.1373/clinchem.2012.185363.

[6]   K. Thanki, R.P. Gangwal, A.T. Sangamwar, S. Jain, Oral delivery of anticancer drugs: Challenges and opportunities, J. Control. Release. 170 (2013) 15–40. https://doi.org/10.1016/j.jconrel.2013.04.020.

[7]   A.F. Dos Santos, D.R.Q. De Almeida, L.F. Terra, M.S. Baptista, L. Labriola, Photodynamic therapy in cancer treatment - an update review, J. Cancer Metastasis Treat. 5 (2019). https://doi.org/10.20517/2394-4722.2018.83.

[8]   H. Peinado, H. Zhang, I.R. Matei, B. Costa-Silva, A. Hoshino, G. Rodrigues, B. Psaila, R.N. Kaplan, J.F. Bromberg, Y. Kang, M.J. Bissell, T.R. Cox, A.J. Giaccia, J.T. Erler, S. Hiratsuka, C.M. Ghajar, D. Lyden, Pre-metastatic niches: Organ-specific homes for metastases, Nat. Rev. Cancer. 17 (2017) 302–317. https://doi.org/10.1038/nrc.2017.6.

[9]   F. Kamangar, G.M. Dores, W.F. Anderson, Patterns of cancer incidence, mortality, and prevalence across five continents: Defining priorities to reduce cancer disparities in different geographic regions of the world, J. Clin. Oncol. 24 (2006) 2137–2150. https://doi.org/10.1200/JCO.2005.05.2308.

[10]   Z.Q. Tao, A. Shi, C. Lu, T. Song, Z. Zhang, J. Zhao, Breast Cancer: Epidemiology and Etiology, Cell Biochem. Biophys. 72 (2015) 333–338. https://doi.org/10.1007/s12013-014-0459-6.

[11]   S. Mittal, H. Kaur, N. Gautam, A.K. Mantha, Biosensors for breast cancer diagnosis: A review of bioreceptors, biotransducers and signal amplification strategies, Biosens. Bioelectron. 88 (2017) 217–231. https://doi.org/10.1016/j.bios.2016.08.028.

[12] L.A. Torre, R.L. Siegel, E.M. Ward, A. Jemal, Global cancer incidence and mortality rates and trends - An update, Cancer Epidemiol. Biomarkers Prev. 25 (2016) 16–27. https://doi.org/10.1158/1055-9965.EPI-15-0578.

[13] S. Pilleron, D. Sarfati, M. Janssen-Heijnen, J. Vignat, J. Ferlay, F. Bray, I. Soerjomataram, Global cancer incidence in older adults, 2012 and 2035: A population-based study, Int. J. Cancer. 144 (2019) 49–58. https://doi.org/10.1002/ijc.31664.

[14] O. Ginsburg, C.H. Yip, A. Brooks, A. Cabanes, M. Caleffi, J.A. Dunstan Yataco, B. Gyawali, V. McCormack, M. McLaughlin de Anderson, R. Mehrotra, A. Mohar, R. Murillo, L.E. Pace, E.D. Paskett, A. Romanoff, A.F. Rositch, J.R. Scheel, M. Schneidman, K. Unger-Saldaña, V. Vanderpuye, T.Y. Wu, S. Yuma, A. Dvaladze, C. Duggan, B.O. Anderson, Breast cancer early detection: A phased approach to implementation, Cancer. 126 (2020) 2379–2393. https://doi.org/10.1002/cncr.32887.

[15] B.S. Yadav, P. Chanana, S. Jhamb, Biomarkers in triple negative breast cancer: A review, World J. Clin. Oncol. 6 (2015) 252–263. https://doi.org/10.5306/wjco.v6.i6.252.

[16] P. Kumar, R. Aggarwal, An overview of triple-negative breast cancer, Arch. Gynecol. Obstet. 293 (2016) 247–269. https://doi.org/10.1007/s00404-015-3859-y.

[17] G. Bianchini, J.M. Balko, I.A. Mayer, M.E. Sanders, L. Gianni, Triple-negative breast cancer: Challenges and opportunities of a heterogeneous disease, Nat. Rev. Clin. Oncol. 13 (2016) 674–690. https://doi.org/10.1038/nrclinonc.2016.66.

[18] T. Ovcaricek, S.G. Frkovic, E. Matos, B. Mozina, S. Borstnar, Triple negative breast cancer - Prognostic factors and survival, Radiol. Oncol. 45 (2011) 46–52. https://doi.org/10.2478/v10019-010-0054-4.

[19] J.L. da Silva, N.C. Cardoso Nunes, P. Izetti, G.G. de Mesquita, A.C. de Melo, Triple negative breast cancer: A thorough review of biomarkers, Crit. Rev. Oncol. Hematol. 145 (2020) 102855. https://doi.org/10.1016/j.critrevonc.2019.102855.

[20] G.J. Morris, S. Naidu, A.K. Topham, F. Guiles, Y. Xu, P. McCue, G.F. Schwartz, P.K. Park, A.L. Rosenberg, K. Brill, E.P. Mitchell, Differences in breast carcinoma characteristics in newly diagnosed African-American and Caucasian patients: A single-institution compilation compared with the national cancer institute's surveillance, epidemiology, and end results database, Cancer. 110 (2007) 876–884. https://doi.org/10.1002/cncr.22836.

[21] L.A. Carey, E.C. Dees, L. Sawyer, L. Gatti, D.T. Moore, F. Collichio, D.W. Ollila, C.I. Sartor, M.L. Graham, C.M. Perou, The triple negative paradox: Primary tumor chemosensitivity of breast cancer subtypes, Clin. Cancer Res. 13 (2007) 2329–2334. https://doi.org/10.1158/1078-0432.CCR-06-1109.

[22] C.A. Hudis, L. Gianni, Triple-Negative Breast Cancer: An Unmet Medical Need, Oncologist. 16 (2011) 1–11. https://doi.org/10.1634/theoncologist.2011-s1-01.

[23] F. Kassam, K. Enright, R. Dent, G. Dranitsaris, J. Myers, C. Flynn, M. Fralick, R. Kumar,

M. Clemons, Survival outcomes for patients with metastatic triple-negative breast cancer: Implications for clinical practice and trial design, Clin. Breast Cancer. 9 (2009) 29–33. https://doi.org/10.3816/CBC.2009.n.005.

[24] C.L. Shapiro, A. Recht, Side Effects of Adjuvant Treatment of Breast Cancer, N. Engl. J. Med. 344 (2001) 1997–2008. https://doi.org/10.1056/nejm200106283442607.

[25] P. Broët, S.M. Scholl, A. De la Rochefordière, A. Fourquet, T. Moreau, Y. De Rycke, B. Asselain, P. Pouillart, Short and long-term effects on survival in breast cancer patients treated by primary chemotherapy: An updated analysis of a randomized trial, Breast Cancer Res. Treat. 58 (1999) 151–156. https://doi.org/10.1023/A:1006339918798.

[26] C. Anders, L.A. Carey, Understanding and treating triple-negative breast cancer, Oncology. 22 (2008) 1233–1239.

[27] N. Gao, X.J. Li, Controlled drug delivery using microfluidic devices, in: Microfluid. Devices Biomed. Appl., 2013: pp. 167–184. https://doi.org/10.1533/9780857097040.2.167.

[28] C. Li, J. Wang, Y. Wang, H. Gao, G. Wei, Y. Huang, H. Yu, Y. Gan, Y. Wang, L. Mei, H. Chen, H. Hu, Z. Zhang, Y. Jin, Recent progress in drug delivery, Acta Pharm. Sin. B. 9 (2019) 1145–1162. https://doi.org/10.1016/j.apsb.2019.08.003.

[29] W.B. Liechty, D.R. Kryscio, B. V. Slaughter, N.A. Peppas, Polymers for drug delivery systems, Annu. Rev. Chem. Biomol. Eng. 1 (2010) 149–173. https://doi.org/10.1146/annurev-chembioeng-073009-100847.

[30] J.K. Mills, D. Needham, Targeted drug delivery, Expert Opin. Ther. Pat. 9 (1999) 1499–1513. https://doi.org/10.1517/13543776.9.11.1499.

[31] H. Maeda, The enhanced permeability and retention (EPR) effect in tumor vasculature: The key role of tumor-selective macromolecular drug targeting, Adv. Enzyme Regul. 41 (2001) 189–207. https://doi.org/10.1016/S0065-2571(00)00013-3.

[32] J. Fang, H. Nakamura, H. Maeda, The EPR effect: Unique features of tumor blood vessels for drug delivery, factors involved, and limitations and augmentation of the effect, Adv. Drug Deliv. Rev. 63 (2011) 136–151. https://doi.org/10.1016/j.addr.2010.04.009.

[33] Y.H. Bae, K. Park, Targeted drug delivery to tumors: Myths, reality and possibility, J. Control. Release. 153 (2011) 198–205. https://doi.org/10.1016/j.jconrel.2011.06.001.

[34] M.F. Attia, N. Anton, J. Wallyn, Z. Omran, T.F. Vandamme, An overview of active and passive targeting strategies to improve the nanocarriers efficiency to tumour sites, J. Pharm. Pharmacol. 71 (2019) 1185–1198. https://doi.org/10.1111/jphp.13098.

[35] A. Béduneau, P. Saulnier, F. Hindré, A. Clavreul, J.C. Leroux, J.P. Benoit, Design of targeted lipid nanocapsules by conjugation of whole antibodies and antibody Fab' fragments, Biomaterials. 28 (2007) 4978–4990. https://doi.org/10.1016/j.biomaterials.2007.05.014.

[36]   P. Deckert, Current Constructs and Targets in Clinical Development for Antibody- Based Cancer Therapy, Curr. Drug Targets. 10 (2009) 158–175. https://doi.org/10.2174/138945009787354502.

[37]   M. Hong, S. Zhu, Y. Jiang, G. Tang, Y. Pei, Efficient tumor targeting of hydroxycamptothecin loaded PEGylated niosomes modified with transferrin, J. Control. Release. 133 (2009) 96–102. https://doi.org/10.1016/j.jconrel.2008.09.005.

[38]   A. Zensi, D. Begley, C. Pontikis, C. Legros, L. Mihoreanu, S. Wagner, C. Büchel, H. von Briesen, J. Kreuter, Albumin nanoparticles targeted with Apo E enter the CNS by transcytosis and are delivered to neurones, J. Control. Release. 137 (2009) 78–86. https://doi.org/10.1016/j.jconrel.2009.03.002.

[39]   F. Canal, M.J. Vicent, G. Pasut, O. Schiavon, Relevance of folic acid/polymer ratio in targeted PEG-epirubicin conjugates, J. Control. Release. 146 (2010) 388–399. https://doi.org/10.1016/j.jconrel.2010.05.027.

[40]   C.W. Kwok, O. Treeck, S. Buchholz, S. Seitz, O. Ortmann, J.B. Engel, Receptors for luteinizing hormone-releasing hormone (GnRH) as therapeutic targets in triple negative breast cancers (TNBC), Target. Oncol. 10 (2015) 365–373. https://doi.org/10.1007/s11523-014-0340-y.

[41]   A.V. Fekete, M., Wittliff, J.L. and Schally, Characteristics and distribution of receptors for [D-TRP6]-luteinizing hormone-releasing hormone, somatostatin, epidermal growth factor, and sex steroids in 500 biopsy samples of human breast cancer., J. Clin. Lab. Anal. 3 (1989) 137–147.

[42]   S. Buchholz, S. Seitz, A. V. Schally, J.B. Engel, F.G. Rick, L. Szalontay, F. Hohla, A. Krishan, A. Papadia, T. Gaiser, G. Brockhoff, O. Ortmann, K. Diedrich, F. Köster, Triple-negative breast cancers express receptors for luteinizing hormone-releasing hormone (LHRH) and respond to LHRH antagonist Cetrorelix with growth inhibition, Int. J. Oncol. 35 (2009) 789–796. https://doi.org/10.3892/ijo-00000391.

[43]   J.D. Obayemi, A.A. Salifu, S.C. Eluu, V.O. Uzonwanne, S.M. Jusu, C.C. Nwazojie, C.E. Onyekanne, O. Ojelabi, L. Payne, C.M. Moore, J.A. King, W.O. Soboyejo, LHRH-Conjugated Drugs as Targeted Therapeutic Agents for the Specific Targeting and Localized Treatment of Triple Negative Breast Cancer, Sci. Rep. 10 (2020) 1–18. https://doi.org/10.1038/s41598-020-64979-1.

[44]   J. Engel, G. Emons, J. Pinski, A. V. Schally, AEZS-108: A targeted cytotoxic analog of LHRH for the treatment of cancers positive for LHRH receptors, Expert Opin. Investig. Drugs. 21 (2012) 891–899. https://doi.org/10.1517/13543784.2012.685128.

[45]   A. V. Schally, A. Nagy, Chemotherapy targeted to cancers through tumoral hormone receptors, Trends Endocrinol. Metab. 15 (2004) 300–310. https://doi.org/10.1016/j.tem.2004.07.002.

[46]   American Cancer Institute, Cancer Facts & Figures 2020, CA. Cancer J. Clin. (2020) 1–76.

[47] N.N. Pavlova, C.B. Thompson, The Emerging Hallmarks of Cancer Metabolism, Cell Metab. 23 (2016) 27–47. https://doi.org/10.1016/j.cmet.2015.12.006.

[48] N. Fortunato, Pathophysiology: The Biologic Basis for Disease in Adults and Children, 1996. https://doi.org/10.1016/s0001-2092(06)63479-0.

[49] P. Anand, A.B. Kunnumakara, C. Sundaram, K.B. Harikumar, S.T. Tharakan, O.S. Lai, B. Sung, B.B. Aggarwal, Cancer is a preventable disease that requires major lifestyle changes, Pharm. Res. 25 (2008) 2097–2116. https://doi.org/10.1007/s11095-008-9661-9.

[50] M. Galukande, J. Schüz, B.O. Anderson, A. Zietsman, C. Adisa, A. Anele, G. Parham, L.F. Pinder, S. Mutumba, D. Lombe, A. Cabanes, M. Foerster, I. Dos-Santos-Silva, Maternally Orphaned Children and Intergenerational Concerns Associated with Breast Cancer Deaths among Women in Sub-Saharan Africa, JAMA Oncol. 7 (2021) 285–289. https://doi.org/10.1001/jamaoncol.2020.6583.

[51] Atlanta: American Cancer Society, Cancer Treatment & Survivorship Facts and Figures 2019-2021, (2019). https://www.cancer.org/content/dam/cancer-org/research/cancer-facts-and-statistics/cancer-treatment-and-survivorship-facts-and-figures/cancer-treatment-and-survivorship-facts-and-figures-2019-2021.pdf.

[52] L.A. Torre, A.M.G. Sauer, M.S. Chen, M. Kagawa-Singer, A. Jemal, R.L. Siegel, Cancer statistics for Asian Americans, Native Hawaiians, and Pacific Islanders, 2016: Converging incidence in males and females, CA. Cancer J. Clin. 66 (2016) 182–202. https://doi.org/10.3322/caac.21335.

[53] G.N. Sharma, R. Dave, J. Sanadya, P. Sharma, K.K. Sharma, Various types and management of breast cancer: An overview, J. Adv. Pharm. Technol. Res. 1 (2010) 109–126.

[54] M. Akram, M. Iqbal, M. Daniyal, A.U. Khan, Awareness and current knowledge of breast cancer, Biol. Res. 50 (2017) 1–23. https://doi.org/10.1186/s40659-017-0140-9.

[55] P.J. Tanis, O.E. Nieweg, R.A. Valdés Olmos, B.B.R. Kroon, Anatomy and physiology of lymphatic drainage of the breast from the perspective of sentinel node biopsy, J. Am. Coll. Surg. 192 (2001) 399–409. https://doi.org/10.1016/S1072-7515(00)00776-6.

[56] N.R. Jagannathan, U. Sharma, Breast tissue metabolism by magnetic resonance spectroscopy, Metabolites. 7 (2017) 25. https://doi.org/10.3390/metabo7020025.

[57] American Cancer Society, Breast Cancer Facts & Figures 2019-2020, Am. Cancer Soc. (2019).

[58] W.E. Barlow, C.D. Lehman, Y. Zheng, R. Ballard-Barbash, B.C. Yankaskas, G.R. Cutter, P.A. Carney, B.M. Geller, R. Rosenberg, K. Kerlikowske, D.L. Weaver, S.H. Taplin, Performance of diagnostic mammography for women with signs or symptoms of breast cancer, J. Natl. Cancer Inst. 94 (2002) 1151–1159. https://doi.org/10.1093/jnci/94.15.1151.

[59]   N.I.R. Yassin, S. Omran, E.M.F. El Houby, H. Allam, Machine learning techniques for breast cancer computer aided diagnosis using different image modalities: A systematic review, Comput. Methods Programs Biomed. 156 (2018) 25–45. https://doi.org/10.1016/j.cmpb.2017.12.012.

[60]   S.H. Jafari, Z. Saadatpour, A. Salmaninejad, F. Momeni, M. Mokhtari, J.S. Nahand, M. Rahmati, H. Mirzaei, M. Kianmehr, Breast cancer diagnosis: Imaging techniques and biochemical markers, J. Cell. Physiol. 233 (2018) 5200–5213. https://doi.org/10.1002/jcp.26379.

[61]   H. Li, Y. Wang, K.J.R. Liu, S.C.B. Lo, M.T. Freedman, Computerized radiographic mass detection - Part II: Decision support by featured database visualization and modular neural networks, IEEE Trans. Med. Imaging. 20 (2001) 302–313. https://doi.org/10.1109/42.921479.

[62]   N. Howlader, K.A. Cronin, A.W. Kurian, R. Andridge, Differences in breast cancer survival by molecular subtypes in the United States, Cancer Epidemiol. Biomarkers Prev. 27 (2018) 619–626. https://doi.org/10.1158/1055-9965.EPI-17-0627.

[63]   C.A. Parise, V. Caggiano, Risk of mortality of node-negative, ER/PR/HER2 breast cancer subtypes in T1, T2, and T3 tumors, Breast Cancer Res. Treat. 165 (2017) 743–750. https://doi.org/10.1007/s10549-017-4383-5.

[64]   M.J. Ellis, V.J. Suman, J. Hoog, R. Goncalves, S. Sanati, C.J. Creighton, K. DeSchryver, E. Crouch, A. Brink, M. Watson, J. Luo, Y. Tao, M. Barnes, M. Dowsett, G.T. Budd, E. Winer, P. Silverman, L. Esserman, L. Carey, C.X. Ma, G. Unzeitig, T. Pluard, P. Whitworth, G. Babiera, J.M. Guenther, Z. Dayao, D. Ota, M. Leitch, J.A. Olson, D.C. Allred, K. Hunt, Ki67 proliferation index as a tool for chemotherapy decisions during and after neoadjuvant aromatase inhibitor treatment of breast cancer: Results from the American college of surgeons oncology group Z1031 trial (alliance), J. Clin. Oncol. 35 (2017) 1061–1069. https://doi.org/10.1200/JCO.2016.69.4406.

[65]   N. Houssami, R.M. Turner, M. Morrow, Meta-analysis of pre-operative magnetic resonance imaging (MRI) and surgical treatment for breast cancer, Breast Cancer Res. Treat. 165 (2017) 273–283. https://doi.org/10.1007/s10549-017-4324-3.

[66]   R. Pearson, R. Milligan, H. Cain, Radioactive iodine-125 seed localisation of breast carcinoma in advance of the day of surgery reduces pre-operative anxiety levels, Eur. J. Surg. Oncol. 43 (2017) S7. https://doi.org/10.1016/j.ejso.2017.01.039.

[67]   J.H. Rowland, K.A. Desmond, B.E. Meyerowitz, T.R. Belin, G.E. Wyatt, P.A. Ganz, Role of breast reconstructive surgery in physical and emotional outcomes among breast cancer survivors, J. Natl. Cancer Inst. 92 (2000) 1422–1429. https://doi.org/10.1093/jnci/92.17.1422.

[68]   R.W. Johnstone, A.A. Ruefli, S.W. Lowe, Apoptosis: A link between cancer genetics and chemotherapy, Cell. 108 (2002) 153–164. https://doi.org/10.1016/S0092-8674(02)00625-6.

[69] S. Masood, Neoadjuvant chemotherapy in breast cancers, Women's Heal. 12 (2016) 480–491. https://doi.org/10.1177/1745505716677139.

[70] S.B. Oppenheimer, Cellular basis of cancer metastasis: A review of fundamentals and new advances, Acta Histochem. (2006). https://doi.org/10.1016/j.acthis.2006.03.008.

[71] A.F. Chambers, A.C. Groom, I.C. MacDonald, Dissemination and growth of cancer cells in metastatic sites, Nat. Rev. Cancer. 2 (2002) 563–572. https://doi.org/10.1038/nrc865.

[72] G. Poste, I.J. Fidler, The pathogenesis of cancer metastasis, Nature. 283 (1980) 139–146. https://doi.org/10.1038/283139a0.

[73] I.J. Fidler, The organ microenvironment and cancer metastasis, Differentiation. 70 (2002) 498–505. https://doi.org/10.1046/j.1432-0436.2002.700904.x.

[74] A.M. Alizadeh, S. Shiri, S. Farsinejad, Metastasis review: from bench to bedside, Tumor Biol. 35 (2014) 8483–8523. https://doi.org/10.1007/s13277-014-2421-z.

[75] S.A. Brooks, H.J. Lomax-Browne, T.M. Carter, C.E. Kinch, D.M.S. Hall, Molecular interactions in cancer cell metastasis, Acta Histochem. 112 (2010) 3–25. https://doi.org/10.1016/j.acthis.2008.11.022.

[76] G. Curigliano, A. Goldhirsch, The triple-negative subtype: New ideas for the poorest prognosis breast cancer, J. Natl. Cancer Inst. - Monogr. (2011) 108–110. https://doi.org/10.1093/jncimonographs/lgr038.

[77] F. Penault-Llorca, G. Viale, Pathological and molecular diagnosis of triple-negative breast cancer: A clinical perspective, Ann. Oncol. 23 (2012) vi19–vi22. https://doi.org/10.1093/annonc/mds190.

[78] R. Ismail-Khan, M.M. Bui, A review of triple-negative breast cancer, Cancer Control. 17 (2010) 173–176. https://doi.org/10.1177/107327481001700305.

[79] R.D. Chacón, M. V. Costanzo, Triple-negative breast cancer, Breast Cancer Res. 12 (2010). https://doi.org/10.1186/bcr2574.

[80] T.C. De Ruijter, J. Veeck, J.P.J. De Hoon, M. Van Engeland, V.C. Tjan-Heijnen, Characteristics of triple-negative breast cancer, J. Cancer Res. Clin. Oncol. 137 (2011) 183–192. https://doi.org/10.1007/s00432-010-0957-x.

[81] P. Sharma, Biology and Management of Patients With Triple-Negative Breast Cancer, Oncologist. 21 (2016) 1050–1062. https://doi.org/10.1634/theoncologist.2016-0067.

[82] C. Liedtke, C. Mazouni, K.R. Hess, F. André, A. Tordai, J.A. Mejia, W.F. Symmans, A.M. Gonzalez-Angulo, B. Hennessy, M. Green, M. Cristofanilli, G.N. Hortobagyi, L. Pusztai, Response to neoadjuvant therapy and long-term survival in patients with triple-negative breast cancer, J. Clin. Oncol. 26 (2008) 1275–1281. https://doi.org/10.1200/JCO.2007.14.4147.

[83]   V. Guarneri, K. Broglio, S.W. Kau, M. Cristofanilli, A.U. Buzdar, V. Valero, T. Buchholz, F. Meric, L. Middleton, G.N. Hortobagyi, A.M. Gonzalez-Angulo, Prognostic value of pathologic complete response after primary chemotherapy in relation to hormone receptor status and other factors, J. Clin. Oncol. 24 (2006) 1037–1044. https://doi.org/10.1200/JCO.2005.02.6914.

[84]   C.M. Perou, T. Sørile, M.B. Eisen, M. Van De Rijn, S.S. Jeffrey, C.A. Ress, J.R. Pollack, D.T. Ross, H. Johnsen, L.A. Akslen, Ø. Fluge, A. Pergammenschlkov, C. Williams, S.X. Zhu, P.E. Lønning, A.L. Børresen-Dale, P.O. Brown, D. Botstein, Molecular portraits of human breast tumours, Nature. 406 (2000) 747–752. https://doi.org/10.1038/35021093.

[85]   A. Prat, E. Pineda, B. Adamo, P. Galván, A. Fernández, L. Gaba, M. Díez, M. Viladot, A. Arance, M. Muñoz, Clinical implications of the intrinsic molecular subtypes of breast cancer, Breast. 24 (2015) S26–S35. https://doi.org/10.1016/j.breast.2015.07.008.

[86]   L. Otvos, E. Surmacz, Targeting the leptin receptor: A potential new mode of treatment for breast cancer, Expert Rev. Anticancer Ther. 11 (2011) 1147–1150. https://doi.org/10.1586/era.11.109.

[87]   E. Paplomata, R. O'Regan, The PI3K/AKT/mTOR pathway in breast cancer: targets, trials and biomarkers, Ther. Adv. Med. Oncol. 6 (2014) 154–166.

[88]   M.A. Khan, V.K. Jain, M. Rizwanullah, J. Ahmad, K. Jain, PI3K/AKT/mTOR pathway inhibitors in triple-negative breast cancer: a review on drug discovery and future challenges, Drug Discov. Today. 24 (2019) 2181–2191. https://doi.org/10.1016/j.drudis.2019.09.001.

[89]   B. Weigelt, J.L. Peterse, L.J. Van't Veer, Breast cancer metastasis: Markers and models, Nat. Rev. Cancer. 5 (2005) 591–602. https://doi.org/10.1038/nrc1670.

[90]   P. Mehlen, A. Puisieux, Metastasis: A question of life or death, Nat. Rev. Cancer. 6 (2006) 449–458. https://doi.org/10.1038/nrc1886.

[91]   S.K. Pal, B.H. Childs, M. Pegram, Triple negative breast cancer: Unmet medical needs, Breast Cancer Res. Treat. 125 (2011) 627–636. https://doi.org/10.1007/s10549-010-1293-1.

[92]   A. Nagy, A. V. Schally, Targeting of cytotoxic luteinizing hormone-releasing hormone analogs to breast, ovarian, endometrial, and prostate cancers, Biol. Reprod. 73 (2005) 851–859. https://doi.org/10.1095/biolreprod.105.043489.

[93]   C. Gründker, J. Ernst, M. Reutter, B.M. Ghadimi, G. Emons, Effective targeted chemotherapy using AEZS-108 (AN-152) for LHRH receptor-positive pancreatic cancers, Oncol. Rep. 26 (2011) 629–635. https://doi.org/10.3892/or.2011.1340.

[94]   C. Gründker, P. Völker, F. Griesinger, A. Ramaswamy, A. Nagy, A. V. Schally, G. Emons, Antitumor effects of the cytotoxic luteinizing hormone-releasing hormone analog AN-152 on human endometrial and ovarian cancers xenografted into nude mice, Am. J. Obstet. Gynecol. 187 (2002) 528–537. https://doi.org/10.1067/mob.2002.124278.

[95] B. Straub, M. Müller, H. Krause, M. Schrader, C. Goessl, R. Heicappell, K. Miller, Increased incidence of luteinizing hormone-releasing hormone receptor gene messenger rna expression in hormone-refractory human prostate cancers, Clin. Cancer Res. 7 (2001) 2340–2343.

[96] C. Föst, F. Duwe, M. Hellriegel, S. Schweyer, G. Emons, C. Gründker, Targeted chemotherapy for triple-negative breast cancers via LHRH receptor, Oncol Rep. 25 (2011) 1481–1487. https://doi.org/10.3892/or.2011.1188.

[97] S. Seitz, S. Buchholz, A.V. Schally, F. Weber, M. Klinkhammer-Schalke, E.C. Inwald, R. Perez, F.G. Rick, L. Szalontay, F. Hohla, S. Segerer, C.W. Kwok, O. Ortmann, J.B. Engel, Triple negative breast cancers express receptors for LHRH and are potential therapeutic targets for cytotoxic LHRH-analogs, AEZS 108 and AEZS 125, BMC Cancer. (2014). https://doi.org/10.1186/1471-2407-14-847.

[98] Z. Kahán, A. Nagy, A. V. Schally, F. Hebert, B. Sun, K. Groot, G. Halmos, Inhibition of growth of MX-1, MCF-7-MIII and MDA-MB-231 human breast cancer xenografts after administration of a targeted cytotoxic analog of somatostatin, AN-238, Int. J. Cancer. 82 (1999) 592–598. https://doi.org/10.1002/(SICI)1097-0215(19990812)82:4<592::AID-IJC20>3.0.CO;2-0.

[99] Z. Kahán, A. Nagy, A. V. Schally, G. Halmos, J.M. Arencibia, K. Groot, Administration of a targeted cytotoxic analog of luteinizing hormone-releasing hormone inhibits growth of estrogen-independent MDA-MB-231 human breast cancers in nude mice, Breast Cancer Res. Treat. 59 (2000) 255–262. https://doi.org/10.1023/A:1006352401912.

[100] J. Hu, J. Obayemi, K. Malatesta, E. Yurkow, D. Adler, W. Soboyejo, Luteinizing hormone-releasing hormone (LHRH) conjugated magnetite nanoparticles as MRI contrast agents for breast cancer imaging, Appl. Sci. 10 (2020) 5175. https://doi.org/10.3390/app10155175.

[101] S.M. Jusu, J.D. Obayemi, A.A. Salifu, C.C. Nwazojie, V. Uzonwanne, O.S. Odusanya, W.O. Soboyejo, Drug-encapsulated blend of PLGA-PEG microspheres: in vitro and in vivo study of the effects of localized/targeted drug delivery on the treatment of triple-negative breast cancer, Sci. Rep. 10 (2020) 1–23. https://doi.org/10.1038/s41598-020-71129-0.

[102] Y. Liu, A.R. Khan, X. Du, Y. Zhai, H. Tan, G. Zhai, Progress in the polymer-paclitaxel conjugate, J. Drug Deliv. Sci. Technol. 54 (2019) 101237. https://doi.org/10.1016/j.jddst.2019.101237.

[103] M.C. Wani, H.L. Taylor, M.E. Wall, P. Coggon, A.T. Mcphail, Plant Antitumor Agents.VI.The Isolation and Structure of Taxol, a Novel Antileukemic and Antitumor Agent from Taxus brevifolia2, J. Am. Chem. Soc. 93 (1971) 2325–2327. https://doi.org/10.1021/ja00738a045.

[104] E.K. Rowinsky, L.A. Cazenave, R.C. Donehower, Taxol: A novel investigational antimicrotubule agent, J. Natl. Cancer Inst. 82 (1990) 1247–1259. https://doi.org/10.1093/jnci/82.15.1247.

[105] R.C. Alves, R.P. Fernandes, J.O. Eloy, H.R.N. Salgado, M. Chorilli, Characteristics, Properties and Analytical Methods of Paclitaxel: A Review, Crit. Rev. Anal. Chem. 48 (2018) 110–118. https://doi.org/10.1080/10408347.2017.1416283.

[106] W.P. McGuire, E.K. Rowinsky, N.B. Rosenhein, F.C. Grumbine, D.S. Ettinger, D.K. Armstrong, R.C. Donehower, Taxol: A unique antineoplastic agent with significant activity in advanced ovarian epithelial neoplasms, Ann. Intern. Med. 111 (1989) 273–279. https://doi.org/10.7326/0003-4819-111-4-273.

[107] J.A. O'Shaughnessy, K.H. Cowan, Current status of paclitaxel in the treatment of breast cancer, Breast Cancer Res. Treat. 33 (1995) 27–37. https://doi.org/10.1007/BF00666068.

[108] Y.N. Cao, L.L. Zheng, D. Wang, X.X. Liang, F. Gao, X.L. Zhou, Recent advances in microtubule-stabilizing agents, Eur. J. Med. Chem. 143 (2018) 806–828. https://doi.org/10.1016/j.ejmech.2017.11.062.

[109] S. Jennewein, R. Croteau, Taxol: Biosynthesis, molecular genetics, and biotechnological applications, Appl. Microbiol. Biotechnol. 57 (2001) 13–19. https://doi.org/10.1007/s002530100757.

[110] A.K. Singla, A. Garg, D. Aggarwal, Paclitaxel and its formulations, Int. J. Pharm. 235 (2002) 179–192. https://doi.org/10.1016/S0378-5173(01)00986-3.

[111] Y.J. Wang, Y.K. Zhang, G.N. Zhang, S.B. Al Rihani, M.N. Wei, P. Gupta, X.Y. Zhang, S. Shukla, S. V. Ambudkar, A. Kaddoumi, Z. Shi, Z.S. Chen, Regorafenib overcomes chemotherapeutic multidrug resistance mediated by ABCB1 transporter in colorectal cancer: In vitro and in vivo study, Cancer Lett. 396 (2017) 145–154. https://doi.org/10.1016/j.canlet.2017.03.011.

[112] R. Liu, W. Xiao, C. Hu, R. Xie, H. Gao, Theranostic size-reducible and no donor conjugated gold nanocluster fabricated hyaluronic acid nanoparticle with optimal size for combinational treatment of breast cancer and lung metastasis, J. Control. Release. 278 (2018) 127–139. https://doi.org/10.1016/j.jconrel.2018.04.005.

[113] J.J. Manfredi, S.B. Horwitz, Taxol: an antimitotic agent with a new mechanism of action, Pharmacol. Ther. 25 (1984) 83–125. https://doi.org/10.1016/0163-7258(84)90025-1.

[114] L.A. Amos, J. Löwe, How Taxol® stabilises microtubule structure, Chem. Biol. 6 (1999) R65–R69. https://doi.org/10.1016/S1074-5521(99)89002-4.

[115] E. Bernabeu, M. Cagel, E. Lagomarsino, M. Moretton, D.A. Chiappetta, Paclitaxel: What has been done and the challenges remain ahead, Int. J. Pharm. 526 (2017) 474–495. https://doi.org/10.1016/j.ijpharm.2017.05.016.

[116] H. Lee, K. Lee, G.P. Tae, Hyaluronic acid-paclitaxel conjugate micelles: Synthesis, characterization, and antitumor activity, Bioconjug. Chem. 19 (2008) 1319–1325. https://doi.org/10.1021/bc8000485.

[117] A. Safavy, J.A. Bonner, H.W. Waksal, D.J. Buchsbaum, G.Y. Gillespie, M.B. Khazaeli, R. Arani, D.T. Chen, M. Carpenter, K.P. Raisch, Synthesis and biological evaluation of paclitaxel-C225 conjugate as a model for targeted drug delivery, Bioconjug. Chem. 14 (2003) 302–310. https://doi.org/10.1021/bc020033z.

[118] S.K. Sahoo, V. Labhasetwar, Enhanced antiproliferative activity of transferrin-conjugated paclitaxel-loaded nanoparticles is mediated via sustained intracellular drug retention, Mol. Pharm. 2 (2005) 373–383. https://doi.org/10.1021/mp050032z.

[119] A. Régina, M. Demeule, C. Ché, I. Lavallée, J. Poirier, R. Gabathuler, R. Béliveau, J.P. Castaigne, Antitumour activity of ANG1005, a conjugate between paclitaxel and the new brain delivery vector Angiopep-2, Br. J. Pharmacol. 155 (2008) 185–197. https://doi.org/10.1038/bjp.2008.260.

[120] F. Dosio, P. Brusa, P. Crosasso, S. Arpicco, L. Cattel, Preparation, characterization and properties in vitro and in vivo of a paclitaxel-albumin conjugate, J. Control. Release. 47 (1997) 293–304. https://doi.org/10.1016/S0168-3659(97)01656-8.

[121] J. Yang, Q. Lv, W. Wei, Z. Yang, J. Dong, R. Zhang, Q. Kan, Z. He, Y. Xu, Bioresponsive albumin-conjugated paclitaxel prodrugs for cancer therapy, Drug Deliv. 25 (2018) 807–814. https://doi.org/10.1080/10717544.2018.1451935.

[122] A. Khanafari, M.M. Assadi, F.A. Fakhr, Review of Prodigiosin, Pigmentation in Serratia marcescens, Online J. Biol. Sci. 6 (2006) 1–13. https://doi.org/10.3844/ojbsci.2006.1.13.

[123] R. Pérez-Tomás, B. Montaner, E. Llagostera, V. Soto-Cerrato, The prodigiosins, proapoptotic drugs with anticancer properties, Biochem. Pharmacol. 66 (2003) 1447–1452. https://doi.org/10.1016/S0006-2952(03)00496-9.

[124] R.A. Manderville, Synthesis, proton-affinity and anti-cancer properties of the prodigiosin-group natural products., Curr. Med. Chem. Anticancer. Agents. 1 (2001) 195–218. https://doi.org/10.2174/1568011013354688.

[125] N. Darshan, H.K. Manonmani, Prodigiosin and its potential applications, J. Food Sci. Technol. 52 (2015) 5393–5407. https://doi.org/10.1007/s13197-015-1740-4.

[126] R. D'Alessio, A. Rossi, Short synthesis of undecylprodigiosine. a new route to 2,2′-bipyrrolyl-pyrromethene systems, Synlett. 1996 (1996) 513–514. https://doi.org/10.1055/s-1996-5485.

[127] R. D'Alessio, A. Bargiotti, O. Carlini, F. Colotta, M. Ferrari, P. Gnocchi, A. Isetta, N. Mongelli, P. Motta, A. Rossi, M. Rossi, M. Tibolla, E. Vanotti, Synthesis and immunosuppressive activity of novel prodigiosin derivatives, J. Med. Chem. 43 (2000) 2557–2565. https://doi.org/10.1021/jm001003p.

[128] B.H. Sang, H.P. Se, J.J. Young, K.K. Young, M.K. Hwan, H.Y. Kyu, Prodigiosin blocks T cell activation by inhibiting interleukin-2Rα expression and delays progression of autoimmune diabetes and collagen-induced arthritis, J. Pharmacol. Exp. Ther. 299 (2001)

415–425.

[129] C.K. Venil, Z.A. Zakaria, W.A. Ahmad, Bacterial pigments and their applications, Process Biochem. 48 (2013) 1065–1079. https://doi.org/10.1016/j.procbio.2013.06.006.

[130] B. Singh, R. Vishwakarma, S. Bharate, QSAR and Pharmacophore Modeling of Natural and Synthetic Antimalarial Prodiginines, Curr. Comput. Aided-Drug Des. 9 (2013) 350–359. https://doi.org/10.2174/15734099113099990020.

[131] D. Ibrahim, T.F. Nazari, J. Kassim, S.H. Lim, Prodigiosin - an antibacterial red pigment produced by Serratia marcescens IBRL USM 84 associated with a marine sponge Xestospongia testudinaria, J. Appl. Pharm. Sci. 4 (2014) 1–6. https://doi.org/10.7324/JAPS.2014.40101.

[132] S. Namazkar, W.A. Ahmad, Spray-dried prodigiosin from Serratia marcescens as a colorant, Biosci. Biotechnol. Res. Asia. 10 (2013) 69–76. https://doi.org/10.13005/bbra/1094.

[133] C. Campàs, M. Dalmau, B. Montaner, M. Barragán, B. Bellosillo, D. Colomer, G. Pons, R. Pérez-Tomás, J. Gil, Prodigiosin induces apoptosis of B and T cells from B-cell chronic lymphocytic leukemia, Leukemia. 17 (2003) 746–750. https://doi.org/10.1038/sj.leu.2402860.

[134] V. Soto-Cerrato, E. Llagostera, B. Montaner, G.L. Scheffer, R. Perez-Tomas, Mitochondria-mediated apoptosis operating irrespective of multidrug resistance in breast cancer cells by the anticancer agent prodigiosin, Biochem. Pharmacol. 68 (2004) 1345–1352. https://doi.org/10.1016/j.bcp.2004.05.056.

[135] E. Llagostera, V. Soto-Cerrato, R. Joshi, B. Montaner, P. Gimenez-Bonafé, R. Pérez-Tomás, High cytotoxic sensitivity of the human small cell lung doxorubicin-resistant carcinoma (GLC4/ADR) cell line to prodigiosin through apoptosis activation, Anticancer. Drugs. 16 (2005) 393–399. https://doi.org/10.1097/00001813-200504000-00005.

[136] T. Kataoka, M. Muroi, S. Ohkuma, T. Waritani, J. Magae, A. Takatsuki, S. Kondo, M. Yamasaki, K. Nagai, Prodigiosin 25-C uncouples vacuolar type H+-ATPase, inhibits vacuolar acidification and affects glycoprotein processing, FEBS Lett. 359 (1995) 53–59. https://doi.org/10.1016/0014-5793(94)01446-8.

[137] C.M. Baldino, J. Parr, C.J. Wilson, S.C. Ng, D. Yohannes, H.H. Wasserman, Indoloprodigiosins from the C-10 bipyrrolic precursor: New antiproliferative prodigiosin analogs, Bioorganic Med. Chem. Lett. 16 (2006) 701–704. https://doi.org/10.1016/j.bmcl.2005.10.027.

[138] R. Francisco, R. Pérez-Tomás, P. Gimènez-Bonafé, V. Soto-Cerrato, P. Giménez-Xavier, S. Ambrosio, Mechanisms of prodigiosin cytotoxicity in human neuroblastoma cell lines, Eur. J. Pharmacol. 572 (2007) 111–119. https://doi.org/10.1016/j.ejphar.2007.06.054.

[139] M. Ayatollahi, G. Ayatollahi, M. Rashidi, S. Hekmatimoghaddam, M. Mosshafi, A. Jebali, M. Iman, H. Shahdadi Sardo, Prodigiosin-Conjugated Aptamer for Attachment to the

Surface of Brain Cancer Cells Mediated by Glutamate Receptor, Colloids Interface Sci. Commun. 24 (2018) 45–48. https://doi.org/10.1016/j.colcom.2018.03.006.

[140] G. Tiwari, R. Tiwari, S. Bannerjee, L. Bhati, S. Pandey, P. Pandey, B. Sriwastawa, Drug delivery systems: An updated review, Int. J. Pharm. Investig. 2 (2012) 2. https://doi.org/10.4103/2230-973x.96920.

[141] D.A. LaVan, T. McGuire, R. Langer, Small-scale systems for in vivo drug delivery, Nat. Biotechnol. 21 (2003) 1184–1191. https://doi.org/10.1038/nbt876.

[142] T.M. Allen, P.R. Cullis, Drug Delivery Systems: Entering the Mainstream, Science (80-.). 303 (2004) 1818–1822. https://doi.org/10.1126/science.1095833.

[143] R. Langer, New methods of drug delivery, Science (80-.). 249 (1990) 1527–1533. https://doi.org/10.1126/science.2218494.

[144] W.R. Gombotz, D.K. Pettit, Biodegradable Polymers for Protein and Peptide Drug Delivery, Bioconjug. Chem. 6 (1995) 332–351. https://doi.org/10.1021/bc00034a002.

[145] V.P. Torchilin, Drug targeting, Eur. J. Pharm. Sci. 11 (2000) S81–S91. https://doi.org/10.1016/S0928-0987(00)00166-4.

[146] G. Manish, S. Vimukta, Target drug delivery system: A Review, Res. J. Chem. Sci. 1 (2011) 135–138. www.isca.in.

[147] N. Mishra, P. Pant, A. Porwal, J. Jaiswal, M. Aquib, Targeted drug delivery: a review, Am. J. Pharm. Tech. Res. 6 (2016) 1–24.

[148] S. Bhatia, Natural polymer drug delivery systems: Nanoparticles, plants, and algae, 2016. https://doi.org/10.1007/978-3-319-41129-3.

[149] J.P. Jain, W. Yenet Ayen, A.J. Domb, N. Kumar, Biodegradable Polymers in Drug Delivery, in: Biodegrad. Polym. Clin. Use Clin. Dev., 2011: pp. 1–58. https://doi.org/10.1002/9781118015810.ch1.

[150] P. Saini, M. Arora, M.N.V.R. Kumar, Poly(lactic acid) blends in biomedical applications, Adv. Drug Deliv. Rev. 107 (2016) 47–59. https://doi.org/10.1016/j.addr.2016.06.014.

[151] Q. Cai, J. Yang, J. Bei, S. Wang, A novel porous cells scaffold made of polylactide-dextran blend by combining phase-separation and particle-leaching techniques, Biomaterials. 23 (2002) 4483–4492. https://doi.org/10.1016/S0142-9612(02)00168-0.

[152] M.I. Sabir, X. Xu, L. Li, A review on biodegradable polymeric materials for bone tissue engineering applications, J. Mater. Sci. 44 (2009) 5713–5724. https://doi.org/10.1007/s10853-009-3770-7.

[153] J.Y. Kim, D.W. Cho, Blended PCL/PLGA scaffold fabrication using multi-head deposition system, Microelectron. Eng. 86 (2009) 1447–1450.

https://doi.org/10.1016/j.mee.2008.11.026.

[154] M.A. Barkat, Harshita, S.S. Das, S. Beg, F.J. Ahmad, Nanotechnology-Based Phytotherapeutics: Current Status and Challenges, in: S. Beg, M.A. Barkat, F.J. Ahmad (Eds.), Nanophytomedicine, Springer Singapore, Singapore, 2020: pp. 1–17. https://doi.org/10.1007/978-981-15-4909-0_1.

[155] M.L. Bruschi, Strategies to Modify the Drug Release from Pharmaceutical Systems, Woodhead Publishing, 2015. https://doi.org/10.1016/C2014-0-02342-8.

[156] M. Whelehan, I.W. Marison, Microencapsulation using vibrating technology, J. Microencapsul. 28 (2011) 669–688. https://doi.org/10.3109/02652048.2011.586068.

[157] M. Lengyel, N. Kállai-Szabó, V. Antal, A.J. Laki, I. Antal, Microparticles, microspheres, and microcapsules for advanced drug delivery, Sci. Pharm. 87 (2019). https://doi.org/10.3390/scipharm87030020.

[158] N.T.T. Uyen, Z.A.A. Hamid, N.X.T. Tram, N. Ahmad, Fabrication of alginate microspheres for drug delivery: A review, Int. J. Biol. Macromol. 153 (2020) 1035–1046. https://doi.org/10.1016/j.ijbiomac.2019.10.233.

[159] B. Wang, L. Hu, T.J. Siahaan, Drug Delivery: Principles and Applications: Second Edition, John Wiley & Sons, 2016. https://doi.org/10.1002/9781118833322.

[160] U. Farooq, R. Malviya, P. Sharma, Advancement in Microsphere Preparation Using Natural Polymers and Recent Patents, Recent Pat. Drug Deliv. Formul. 8 (2014) 111–125. https://doi.org/10.2174/1872211308666140218110520.

[161] I. Marison, A. Peters, C. Heinzen, Liquid Core Caspules for Applications in Biotechnology, in: Springer, 2004: pp. 185–204. https://doi.org/10.1007/978-94-017-1638-3_10.

[162] J. Berg, D. Sundberg, B. Kronberg, Microencapsulation of emulsified oil droplets by in-situ vinyl polymerization, J. Microencapsul. 6 (1989) 327–337. https://doi.org/10.3109/02652048909019915.

[163] A.R. Kulkarni, K.S. Soppimath, T.M. Aminabhavi, A.M. Dave, M.H. Mehta, Glutaraldehyde crosslinked sodium alginate beads containing liquid pesticide for soil application, J. Control. Release. 63 (2000) 97–105. https://doi.org/10.1016/S0168-3659(99)00176-5.

[164] F. Weinbreck, R. de Vries, P. Schrooyen, C.G. de Kruif, Complex coacervation of whey proteins and gum arabic, Biomacromolecules. 4 (2003) 293–303. https://doi.org/10.1021/bm025667n.

[165] Y. Guo, Y. Yang, L. He, R. Sun, C. Pu, B. Xie, H. He, Y. Zhang, T. Yin, Y. Wang, X. Tang, Injectable Sustained-Release Depots of PLGA Microspheres for Insoluble Drugs Prepared by hot-Melt Extrusion, Pharm. Res. 34 (2017) 2211–2222. https://doi.org/10.1007/s11095-017-2228-x.

[166] A.R. de Oliveira, P.C. Mesquita, P.R.L. Machado, K.J.S. Farias, Y.M.B. de Almeida, M.F. Fernandes-Pedrosa, A.M. Cornélio, E.S.T. do Egito, A.A. da Silva-Júnior, Monitoring structural features, biocompatibility and biological efficacy of gamma-irradiated methotrexate-loaded spray-dried microparticles, Mater. Sci. Eng. C. 80 (2017) 438–448. https://doi.org/10.1016/j.msec.2017.06.013.

[167] E.A. Makris, A.H. Gomoll, K.N. Malizos, J.C. Hu, K.A. Athanasiou, Repair and tissue engineering techniques for articular cartilage, Nat. Rev. Rheumatol. 11 (2015) 21–34. https://doi.org/10.1038/nrrheum.2014.157.

[168] J.P. Vacanti, C.A. Vacanti, The History and Scope of Tissue Engineering, in: Princ. Tissue Eng. Fourth Ed., 2013: pp. 3–8. https://doi.org/10.1016/B978-0-12-398358-9.00001-X.

[169] R. Langer, J.P. Vacanti, Tissue engineering, Science (80-.). 260 (1993) 920–926. https://doi.org/10.1126/science.8493529.

[170] C.Y. Lin, R.M. Schek, A.S. Mistry, X. Shi, A.G. Mikos, P.H. Krebsbach, S.J. Hollister, Functional bone engineering using ex vivo gene therapy and topology-optimized, biodegradable polymer composite scaffolds, Tissue Eng. 11 (2005) 1589–1598. https://doi.org/10.1089/ten.2005.11.1589.

[171] F. Akter, Principles of Tissue Engineering, in: Tissue Eng. Made Easy, 2016: pp. 3–16. https://doi.org/10.1016/B978-0-12-805361-4.00002-3.

[172] P.X. Ma, Biomimetic materials for tissue engineering, Adv. Drug Deliv. Rev. 60 (2008) 184–198. https://doi.org/10.1016/j.addr.2007.08.041.

[173] S. Yang, K.F. Leong, Z. Du, C.K. Chua, The design of scaffolds for use in tissue engineering. Part I. Traditional factors, Tissue Eng. 7 (2001) 679–689. https://doi.org/10.1089/107632701753337645.

[174] J.M. Holzwarth, P.X. Ma, Biomimetic nanofibrous scaffolds for bone tissue engineering, Biomaterials. 32 (2011) 9622–9629. https://doi.org/10.1016/j.biomaterials.2011.09.009.

[175] L.G. Griffith, G. Naughton, Tissue engineering - Current challenges and expanding opportunities, Science (80-.). 295 (2002). https://doi.org/10.1126/science.1069210.

[176] Y. Ikada, Challenges in tissue engineering, J. R. Soc. Interface. 3 (2006) 589–601. https://doi.org/10.1098/rsif.2006.0124.

[177] G. Rijal, W. Li, 3D scaffolds in breast cancer research, Biomaterials. 81 (2016) 135–156. https://doi.org/10.1016/j.biomaterials.2015.12.016.

[178] J.D. Obayemi, S.M. Jusu, A.A. Salifu, S. Ghahremani, M. Tadesse, V.O. Uzonwanne, W.O. Soboyejo, Degradable porous drug-loaded polymer scaffolds for localized cancer drug delivery and breast cell/tissue growth, Mater. Sci. Eng. C. 112 (2020) 110794. https://doi.org/10.1016/j.msec.2020.110794.

[179] B. Subia, T. Dey, S. Sharma, S.C. Kundu, Target specific delivery of anticancer drug in silk fibroin based 3D distribution model of bone-breast cancer cells, ACS Appl. Mater. Interfaces. 7 (2015) 2269–2279. https://doi.org/10.1021/am506094c.

[180] L. Wang, J.A. Johnson, Q. Zhang, E.K. Beahm, Combining decellularized human adipose tissue extracellular matrix and adipose-derived stem cells for adipose tissue engineering, Acta Biomater. 9 (2013) 8921–8931. https://doi.org/10.1016/j.actbio.2013.06.035.

[181] H. Wu, T. Zhou, L. Tian, Z. Xia, F. Xu, Self-Assembling RADA16-I Peptide Hydrogel Scaffold Loaded with Tamoxifen for Breast Reconstruction, Biomed Res. Int. 2017 (2017). https://doi.org/10.1155/2017/3656193.

[182] A. Baldwin, L. Uy, A. Frank-Kamenetskii, L. Strizzi, B.W. Booth, The in vivo biocompatibility of novel tannic acid-collagen type I injectable bead scaffold material for breast reconstruction post-lumpectomy, J. Biomater. Appl. 34 (2020) 1315–1329. https://doi.org/10.1177/0885328219899238.

[183] R.D. Rehnke, M.A. Schusterman, J.M. Clarke, B.C. Price, U. Waheed, R.E. Debski, S.F. Badylak, J.P. Rubin, Breast Reconstruction Using a Three-Dimensional Absorbable Mesh Scaffold and Autologous Fat Grafting: A Composite Strategy Based on Tissue-Engineering Principles, Plast. Reconstr. Surg. 146 (2020) 409E-413E. https://doi.org/10.1097/PRS.0000000000007172.

[184] V.M. Pathak, Navneet, Review on the current status of polymer degradation: a microbial approach, Bioresour. Bioprocess. 4 (2017) 1–31. https://doi.org/10.1186/s40643-017-0145-9.

[185] A. Göpferich, Mechanisms of polymer degradation and erosion, Biomaterials. 17 (1996) 103–114. https://doi.org/10.1016/0142-9612(96)85755-3.

[186] J.A. Tamada, R. Langer, Erosion kinetics of hydrolytically degradable polymers, Proc. Natl. Acad. Sci. U. S. A. 90 (1993) 552–556. https://doi.org/10.1073/pnas.90.2.552.

[187] F.P. La Mantia, M. Morreale, L. Botta, M.C. Mistretta, M. Ceraulo, R. Scaffaro, Degradation of polymer blends: A brief review, Polym. Degrad. Stab. 145 (2017) 79–92. https://doi.org/10.1016/j.polymdegradstab.2017.07.011.

[188] H.S. Azevedo, F.M. Gama, R.L. Reis, In vitro assessment of the enzymatic degradation of several starch based biomaterials, Biomacromolecules. 4 (2003) 1703–1712. https://doi.org/10.1021/bm0300397.

[189] T. Murase, T. Iwata, Y. Doi, Direct observation of enzymatic degradation behavior of poly[(R)-3-hydroxybutyrate] lamellar single crystals by atomic force microscopy, Macromolecules. 34 (2001) 5848–5853. https://doi.org/10.1021/ma001505c.

[190] K. Numata, T. Hirota, Y. Kikkawa, T. Tsuge, T. Iwata, H. Abe, Y. Doi, Enzymatic degradation processes of lamellar cyrstals in thin films for poly[(R)-3-hydroxybutyric acid] and its copolymers revealed by real-time atomic force microscopy, Biomacromolecules. 5

(2004) 2186–2194. https://doi.org/10.1021/bm0497670.

[191] Y. Cao, B. Wang, Biodegradation of silk biomaterials, Int. J. Mol. Sci. 10 (2009) 1514–1524. https://doi.org/10.3390/ijms10041514.

[192] L.A. Matheson, R.S. Labow, J.P. Santerre, Biodegradation of polycarbonate-based polyurethanes by the human monocyte-derived macrophage and U937 cell systems, J. Biomed. Mater. Res. 61 (2002) 505–513. https://doi.org/10.1002/jbm.10286.

[193] J.P. Mahalik, G. Madras, Effect of the alkyl group substituents on the thermal and enzymatic degradation of poly(n-alkyl acrylates), Ind. Eng. Chem. Res. 44 (2005) 4171–4177. https://doi.org/10.1021/ie0500164.

[194] A. Banerjee, K. Chatterjee, G. Madras, Enzymatic degradation of polymers: A brief review, Mater. Sci. Technol. (United Kingdom). 30 (2014) 567–573. https://doi.org/10.1179/1743284713Y.0000000503.

[195] Y.S. Chen, T.C. Kao, G.J. Yu, J.P. Sheu, A mobile butterfly-watching learning system for supporting independent learning, in: Proc. - 2nd IEEE Int. Work. Wirel. Mob. Technol. Educ., 2004: pp. 11–18. https://doi.org/10.1021/bm034388c.

[196] Z. Jedliński, M. Kowalczuk, P. Kurcok, L. Brzoskowska, J. Franek, Anionic block polymerization of β-lactones initiated by potassium solutions, 1. Synthesis of poly(4-methyl-2-oxetanone-block-2-oxetanone), Die Makromol. Chemie. 188 (1987) 1575–1582. https://doi.org/10.1002/macp.1987.021880704.

[197] Y.W. Tang, R.S. Labow, J.P. Santerre, Isolation of methylene dianiline and aqueous-soluble biodegradation products from polycarbonate-polyurethanes, Biomaterials. 24 (2003) 2805–2819. https://doi.org/10.1016/S0142-9612(03)00081-4.

[198] S.L. Elliott, J.D. Fromstein, J.P. Santerre, K.A. Woodhouse, Identification of biodegradation products formed by L-phenylalanine based segmented polyurethaneureas, J. Biomater. Sci. Polym. Ed. 13 (2002) 691–711. https://doi.org/10.1163/156856202320269166.

[199] K. Yamashita, Y. Kikkawa, K. Kurokawa, Y. Doi, Enzymatic degradation of poly(L-lactide) film by proteinase K: Quartz crystal microbalance and atomic force microscopy study, Biomacromolecules. 6 (2005) 850–857. https://doi.org/10.1021/bm049395v.

[200] D. Walsh, T. Furuzono, J. Tanaka, Preparation of porous composite implant materials by in situ polymerization of porous apatite containing ε-caprolactone or methyl methacrylate, Biomaterials. 22 (2001) 1205–1212. https://doi.org/10.1016/S0142-9612(00)00268-4.

[201] F. Bray, J. Ferlay, I. Soerjomataram, R.L. Siegel, L.A. Torre, A. Jemal, Global cancer statistics 2018: GLOBOCAN estimates of incidence and mortality worldwide for 36 cancers in 185 countries, CA. Cancer J. Clin. 68 (2018) 394–424. https://doi.org/10.3322/caac.21492.

[202] World Health Organization, World Health Organization Facts Sheet, Cancer - Fact Sheets. (2019) 1. https://www.who.int/news-room/fact-sheets/detail/cancer (accessed September 10, 2019).

[203] World Health Organization, World Health Organization - Key Facts on Cancer, Cancer - Key Facts. (2019) 1. https://www.who.int/cancer/resources/keyfacts/en/ (accessed September 9, 2019).

[204] R.L. Siegel, K.D. Miller, A. Jemal, Cancer statistics, 2016, CA. Cancer J. Clin. 66 (2016) 7–30. https://doi.org/10.3322/caac.21332.

[205] B.O. Anderson, C.H. Yip, R.A. Smith, R. Shyyan, S.F. Sener, A. Eniu, R.W. Carlson, E. Azavedo, J. Harford, Guideline implementation for breast healthcare in low-income and middle-income countries: Overview of the breast health global initiative Global Summit 2007, Cancer. 113 (2008) 2221–2243. https://doi.org/10.1002/cncr.23844.

[206] F. Podo, L.M.C. Buydens, H. Degani, R. Hilhorst, E. Klipp, I.S. Gribbestad, S. Van Huffel, H. W.M. van Laarhoven, J. Luts, D. Monleon, G.J. Postma, N. Schneiderhan-Marra, F. Santoro, H. Wouters, H.G. Russnes, T. Sørlie, E. Tagliabue, A.L. Børresen-Dale, Triple-negative breast cancer: Present challenges and new perspectives, Mol. Oncol. 4 (2010) 209–229. https://doi.org/10.1016/j.molonc.2010.04.006.

[207] M. De Laurentiis, D. Cianniello, R. Caputo, B. Stanzione, G. Arpino, S. Cinieri, V. Lorusso, S. De Placido, Treatment of triple negative breast cancer (TNBC): Current options and future perspectives, Cancer Treat. Rev. 36 (2010). https://doi.org/10.1016/S0305-7372(10)70025-6.

[208] H.A. Wahba, H.A. El-Hadaad, Current approaches in treatment of triple-negative breast cancer, Cancer Biol. Med. 12 (2015) 106–116. https://doi.org/10.7497/j.issn.2095-3941.2015.0030.

[209] A. Gucalp, T.A. Traina, Triple-Negative Breast Cancer: Adjuvant Therapeutic Options, Chemother. Res. Pract. 2011 (2011) 1–13. https://doi.org/10.1155/2011/696208.

[210] P.D. Ryan, N.M. Tung, S.J. Isakoff, M. Golshan, A. Richardson, A.D. Corben, B.L. Smith, R. Gelman, E.P. Winer, J.E. Garber, Neoadjuvant cisplatin and bevacizumab in triple negative breast cancer (TNBC): Safety and efficacy, J. Clin. Oncol. 27 (2009) 551–551. https://doi.org/10.1200/jco.2009.27.15_suppl.551.

[211] A.S. Meyer, M.A. Miller, F.B. Gertler, D.A. Lauffenburger, The receptor AXL diversifies EGFR signaling and limits the response to EGFR-targeted inhibitors in triple-negative breast cancer cells, Sci. Signal. 6 (2013). https://doi.org/10.1126/scisignal.2004155.

[212] L.A. Carey, H.S. Rugo, P.K. Marcom, W. Irvin, M. Ferraro, E. Burrows, X. He, C.M. Perou, E.P. Winer, TBCRC 001: EGFR inhibition with cetuximab added to carboplatin in metastatic triple-negative (basal-like) breast cancer, J. Clin. Oncol. 26 (2008) 1009–1009. https://doi.org/10.1200/jco.2008.26.15_suppl.1009.

[213] A. Bosch, P. Eroles, R. Zaragoza, J.R. Viña, A. Lluch, Triple-negative breast cancer: Molecular features, pathogenesis, treatment and current lines of research, Cancer Treat. Rev. 36 (2010) 206–215. https://doi.org/10.1016/j.ctrv.2009.12.002.

[214] Y.H. Ibrahim, C. García-García, V. Serra, L. He, K. Torres-Lockhart, A. Prat, P. Anton, P. Cozar, M. Guzmán, J. Grueso, O. Rodríguez, M.T. Calvo, C. Aura, O. Díez, I.T. Rubio, J. Pérez, J. Rodón, J. Cortés, L.W. Ellisen, M. Scaltriti, J. Baselga, PI3K inhibition impairs BRCA1/2 expression and sensitizes BRCA-proficient triple-negative breast cancer to PARP inhibition, Cancer Discov. 2 (2012) 1036–1047. https://doi.org/10.1158/2159-8290.CD-11-0348.

[215] J.C. Montero, A. Esparís-Ogando, M.F. Re-Louhau, S. Seoane, M. Abad, R. Calero, A. Ocaña, A. Pandiella, Active kinase profiling, genetic and pharmacological data define mTOR as an important common target in triple-negative breast cancer, Oncogene. 33 (2014) 148–156. https://doi.org/10.1038/onc.2012.572.

[216] V.S. Jamdade, N. Sethi, N.A. Mundhe, P. Kumar, M. Lahkar, N. Sinha, Therapeutic targets of triple-negative breast cancer: A review, Br. J. Pharmacol. 172 (2015) 4228–4237. https://doi.org/10.1111/bph.13211.

[217] R.S. Finn, J. Dering, C. Ginther, C.A. Wilson, P. Glaspy, N. Tchekmedyian, D.J. Slamon, Dasatinib, an orally active small molecule inhibitor of both the src and abl kinases, selectively inhibits growth of basal-type/"triple- negative" breast cancer cell lines growing in vitro, Breast Cancer Res. Treat. 105 (2007) 319–326. https://doi.org/10.1007/s10549-006-9463-x.

[218] Y. Danyuo, J.D. Obayemi, S. Dozie-Nwachukwu, C.J. Ani, O.S. Odusanya, Y. Oni, N. Anuku, K. Malatesta, W.O. Soboyejo, Prodigiosin release from an implantable biomedical device: Kinetics of localized cancer drug release, Mater. Sci. Eng. C. 42 (2014) 734–745. https://doi.org/10.1016/j.msec.2014.06.008.

[219] J.D. Obayemi, Y. Danyuo, S. Dozie-Nwachukwu, O.S. Odusanya, N. Anuku, K. Malatesta, W. Yu, K.E. Uhrich, W.O. Soboyejo, PLGA-based microparticles loaded with bacterial-synthesized prodigiosin for anticancer drug release: Effects of particle size on drug release kinetics and cell viability, Mater. Sci. Eng. C. 66 (2016) 51–65. https://doi.org/10.1016/j.msec.2016.04.071.

[220] S.O. Dozie-Nwachukwu, Y. Danyuo, J.D. Obayemi, O.S. Odusanya, K. Malatesta, W.O. Soboyejo, Extraction and encapsulation of prodigiosin in chitosan microspheres for targeted drug delivery, Mater. Sci. Eng. C. 71 (2017) 268–278. https://doi.org/10.1016/j.msec.2016.09.078.

[221] C.P. Tsai, C.Y. Chen, Y. Hung, F.H. Chang, C.Y. Mou, Monoclonal antibody-functionalized mesoporous silica nanoparticles (MSN) for selective targeting breast cancer cells, J. Mater. Chem. 19 (2009) 5737–5743. https://doi.org/10.1039/b905158a.

[222] J. Hu, J.D. Obayemi, K. Malatesta, A. Košmrlj, W.O. Soboyejo, Enhanced cellular uptake of LHRH-conjugated PEG-coated magnetite nanoparticles for specific targeting of triple

negative breast cancer cells, Mater. Sci. Eng. C. 88 (2018) 32–45. https://doi.org/10.1016/j.msec.2018.02.017.

[223] J.W. Park, Liposome-based drug delivery in breast cancer treatment, Breast Cancer Res. 4 (2002) 95–99. https://doi.org/10.1186/bcr432.

[224] N. Malik, E.G. Evagorou, R. Duncan, Dendrimer-platinate: A novel approach to cancer chemotherapy, Anticancer. Drugs. 10 (1999) 767–776. https://doi.org/10.1097/00001813-199909000-00010.

[225] Y. Zhang, H. Zhang, X. Wang, J. Wang, X. Zhang, Q. Zhang, The eradication of breast cancer and cancer stem cells using octreotide modified paclitaxel active targeting micelles and salinomycin passive targeting micelles, Biomaterials. 33 (2012) 679–691. https://doi.org/10.1016/j.biomaterials.2011.09.072.

[226] C. Wang, J. Chen, T. Talavage, J. Irudayaraj, Gold Nanorod/Fe3O4 nanoparticle "nano-pearl- necklaces" for simultaneous targeting, dual-mode imaging, and photothermal ablation of cancer cells, Angew. Chemie - Int. Ed. 48 (2009) 2759–2763. https://doi.org/10.1002/anie.200805282.

[227] D. Rosenblum, N. Joshi, W. Tao, J.M. Karp, D. Peer, Progress and challenges towards targeted delivery of cancer therapeutics, Nat. Commun. 9 (2018) 1–2. https://doi.org/10.1038/s41467-018-03705-y.

[228] S.D. Bruck, Pharmacological Basis of Controlled Drug Delivery, in: Control. Drug Deliv., CRC Press, 2019: pp. 1–14. https://doi.org/10.1201/9780429262258-1.

[229] L. Brannon-Peppas, J.O. Blanchette, Nanoparticle and targeted systems for cancer therapy, Adv. Drug Deliv. Rev. 64 (2012) 206–212. https://doi.org/10.1016/j.addr.2012.09.033.

[230] R. Langer, Drug delivery and targeting, Nature. 392 (1998) 5–10. https://doi.org/10.1016/s0378-5173(02)00260-0.

[231] I. Melero, S. Hervas-Stubbs, M. Glennie, D.M. Pardoll, L. Chen, Immunostimulatory monoclonal antibodies for cancer therapy, Nat. Rev. Cancer. 7 (2007) 95–106. https://doi.org/10.1038/nrc2051.

[232] A. Kumari, S.K. Yadav, S.C. Yadav, Biodegradable polymeric nanoparticles based drug delivery systems, Colloids Surfaces B Biointerfaces. 75 (2010) 1–18. https://doi.org/10.1016/j.colsurfb.2009.09.001.

[233] M.L. Hans, A.M. Lowman, Biodegradable nanoparticles for drug delivery and targeting, Curr. Opin. Solid State Mater. Sci. 6 (2002) 319–327. https://doi.org/10.1016/S1359-0286(02)00117-1.

[234] H.K. Makadia, S.J. Siegel, Poly Lactic-co-Glycolic Acid (PLGA) as biodegradable controlled drug delivery carrier, Polymers (Basel). 3 (2011) 1377–1397. https://doi.org/10.3390/polym3031377.

[235] K. Knop, R. Hoogenboom, D. Fischer, U.S. Schubert, Poly(ethylene glycol) in drug delivery: Pros and cons as well as potential alternatives, Angew. Chemie - Int. Ed. 49 (2010) 6288–6308. https://doi.org/10.1002/anie.200902672.

[236] K.E. Uhrich, S.M. Cannizzaro, R.S. Langer, K.M. Shakesheff, Polymeric Systems for Controlled Drug Release, Chem. Rev. 99 (1999) 3181–3198. https://doi.org/10.1021/cr940351u.

[237] O. Pillai, R. Panchagnula, Polymers in drug delivery, Curr. Opin. Chem. Biol. 5 (2001) 447–451. https://doi.org/10.1016/S1367-5931(00)00227-1.

[238] R.W. Korsmeyer, R. Gurny, E. Doelker, P. Buri, N.A. Peppas, Mechanisms of solute release from porous hydrophilic polymers, Int. J. Pharm. 15 (1983) 25–35. https://doi.org/10.1016/0378-5173(83)90064-9.

[239] S.S. Shah, Y. Cha, C.G. Pitt, Poly (glycolic acid-co-dl-lactic acid): diffusion or degradation controlled drug delivery?, J. Control. Release. 18 (1992) 261–270. https://doi.org/10.1016/0168-3659(92)90171-M.

[240] R.B. Patil, P.B., Uphade, K.B. and Saudagar, A REVIEW: OSMOTIC DRUG DELIVERY SYSTEM., Pharma Sci. Monit. 9 (2018).

[241] Y. Danyuo, C.J. Ani, A.A. Salifu, J.D. Obayemi, S. Dozie-Nwachukwu, V.O. Obanawu, U.M. Akpan, O.S. Odusanya, M. Abade-Abugre, F. McBagonluri, W.O. Soboyejo, Anomalous Release Kinetics of Prodigiosin from Poly-N-Isopropyl-Acrylamid based Hydrogels for The Treatment of Triple Negative Breast Cancer, Sci. Rep. 9 (2019) 1–14. https://doi.org/10.1038/s41598-019-39578-4.

[242] Z. Song, R. Feng, M. Sun, C. Guo, Y. Gao, L. Li, G. Zhai, Curcumin-loaded PLGA-PEG-PLGA triblock copolymeric micelles: Preparation, pharmacokinetics and distribution in vivo, J. Colloid Interface Sci. 354 (2011) 116–123. https://doi.org/10.1016/j.jcis.2010.10.024.

[243] W. Jiang, S.P. Schwendeman, Stabilization and controlled release of bovine serum albumin encapsulated in poly(D, L-lactide) and poly(ethylene glycol) microsphere blends, Pharm. Res. 18 (2001) 878–885. https://doi.org/10.1023/A:1011009117586.

[244] M. Stack, D. Parikh, H. Wang, L. Wang, M. Xu, J. Zou, J. Cheng, H. Wang, Electrospun nanofibers for drug delivery, in: Electrospinning Nanofabrication Appl., 2018: pp. 735–764. https://doi.org/10.1016/B978-0-323-51270-1.00025-X.

[245] P. Kesarwani, R.K. Tekade, N.K. Jain, Spectrophotometric estimation of paclitaxel, Int. J. Adv. Pharm. Sci. 2 (2011) 29–32.

[246] Y.M. Park, E.K., Lee, S.B. and Lee, Preparation and characterization of methoxy poly (ethylene glycol)/poly (ε-caprolactone) amphiphilic block copolymeric nanospheres for tumor-specific folate-mediated targeting of anticancer drugs., Biomaterials. 26 (2005) 1053–1061.

[247] J.D. Obayemi, J. Hu, V.O. Uzonwanne, O.S. Odusanya, K. Malatesta, N. Anuku, W.O. Soboyejo, Adhesion of ligand-conjugated biosynthesized magnetite nanoparticles to triple negative breast cancer cells, J. Mech. Behav. Biomed. Mater. 68 (2017) 276–286. https://doi.org/10.1016/j.jmbbm.2017.02.004.

[248] D.M. Euhus, C. Hudd, M.C. Laregina, F.E. Johnson, Tumor measurement in the nude mouse, J. Surg. Oncol. 31 (1986) 229–234. https://doi.org/10.1002/jso.2930310402.

[249] M.M. Tomayko, C.P. Reynolds, Determination of subcutaneous tumor size in athymic (nude) mice, Cancer Chemother. Pharmacol. 24 (1989) 148–154. https://doi.org/10.1007/BF00300234.

[250] S. Dash, P.N. Murthy, L. Nath, P. Chowdhury, Kinetic modeling on drug release from controlled drug delivery systems, Acta Pol. Pharm. - Drug Res. 67 (2010) 217–223.

[251] P. Costa, J.M. Sousa Lobo, Modeling and comparison of dissolution profiles, Eur. J. Pharm. Sci. 13 (2001) 123–133. https://doi.org/10.1016/S0928-0987(01)00095-1.

[252] N.A. Narasimhan, B., Mallapragada, S.K. and Peppas, Release kinetics, data interpretation., Encycl. Control. Drug Deliv. 2 (1999) 921–935.

[253] T. Higuchi, Mechanism of sustained-action medication. Theoretical analysis of rate of release of solid drugs dispersed in solid matrices, J. Pharm. Sci. 52 (1963) 1145–1149. https://doi.org/10.1002/jps.2600521210.

[254] J.M. Smith, Introduction to chemical engineering thermodynamics, J. Chem. Educ. 27 (1950) 584. https://doi.org/10.1021/ed027p584.3.

[255] A. Sari, M. Tuzen, D. Citak, M. Soylak, Equilibrium, kinetic and thermodynamic studies of adsorption of Pb(II) from aqueous solution onto Turkish kaolinite clay, J. Hazard. Mater. 149 (2007) 283–291. https://doi.org/10.1016/j.jhazmat.2007.03.078.

[256] B. Amsden, Tissue engineering and novel delivery systems, CRC, 2005. https://doi.org/10.1016/j.jconrel.2005.01.023.

[257] M. Chieng, B., Ibrahim, N., Yunus, W. and Hussein, Poly (lactic acid)/poly (ethylene glycol) polymer nanocomposites: effects of graphene nanoplatelets., Polymers (Basel). 6 (2014) 93–104.

[258] C. D'Avila Carvalho Erbetta, Synthesis and Characterization of Poly(D,L-Lactide-co-Glycolide) Copolymer, J. Biomater. Nanobiotechnol. 03 (2012) 208–225. https://doi.org/10.4236/jbnb.2012.32027.

[259] A.T.C.R. Silva, B.C.O. Cardoso, M.E.S.R. e Silva, R.F.S. Freitas, R.G. Sousa, Synthesis, Characterization, and Study of PLGA Copolymer <i>in Vitro</i> Degradation, J. Biomater. Nanobiotechnol. 06 (2015) 8–19. https://doi.org/10.4236/jbnb.2015.61002.

[260] A. Alemdar, N. Güngör, O.I. Ece, O. Atici, The rheological properties and characterization

of bentonite dispersions in the presence of non-ionic polymer PEG, J. Mater. Sci. 40 (2005) 171–177. https://doi.org/10.1007/s10853-005-5703-4.

[261] A. Gorajana, C.C. Ying, Y. Shuang, P. Fong, Z. Tan, J. Gupta, M. Talekar, M. Sharma, S. Garg, Development of Solid Dispersion Systems of Dapivirine to Enhance its Solubility, Curr. Drug Deliv. 10 (2013) 309–316. https://doi.org/10.2174/1567201811310030007.

[262] K.F. Martins, A.D. Messias, F.L. Leite, E.A.R. Duek, Preparation and characterization of paclitaxel-loaded PLDLA microspheres, Mater. Res. 17 (2014) 650–656. https://doi.org/10.1590/S1516-14392014005000028.

[263] M. Qiao, D. Chen, X. Ma, Y. Liu, Injectable biodegradable temperature-responsive PLGA-PEG-PLGA copolymers: Synthesis and effect of copolymer composition on the drug release from the copolymer-based hydrogels, Int. J. Pharm. 294 (2005) 103–112. https://doi.org/10.1016/j.ijpharm.2005.01.017.

[264] B. Zhang, P. Sai Lung, S. Zhao, Z. Chu, W. Chrzanowski, Q. Li, Shape dependent cytotoxicity of PLGA-PEG nanoparticles on human cells, Sci. Rep. 7 (2017). https://doi.org/10.1038/s41598-017-07588-9.

[265] Q. Xu, J.T. Czernuszka, Controlled release of amoxicillin from hydroxyapatite-coated poly(lactic-co-glycolic acid) microspheres, J. Control. Release. 127 (2008) 146–153. https://doi.org/10.1016/j.jconrel.2008.01.017.

[266] Z. gang Zhang, A. ping Sun, L. xia Long, Effect of physicochemical properties of drugs on morphology and release of microspheres, J. Med. Biol. Eng. 34 (2014) 293–298. https://doi.org/10.5405/jmbe.1070.

[267] R. Yang, X. Han, K. Shi, G. Cheng, C.K. Shim, F. Cui, Cationic formulation of paclitaxel-loaded poly D,L-lactic-co-glycolic acid (PLGA) nanoparticles using an emulsion-solvent diffusion method, Asian J. Pharm. Sci. 4 (2009) 89–95.

[268] L.S.C. Wan, P.W.S. Heng, L.F. Wong, Relationship between swelling and drug release in a hydrophilic matrix, Drug Dev. Ind. Pharm. 19 (1993) 1201–1210. https://doi.org/10.3109/03639049309063012.

[269] S.J. Siegel, J.B. Kahn, K. Metzger, K.I. Winey, K. Werner, N. Dan, Effect of drug type on the degradation rate of PLGA matrices, Eur. J. Pharm. Biopharm. 64 (2006) 287–293. https://doi.org/10.1016/j.ejpb.2006.06.009.

[270] V.A. Spencer, Actin-towards a deeper understanding of the relationship between tissue context, cellular function and tumorigenesis, Cancers (Basel). 3 (2011) 4269–4280. https://doi.org/10.3390/cancers3044269.

[271] K.J. Green, R.D. Goldman, The effects of taxol on cytoskeletal components in cultured fibroblasts and epithelial cells, Cell Motil. 3 (1983) 283–305. https://doi.org/10.1002/cm.970030402.

[272] R.D. Goldman, S. Khuon, Y.H. Chou, P. Opal, P.M. Steinert, The function of intermediate filaments in cell shape and cytoskeletal integrity, J. Cell Biol. 134 (1996) 971–983. https://doi.org/10.1083/jcb.134.4.971.

[273] S. Taranejoo, M. Janmaleki, M. Pachenari, S.M. Seyedpour, R. Chandrasekaran, W. Cheng, K. Hourigan, Dual effect of F-actin targeted carrier combined with antimitotic drug on aggressive colorectal cancer cytoskeleton: Allying dissimilar cell cytoskeleton disrupting mechanisms, Int. J. Pharm. 513 (2016) 464–472. https://doi.org/10.1016/j.ijpharm.2016.09.056.

[274] C.W. Gourlay, L.N. Carpp, P. Timpson, S.J. Winder, K.R. Ayscough, A role for the actin cytoskeleton in cell death and aging in yeast, J. Cell Biol. 164 (2004) 803–809. https://doi.org/10.1083/jcb.200310148.

[275] C.W. Gourlay, K.R. Ayscough, A role for actin in aging and apoptosis, Biochem. Soc. Trans. 33 (2005) 1260–1264. https://doi.org/10.1042/BST20051260.

[276] W. Bursch, K. Hochegger, L. Török, B. Marian, A. Ellinger, R.S. Hermann, Autophagic and apoptotic types of programmed cell death exhibit different fates of cytoskeletal filaments, J. Cell Sci. 113 (2000) 1189–1198. https://doi.org/10.1242/jcs.113.7.1189.

[277] Z. Abbas, S. Rehman, An Overview of Cancer Treatment Modalities, in: Neoplasm, 2018: pp. 139–57. https://doi.org/10.5772/intechopen.76558.

[278] A. Mitra, B. Dey, Chitosan microspheres in novel drug delivery systems, Indian J. Pharm. Sci. 73 (2011) 355–366. https://doi.org/10.4103/0250-474X.95607.

[279] B. Tyler, D. Gullotti, A. Mangraviti, T. Utsuki, H. Brem, Polylactic acid (PLA) controlled delivery carriers for biomedical applications, Adv. Drug Deliv. Rev. 107 (2016) 163–175. https://doi.org/10.1016/j.addr.2016.06.018.

[280] M. Mir, N. Ahmed, A. ur Rehman, Recent applications of PLGA based nanostructures in drug delivery, Colloids Surfaces B Biointerfaces. 159 (2017) 217–231. https://doi.org/10.1016/j.colsurfb.2017.07.038.

[281] S. Fredenberg, M. Wahlgren, M. Reslow, A. Axelsson, The mechanisms of drug release in poly(lactic-co-glycolic acid)-based drug delivery systems - A review, Int. J. Pharm. 415 (2011) 34–52. https://doi.org/10.1016/j.ijpharm.2011.05.049.

[282] N. Kamaly, B. Yameen, J. Wu, O.C. Farokhzad, Degradable controlled-release polymers and polymeric nanoparticles: mechanisms of controlling drug release, Chem. Rev. 116 (2016) 2602–2663.

[283] M.M. Anwar, M. Shalaby, A.M. Embaby, H. Saeed, M.M. Agwa, A. Hussein, Prodigiosin/PU-H71 as a novel potential combined therapy for triple negative breast cancer (TNBC): preclinical insights, Sci. Rep. 10 (2020) 1–5. https://doi.org/10.1038/s41598-020-71157-w.

[284] B.A. Weaver, How Taxol/paclitaxel kills cancer cells, Mol. Biol. Cell. 25 (2014) 2677–2681.

[285] R. Renneberg, Biotech History: Yew trees, paclitaxel synthesis and fungi, Biotechnol. J. Healthc. Nutr. Technol. 2 (2007) 1207–1209.

[286] Y. Fu, W.J. Kao, Drug release kinetics and transport mechanisms of non-degradable and degradable polymeric delivery systems, Expert Opin. Drug Deliv. 7 (2010) 429–444. https://doi.org/10.1517/17425241003602259.

[287] M.C.L.C. Freire, F. Alexandrino, H.R. Marcelino, P.H. de S. Picciani, K.G. de H. e Silva, J. Genre, A.G. de Oliveira, E.S.T. do Egito, Understanding drug release data through thermodynamic analysis, Materials (Basel). 10 (2017) 651. https://doi.org/10.3390/ma10060651.

[288] G. Maria, I. Luta, Precautions in using global kinetic and thermodynamic models for characterization of drug release from multivalent supports, Chem. Pap. 65 (2011) 542–552. https://doi.org/10.2478/s11696-011-0041-2.

[289] J. Wang, A. Shi, D. Agyei, Q. Wang, Formulation of water-in-oil-in-water (W/O/W) emulsions containing trans-resveratrol, RSC Adv. 7 (2017) 35917–35927. https://doi.org/10.1039/c7ra05945k.

[290] S. Parveen, S.K. Sahoo, Long circulating chitosan/PEG blended PLGA nanoparticle for tumor drug delivery, Eur. J. Pharmacol. 670 (2011) 372–383. https://doi.org/10.1016/j.ejphar.2011.09.023.

[291] K. Al Rubeaan, M. Rafiullah, S. Jayavanth, Oral insulin delivery systems using chitosan-based formulation: A review, Expert Opin. Drug Deliv. 13 (2016) 223–237. https://doi.org/10.1517/17425247.2016.1107543.

[292] A.A. Abd-Rabou, H.H. Ahmed, CS-PEG decorated PLGA nano-prototype for delivery of bioactive compounds: A novel approach for induction of apoptosis in HepG2 cell line, Adv. Med. Sci. 62 (2017) 357–367. https://doi.org/10.1016/j.advms.2017.01.003.

[293] D.N. Kapoor, A. Bhatia, R. Kaur, R. Sharma, G. Kaur, S. Dhawan, PLGA: A unique polymer for drug delivery, Ther. Deliv. 6 (2015) 41–58. https://doi.org/10.4155/tde.14.91.

[294] F. Sadoughi, M.A. Mansournia, S.M. Mirhashemi, The potential role of chitosan-based nanoparticles as drug delivery systems in pancreatic cancer, IUBMB Life. 72 (2020) 872–883.

[295] A. Hassani Najafabadi, M. Abdouss, S. Faghihi, Synthesis and evaluation of PEG-O-chitosan nanoparticles for delivery of poor water soluble drugs: Ibuprofen, Mater. Sci. Eng. C. 41 (2014) 91–99. https://doi.org/10.1016/j.msec.2014.04.035.

[296] E. Sánchez-López, M.A. Egea, A. Cano, M. Espina, A.C. Calpena, M. Ettcheto, A. Camins, E.B. Souto, A.M. Silva, M.L. García, PEGylated PLGA nanospheres optimized by design

of experiments for ocular administration of dexibuprofen-in vitro, ex vivo and in vivo characterization, Colloids Surfaces B Biointerfaces. 145 (2016) 241–250. https://doi.org/10.1016/j.colsurfb.2016.04.054.

[297] Jha, M.K., Rahman, M.H. and Rahman, M.M., Biphasic oral solid drug delivery system: A review., Int. J. Pharm. Sci. Res. 2 (2011) 1108.

[298] J. Yoo, Y.Y. Won, Phenomenology of the Initial Burst Release of Drugs from PLGA Microparticles, ACS Biomater. Sci. Eng. 6 (2020) 6053–6062. https://doi.org/10.1021/acsbiomaterials.0c01228.

[299] A.C. Society, Breast Cancer Facts & Figures 2018-2019, Side Eff. Med. Cancer Ther. Prev. Treat. Second Ed. (2018).

[300] A. Migowski, A detecção precoce do câncer de mama e a interpretação dos resultados de estudos de sobrevida, Cienc. e Saude Coletiva. 20 (2015) 1309–1310. https://doi.org/10.1590/1413-81232015204.17772014.

[301] S. Senapati, A.K. Mahanta, S. Kumar, P. Maiti, Controlled drug delivery vehicles for cancer treatment and their performance, Signal Transduct. Target. Ther. 3 (2018) 1–9. https://doi.org/10.1038/s41392-017-0004-3.

[302] A.C. Society, Breast Cancer Facts and Figures 2017-2018, 2017.

[303] A. Argyraki, M. Markvart, C. Stavnsbjerg, K.N. Kragh, Y. Ou, L. Bjørndal, T. Bjarnsholt, P.M. Petersen, Y. Muramoto, M. Kimura, S. Nouda, I.N. Solution, T. Takayoshi, M. Takuya, S. Jun, N. Norimichi, T. Kenji, H. Hideki, U. Germicidal, I. Handbook, F. Science, F. Science, N. Science, T. Scholarship, A. Note, A. Note, D. Welch, M. Buonanno, I. Shuryak, G. Randers-Pehrson, H.M. Spotnitz, D.J. Brenner, Y. Huo, K. Aboud, H. Kang, L.E. Cutting, A. Bennett, W.C.M.A. De Melo, P. Avci, M.N. De Oliveira, A. Gupta, D. Vecchio, M. Sadasivam, R. Chandran, Y.Y. Huang, R. Yin, L.R. Perussi, G.P. Tegos, J.R. Perussi, T. Dai, M.R. Hamblin, E. Connolly, M.J. Lee, J.S. Kwon, H.B. Jiang, E.H. Choi, G. Park, K.M. Kim, J. Shin, S. Kim, D. Kim, D. Kang, （生物用）HHS Public Access, 2015 IEEE Summer Top. Meet. Ser. SUM 2015. 10 (2018) 1–13. https://doi.org/10.1038/s41598-019-39414-9.

[304] C. Desantis, R. Siegel, A. Jemal, Breast Cancer Facts & Figures 2015-2016, Surveill. Heal. Serv. Res. Progr. (2015). https://doi.org/10.1016/B978-1-4377-1757-0.00028-7.

[305] J.A. Marks, L.A. Wegiel, L.S. Taylor, K.J. Edgar, Pairwise polymer blends for oral drug delivery, J. Pharm. Sci. 103 (2014) 2871–2883. https://doi.org/10.1002/jps.23991.

[306] Q. Zhan, B. Shen, X. Deng, H. Chen, J. Jin, X. Zhang, C. Peng, H. Li, Drug-eluting scaffold to deliver chemotherapeutic medication for management of pancreatic cancer after surgery, Int. J. Nanomedicine. 8 (2013) 2465–2472. https://doi.org/10.2147/ijn.s47666.

[307] W. Sun, Z. Gu, Engineering DNA scaffolds for delivery of anticancer therapeutics, Biomater. Sci. 3 (2015) 1018–1024. https://doi.org/10.1039/c4bm00459k.

[308] K.S. Soppimath, T.M. Aminabhavi, A.R. Kulkarni, W.E. Rudzinski, Biodegradable polymeric nanoparticles as drug delivery devices, J. Control. Release. 70 (2001) 1–20. https://doi.org/10.1016/S0168-3659(00)00339-4.

[309] S. Kumar, S. Singh, S. Senapati, A.P. Singh, B. Ray, P. Maiti, Controlled drug release through regulated biodegradation of poly(lactic acid) using inorganic salts, Int. J. Biol. Macromol. 104 (2017) 487–497. https://doi.org/10.1016/j.ijbiomac.2017.06.033.

[310] N. Bhattarai, J. Gunn, M. Zhang, Chitosan-based hydrogels for controlled, localized drug delivery, Adv. Drug Deliv. Rev. 62 (2010) 83–99. https://doi.org/10.1016/j.addr.2009.07.019.

[311] A.J. Meinel, O. Germershaus, T. Luhmann, H.P. Merkle, L. Meinel, Electrospun matrices for localized drug delivery: Current technologies and selected biomedical applications, Eur. J. Pharm. Biopharm. 81 (2012) 1–13. https://doi.org/10.1016/j.ejpb.2012.01.016.

[312] S.S. Rao, G.G. Bushnell, S.M. Azarin, G. Spicer, B.A. Aguado, J.R. Stoehr, E.J. Jiang, V. Backman, L.D. Shea, J.S. Jeruss, Enhanced survival with implantable scaffolds that capture metastatic breast cancer cells in vivo, Cancer Res. 76 (2016) 5209–5218. https://doi.org/10.1158/0008-5472.CAN-15-2106.

[313] H.G. Yi, Y.J. Choi, K.S. Kang, J.M. Hong, R.G. Pati, M.N. Park, I.K. Shim, C.M. Lee, S.C. Kim, D.W. Cho, A 3D-printed local drug delivery patch for pancreatic cancer growth suppression, J. Control. Release. 238 (2016) 231–241. https://doi.org/10.1016/j.jconrel.2016.06.015.

[314] J.S. Son, M. Appleford, J.L. Ong, J.C. Wenke, J.M. Kim, S.H. Choi, D.S. Oh, Porous hydroxyapatite scaffold with three-dimensional localized drug delivery system using biodegradable microspheres, J. Control. Release. 153 (2011) 133–140. https://doi.org/10.1016/j.jconrel.2011.03.010.

[315] H. Soltanian, H. Okada, Understanding genetic analysis for breast cancer and its implications for plastic surgery, Aesthetic Surg. J. 28 (2008) 85–91. https://doi.org/10.1016/j.asj.2007.10.002.

[316] U.S. Food, D. Administration, FDA, FDA Update on the Safety of Silicone Gel-Filled Breast Implants Center for Devices and Radiological Health, Cent. Devices Radiol. Heal. U.S. Food Drug Adm. (2011) 63. http://www.fda.gov/downloads/medicaldevices/productsandmedicalprocedures/Implantsandprosthetics/Breastimplants/Ucm260090.Pdf (accessed February 7, 2018).

[317] S.H. Oh, S.G. Kang, E.S. Kim, S.H. Cho, J.H. Lee, Fabrication and characterization of hydrophilic poly(lactic-co-glycolic acid)/poly(vinyl alcohol) blend cell scaffolds by melt-molding particulate-leaching method, Biomaterials. 24 (2003) 4011–4021. https://doi.org/10.1016/S0142-9612(03)00284-9.

[318] C.M. Nelson, M.J. Bissell, Modeling dynamic reciprocity: Engineering three-dimensional culture models of breast architecture, function, and neoplastic transformation, Semin.

Cancer Biol. 15 (2005) 342–352. https://doi.org/10.1016/j.semcancer.2005.05.001.

[319] C.W. Patrick, Adipose tissue engineering: The future of breast and soft tissue reconstruction following tumor resection, Semin. Surg. Oncol. 19 (2000) 302–311. https://doi.org/10.1002/1098-2388(200010/11)19:3<302::AID-SSU12>3.0.CO;2-S.

[320] M.P. Chhaya, F.P.W. Melchels, B.M. Holzapfel, J.G. Baldwin, D.W. Hutmacher, Sustained regeneration of high-volume adipose tissue for breast reconstruction using computer aided design and biomanufacturing, Biomaterials. 52 (2015) 551–560. https://doi.org/10.1016/j.biomaterials.2015.01.025.

[321] P. Ahangar, E. Akoury, A.S.R.G. Luna, A. Nour, M.H. Weber, D.H. Rosenzweig, Nanoporous 3D-printed scaffolds for local doxorubicin delivery in bone metastases secondary to prostate cancer, Materials (Basel). 11 (2018) 1485. https://doi.org/10.3390/ma11091485.

[322] G.Y. Lee, P.A. Kenny, E.H. Lee, M.J. Bissell, Three-dimensional culture models of normal and malignant breast epithelial cells, Nat. Methods. 4 (2007) 359–365. https://doi.org/10.1038/nmeth1015.

[323] C. Fischbach, R. Chen, T. Matsumoto, T. Schmelzle, J.S. Brugge, P.J. Polverini, D.J. Mooney, Engineering tumors with 3D scaffolds, Nat. Methods. 4 (2007) 855–860. https://doi.org/10.1038/nmeth1085.

[324] H.J. Sung, C. Meredith, C. Johnson, Z.S. Galis, The effect of scaffold degradation rate on three-dimensional cell growth and angiogenesis, Biomaterials. 25 (2004) 5735–5742. https://doi.org/10.1016/j.biomaterials.2004.01.066.

[325] A. Newman, G. Knipp, G. Zografi, Assessing the performance of amorphous solid dispersions, J. Pharm. Sci. 101 (2012) 1355–1377. https://doi.org/10.1002/jps.23031.

[326] T.W.A. Gould, J.P. Birchall, A.S. Mallick, T. Alliston, L.R. Lustig, K.M. Shakesheff, C. V. Rahman, Development of a porous poly(DL-lactic acid-co-glycolic acid)-based scaffold for mastoid air-cell regeneration, Laryngoscope. 123 (2013) 3156–3161. https://doi.org/10.1002/lary.24173.

[327] C. V. Rahman, G. Kuhn, L.J. White, G.T.S. Kirby, O.P. Varghese, J.S. Mclaren, H.C. Cox, F.R.A.J. Rose, R. Muller, J. Hilborn, K.M. Shakesheff, PLGA/PEG-hydrogel composite scaffolds with controllable mechanical properties, J. Biomed. Mater. Res. - Part B Appl. Biomater. 101 (2013) 648–655. https://doi.org/10.1002/jbm.b.32867.

[328] C. V. Rahman, D. Ben-David, A. Dhillon, G. Kuhn, T.W.A. Gould, R. Müller, F.R.A.J. Rose, K.M. Shakesheff, E. Livne, Controlled release of BMP-2 from a sintered polymer scaffold enhances bone repair in a mouse calvarial defect model, J. Tissue Eng. Regen. Med. 8 (2014) 59–66. https://doi.org/10.1002/term.1497.

[329] G.A. Ilevbare, H. Liu, K.J. Edgar, L.S. Taylor, Effect of binary additive combinations on solution crystal growth of the poorly water-soluble drug, ritonavir, Cryst. Growth Des. 12

(2012) 6050–6060. https://doi.org/10.1021/cg301169t.

[330] Pradip, C. Maltesh, P. Somasundaran, R.A. Kulkarni, S. Gundiah, Polymer-Polymer Complexation in Dilute Aqueous Solutions: Poly(acrylic acid)-Poly(ethylene oxide) and Poly(acrylic acid)-Poly(vinylpyrrolidone), Langmuir. 7 (1991) 2108–2111. https://doi.org/10.1021/la00058a024.

[331] V. Umesh, A.D. Rape, T.A. Ulrich, S. Kumar, Microenvironmental stiffness enhances glioma cell proliferation by stimulating epidermal growth factor receptor signaling, PLoS One. 9 (2014) 101771. https://doi.org/10.1371/journal.pone.0101771.

[332] S. Eshraghi, S. Das, Mechanical and microstructural properties of polycaprolactone scaffolds with one-dimensional, two-dimensional, and three-dimensional orthogonally oriented porous architectures produced by selective laser sintering, Acta Biomater. 6 (2010) 2467–2476. https://doi.org/10.1016/j.actbio.2010.02.002.

[333] C.M. Agrawal, R.B. Ray, Biodegradable polymeric scaffolds for musculoskeletal tissue engineering, J. Biomed. Mater. Res. 55 (2001) 141–150. https://doi.org/10.1002/1097-4636(200105)55:2<141::AID-JBM1000>3.0.CO;2-J.

[334] P. Sarazin, X. Roy, B.D. Favis, Controlled preparation and properties of porous poly(L-lactide) obtained from a co-continuous blend of two biodegradable polymers, Biomaterials. 25 (2004) 5965–5978. https://doi.org/10.1016/j.biomaterials.2004.01.065.

[335] S.J. Bryant, R.J. Bender, K.L. Durand, K.S. Anseth, Encapsulating chondrocytes in degrading PEG hydrogels with high modulus: Engineering gel structural changes to facilitate cartilaginous tissue production, Biotechnol. Bioeng. 86 (2004) 747–755. https://doi.org/10.1002/bit.20160.

[336] A.L. McKnight, J.L. Kugel, P.J. Rossman, A. Manduca, L.C. Hartmann, R.L. Ehman, MR elastography of breast cancer: Preliminary results, Am. J. Roentgenol. 178 (2002) 1411–1417. https://doi.org/10.2214/ajr.178.6.1781411.

[337] M.J. Paszek, N. Zahir, K.R. Johnson, J.N. Lakins, G.I. Rozenberg, A. Gefen, C.A. Reinhart-King, S.S. Margulies, M. Dembo, D. Boettiger, D.A. Hammer, V.M. Weaver, Tensional homeostasis and the malignant phenotype, Cancer Cell. 8 (2005) 241–254. https://doi.org/10.1016/j.ccr.2005.08.010.

[338] E.E.W. Van Houten, M.M. Doyley, F.E. Kennedy, J.B. Weaver, K.D. Paulsen, Initial in vivo experience with steady-state subzone-based MR elastography of the human breast, J. Magn. Reson. Imaging. 17 (2003) 72–85. https://doi.org/10.1002/jmri.10232.

[339] O.I. Corrigan, X. Li, Quantifying drug release from PLGA nanoparticulates, Eur. J. Pharm. Sci. 37 (2009) 477–485. https://doi.org/10.1016/j.ejps.2009.04.004.

[340] E.D. Pereira, R. Cerruti, E. Fernandes, L. Peña, V. Saez, J.C. Pinto, J.A. Ramón, G.E. Oliveira, F.G. De Souza, Influence of PLGA and PLGA-PEG on the dissolution profile of oxaliplatin, Polimeros. 26 (2016) 137–143. https://doi.org/10.1590/0104-1428.2323.

[341] S.C. Baker, G. Rohman, J. Southgate, N.R. Cameron, The relationship between the mechanical properties and cell behaviour on PLGA and PCL scaffolds for bladder tissue engineering, Biomaterials. 30 (2009) 1321–1328. https://doi.org/10.1016/j.biomaterials.2008.11.033.

[342] Y. Danyuo, C.J. Ani, J.D. Obayemi, S. Dozie-Nwachukwu, O.S. Odusanya, Y. Oni, N. Anuku, K. Malatesta, W.O. Soboyejo, Prodigiosin Release from an Implantable Biomedical Device: Effect on Cell Viability, Adv. Mater. Res. (2015). https://doi.org/10.4028/www.scientific.net/amr.1132.3.

[343] A. Salerno, E. Di Maio, S. Iannace, P.A. Netti, Tailoring the pore structure of PCL scaffolds for tissue engineering prepared via gas foaming of multi-phase blends, J. Porous Mater. 19 (2012) 181–188. https://doi.org/10.1007/s10934-011-9458-9.

[344] S.J. Hollister, Porous scaffold design for tissue engineering, Nat. Mater. 4 (2005) 518–524. https://doi.org/10.1038/nmat1421.

[345] F. Causa, P.A. Netti, L. Ambrosio, A multi-functional scaffold for tissue regeneration: The need to engineer a tissue analogue, Biomaterials. 28 (2007) 5093–5099. https://doi.org/10.1016/j.biomaterials.2007.07.030.

[346] R. Zhang, P.X. Ma, Poly(α-hydroxyl acids)/hydroxyapatite porous composites for bone-tissue engineering. I. Preparation and morphology, J. Biomed. Mater. Res. 44 (1999) 446–455. https://doi.org/10.1002/(SICI)1097-4636(19990315)44:4<446::AID-JBM11>3.0.CO;2-F.

[347] Y.Y. Hsu, J.D. Gresser, D.J. Trantolo, C.M. Lyons, P.R.J. Gangadharam, D.L. Wise, Effect of polymer foam morphology and density on kinetics of in vitro controlled release of isoniazid from compressed foam matrices, J. Biomed. Mater. Res. 35 (1997) 107–116. https://doi.org/10.1002/(SICI)1097-4636(199704)35:1<107::AID-JBM11>3.0.CO;2-G.

[348] K.G. Janoria, A.K. Mitra, Effect of lactide/glycolide ratio on the in vitro release of ganciclovir and its lipophilic prodrug (GCV-monobutyrate) from PLGA microspheres, Int. J. Pharm. 338 (2007) 133–141. https://doi.org/10.1016/j.ijpharm.2007.01.038.

[349] V.A. De Mello, E. Ricci-Júnior, Encapsulation of naproxen in nanostructured system: Structural characterization and in Vitro release studies, Quim. Nova. 34 (2011) 933–939. https://doi.org/10.1590/s0100-40422011000600004.

[350] A. Samani, J. Zubovits, D. Plewes, Elastic moduli of normal and pathological human breast tissues: An inversion-technique-based investigation of 169 samples, Phys. Med. Biol. 52 (2007) 1565–1576. https://doi.org/10.1088/0031-9155/52/6/002.

[351] A. Samani, D. Plewes, An inverse problem solution for measuring the elastic modulus of intact ex vivo breast tissue tumours, Phys. Med. Biol. 52 (2007) 1247–1260. https://doi.org/10.1088/0031-9155/52/5/003.

[352] A. Samani, J. Bishop, C. Luginbuhl, D.B. Plewes, Measuring the elastic modulus of ex vivo

small tissue samples, Phys. Med. Biol. 48 (2003) 2183–2198. https://doi.org/10.1088/0031-9155/48/14/310.

[353] S.H. Huang, T.T. Hsu, T.H. Huang, C.Y. Lin, M.Y. Shie, Fabrication and characterization of polycaprolactone and tricalcium phosphate composites for tissue engineering applications, J. Dent. Sci. 12 (2017) 33–43. https://doi.org/10.1016/j.jds.2016.05.003.

[354] G.M. Balachander, S.A. Balaji, A. Rangarajan, K. Chatterjee, Enhanced Metastatic Potential in a 3D Tissue Scaffold toward a Comprehensive in Vitro Model for Breast Cancer Metastasis, ACS Appl. Mater. Interfaces. 7 (2015) 27810–27822. https://doi.org/10.1021/acsami.5b09064.

[355] Y.M. Wang, H. Sato, I. Adachi, I. Horikoshi, Preparation and characterization of poly(lactic-co-glycolic acid) microspheres for targeted delivery of a novel anticancer agent, Taxol, Chem. Pharm. Bull. 44 (1996) 1935–1940. https://doi.org/10.1248/cpb.44.1935.

[356] D.R. Liston, M. Davis, Clinically relevant concentrations of anticancer drugs: A guide for nonclinical studies, Clin. Cancer Res. 23 (2017) 3489–3498. https://doi.org/10.1158/1078-0432.CCR-16-3083.

[357] Z.G. Tang, J.T. Callaghan, J.A. Hunt, The physical properties and response of osteoblasts to solution cast films of PLGA doped polycaprolactone, Biomaterials. 26 (2005) 6618–6624. https://doi.org/10.1016/j.biomaterials.2005.04.013.

[358] H.J. Sung, J. Su, J.D. Berglund, B. V. Russ, J.C. Meredith, Z.S. Galis, The use of temperature-composition combinatorial libraries to study the effects of biodegradable polymer blend surfaces on vascular cells, Biomaterials. 26 (2005) 4557–4567. https://doi.org/10.1016/j.biomaterials.2004.11.034.

[359] L.L. Lao, N.A. Peppas, F.Y.C. Boey, S.S. Venkatraman, Modeling of drug release from bulk-degrading polymers, Int. J. Pharm. 418 (2011) 28–41. https://doi.org/10.1016/j.ijpharm.2010.12.020.

[360] C.H. Wu, Adsorption of reactive dye onto carbon nanotubes: Equilibrium, kinetics and thermodynamics, J. Hazard. Mater. 144 (2007) 93–100. https://doi.org/10.1016/j.jhazmat.2006.09.083.

[361] S. Vasiliu, I. Bunia, S. Racovita, V. Neagu, Adsorption of cefotaxime sodium salt on polymer coated ion exchange resin microparticles: Kinetics, equilibrium and thermodynamic studies, Carbohydr. Polym. 85 (2011) 376–387. https://doi.org/10.1016/j.carbpol.2011.02.039.

[362] C. Ferrero, D. Massuelle, E. Doelker, Towards elucidation of the drug release mechanism from compressed hydrophilic matrices made of cellulose ethers. II. Evaluation of a possible swelling-controlled drug release mechanism using dimensionless analysis, J. Control. Release. 141 (2010) 223–233. https://doi.org/10.1016/j.jconrel.2009.09.011.

[363] H. Antheunis, J.C. Van Der Meer, M. De Geus, A. Heise, C.E. Koning, Autocatalytic

equation describing the change in molecular weight during hydrolytic degradation of aliphatic polyesters, Biomacromolecules. 11 (2010) 1118–1124. https://doi.org/10.1021/bm100125b.

[364] Z. Pan, J. Ding, Poly(lactide-co-glycolide) porous scaffolds for tissue engineering and regenerative medicine, Interface Focus. 2 (2012) 366–377. https://doi.org/10.1098/rsfs.2011.0123.

[365] A.C. Society, What Are the Different Types of Chemotherapy Drugs?, (n.d.).

[366] B. Montaner, S. Navarro, M. Piqué, M. Vilaseca, M. Martinell, E. Giralt, J. Gil, R. Pérez-Tomás, Prodigiosin from the supernatant of Serratia marcescens induces apoptosis in haematopoietic cancer cell lines, Br. J. Pharmacol. 131 (2000) 585–593. https://doi.org/10.1038/sj.bjp.0703614.

[367] T. Azuma, N. Watanabe, H. Yagisawa, H. Hirata, M. Iwamura, Y. Kobayashi, Induction of apoptosis of activated murine splenic T cells by cycloprodigiosin hydrochloride, a novel immunosuppressant, Immunopharmacology. 46 (2000) 29–37. https://doi.org/10.1016/S0162-3109(99)00153-8.

[368] B. Montaner, R. Pérez-Tomás, Prodigiosin-induced apoptosis in human colon cancer cells, Life Sci. 68 (2001) 2025–2036. https://doi.org/10.1016/S0024-3205(01)01002-5.

[369] R. Pérez-Tomás, B. Montaner, Effects of the proapoptotic drug prodigiosin on cell cycle-related proteins in Jurkat T cells, Histol. Histopathol. 18 (2003) 379–385. https://doi.org/10.14670/HH-18.379.

[370] E. Jubeli, A. Khzam, N. Yagoubi, Cells integration onto scaffolds prepared from polyester based polymers–importance of polymer thermal properties in addition to hydrophilicity, Int. J. Polym. Mater. Polym. Biomater. 68 (2019) 1068–1077. https://doi.org/10.1080/00914037.2018.1525549.

[371] S. Prabhakar, Translational research challenges: Finding the right animal models, J. Investig. Med. 60 (2012) 1141–1146. https://doi.org/10.2310/JIM.0b013e318271fb3b.

[372] O. Lorbach, M.H. Baums, T. Kostuj, S. Pauly, M. Scheibel, A. Carr, N. Zargar, M.F. Saccomanno, G. Milano, Advances in biology and mechanics of rotator cuff repair, Knee Surgery, Sport. Traumatol. Arthrosc. 23 (2015) 530–541. https://doi.org/10.1007/s00167-014-3487-2.

[373] I. Ribitsch, P.M. Baptista, A. Lange-Consiglio, L. Melotti, M. Patruno, F. Jenner, E. Schnabl-Feichter, L.C. Dutton, D.J. Connolly, F.G. van Steenbeek, J. Dudhia, L.C. Penning, Large Animal Models in Regenerative Medicine and Tissue Engineering: To Do or Not to Do, Front. Bioeng. Biotechnol. 8 (2020). https://doi.org/10.3389/fbioe.2020.00972.

[374] N. Shanks, R. Greek, J. Greek, Are animal models predictive for humans?, Philos. Ethics, Humanit. Med. 4 (2009) 1–20. https://doi.org/10.1186/1747-5341-4-2.

[375] A.J. Minn, Y. Kang, I. Serganova, G.P. Gupta, D.D. Giri, M. Doubrovin, V. Ponomarev, W.L. Gerald, R. Blasberg, J. Massagué, Distinct organ-specific metastatic potential of individual breast cancer cells and primary tumors, J. Clin. Invest. 115 (2005) 44–55. https://doi.org/10.1172/JCI22320.